Investigating genotype-phenotype correlations and potential therapies for laminopathies

Scharner, Juergen

Awarding institution:
King's College London

Investigating genotype-phenotype correlations and potential therapies for laminopathies

Juergen Scharner

Thesis submitted to King's College London
in partial fulfilment of the requirements for the degree of

Doctor of Philosophy

Randall Division of Cell and Molecular Biophysics

June 2012

Abstract

Laminopathies are a heterogeneous group of diseases associated with mutations in A-type lamins, which together with B-type lamins, form the nuclear lamina: a proteinaceous network underlying the nuclear membrane. A-type lamins are encoded by the *LMNA* gene, and more than 300 mutations have been described, associated with more than 16 phenotypes. The majority of mutations affect striated muscle to cause Emery-Dreifuss muscular dystrophy (EDMD) or cardiomyopathy, while others result in lipodystrophy, neuropathy or premature ageing syndromes. However, clear genotype-phenotype correlations are not established, the pathogenic mechanisms are little understood and therapies are lacking.

This thesis first explores genotype-phenotype for *LMNA* mutations and makes correlations by characterising both physical-chemical properties of the amino-acid change, and position in the 3D structure of lamin A. *LMNA* mutations associated with muscular dystrophies, premature ageing disorders and lipodystrophies clustered in the Ig-fold domain of lamin A and resulted in a similar change in charge, suggesting that modification of specific protein-protein interactions contribute to different phenotypes.

Next, I investigated the effects of four pathogenic EDMD mutations on nuclear morphology, nuclear protein distribution and myogenic cell function. I found that some mutations led to severe nuclear deformations and mislocalisation of lamin B, while others caused accumulation of lamin A-positive nuclear foci. Myogenic differentiation was mildly affected by some mutant lamin A species.

Finally, I describe a series of proof-of-principle experiments investigating a potential therapeutic intervention for laminopathies. A lamin A variant with a deletion corresponding to regions encoded by exon 5, removing 42 amino acids in the central rod domain, localised correctly. It could also rescue both abnormal nuclear morphology, and correct lamin B1 and emerin localisation in *lmna*-null embryonic fibroblasts.

This work advances the current understanding of genotype-phenotype correlations in laminopathies and provides proof-of-principle that oligonucleotide-mediated exon skipping is a potential therapy for certain laminopathies.

Acknowledgements

I want to acknowledge all those who helped to make this thesis possible. First I would like to thank Peter Zammit, my supervisor and mentor during the past 4 years who gave me the opportunity to work in his team and Elisabeth Ehler, my secondary supervisor for her support during my time at King's. My thanks also go to Juliet Ellis who provided fruitful suggestions to all areas of my research.

During my project I worked and published together with Viola Gnocchi who I whish to thank especially for her help in the lab during my first few weeks.

I would also like to thank my other lab mates Rob, Paul, Fred, Nico, Mathieu, Jackie, Janet, Louise for all their help in the lab but also for sharing a fun time outside the lab.

I also want to thank Franca Fraternali who provided interesting ideas for the bioinformatics analysis and taught me how to use PyMol to manipulate and visualise different 3D structures of proteins.

Eric Schirmer provided interesting comments on the exon skipping constructs and offered his help to develop the project further.

Finally, I would like to thank those closest to me; my girl friend En-Min for all her support and encouragement during the past four years and most of all my family for their confidence in me. My parents, Karl and Isolde Scharner, have always been supportive both emotionally and financially and without their help this thesis would not exist.

Table of Contents

List of figures

List of Tables

Appendices

Abbreviations

AON	Antisenseoligonucleotide
AR-CMT	Autosomal dominant Charcot-Marie Tooth disease
ATP	Adenosine triphosphate
AV	Atrio-ventricuar
BAF	Barrier-to autointegration factor
BMD	Becker muscular dystrophy
BrdU	5-bromo-2'-deoxyuridine
Cdk	cyclin dependent kinase
CMD	Congenital muscular dystrophy
CPP	Cell-penetrating peptide
CR	Contour ratio
DAPC	Dystrophin-associated protein complex
DCM-CD	Dilated cardiomyopathy with conduction system disorder
DGC	Dystrophin-glycoprotein complex
DMD	Duchene muscular dystrophy
ECM	Extracellular matrix
EDL	Extensor digitorum longus
EDMD	Emery-Dreifuss muscular dystrophy
Erk	Extracellular signal-regulated protein kinase
FPLD	Familial partial lipodystrophy
FRAP	Fluorescence recovery after photobleaching
FTI	Farnesyltransferase inhibitor
HGPS	Hutchinson-Gilford progeria syndrome
ICD	Implantable cardioverter-defibrillator
Ig	Immunoglobulin
LAD	Lamin associated domain
LAP	Lamin associated protein
LEM	LAP2-emerin-MAN1
LGMD	Limb-girdle muscular dystrophy
LNA	Locked nucleic acid
MADA	Mandibuacral dyspasia with type A lipodystrophy
MAPK	Mitogen-activated protein kinase
MIG	*pMSCV-IRES-eGFP* retroviral vector
MRF	Myogenic regulatory factor
MyHC	Myosin heavy chain
NET	Nuclear envelope transmembrane protein
NMD	Nonsense mediated decay
NMR	Nuclear magnetic resonance
NPC	Nuclear pore complex

PCNA	Proliferating cell nuclear antigen
PKC	Protein kinase C
PNA	Peptide nucleic acid
pMEFs	primary mouse embryonic fibroblasts
POI	Phenotype outcome index
POPS	Parameter optimised surfaces
PP1	Protein phosphatase 1
PTC	Premature translation termination codon
RD	Restrictive dermopathy
SASA	Solvent accessible surface area
SNP	Single nucleotide polymorphism
SREBP1	Sterol regulatory element binding protein 1
UMD	Universal mutation database
ZMPSTE24	Zink-metalloproteinase STE24

Standard abbreviations and abbreviations for common chemicals are not listed

Chapter 1

Introduction

Mutations in the nuclear lamina protein *LMNA* cause a series of diseases, collectively called laminopathies, affecting various tissues. In particular, EDMD affects skeletal muscle. This thesis explores lamin mutations that underlie laminopathies and examines mutation location in chapter 3 and attempts to make genotype-phenotype correlations. Chapters 4 and 5 investigate the effects of four pathogenic EDMD mutations on myogenic cell nuclear structure and function. Finally chapter 6 describes a series of proof-of-principle experiments investigating potential therapeutic interventions for certain laminopathies. As such I will begin with introducing skeletal muscle, then describe nuclear structure and the role of the nuclear envelope as well as lamins and their binding partners, before covering disease phenotypes of laminpathies and the current understanding of the pathogenic mechanism of mutant lamin A.

1.1 Skeletal muscle in health and disease

1.1.1 Muscle structure and function

Skeletal muscle represents just over 30% of body weight for women and around 38% for men making it the most abundant tissue of the body (Janssen et al., 2000). The function of skeletal muscle is to provide coordinated body movements through attachment to the skeleton via tendons. To ensure proper function it is heavily vascularised and intensively innervated. Skeletal muscle is organised in a hierarchical structure, depicted in figure 1.1. Each muscle is formed by thousands of myofibres, the functional units, organised in fibre bundles called fascicles. Myofibres themselves are packed with myofibrils, which contain bundles of actin and myosin, forming the contractile apparatus of skeletal muscle (reviewed in (Grefte et al., 2007)).

Myofibrils contain actin and myosin filaments organised into sarcomeres, the contractile units of skeletal muscle. The sarcomere arrangement also gives myofibres a striated appearance under the microscope. Neighbouring sarcomeres share a Z-disc which provides a scaffold for the attachment of thin filaments formed by filamentous actin and the tropomyosin-troponin complex. Thick filaments which are formed by myosin subunits are anchored at the M-band. The area spanned by the thick filament is known as the A-band. The area on both sides to the Z-disc which is not occupied by thick filaments is knows as the I-band. Myosin heads attach to the thin filaments and provide contraction driven by ATP, the sliding filament theory (Huxley and Niedergerke, 1954; Huxley and Hanson, 1954). For a muscle to contract, fibres depolarise as a consequence of nerve

activation and release Ca^{2+} ions into the cytoplasm. Relaxation of muscle is passive and requires a counteracting muscle to contract (reviewed in (Sparrow and Schock, 2009)).

The myosin heavy chain (MyHC) subtype present in the myofibrils of a myofibre determine its fibre type. In man, three fibre types are present: slow twitch type I and fast twitch type IIa and type IIx fibres. Fibres of different types differ from each other in terms of their resistance to fatigue and the power produced. Type I fibres are fatigue resistant and provide little force. Type IIa and IIx provide higher force but are less resistant to fatigue. The fibre type composition and distribution varies between muscles depending on their use in the organism, for example postural support versus lifting (reviewed in Schiaffino and Reggiani (2011)). Other mammals (apart from man) also have fast type IIb fibres in addition to the fibre types listed above (Gorza, 1990).

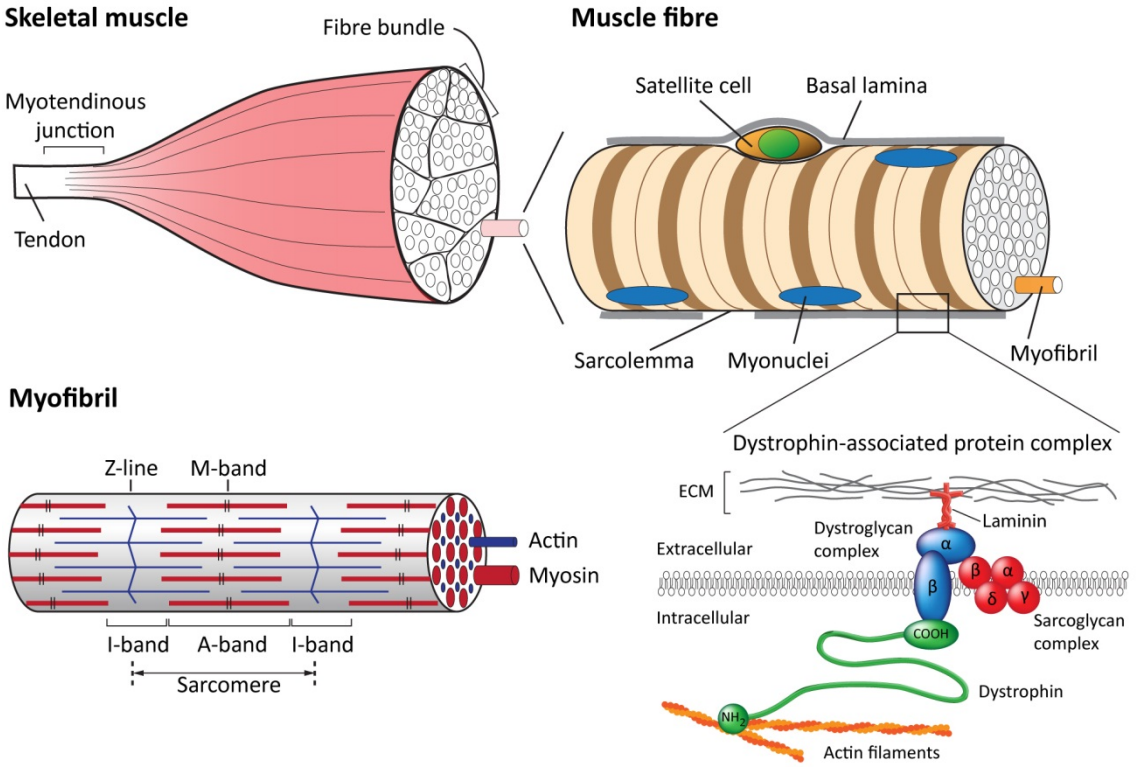

Figure 1.1 The structure of skeletal muscle. Skeletal muscle is formed by bundles of myofibres and ends with tendons on either side which are attached to the skeleton. Myofibres are multinucleated cells formed by the fusion of myoblasts. Their cell wall (sarcolemma) is covered by a basal lamina. Located beneath the basal lamina are muscle stem cells (satellite cells) which provide new myoblasts for homeostasis and repair. Muscle fibres are packed with myofibrils which contain sarcomeres. A sarcomere is a contractile unit and consists of thick and thin filaments. The sarcomere arrangement of alternating A and I-bands give skeletal muscle fibres their striated appearance. The dystrophin-associated protein complex (DAPC) (also dystrophin-glycoprotein complex, DGC) directly links the actin cytoskeleton to the extracellular matrix (ECM) and provides structural stability to the contracting myofibre. Its main components are dystrophin (green), the dystroglycan-complex (blue) and the sarcoglycan-complex (red).

Skeletal muscle, which is striated and under voluntary control, represents only one of three types of muscle cells in mammals. The others are involuntary including cardiac muscle and smooth muscle cells.

Cardiac muscle resembles skeletal muscle in that the actin and myosin filaments are also arranged in sarcomeres giving them a striated appearance. In contrast to skeletal muscle fibres however, cardiomyocytes do not form large syncytia and are not innervated individually. Cardiomyocytes are rod shaped and form a branched network of cells which are connected with each other through the intercalated disk providing (1) mechanical attachment through the fascia adherens (anchoring actin filaments to the intercalated disc) and desmosomes as well as (2) electrical coupling through gap junctions allowing the action potential to pass across adjacent cells (Perriard et al., 2003).

Smooth muscle cells are arranged in sheets or layers of cells and found in multiple tissues in the body including blood vessels, stomach, intestines, airways etc. Smooth muscle cells lack the striated pattern and are innervated by the autonomous nervous system. However, contraction can also be indiced by hormones (Webb, 2003).

1.1.2 Muscle development and regeneration

1.1.2.1 Early embryonic development of skeletal muscle

During gastrulation in early embryonic development a mesodermal layer is formed between the endoderm and ectoderm. The mesoderm forms connective tissue, cartilage, bones, blood, blood vessels and muscle. Nearly all skeletal muscles (with the exception of certain head muscles which are of cephalic mesenchymal origin) are derived from the paraxial mesoderm which forms cell clusters (somites) on either side of the neural tube and notochord. Later in development, the dorsal part of the somite forms the dermomyotome which is characterised by the expression of two members of the paired/homeodomain transcription factors, Pax3 and Pax7 (Relaix et al., 2004). Within the dermomyotome two distinct muscle lineages exist, the epaxial lineage forming the deep back muscles and the hypaxial lineage giving rise to intercostal, abdominal and limb muscles. After formation of the dermomyotome, some muscle progenitor cells migrate from the dorsolateral lip into the limb buds while maintaining Pax3 expression, to seed sites including the limbs and diaphragm with muscle progenitors. Other cells delaminate from the dermomyotome and downregulate Pax3 expression, then up-regulate expression of myogenic regulatory factors (MRFs) such as Myf5 and MyoD giving rise to the myotome where they form embryonic fibres (primary myogenesis). Later in embryogenesis, the remaining Pax3/Pax7 positive cells migrate from the dermomyotome into the myotome and contribute to muscle development (secondary myogenesis) where fetal fibres are formed (reviewed in (Bryson-Richardson and Currie, 2008; Grefte et al., 2007; Muntoni et al., 2002)).

1.1.2.2 Muscle satellite cells

The myofibre is a syncytium formed by fusion of mononucleated myoblasts. Importantly, they also giving rise to satellite cells, the muscle resident stem cell, which are responsible for postnatal muscle growth (Moss and Leblond, 1971). In mature muscle they become mitotically quiescent (Schultz et al., 1978) and are located beneath the basal lamina and resting on the plasmalemma of the myofibre. These are the muscle resident stem cells, crucial in muscle homeostasis and repair (reviewed in Zammit (2008)).

The mechanism of muscle regeneration has been of interest to anatomists and physiologists since the mid-19th century (reviewed in Scharner and Zammit (2011)). It was observed that muscle has a remarkable capacity to regenerate which occurs in three phases: inflammation, tissue formation and tissue remodelling. The source of muscle regeneration was long unknown until Mauro and Katz identified cells at the edge of skeletal muscle fibres which they termed satellite cells (Katz, 1961; Mauro, 1961). Satellite cells are by definition quiescent myogenic cells and show the adult stem cell characteristics of proliferation, differentiation and self-renewal. Muscle satellite cells from adult muscle are well characterized with respect to markers and strongly express Pax7 (Seale et al., 2000), M-cadherin (Irintchev et al., 1994), Myf5 and the surface marker CD34 (Beauchamp et al., 2000).

1.1.2.3 Adult muscle regeneration and repair

When muscle is injured by either trauma or disease, myofibres become necrotic and release cytoplasmic proteins such as muscle creatin kinase (MCK) into the blood stream. This is followed by an inflammatory response and the infiltration of muscle tissue with neutrophils and macrophages (Charge and Rudnicki, 2004). Concomitantly, the trauma induces the activation of quiescent satellite cells which migrate underneath the basal lamina to the site of injury or across to neighbouring myofibres if the basal lamina is breached (Collins et al., 2005).

Myogenic progression and differentiation during adult myogenesis closely resembles embryonic development and also involves Pax7 and MRFs (summarised in Fig. 1.2) (Zammit et al., 2006a). What cues trigger satellite cell activation upon injury remain to be fully determined and may vary depending on the type of injury. One pathway implicated in satellite cell activation is through the hepatocyte growth factor (HGF). HGF is present in the basal lamina of muscle fibers and satellite cells express the HGF receptor c-Met (Tatsumi and Allen, 2004). Exogenous HGF has been shown to induce satellite cell activation in vivo while blocking HGF by antibodies prevents satellite cell activation (Tatsumi et al., 1998).

After activation, quiescent satellite cells overcome the G0-G1 block, enter the cell cycle and start to proliferate (at this stage they become myoblasts). Proliferating myoblasts are characterised by the rapid up-regulation of MyoD and Myf5 (Cooper et al., 1999; Cornelison and Wold, 1997). During the proliferative phase some cells down-regulate MyoD, exit the cell cycle and return to quiescence, expressing Pax7. These cells undergo self-renewal and will be available for further regeneration.

The remaining cells commit to the myogenic program by down-regulating Pax7 and inducing the expression of myogenin and MRF4 (Zammit et al., 2004). The terminal differentiation program then continues with the expression of the cell cycle arrest protein p21 and permanent exit from cell cycle at G0 (Guo et al., 1995). Individual myoblasts continue to fuse and form myotubes or nascent myofibers and start to express muscle specific proteins such as MyHC. These myofibres continue to grow by the addition of myoblasts and start to assemble myofibrils and sarcomeres before they get innervated and fully integrated into the regenerated muscle. Early stages of regeneration are histologically characterised by inflammatory infiltration and necrotic fibres containing cellular debris. Later stages are characterised by a large variation in fibre size and the presence of myofibres with centrally located nuclei (Charge and Rudnicki, 2004). Unaffected fibres may show compensatory hypertrophy. In man, the entire regeneration process is completed in approx. three weeks and myonuclei assume their peripheral position within one to three months (McNally and Pytel, 2007).

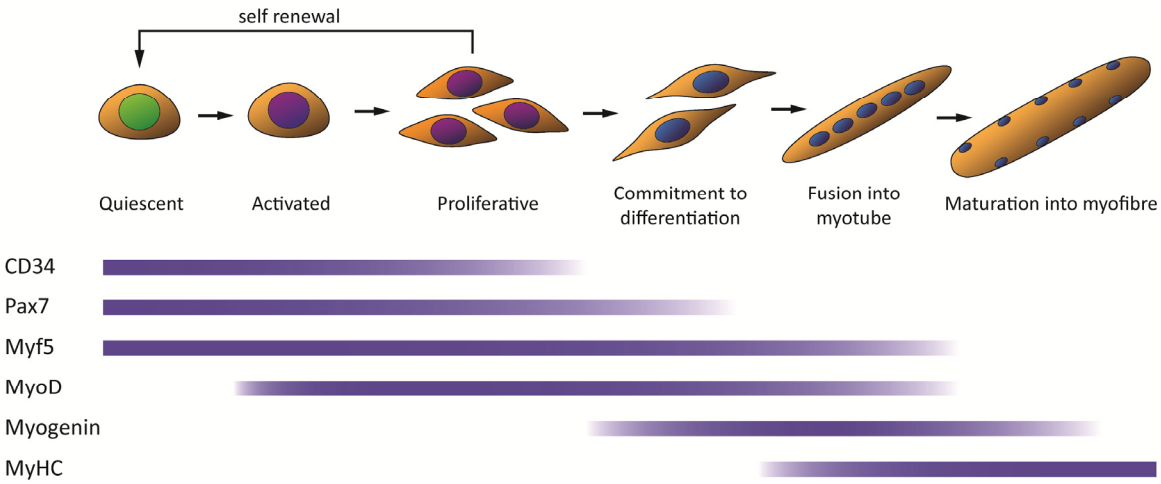

Figure 1.2 The myogenic program of satellite cells. Quiescent satellite cells lie dormant beneath the basal lamina of skeletal muscle fibres and express CD34, Pax7 and Myf5. Activated satellite cells start to proliferate and express MyoD together with Pax7. At this point some cells down-regulate MyoD and exit the cell cycle (self-renewal) while others exit the cell cycle and start to express myogenin (commitment). Cells continue to fuse to form nascent multinucleated myotubes and continue to grow to form mature myofibres (modified from Zammit et al. (2004) and Zammit et al. (2006a)).

Besides satellite cells, cells of non-muscle origin have also been implicated in skeletal muscle regeneration. These include interstitial cells (Tamaki et al., 2002), endothelial-associated cells (De Angelis et al., 1999) side population cells (Asakura et al., 2002) as well as bone marrow derived myogenic progenitors (LaBarge and Blau, 2002). However, genetic ablation of satellite cells in adult mice has been shown to completely block regenerative myogenesis, demonstrating their absolute

requirement to regenerate muscle damaged by injury (Lepper et al., 2011), and so presumably also disease.

1.1.3 Muscular dystrophies

Many diseases affect skeletal muscle. Of particular interest are the muscular dystrophies which include a large range of disorders all characterised by muscle weakness and wasting though they vary in severity, type of muscle groups affected and heart involvement (Emery, 2002). Since muscular dystrophies result in muscle fibre damage and sometimes degeneration, hallmarks of on-going regeneration such as centrally nucleated myofibres, are often seen. Muscular dystrophies can be subdivided in a number of ways, including muscle groups affected, type of gene mutated etc. In general, muscular dystrophies can be classified into two distinct groups: (1) Diseases with pathologies directly caused by proteins predominantly expressed in muscle (2) diseases caused by widely expressed nuclear proteins (Morgan and Zammit, 2010).

1.1.3.1 Muscular dystrophies directly related genes predominantly expressed in muscle

The most common muscular dystrophy is Duchenne muscular dystrophy (DMD), which is caused by mutations in the *DMD* gene encoding dystrophin, located on the X-chromosome (Hoffman et al., 1987). DMD boys suffer from early onset muscle weakness resulting in delayed walking and calf hypertrophy. Patients are usually wheelchair bound by the mid-teens and usually die from cardiac failure or respiratory arrest in their mid- to late twenties (Hoffman et al., 1987; Muntoni et al., 2003). In DMD patients, dystrophin expression is usually lost due to nonsense mutation or large deletions resulting in a frameshift. In frame deletions in *DMD* that result in a shorter but partially functional dystrophin protein are associated with Becker muscular dystrophy (BMD) (Chaturvedi et al., 2001; Muntoni et al., 2003). BMD patients usually have a milder disease, with later onset of symptoms and can remain ambulant for life (McNally and Pytel, 2007). Treatment for DMD is currently not available, however, gene therapy including splice modulation by antisense oligonucleotides to restore dystrophin expression are currently being tested in clinical trials (Cirak et al., 2011; Goemans et al., 2011).

The different phenotype between DMD and BMD shows the importance of dystrophin to the muscle. Dystrophin is a large protein and a main part of the dystrophin-associated glycoprotein complex (DGC) (Fig. 1.1). The cysteine-rich C-terminus of dystrophin directly binds to β-dystroglycan, a transmembrane protein located at the sarcolemma, which is connected to the extracellular matrix via α-dystroglycan (Ibraghimov-Beskrovnaya et al., 1992). The central part of dystrophin contains 24 spectrin repeats interrupted by four hinge points (Koenig and Kunkel, 1990) and at its N-terminus is a calponin-like actin binding domain, which binds to F-actin of the cytoskeleton (Rybakova et al., 2000). Hence, dystrophin forms a strong link between the cytoskeleton and the extracellular matrix. A disruption of this link induces pathological myofibre

damage, which leads to successive rounds of regeneration (Straub et al., 1997). Over time muscle tissue gets replaced by adipose and connective tissue leading to the failure of the muscle.

Other examples of genes primarily expressed in muscle and involved in muscular dystrophy are sarcoglycans and dysferlin, both associated with limb-girdle muscular dystrophy (LGMD), which resembles Duchene-type dystrophy (McNally and Pytel, 2007). Sarcoglycans are transmembrane proteins located at the sarcolemma and form a unit with the DGC (Ozawa et al., 2005) (Fig. 1.1). Mutations in sarcoglycans also disrupt the DGC, leading to myofibre damage and muscular dystrophy.

In contrast, dysferlin, also a membrane bound protein, is not associated with the DGC and plays a different pathogenic role when disrupted. Dysferlin is highly expressed in skeletal and cardiac muscle and has been shown to play a role in vesicle trafficking and membrane repair. Loss of dysferlin results in defective membrane repair and progressive myofibre loss, and leads to a dystrophic phenotype (Bansal et al., 2003).

1.1.3.2 Muscular dystrophies caused by nuclear proteins

In addition to mutations in genes primarily expressed in muscle tissues, muscular dystrophies are also caused by mutations in ubiquitously expressed nuclear proteins. Examples are oculopharyngeal muscular dystrophy (OPMD), associated with nuclear aggregates of poly A binding protein 1 (PABPN1) (Fan et al., 2001) and Emery-Dreifuss muscular dystrophy (EDMD) which is associated with mutations in proteins of the inner and outer nuclear membranes (emerin (Bione et al., 1994) and nesprins (Zhang et al., 2007)) or nuclear lamins (Bonne et al., 1999).

EDMD was first described by Alan Emery and Fritz Dreifuss in 1966 as an "unusual type of benign X-linked muscular dystrophy" that is distinct from DMD and BMD (Emery and Dreifuss, 1966). EDMD is characterized by the clinical triad of (1) early joint contractures of elbows, Achilles tendons and posterior neck, (2) childhood onset of slowly progressive muscle wasting with an early humero-peroneal distribution later affecting the limb-girdle musculature and (3) adult onset cardiac disease, which is characterised by cardiomyopathy, atrio-ventricular conduction defect and arrhythmias (Emery, 2000).

Skeletal muscle biopsies from EDMD patients show mild dystrophic changes including split, necrotic and regenerating fibres with central nuclei. Muscle fibres are variable in size (hypertrophic and atrophic) and an increase in endomysial connective tissue is frequently observed (Mittelbronn et al., 2006; Sewry et al., 2001). Unlike DMD, EDMD is not associated with repeated rounds of muscle degeneration and regeneration. Currently there is no treatment available for EDMD. However, if diagnosed early, patients receive a pacemaker or implantable cardioverter-defibrillator (ICD) to prevent sudden cardiac death, which is the primary cause of death in EDMD patients.

There are three forms of EDMD, the X-linked form (X-EDMD) is caused by mutations in *EMD* (Bione et al., 1994) and *FHL1* (Gueneau et al., 2009), the autosomal dominant (AD) and autosomal

recessive forms are both caused by mutations in *LMNA* (Bonne et al., 1999; Raffaele Di Barletta et al., 2000). The *FHL1* gene encodes a LIM domain protein containing two zinc fingers in tandem which has been implicated in sarcomere assembly (Gueneau et al., 2009; McGrath et al., 2006). EMD encodes emerin, a transmembrane protein located at the inner nuclear membrane and *LMNA* encodes A-type lamins forming the nuclear lamina underlying the inner nuclear membrane. Mutations in *EMD* usually result in a loss of emerin expression while the majority of *LMNA* mutations that cause EDMD are missense mutations. The functions of emerin and lamin, as well their role in disease pathology are reviewed in detail in the sections below.

The overall prevalence for EDMD is approx. 1:50,000 (Juliet Ellis, personal communication) however for X-EDMD it is estimated to be 1:100,000 (Bonne et al., 1993). Also, of all diagnosed EDMD patients, 56%-64% do express emerin and have no mutation identified in *EMD*, *FHL1* or *LMNA* suggesting that yet unidentified genes play a role in EDMD pathology (Gueneau et al., 2009; Meinke et al., 2011).

Mutations in *LMNA* have also been associated with other muscular dystrophies such as lamin-associated congenital muscular dystrophy (L-CMD) (Quijano-Roy et al., 2008), limb-girdle muscular dystrophy (LGMD1B) (Muchir et al., 2000) and cardiomyopathy with conduction defects (DCM-CD) (Fatkin et al., 1999) as well as other disorders. The diseases caused by mutations in lamins (collectively called laminopathies) are reviewed in section 1.4.

1.1.3.3 Potential contribution of a dysfunctional satellite cell pool to muscular dystrophy

Satellite cells have been suggested to contribute to both muscle protein specific muscular dystrophies as well as muscular dystrophies associated with ubiquitously expressed genes (Gnocchi et al., 2008; Morgan and Zammit, 2010). Satellite cells can either contribute indirectly to the pathology by exhaustion of satellite cells or directly by a defective pool which is unable to progress through one or more steps in the myogenic pathway.

The former has been shown to be the case in the pathology of DMD. Excessive myofibre damage caused by the lack of dystrophin protein induces myofibre degeneration and satellite cell mediated repair (Straub et al., 1997). Since satellite cell derived myofibres also lack dystrophin, the muscle will continue to accumulate myofibre damage and be replaced in subsequent rounds of regeneration. These chronic rounds of degeneration and repair lead to a decline in the replicative capacity of myoblasts (Webster and Blau, 1990). This constant demand for a large number of satellite cells may ultimately lead to their exhaustion, resulting in a progression of the dystrophic phenotype. Indeed the dystrophic phenotype is worse in mice where telomerase is inactivated, presumably due to limited satellite cell proliferation (Sacco et al., 2010).

In contrast, pathogenic mutations in nuclear proteins might affects satellite cells directly. Mutations may delay satellite cell activation from quiescence; they may affect myoblast proliferation and expansion; block their ability to differentiate and form new myofibres; or hinder their fusion to

existing fibres (Morgan and Zammit, 2010). On one hand, defective satellite cells may affect muscle in pre- or postnatal development, where satellite cells continue to supply myoblasts, which could explain congenital muscular dystrophy. On the other hand, defective satellite cells could also affect muscle homeostasis and repair in adult muscle which could explain the pathology of late onset muscular dystrophies (Morgan and Zammit, 2010). One example where defective satellite cells may play a role is in the pathology of EDMD, by targeting cell cycle dependent events since EDMD proteins are known to have an indirect role in these (Gnocchi et al., 2008; Morgan and Zammit, 2010). Lamins and emerin as well as their interacting proteins demonstrate a large array of functions in the nucleus including chromatin organisation, cell cycle regulation and gene transcription. The role of emerin and lamin in myoblast function will be reviewed in the sections below.

1.2 The nuclear envelope

1.2.1 Structure and function of the nuclear envelope

In eukaryotes, the genetic material is confined in the largest organelle of the cell, the nucleus. Each nucleus is delimited by a structure called nuclear envelope consisting of two phospholipid bilayers (the inner and outer nuclear membrane) as well as the nuclear lamina, a proteinaceous meshwork underlying the inner nuclear membrane (Hetzer, 2010; Pederson, 2011). The outer nuclear membrane is continuous with membranes forming the endoplasmic reticulum. Although the inner and outer nuclear membranes are continuous, they maintain a specific protein composition (see below). The inner nuclear membrane is closely associated and structurally supported by the underlying nuclear lamina which is formed by a sheet of intermediate filament proteins (Dechat et al., 2010). Spotted throughout the nuclear envelope are nuclear pore complexes (NPCs) penetrating the nuclear membranes and the nuclear lamina. NPCs allow bidirectional trafficking of high molecular weight molecules such as nucleic acids and proteins between the nucleus and the cytoplasm (Wente and Rout, 2010). The main function of the nuclear envelope is to protect the genetic information and to provide a compartment to concentrate enzymes and substrates for biochemical processes at work in the nucleus such as DNA replication, transcription, RNA processing and ribosome synthesis.

1.2.2 Nuclear envelope proteins

To date, a large number of proteins have been described to be associated with the nuclear envelope. These include transmembrane proteins located at the inner or outer nuclear membrane as well as nuclear lamins and lamin associated proteins (Wilson and Foisner, 2010). Figure 1.3 gives an overview of the nuclear envelope and its components and their interaction with regulatory proteins and signalling cascades. A short description of the major nuclear envelope proteins is given below.

1.2.2.1 Emerin

Emerin is a serine-rich transmembrane protein located at the inner nuclear membrane and is widely expressed in humans as shown by mRNA and protein studies (Bione et al., 1994; Nagano et al., 1996). The N-terminus of emerin contains a LEM domain (common to LAP2, emerin and MAN1) which binds barrier-to-autointegration factor (BAF), a small DNA crosslinking molecule (Lee et al., 2001). Emerin has been shown to interact with a multitude of binding partners including structural proteins such as lamins (Clements et al., 2000), actin (Fairley et al., 1999) and nesprins (Zhang et al., 2005) as well as transcriptional repressors such as germ-cell-less (GCL) (Holaska et al., 2003) and BCL2-associated transcription factor (Btf) (Haraguchi et al., 2004). The localisation of emerin to the nuclear envelope has been shown to be lamin A dependent (Sullivan et al., 1999; Vaughan et al., 2001).

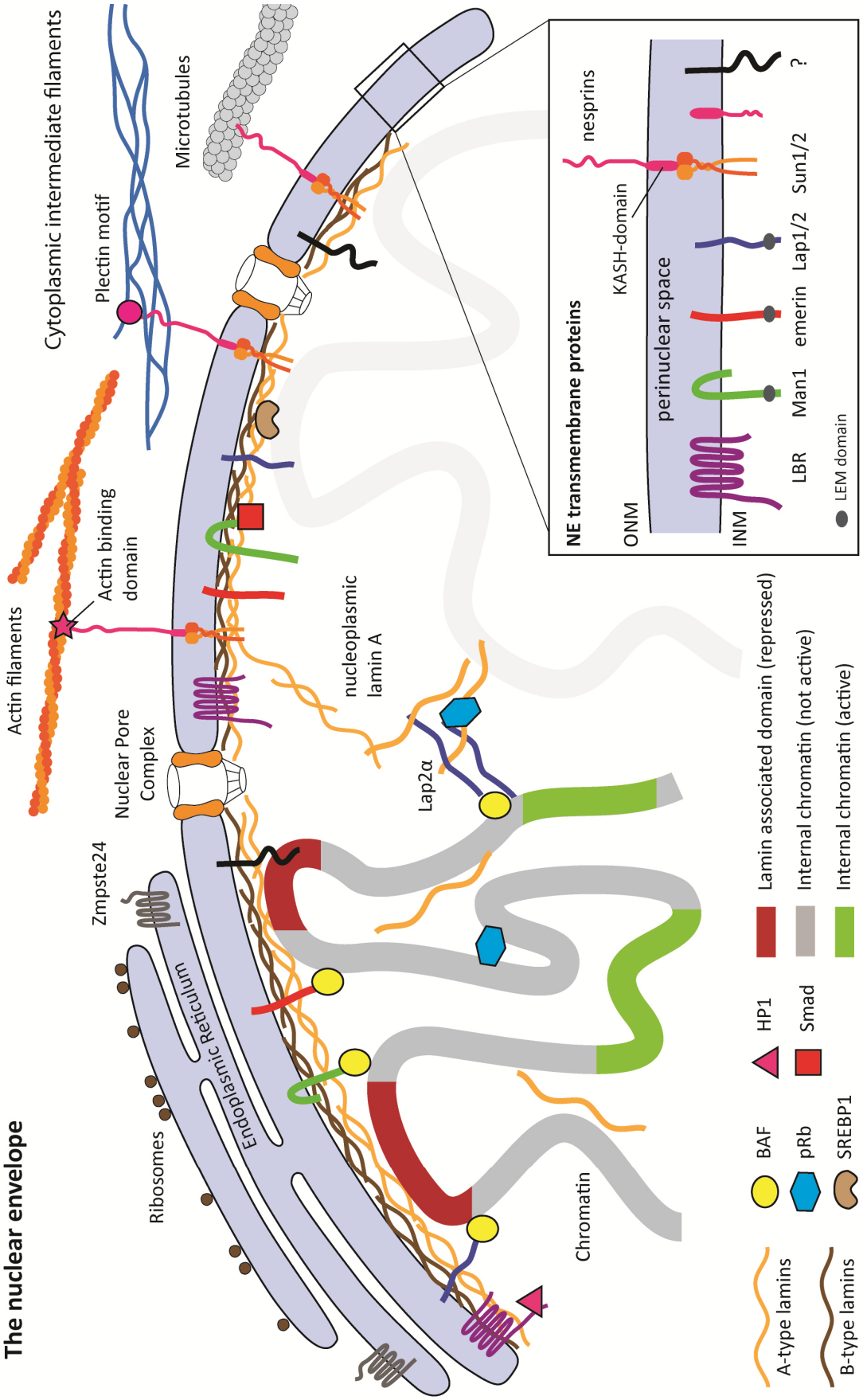

Figure 1.3 Structure and function of the nuclear envelope. Schematic representation of the nuclear envelope, and the interaction of nuclear envelope transmembrane proteins with the nuclear lamina and chromatin. See main text for a detailed explanation. ? represents unknown/undescribed nuclear envelope transmembrane proteins.

Mutations in *EMD* are associated with X-linked Emery-Dreifuss muscular dystrophy mainly due to nonsense mutations resulting in a loss of emerin expression (Bione et al., 1994; Nagano et al., 1996; Yates and Wehnert, 1999). However, missense mutations and in-frame deletions in *EMD* have also been associated with X-EDMD (Brown et al., 2011). Emerin null mice do not display an obvious skeletal muscle phenotype or joint abnormalities (Melcon et al., 2006; Ozawa et al., 2006). However, mice greater 40 weeks of age demonstrate a prolongation of atrioventricular conduction time (Ozawa et al., 2006). In a genome wide expression analysis hearts from emerin null mice showed increased Erk1/2 mitogen-activated protein kinase (MAPK) signalling and activation of downstram targets (Muchir et al., 2007a).

1.2.2.2 Lamin B receptor

The lamin B receptor (LBR) is targeted to the inner nuclear membrane via 8 transmembrane domains (Worman et al., 1990). The LBR directly binds lamin B and has been shown to interact with double stranded DNA (Ye and Worman, 1994), the heterochromatin-associated protein-1 (HP1) (Ye and Worman, 1996), chromatin associated protein HA95, lamin associated protein-2β (LAP2β) and emerin (Martins et al., 2000). HP1 directly interacts with methylated H3K9 via its chromo domain bridging the nuclear lamina with heterochromatin (Ye et al., 1997). LBR also has a conserved Tudor domain which binds H4K20me2 and a sterol reductase domain, the function of which is unclear. Taken together, LBR might play a role in post-mitotic nuclear reformation as well as compartmentalisation of heterochromatin in the interphase nucleus (reviewed in Olins et al. (2010)).

1.2.2.3 Lamin associated proteins

The lamin associated polypeptide (LAP) family is encoded by two genes. LAP1 proteins (LAP1A, LAP1B and LAP1C) as well as two out of six LAP2 proteins (LAP2β-ε) contain a C-terminal transmembrane domain and are localised to the inner nuclear membrane. LAP2α and LAP2ζ lack the transmembrane domain and are found in the nucleoplasm (Berger et al., 1996; Foisner and Gerace, 1993). All LAP isoforms share an N-terminal LEM-domain which binds BAF (Furukawa, 1999; Shumaker et al., 2001) (see section 1.2.2.1). LAP1A and LAP1B have been shown to bind to A and B-type lamins, whereas LAP2C only binds lamin B (Foisner and Gerace, 1993).

Lap2α directly interacts with nucleoplasmic lamin A (Dechat et al., 2000) and together, they have been shown to form a complex with the retinoblastoma protein (pRb) (Markiewicz et al., 2002). Overexpression of Lap2α in vitro results in cell cycle repression of E2F-dependent transcription in an pRb dependent manner (Dorner et al., 2006) while loss of Lap2α has different effects on the cell cycle depending on the organism for yet unknown reasons. In human fibroblasts, loss of Lap2a induces cell cyle arrest (Pekovic et al., 2007) while in mice, loss of Lap2α (Naetar et al., 2008) or lamin A/C (Nitta et al., 2006; Van Berlo et al., 2005) is associated with cell cycle progression. Interestingly, knocking out Lap2α in mice has been shown to induce a cardiac phenotype and result

in delayed satellite differentiation, although delayed muscle regeneration was not observed (Gotic et al., 2010a; Gotic et al., 2010b).

1.2.2.4 SUN-domain proteins

SUN (Sad1, UNC-84 homology) domain proteins SUN1 and SUN2 are located to the INM and have a central helical coil domain that mediates dimerization (Tzur et al., 2006). The N-terminal domain is exposed to the nucleoplasm and has been shown to interact directly with A-type lamins (Haque et al., 2006) as well as emerin and short nesprin-2 isoforms (Haque et al., 2010). The C-terminal SUN-domain protrudes into the perinuclear space and interacts with the KASH (Klarsicht, ANC1, Syne homology) domain found in nesprins, forming the LINC complex (linker of nucleoskeleton and cytoskeleton) (Crisp et al., 2006; Padmakumar et al., 2005). Disruption of the LINC complex has been shown to induce defects in nuclear morphology (Khatau et al., 2009) and affect the localisation of skeletal muscle nuclei as well as strain transmission between the cytoplasm and nucleus (Lombardi et al., 2011; Zhang et al., 2010).

1.2.2.5 Nesprins

Nesprins (Nuclear envelope spectrin repeat proteins) comprise of a large protein family of spectrin repeat proteins encoded by four genes (*SYNE1-4*) (Mellad et al., 2011). Nesprins are characterised by a central rod region, variable in length, and a C-terminal KASH transmembrane domain which facilitates nuclear membrane localisation and interacts with the SUN-domain in the perinuclear space forming the LINC complex (Crisp et al., 2006; Padmakumar et al., 2005). Two giant isoforms (nesprin-1 and 2) have N-terminal calponin homology (CH) domains which bind to F-actin. Nesprin 3 has an N-terminal plectin-binding motif which interacts with cytoplasmic intermediate filament proteins and nesprin-4 directly interacts with microtubules (Roux et al., 2009; Wilhelmsen et al., 2005; Zhen et al., 2002). Nesprins are localised both to the ONM and INM depending on their size and interaction partners (Razafsky and Hodzic, 2009). Human patients with missense mutations in nesprin-1 and 2 (Zhang et al., 2007) as well as mice with a deletion of the KASH domain in nesprin-1 (Puckelwartz et al., 2009), show a skeletal muscle phenotype resembling EDMD. However, it has not been excluded that the missense mutations are in fact polymorphisms in these patients and thus not EDMD-causing.

1.2.2.6 MAN1

MAN1 (also known as LEMD3) is an integral protein of the INM. Located at the N-terminus is a LEM domain, located on the C-terminus is a winged helix domain which binds DNA, and an RR-motif which is a binding site for regulatory Smads (R-Smads) (Bengtsson, 2007). MAN1 is anchored to the INM via two transmembrane domains meaning that both the N-and C-terminal end of the protein are inside the nucleoplasm. Being able to bind R-Smads but not inhibitory Smads, MAN1 acts as an inhibitor of BMP and TGF-β signalling. Overexpression of MAN1 has been shown to block transcription of BMP and TGF-β targets upon cytokine stimulation. At the

same time, loss of MAN1 at the INM results in increased TGF-β signalling (Lin et al., 2005). Loss-of-function mutations in MAN1 result in osteopoikilosis, Buschke-Ollendorff syndrome and melorheostosis, phenotypes characterised by increased bone density and associated with increased TGF-β signalling (Hellemans et al., 2004).

1.2.2.7 Other/novel nuclear envelope transmembrane proteins (NETs)

Other nuclear envelope transmembrane proteins include a large number of uncharacterised nuclear envelope transmembrane proteins (NETs). In 2003 Schirmer E.C. and colleagues performed a large scale proteomics analysis on the nuclear envelope which resulted in the identification of 67 novel proteins (Schirmer et al., 2003). Some of the novel NETs are ubiquitously expressed and have been shown to regulate the cell cycle (Korfali et al., 2011) while others have a tissue specific chromatin organisation expression pattern and are involved in the regulation of differentiation (Schirmer EC, personal communication).

1.2.2.8 Nuclear lamins

Nuclear lamins are the major component of the nuclear envelope and form the nuclear lamina, a proteinaceous network underlying the inner nuclear membrane. Lamins are members of the intermediate filament protein family and divided into A-type lamins (lamins A and C) and B-type lamins (lamin B1 and lamin B2). Mutations in lamins have been shown to cause a variety of diseases with a large range of phenotypes collectively called laminopathies (reviewed in the following sections).

1.3 Type V intermediate filaments: nuclear lamins

1.3.1 The intermediate filament protein family

Intermediate filament (IF) proteins by definition assemble into filaments 9-10nm in diameter and are a major component of the cytoskeleton and nucleoskeleton (Herrmann and Aebi, 2004). Intermediate filaments were named because of their intermediate size forming a cytoarchitectural bridge between microfilaments (MFs, 7nm in diameter) and microtubules (MTs, 20-25nm in diameter) (Ishikawa et al., 1968). MFs and MTs are rather sensitive to shear stress compared to IFs which show more viscoelastic properties under the same conditions (Janmey et al., 1998).

IF proteins are grouped into five sequence homology classes (SHCs). These are acidic keratins (SHC I), basic keratins (SHC II), desmin-/vimentin type proteins (SHC III), neurofilament proteins (SHC IV) and later discovered insoluble members of the nuclear lamina, the lamins (SHC V) (Herrmann and Aebi, 2004). To date, 73 intermediate filament proteins have been described in human where keratins (54/73 form the largest group) (Szeverenyi et al., 2008).

All IF proteins share a common tripartite domain organisation formed by the central rod domain flanked by a short N-terminal head domain and a larger C-terminal tail domain (Fuchs and Weber, 1994). The central rod domain is highly conserved between intermediate filaments and is characterised by a heptad substructure which allows the formation α-helical coiled-coils leading to dimerisation of two IF proteins ((Herrmann and Aebi, 2004), Appendix 1).

1.3.2 Discovery and evolutional origin of lamins

The nuclear lamina (then known as 'fibrous lamina' from studies in the *Amoeba* (Pappas, 1956)) was first described in vertebrate cells in an ultrastructural analysis of nuclei from various animals including leech, cat and guinea pig (Fawcett, 1966). Later, Larry Gerace and colleagues raised antibodies against 3 polypeptide chains (P70, P67 and P60, later termed lamins A, B and C) present in the nuclear lamina, which they isolated together with nuclear pore complexes from rat liver nuclei (Gerace et al., 1978). The antibodies were used in immunofluorescence staining and marked the nuclear lamina in K22 rat liver cells. Importantly, Gerace et al. also noted a disintegration of the lamina in mitotic cells stained with antibodies raised against P70 (lamin A) and concluded correctly that a major portion of the lamina is in fact a polymer which undergoes reversible disassembly during mitosis (Gerace et al., 1978). In a follow up paper they analysed lamin A, C and B individually and found that mitotic lamins A and C occur in a soluble state, while mitotic lamin B is membrane associated. Further, the analysis of the isoelectric point of mitotic lamins led them to the conclusion that reversible enzymatic phosphorylation of lamins may be involved in modulating the polymerisation state of the lamina during mitosis (Gerace and Blobel, 1980). This landmark paper sparked the field of lamin research which is growing larger ever since.

The main difference between cytoplasmic IFs and nuclear lamins in vertebrates is that the central rod domain of lamins is 42 amino acids (six heptads) longer. Lamins also have a nuclear localisation signal (NLS) and a C-terminal CaaX cassette which serves as a target for a series of posttranslational modifications both lacking in cytoplasmic IFs. Lamins are found in all metazoans however simple metazoans only express nuclear IFs suggesting that cytoplasmic IFs originated from an *ur*-lamin (Erber et al., 1999). Further, the rod domains of invertebrate IFs is the 42 amino acids longer than that if vertebrate IFs and therefore closer to nuclear lamins supporting this theory (Weber et al., 1988; Weber et al., 1989).

Invertebrates have only one lamin gene with exceptions such as *D. melanogaster* which expresses two nuclear lamins, lamin A and B. Vertebrates have four lamin genes (encoding lamin B1, B2, LIII and lamin A), acquired after two rounds of genome duplications that possibly occurred in the ancestral vertebrates. Amphibians, fish and birds still possess all four lamin genes; mammals however have lost the LIII gene (reviewed in (Peter and Stick, 2012)).

1.3.3 Lamin genes and proteins

Lamins are divided into two groups based on their sequence homology, structural features and dynamic properties: (**1**) A-type lamins (Lamin A, A-Δ10 and C) expressed by the *LMNA* gene through alternative splicing (Fig. 1.2) and (**2**) B-type lamins (lamin B1 and B2) expressed by *LMNB1* and *LMNB2* respectively. Both lamin types are described in detail below.

1.3.3.1 A-type lamins

A-type lamins are expressed in all vertebrates by the *LMNA* gene located on human chromosome 1q (Lin and Worman, 1993; Wydner et al., 1996). The *LMNA* gene contains 12 exons and is alternatively spliced to give rise to 3 proteins: lamin A, lamin A-Δ10 and lamin C (Fig. 1.4). Lamin A is produced by alternative splicing of exon 10. It is 664 amino acids in length and the longest isoform of A-type lamins. The lamin C protein ends at exon 10 which makes it identical to lamin A up to codon 566. The last six amino acids (567-572) are unique to lamin C (Lin and Worman, 1993). Lamin A-Δ10 lacks exon 10, shortening the tail domain by 30 amino acids (Fig. 1.4) (Machiels et al., 1996).

The major isoforms, lamin A and C, are expressed in the majority of differentiated cells but are lacking in embryonic stem cells (ESCs) (Constantinescu et al., 2006). In most tissues, lamin A and C are expressed at equal levels. In the brain however, lamin C is the predominant form of A-type lamin, likely due to the expression of miR-9, a brain-specific microRNA which has been shown to specifically down-regulate lamin A (Jung et al., 2011). The minor isoform lamin A-Δ10 has been detected in tumour cell lines as well as several normal cell types but is not well characterised (Machiels et al., 1996). In mouse, the *LMNA* gene has been shown to give rise to a fourth splice

variant termed lamin C2. Lamin C2 has an alternative start site in *LMNA* intron 1 and its expression is restricted to the germline (Furukawa et al., 1994).

In man, loss of A-type lamins is postnatally lethal (van Engelen et al., 2005). In mice however, absence of lamin A and C does not produce an embryonic phenotype but the mice suffer growth retardation, muscle dystrophy and die prematurely (Sullivan et al., 1999).

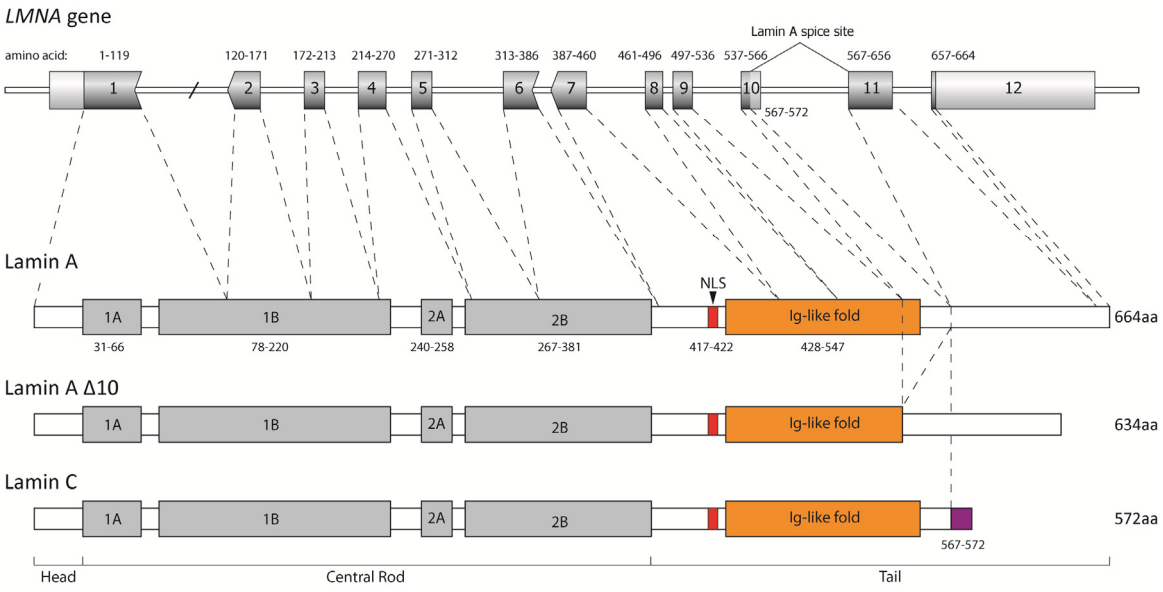

Figure 1.4 The *LMNA* gene and lamin proteins. The *LMNA* gene is alternatively spliced and gives rise to lamin A, lamin AΔ10 and lamin C. The C-terminal end of lamin C (residues 567-572, highlighted in purple) is specific to lamin C.

1.3.3.2 B-type lamins

B-type lamins (lamin B1 or lamin B2) are encoded by *LMNB1* and *LMNB2* respectively and all metazoans express at least one B-type lamin (Hoger et al., 1990; Vorburger et al., 1989). In mice, *LMNB2* has been shown to give rise to an alternative splice product, lamin B3, which is restricted to the germline (Furukawa and Hotta, 1993). In mammals, at least one B-type lamin is expressed in all somatic cell types including undifferentiated cells in early stages of embryonic development (Liu et al., 2011; Stewart and Burke, 1987).

B-type lamins have been associated with the assembly of the mitotic spindle matrix as well as DNA replication, genome organisation and apoptosis and are therefore thought to be essential for proliferation and cell survival (Guelen et al., 2008; Harborth et al., 2001; Liu et al., 2000; Tsai et al., 2006). Mice with homozygous mutations disrupting the lamin B1 protein develop lung and bone defects during embryogenesis and die at birth, even though lamin B2 is expressed normally (Vergnes et al., 2004). Fibroblasts from lamin B1 mutant mice display severely dysmorphic nuclei, impaired differentiation and premature senescence (Vergnes et al., 2004).

Recently, several groups have challenged the essential role of B-type lamins in basic cell function and produced a series of publications which reshaped the current view. Using a conditional knockout system, Yang et al. showed that keratinocytes which lack both lamin B1 and lamin B2 have no defects in cell proliferation and have normal skin or hair development (Yang et al., 2011). The same group showed that forebrain-specific removal of lamin B1 and B2 results in severe atrophy of the cortex, demonstrating an essential role in brain development (Coffinier et al., 2011). Using a total lamin B knockout mouse, Kim et al. found that B-type lamins are essential for organogenesis and brain development confirming results obtained in the conditional knockout. Interestingly, ES cells from the total knockout which lack all A and B-type lamins showed no abnormalities in emerin localisation or nuclear shape (Kim et al., 2011).

In man, loss-of-function mutations in lamin B are not described. However, a gene duplication of *LMNB1* is associated with autosomal dominant leukodystrophy, a neurological disorder characterised by myelin loss in the central nervous system (Padiath et al., 2006).

1.3.3.3 Posttranslational processing of prelamin A

All lamins (except lamin C) are expressed as a pre-form and end in a C-terminal CAAX cassette which undergoes a highly structured sequence of posttranslational modifications before mature lamins are incorporated into the nuclear lamina (Fig. 1.5). The CAAX cassette consists of a cysteine, two aliphatic amino acids and any COOH-terminal amino acid (Davies et al., 2009).

The first step in this maturation process is a posttranslational prenylation step, where a 15-carbon farnesyl or a 20-carbon geranylgeranyl lipid is added to the thiol group of the cysteine, depending on the last (X) residue. When the last residue is a leucine or phenylalanine, the cysteine is geranylgeranylated by geranylgeranyltransferase type I (GGTase-I), otherwise (as it is the case for lamins) it is farnesylated by farnesyltransferase (FTase) (Zhang and Casey, 1996).

Next, the last three amino acids (AAX) are cleaved off by either RCE1 (Ras converting enzyme-1) or ZMPSTE2424 (Zink-metalloproteinase STE24), both metalloproteinases located on the membrane of the endoplasmic reticulum (Schmidt et al., 1998). The farnesylated cysteine residue is then carboxymethylated by ICMT (isoprenyl-cysteine-carboxyl-methyl-transferase), another ER bound enzyme (Dai et al., 1998). Lamins A and B share these first three modifications steps.

Mature B-type lamins remain permanently farnesylated and are believed to be membrane associated through their hydrophobic farnesyl group (Farnsworth et al., 1989). Prelamin A undergoes a second endoproteolytic cleavage step carried out by Zmpste24, the only enzyme known so far to perform this cleavage (Bergo et al., 2002; Pendas et al., 2002). This final cut removes the last 15 amino acids including the farnesyl-cysteine and solubilizes the mature form of lamin A before it gets targeted to the nuclear lamina.

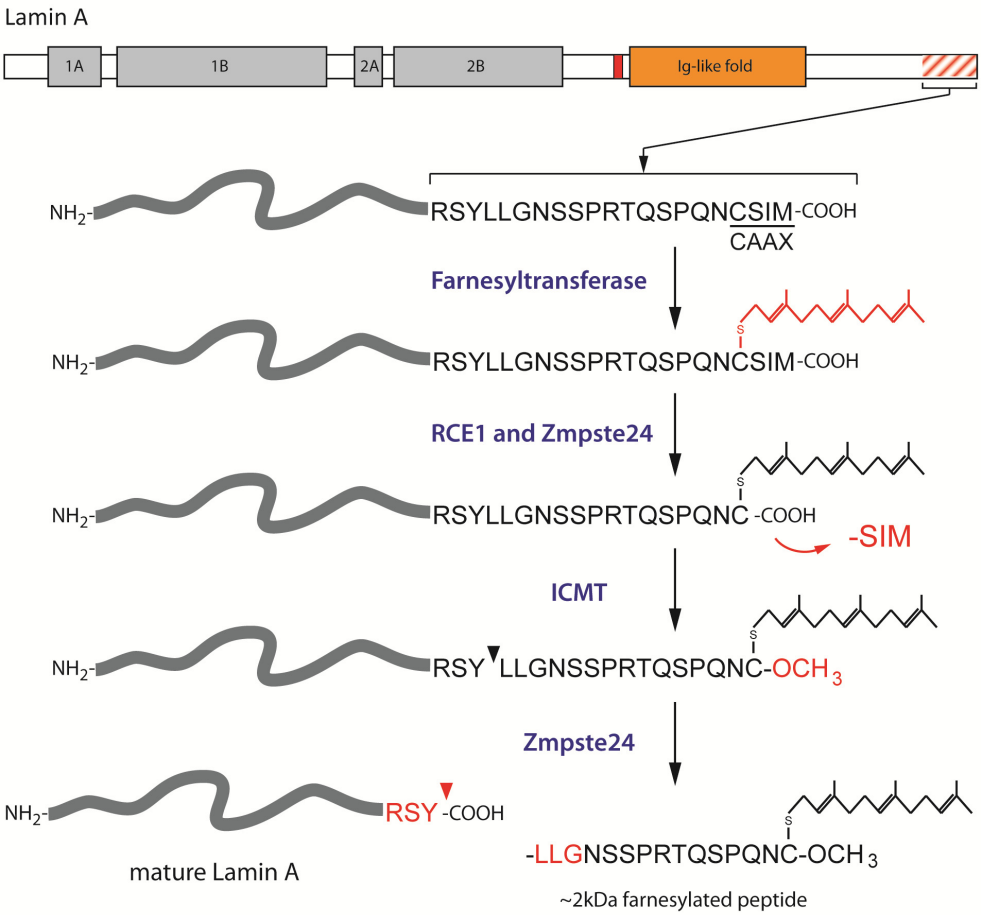

Figure 1.5 Posttranslational processing of prelamin A. In a sequence of prelamin A prenylation, the first endoproteolytic cleavage, methylation and the second endoproteolytic cleavage, the last 18 amino acids of the C-terminal tail of prelamin A are removed which forms mature lamin A. Lamin B lacks the second proteolytic cleavage site and stays permanently farnesylated.

Faulty posttranslational processing of prelamin A is associated with a number of pathologies. A 50 amino acid deletion in the tail domain of lamin A, caused by a point mutation (c.1824C>T; p.G608G) which activates a cryptic splice site in exon 11, has been shown to cause Hutchinson-Gilford progeria syndrome (HGPS), a premature ageing syndrome (De Sandre-Giovannoli et al., 2003; Eriksson et al., 2003). The protein product with the deletion (termed progerin) lacks the second endoproteolytic cleavage site and remains permanently farnesylated. Similarly, mutations in ZMPSTE24 also lead to permanently farnesylated prelamin A, resulting in restrictive dermopathy (RD) and other progeroid phenotypes (Agarwal et al., 2003; Navarro et al., 2004; Shackleton et al., 2005). Further, missense mutations of residues in the Zmpste24 recognition site (RSYLLG) have been shown to partially inhibit cleavage by ZMPSTE24 (Barrowman et al., 2012) and are associated with a large array of phenotypes including muscular dystrophy and premature ageing (Csoka et al., 2004; Genschel et al., 2001; Rankin et al., 2008). For a detailed description of the pathology and pathogenic mechanism of progerin, see section 1.4.

1.3.4 Structure and assembly of A-type lamins

Lamins, like all intermediate filament proteins, are characterised by a tripartite structural organisation which consists of a short globular head domain, a central rod domain and a long globular tail domain. The basic features of lamin A are schematically represented in figure 1.6.

1.3.4.1 The central rod domain

The central rod domain of lamin A is formed of 2 α-helical coils, coil 1 and coil 2, separated by a flexible hinge region (L12). Coil 1 and coil 2 are subdivided by linkers L1 and L2 respectively which are relatively rigid and seem to adopt an α-helical conformation (North et al., 1994; Smith et al., 2002) (Fig. 1.6A). Coils 1 and 2 are characterised by a heptad repeat pattern typical for α-helices which engage in coiled-coil interaction (Conway and Parry, 1990; Herrmann and Aebi, 2004; Mason and Arndt, 2004).

In a typical α-helical, approximately 70-75% of the a and d positions in the heptad repeat pattern $(a\text{-}b\text{-}c\text{-}d\text{-}e\text{-}f\text{-}g)_n$ are hydrophobic residues (Conway and Parry, 1990). These are on average 3.5 residues apart and will form a stripe of hydrophobic residues on the surface of the α-helix, which facilitates hydrophobic interaction of two or more α-helices (Fig. 1.6B) (Parry et al., 2008). Importantly, helix-stabilising hydrogen bonds in the vicinity of hydrophobic residues are slightly shorter than those further away resulting in the helices coiling around each other in a left-handed manner (Cohen and Parry, 1990). The α-helical coiled-coil formation of part of the lamin A central rod domains was confirmed by crystal structure (Strelkov et al., 2004). A typical example of a heptad repeat sequence (taken from the lamin A central rod domain) is illustrated in figure 1.6C.

Approximately 30 amino acids of the C- and N-terminal ends of coil 1 and coil 2 of lamin A respectively, are highly conserved among IFs. These intermediate filament consensus motifs (IFCMs) are thought to play a crucial role in filament assembly (Kapinos et al., 2010). Structural data show that rod fragments of lamin A containing IFCMs form relatively labile coiled coils which might promote "unzipping" of lamin A dimers and allow α-helices to engage in interaction with a neighbouring dimer (Kapinos et al., 2011). This hypothesis is supported by the observation that vimentin with a mutated IFCM demonstrated an increased thermodynamic stability but fails to form long filaments *in vitro* and *in situ* (Meier et al., 2009).

1.3.4.2 The Ig-like fold domain

The tail region of all lamin proteins contains a conserved Immunoglobulin-like fold (Ig-like fold) domain. In lamin A, it stretches from residue 428-547 and comprises two β-sheets which fold to form a β-sandwich. The 3D structure of the Ig-fold domain has been solved independently by Krimm et al. (2002) and Dhe-Paganon et al. (2002) (Fig. 1.4D).

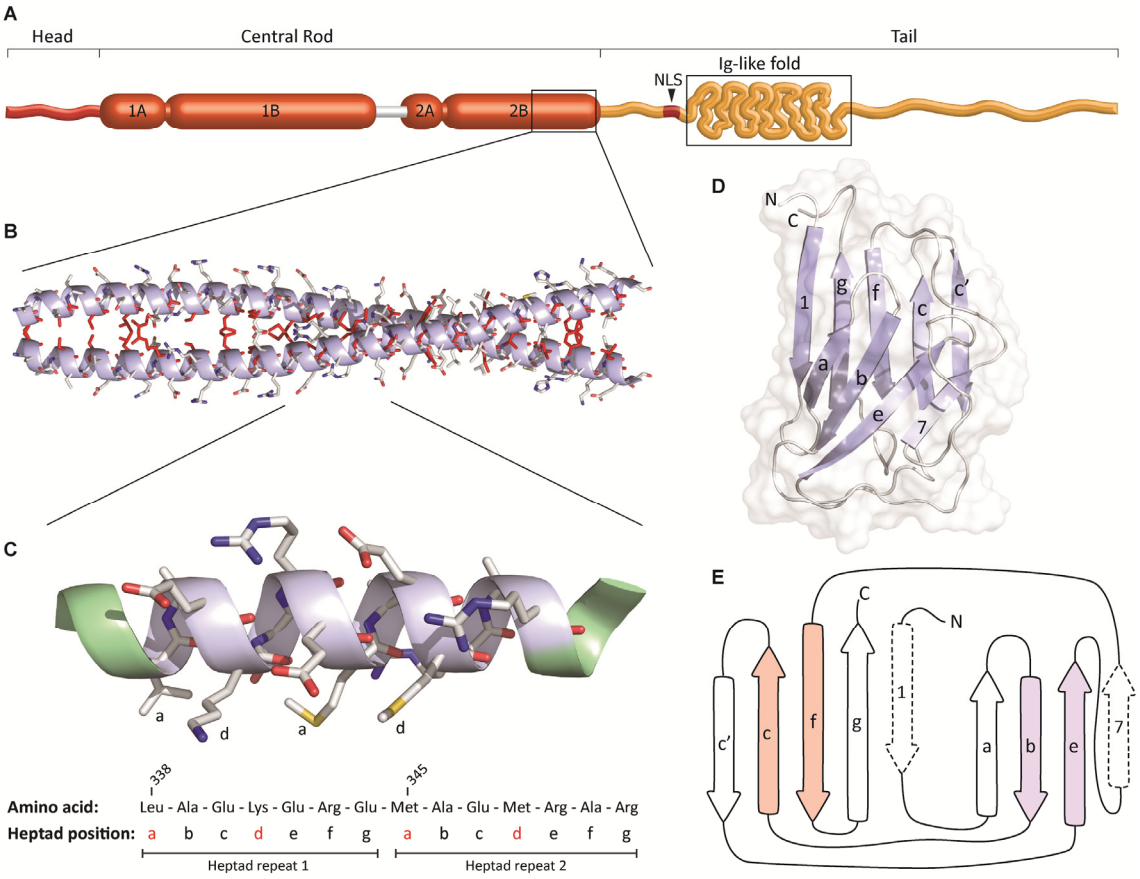

Figure 1.6 Structures of the central rod domain and Ig-fold domain of lamin A. (**A**) Schematic of the lamin A protein. (**B**) Structure of α-helical coiled coil formed by part of central rod domain of lamin A. Residues on heptad repeat positions a and d are highlighted in red and form a seam at the interface of the two α-helices (taken from (Kapinos et al., 2011)). (**C**) Two consecutive heptad repeats (residues 338-351) from the human lamin A central rod domain are shown. Sequences of α-helical coiled-coils display a periodicity of seven amino acids (heptad repeats) with nonpolar amino acids occupying heptad positions a and d. Occasionally charged amino acids are located on position a or d such as lysine 341. In this case, lysine 341 forms a salt bridge with a glutamate residue of the neighbouring α-helix, reinforcing the coiled coil (Kapinos et al., 2011). (**D**) NMR structure of the Ig-like fold domain of lamin A (Krimm et al., 2002). Two β-sheets comprised of nine strands forming a β-sandwich are shown in cartoon representation. The surface of the molecule is indicated in faint grey. (**E**) Two dimensional representation of the lamin A Ig-like fold. Amino acid residues located on strands c and f (orange) as well as b and e (lavender) form a hydrophobic core, stabilising the structure of the Ig-like fold.

Ig-folds (as the name suggests) were first described in immunoglobulins and have seven to nine antiparallel β-strands forming two distinct β-pleated sheets which fold into a β-sandwich (Bork et al., 1994). Ig-folds and Ig-like folds both have the same structural arrangement though the number of strands and their arrangement does vary between different proteins. Common to all Ig-like domains is a 2-plus-2 stranded hydrophobic structural core formed by strands e and b of one β-sheet and strands f and c of the other (Bork et al., 1994). Residues in this common core are aligned against each other which makes it is less flexible as compared to surrounding strands. Disruptions to core residues are thought to disrupt the stability of the domain, interfering with its function (Krimm et al., 2002).

In lamins, the Ig-fold has been shown to bind to a large number of interacting proteins (see section 1.3.5). It has also been shown that the Ig-like fold also plays a role in lamin assembly. Introduction of a lamin B3 Ig-fold motif into *Xenopus* oocytes has been shown to be sufficient to inhibit lamin polymerisation (Shumaker et al., 2005).

1.3.4.3 Lamin filament assembly and disassembly

Intermediate filaments assemble in 3 different assembly groups: 1 2 and 3 (reviewed in Herrmann and Aebi (2004)). The assembly of nuclear lamin (assembly group 3) is illustrated in figure 1.7. Initially, two lamin monomers form a parallel dimer by a coiled-coil α-helix of the central rod domains. These lamin dimers form polar head to tail polymers, which associate with other head-to-tail polymers in an antiparallel fashion to build 10nm IF fibres (Ben-Harush et al., 2009). In contrast, cytoplasmic IF dimers (assembly group 1 and 2) associate laterally to build antiparallel tetramers and unit length filaments (10nm in diameter), which elongate to form IF fibres (Herrmann et al., 2009; Stuurman et al., 1998).

A and B-type lamins form separate filament networks as seen by whole mount electron microscopy in Xenopus oocytes (Goldberg et al., 2008) and high resolution confocal microscopy of human cells (Shimi et al., 2008). However there is strong evidence that these two networks interact with each other such as the mislocalisation of lamin B in cells lacking A-type lamins as well as cell expressing mutant lamin A (Muchir et al., 2004; Ostlund et al., 2001; Sullivan et al., 1999; Taimen et al., 2009).

Lamin A and C have been shown to form heterodimers *in vitro*, however, whether they also heterodimerise *in vivo* and form a filament network is in question (Herrmann H., personal communication). Pull down assays of the soluble A-type lamin fraction has shown that lamin A and C completely segregate, suggesting that, at least in the soluble fraction, lamin A and C do not form heterodimers (Kolb et al., 2011).

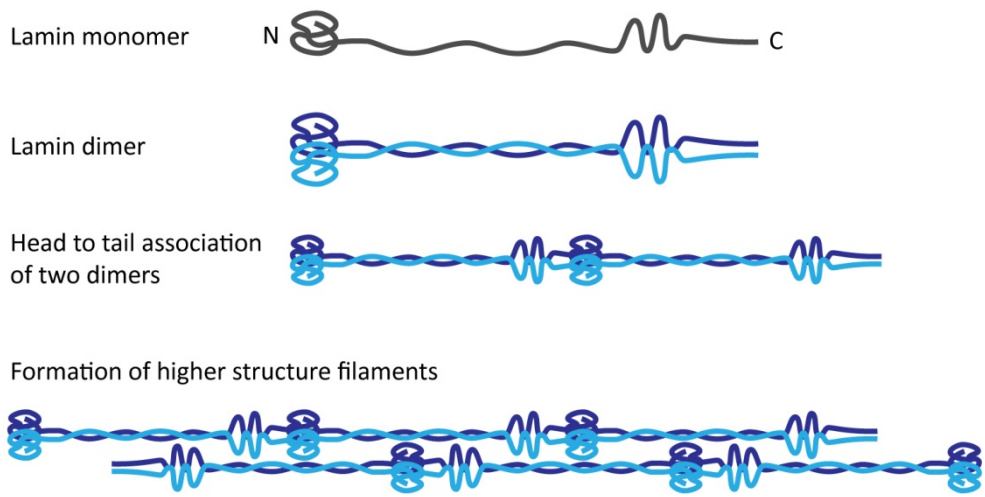

Figure 1.7 Mechanism of lamin filament assembly. Two lamin monomers dimerise and associate into polymers in a head-to-tail arrangement. Multiple of these primary filaments continue to associate laterally with other head-to-tail polymers to form 10nm intermediate filament fibres.

During mitosis the lamin filament network is disassembled in a process called nuclear envelope breakdown (NEBD). In this process cyclin dependent kinase-1 (Cdk1), protein kinase C (PKC) and other mitotic kinases phosphorylate lamins, Nups, LAP2 and LBR, leading to depolymerisation and solubilisation of lamins (Guttinger et al., 2009; Margalit et al., 2005). In late anaphase and telophase, the nuclear envelope attaches to and spreads around the condensed chromatin in the daughter cells, possibly with the help of the DNA-binding activity of some INM proteins (Ulbert et al., 2006). Concomitantly, NPCs get integrated into the newly forming NE. Once the nuclear membrane is formed around the chromosomes, B-type lamins get dephosphorylated by protein phosphatase 1 (PP1) and start to assemble at the nuclear lamina (Steen and Collas, 2001). A-type lamins are imported through the newly formed NPCs and assemble to reform an intact nuclear lamina (Broers et al., 1999).

1.3.5 Lamin binding proteins and their implication in disease

Lamins interact with a large variety of nuclear proteins and are therefore involved in numerous cellular processes and mutations in lamins result in a range of phenotypes termed laminopathies (Wilson and Foisner, 2010; Zastrow et al., 2004). The pathogenic mechanism for the majority of *LMNA* mutations is still unknown. However, proposed disease mechanisms for laminopathies are closely linked to the function of lamins and lamin interacting proteins (Broers et al., 2006; Worman and Bonne, 2007).

The functions of lamins and their interacting proteins can be classified into 3 major groups: (1) maintaining the integrity of nuclear structure and mechanics, (2) regulation of DNA replication and cell cycle and (3) modulation of gene expression and cell signalling pathways. The major lamin

interacting proteins described so far as well as the region in lamin A they bind to are depicted in figure 1.8. For details in their implication in disease refer to section 1.4.2.

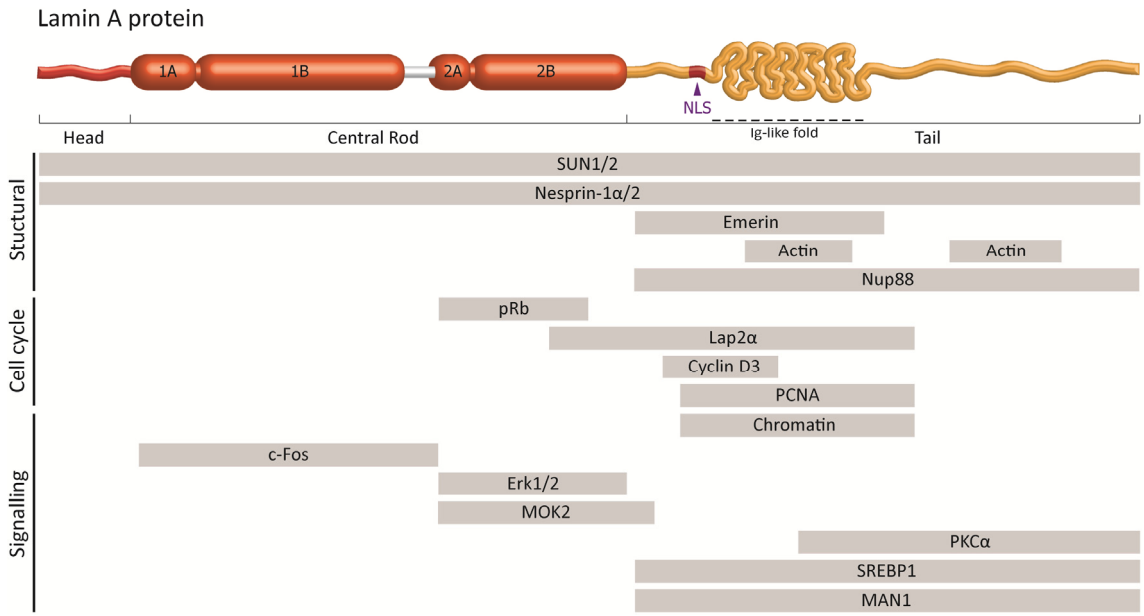

Figure 1.8 Lamin A interacting proteins. The schematic shows the lamin A protein and lamin A interaction partners, modified and updated from Zastrow et al. (2004).

Lamin binding proteins include structural proteins: SUN1/2 (Haque et al., 2006; Haque et al., 2010), nesprin-1α (Mislow et al., 2002), nesprin-2 (Zhang et al., 2005), emerin (Lee et al., 2001; Sakaki et al., 2001), actin (Sasseville and Langelier, 1998; Simon et al., 2010) and Nup88 (Lussi et al., 2011); proteins involved in cell cycle regulation: pRb (Ozaki et al., 1994), Lap2α (Dechat et al., 2000), cyclin D3 (Mariappan et al., 2007) and PCNA (Shumaker et al., 2008); and proteins involved in gene transcription and cell signalling: c-Fos, Erk1/2 (Gonzalez et al., 2008), MOK2 (Dreuillet et al., 2002), PKCα (Martelli et al., 2002), SREBP1 (Lloyd et al., 2002) and MAN1 (Mansharamani and Wilson, 2005). Lamins also bind to chromatin directly (Stierle et al., 2003).

1.4 Laminopathies

1.4.1 Types of laminopathies

Laminopathies are a heterogeneous group of diseases associated with defects in A-type lamins and can be separated into primary and secondary laminopathies.

Primary laminopathies result from mutations in the *LMNA* gene and encompass at least 16 different diseases that can be categorised into 4 major phenotypic groups: (1) diseases affecting striated muscle, either skeletal muscle with/without cardiac involvement or cardiac muscle only, (2) lipodystrophy disorders affecting white adipose tissue and/or the skeleton, (3) peripheral neuropathy associated with demyelination of motor neurons, (4) premature aging syndromes. Some *LMNA* mutations have been associated with isolated phenotypes or heterogeneous disorders comprising overlapping pathologies in different tissues (summarised in table 1.1) (Worman 2012).

Table 1.1 Categories of Laminopathies

Skeletal muscle phenotype (with/without cardiac involvement)	**MIM#**	**Ref. where first described**
AD-Emery Dreifuss Muscular Dystrophy (AD-EDMD)	181350	(Bonne et al., 1999)
AR-Emery Dreifuss Muscular Dystrophy (AR-EDMD)	181350	(Raffaele Di Barletta et al., 2000)
Limb-girdle muscular dystrophy type 1B (LGMD1B)	159001	(Muchir et al., 2000)
LMNA associated congenital muscular dystrophy (L-CMD)	613205	(Quijano-Roy et al., 2008)
Cardiac only phenotype	**MIM#**	
Dilated Cardiomyopathy with conduction defects (DCM-CD)	115200	(Fatkin et al., 1999)
Premature ageing phenotypes	**MIM#**	
Hutchinson-Gilford Progeria Syndrome (HGPS)	176670	(Eriksson et al., 2003)
Atypical Werner Syndrome (WS)	277700	(Chen et al., 2003)
Mandibuacral dyspasia with type A lipodystrophy (MADA)	248370	(Novelli et al., 2002)
Restricted Dermopathy (RD)	275210	(Navarro et al., 2004)
Lipodystrophy syndromes	**MIM#**	
Dunningan-type Familial Partial Lipodystrophy (FPLD2)	151660	(Shackleton et al., 2000)
Köbberling-type Familial Partial Lipodystrophy (FPLD1)	608600	(Savage et al., 2004)
Neuropathies	**MIM#**	
Charcot Marie Tooth Disease type 2B1 (CMT-2B1)	605588	(De Sandre-Giovannoli et al., 2002)
Autosomal dominant spinal muscular dystrophy (AD-SMA)	182980	(Rudnik-Schoneborn et al., 2007)
Other phenotypes	**MIM#**	
Heart-Hand Syndrome	610140	(Renou et al., 2008)
Metabolic Syndrome		(Decaudain et al., 2007)

Secondary laminopathies are caused by mutations in Zmpste24, leading to defects in posttranslational modification of A-type lamins and include restrictive dermopathy (Navarro et al., 2004) and Mandibuloacral dysplasia (Agarwal et al., 2003).

1.4.1.1 Striated muscle laminopathies

Mutations affecting striated muscle can be divided into those resulting in skeletal muscle laminopathies with or without cardiac involvement, and those affecting cardiac tissue only.

The first mutations identified in the *LMNA* gene were those causing autosomal dominant Emery-Dreifuss muscular dystrophy (AD-EDMD) characterised by the clinical triad consisting of joint contractures, slowly progressive muscle weakness with a humero-peroneal distribution and cardiac involvement (Bonne et al., 1999), see section 1.1.3.2 for details.

Soon after, mutations causing an autosomal recessive (AR) form of EDMD and limb-girdle muscular dystrophy type 1B (LGMD1B) were identified (Muchir et al., 2000; Raffaele Di Barletta et al., 2000). LGMD1B is an autosomal dominantly inherited and slowly progressive muscle dystrophy involving muscles in hip and shoulders (limb-girdle musculature) and age related cardiac conduction defects and cardiomyopathy. The main difference to EDMD is the involved muscle groups and the absence of contractures (van der Kooi et al., 1997).

In 2008, lamin mutations were shown to be associated with a severe early-onset congenital form of muscular dystrophy (L-CMD) (Quijano-Roy et al., 2008). L-CMD patients showed upper proximal and lower distal muscular weakness, rigid spine, contractures and cardiac arrhythmias, which resembles the phenotype seen in EDMD patients.

Another striated muscle pathology involving mutations in lamin A/C is dilated cardiomyopathy with conduction system disorder (DCM-CD) (Fatkin et al., 1999). Hearts of DCM-CD patients present with ventricular dilation, reduced systolic function and conduction defects including sinus bradycardia, atrioventricular conduction block, or atrial arrhythmias. Skeletal muscle involvement and joint contractures are not observed in DCM-CD patients (Fatkin et al., 1999).

Mutations resulting in striated muscle laminopathies include missense mutations, nonsense mutations, insertions, deletions and splice site mutations distributed throughout the protein (www.umd.be/LMNA). A clear genotype-phenotype correlation has not been observed so far within this group of laminopathies and is further explored in chapter 3.

1.4.1.2 Premature ageing syndromes

A number of *LMNA* mutations result in premature ageing syndromes, a group of diseases characterised by the early onset of features resembling normal ageing.

Hutchinson-Gilford progeria syndrome (HGPS), likely to be the best known premature ageing syndrome, is a rare genetic disorder that occurs in one out of 4-8 million births. The clinical aspects were first described by Hutchinson (1886) by and Gilford (1897). The earliest signs of HGPS

appear by the age of 3 and are a severe growth retardation and loss of scalp hair, followed by the appearance of characteristic facial dysmorphic traits including a visible vein across the nasal bridge.

Patients also develop lipodystrophy especially in facial areas, osteolysis and a thin and atrophic skin. The cardiovascular system is severely affected and patients suffer from cardiomyopathy and atherosclerosis, the muscle mass decreases and joints stiffen. By the age of 9, strokes are very frequent, causing seizures, headache, vertigo, and limb weakness. HGPS patients have an average life expectancy of 13.5 years with myocardial infarction as the leading cause of death (Hennekam, 2006; Merideth et al., 2008).

In the majority of patients, these phenotypes are caused by a de novo single base mutation in codon 608 at exon 11 of the *LMNA* gene (c.1824C>T/p.G608G) which leads to the activation of a cryptic splicing donor site in the *LMNA* gene resulting in an in-frame deletion of 150 nucleotides (De Sandre-Giovannoli et al., 2003; Eriksson et al., 2003). The incorrectly spliced m-RNA gives rise to lamin A with an internal deletion of 50 amino acids called progerin. This protein lacks the second endoproteolytic cleavage site recognized by Zmpste24 and therefore remains permanently farnesylated. Accumulation of progerin or full length farnesylated lamin A at the nuclear envelope results in severely dysmorphic nuclei, mislocalisation of nuclear envelope proteins, accumulation of DNA damage by defective DNA repair and premature senescence (Goldman et al., 2004; Liu et al., 2005; Scaffidi and Misteli, 2005). Many (but not all; see Verstraeten et al. (2006)) mutations in *LMNA* which result in HGPS and progeroid phenotypes, have the accumulation of farnesylated lamin A in common, either caused by missense mutations or similar splicing defects as described above (Navarro et al., 2004).

Progeroid phenotypes, similar to HGPS but with atypical features, include atypical Werner's syndrome (WS), Mandibacra dysplasia (MADA) and restrictive dermopathy (RD). The clinical features of WS are similar to HGPS however the life expectancy is higher in patients with WS (Chen et al., 2003). Patients with RD, a severe progeroid disease with similarities to HGPS, however, die soon after birth (Navarro et al., 2004). Patients with MADA are characterised by growth retardation, craniofacial abnormalities, osteolysis as well as a generalised lipodystrophy, however they survive until adulthood (Novelli et al., 2002). Recessive null mutations in Zmpste24 have also been shown to cause RD (Navarro et al., 2004) while mutations reducing, but not abolishing Zmpste24 activity are associated with the less severe MAD type B phenotype (Agarwal et al., 2003) and other progeroid phenotypes (Shackleton et al., 2005).

1.4.1.3 Lipodystrophy disorders

The most prevalent lipodystrophy disorder caused by mutations in *LMNA* is the Dunningan-type Familial Partial Lipodystrophy (FPLD2) (Shackleton et al., 2000). The disease is primarily characterised by abnormal subcutaneous adipose tissue distribution, shifting from limbs to the face and neck, beginning in late childhood or early adult life. Other features of FPLD include metabolic

abnormalities including insulin-resistance, liver steatosis which may lead to cirrhosis, and premature atherosclerosis (Bidault et al., 2011).

The majority of affected individuals harbour mutations on residue R482 located in the Ig-fold domain, which results in the loss of a positive charge on the surface of the domain. However, FPLD2 mutations are also found in other parts of the protein including the central rod domain and tail domain (www.umd.be/LMNA).

In addition to the Dunningan-type, *LMNA* mutations also cause Köbberling-type familial partial lipodystrophy (FPLD1) as found in a family compound heterozygous for *LMNA* mutations p.S583L and p.T528M (Savage et al., 2004). FPLD1 has a very similar phenotypic manifestation to FPLD2 however subcutaneous truncal fat is preserved in these patients.

1.4.1.4 Laminopathies affecting the peripheral nervous system

A small number of *LMNA* mutations affect axonal myelination of peripheral neurons which results in autosomal recessive Charcot-Marie-Tooth disease type 2 (ARCMT2) (De Sandre-Giovannoli et al., 2002). The majority of patients are homozygous for p.R298C and suffer from lower proximal and upper limb muscle weakness likely to be a secondary effect to the neuropathy. The onset of disease is variable and ranges from 6 to 27 years (Bernard et al., 2006). Demyelinating neuropathies are assumed to originate from defective Schwann cells resulting in improper myelination or demyelination which leads to axonal loss. Histologically, nerve bundles in CMT2 patients show an abundance of unmyelinated fibres as well as a reduced fibre density (De Sandre-Giovannoli et al., 2002). Interestingly, *lmna*-null mice have a peripheral neuropathy resembling the phenotype seen in CMT2 patients (De Sandre-Giovannoli et al., 2002). How mutations in lamins may affect Schwann cells is not known. However, with a mouse model currently in progress we might soon have insight into the pathogenic role of *LMNA* mutations in CMT2.

1.4.2 How do mutations in lamins cause disease?

Ever since *LMNA* mutations have been associated with pathologies research has been conducted to elucidate the pathogenic mechanism behind different laminopathies. From this research three non-mutually exclusive hypotheses emerged: the 'mechanical stress' hypothesis, the 'gene expression' hypothesis and the 'cell proliferation' hypothesis (Broers et al., 2006; Worman, 2012; Worman and Bonne, 2007).

1.4.2.1 The 'mechanical stress' hypothesis

Given the nature of intermediate filaments, it is not surprising that lamins play a major role in maintaining the nuclear architecture and protecting the nuclear membrane from tearing especially in cells subjected to mechanical stress such as skeletal and cardiac muscle. Nuclei in *lmna*-null MEFs show severe deformations as well as defective mechanotransduction and reduced viability under mechanical stress (Lammerding et al., 2004). Lamin A/C and emerin have been shown to directly

interact with each other (Lee et al., 2001; Sakaki et al., 2001) and mutations in both proteins result in EDMD. Ultrastructural analysis of skeletal muscle from patients with autosomal dominant EDMD and X-linked EDMD reveals widespread breakage of nuclear envelopes and leakage of chromatin into the cytoplasm (Fidzianska and Hausmanowa-Petrusewicz, 2003; Fidzianska et al., 1998; Park et al., 2009), providing a potential pathogenic mechanism for *LMNA* mutations.

A disruption of the interaction of lamins with members of the LINC complex might contribute to the pathology of mutations. The LINC complex (composed of SUN-domain proteins and nesprins) forms a direct link between the nuclear lamina and all three cytoskeletal protein networks, cytoplasmic IFs, F-actin and tubulin (section 1.2.2). Disruption of the LINC complex has been shown to induce defects in nuclear morphology (Khatau et al., 2009) and affect the localisation of skeletal muscle nuclei as well as strain transmission between the cell and nucleus (Lombardi et al., 2011; Zhang et al., 2010), while mutations in giant nesprins 1 and 2 result in a pathology resembling that of EDMD (Zhang et al., 2007).

SUN-domain proteins have also been suggested to play a role in the pathology of EDMD and HGPS (Haque et al., 2010). Both EDMD and HGPS mutations were shown to disrupt the interaction between lamin A and SUN1/2, however, HGPS mutations resulted in an increased expression of SUN1 at the nuclear envelope (Haque et al., 2010). Accumulation of SUN1 at the nuclear envelope was also found in *lmna*-null cells (Chen et al., 2012) and prelamin A-mediated accumulation of SUN1 in myonuclei has been shown to play a role in nuclear positioning (Mattioli et al., 2011) suggesting that SUN1 is implicated in the pathogenic mechanism of laminopathies. Indeed, removal of SUN1 can rescue cellular phenotypes commonly found in HGPS cells including nuclear deformations, lamin B localisation and premature senescence. Further, knocking down SUN1 improves body weight and life span of *lmna*-null mice as well as mice expressing farnesylated lamin A (Chen et al., 2012). Together, this suggests that SUN1 accumulation is a common pathogenic event in HGPS disorders and provides a potential target for future therapies. However, whether SUN1 plays a similar pathogenic role in other laminopathies remains to be determined.

1.4.2.2 The 'gene expression' hypothesis

Lamins are able to directly and indirectly bind chromatin, transcription factors and members of cell signalling cascades. Mutations in lamins might therefore affect cell/tissue function by directly modulating gene expression and regulation.

High resolution mapping of the interaction of the entire genome of human fibroblasts with the nuclear lamina revealed that lamin associated domains (LADs) show low gene expression indicating a repressive chromatin environment (Guelen et al., 2008). Altered lamina-chromatin interaction induced by mutation might therefore change the chromosome organisation in a cell and globally affect gene transcription with unpredictable consequences. Similarly, an indirect disruption of lamina-chromatin interaction via LEM-domain proteins and BAF may lead to a similar result.

Lamin A has also been shown to be involved in the regulation of the Erk1/2 branch of the mitogen activated protein kinase (MAPK) pathway (Emerson et al., 2009; Gonzalez et al., 2008). Upon mitogen stimulation of serum starved cells, extracellular regulated kinase 1 and 2 (Erk1/2) is phosphorylated and in turn phosphorylates and activates c-Fos. Following activation, c-Fos, a member of the AP-1 family of transcription factors, dimerises with other AP-1 proteins and initiates transcription of AP-1 target genes involved in proliferation, differentiation and apoptosis (Andres and Gonzalez, 2009). Lamin A binds to both Erk1/2 and c-Fos and might therefore play an important role in modulating Erk signalling (Gonzalez et al., 2008).

Indeed, the localisation of c-Fos to the nuclear envelope is dependent on A-type lamins (Ivorra et al., 2006) and in fibroblasts from EDMD patients, the phosphorylation of Erk1/2 was initially delayed and then hyperactivated upon cell stimulation and cells exhibited increased proliferation (Emerson et al., 2009). Gene expression analysis in hearts of EMD null mice as well as mice expressing the EDMD mutation lamin A-H222P revealed an activation of MAPK signalling which precedes the cardiac phenotype. This suggests that activation of MAPK signalling could be involved in the pathogenic mechanism of heart disease in EDMD (Muchir et al., 2007a; Muchir et al., 2007b). Inhibition of Erk signalling in the H222P mice has been shown to delay the development of left ventricular dilatation confirming the involvement of MAPK signalling in the development of cardiomyopathy and preparing the way for therapeutic interventions (Muchir et al., 2009).

Lamin A does also bind to sterol-regulatory-element binding protein 1 (SREBP1) a transcription factor involved in lipid homeostasis, adipogenesis and insulin sensibility. The SREBP1 binding site was mapped to the Ig-fold of lamin A which harbours several mutations associated with FPLD2, suggesting it might play a role in the pathogenesis of the disease phenotype (Lloyd et al., 2002). Various mutations in lamin A inhibited the interaction with SREBP1 (Lloyd et al., 2002) and in presence of farnesylated lamin A, SREBP1 was observed to accumulate at the nuclear envelope together with a down-regulation of PPARγ (Peroxisome proliferator-activated receptor γ) (Capanni et al., 2005). Taken together these results support the theory of an involvement of SREBP1 in FPLD pathology.

Lamin and emerin have been shown to directly interact with MAN1 and could therefore modulate TGF-β and BMP signalling (section 1.2.2.6). If altered TGF-β or BMP signalling is involved in laminopathies is not known yet. However, BMP signalling could indirectly play a role by affecting muscle satellite cells where active BMP signalling is required to maintain proliferation and prevent premature differentiation (Ono et al., 2011).

In addition to the above, microRNAs which are predicted to be involved in several cell signalling pathways, including MAPK, TGF-β and Wnt, have recently been implicated in the pathology of *LMNA* associated muscular dystrophy (Sylvius et al., 2011). Interestingly, miR-100, which was upregulated in patient samples, induced myogenic differentiation when expressed in C2C12 cells

while overexpression of miR-335 induced proliferation (Sylvius et al., 2011), which implies an involvement of myoblasts in the disease pathology.

1.4.2.3 The 'Cell proliferation/differentiation' hypothesis

Defective cell proliferation and differentiation might have several implications in laminopathies especially in tissues that are maintained by adult stem cells such as skeletal muscle.

One key regulator of cell cycle progression is the retinoblastoma protein (pRb). In quiescent cells, pRb is hypophosphorylated and bound to E2F transcription factors, thereby inactivating them. In proliferating cells, the cyclin D/cdk4 and 6 complex hyperphosphorylates pRb which results in the release of E2F and the activation of genes involved in G1/S transition (De Falco et al., 2006). Nucleoplasmic A-type lamins have been shown to directly interact with the cell cycle regulator pRb in complex with Lap2α, tethering pRb to the nucleoskeleton and modulating its phosphorylation (Markiewicz et al., 2002; Markiewicz et al., 2005).

In mice, loss of Lap2α (Naetar et al., 2008) or lamin A/C (Nitta et al., 2006; Van Berlo et al., 2005) is associated with cell cycle progression while in human fibroblasts, loss of Lap2a induces cell cyle arrest (Pekovic et al., 2007) for yet unknown reasons.

The pRb pathway also plays a role in myoblast differentiation. Interaction of pRb and MyoD is required for the hypophosphorylation of pRb and subsequent cell cycle exit and differentiation (Gu et al., 1993). *Lmna*-null satellite cell-derived myoblasts display decreased pRb and MyoD protein levels as well as reduced differentiation potential in vitro (Frock et al., 2006). Moreover, gene expression studies in EDMD patient samples with mutations in *LMNA* and *EMD* suggest that key interactions between pRb and MyoD at the nuclear envelope fail at the point of cell cycle exit leading to poorly coordinated phosphorylation and acetylation steps (Bakay et al., 2006).

Other lamin A interacting proteins associated with cell cycle progression are cyclin D3 which is involved in G1/S transition (Mariappan et al., 2007) and the DNA elongation factor PCNA (proliferating cell nuclear antigen) (Shumaker et al., 2008), which suggest that lamin A plays additional roles in cell cycle control.

1.4.2.4 Genotype-Phenotype correlation in laminopathies

To date more than 300 different mutations have been described in the *LMNA* gene (www.umd.be/LMNA). These include mainly missense mutations but also nonsense mutations, insertions, deletions and splice site mutations. However, a clear genoype-phenotype correlation is not yet established (reviewed in Scharner et al. (2010)). The elucitation of genotype-phenotype correlations using a bioinformatics approach is the aim of chapter 3, where I will highlight the current understanding of genotype-phenotype correlations on laminopathies.

1.5 Thesis aim

Laminopathies are a heterogeneous group of diseases associated with mutations in A-type lamins, which together with B-type lamins, form the nuclear lamina: a proteinaceous network underlying the nuclear membrane. A-type lamins are encoded by the *LMNA* gene, and more than 300 mutations have been described, associated with more than 16 phenotypes. The majority of mutations affect striated muscle to cause Emery-Dreifuss muscular dystrophy (EDMD) or cardiomyopathy, while others result in lipodystrophy, neuropathy or premature ageing syndromes. However, clear genotype-phenotype correlations are not established, the pathogenic mechanisms are little understood and therapies are lacking.

The aim of this thesis is: (**1**) to advance the current understanding of genotype-phenotype correlations in laminopathies by analysing both physical-chemical properties of the amino-acid change, and position in the 3D structure of lamin A of a large number of mutations in the context of different pathologies (**2**) to provide insight into the effects of pathogenic Emery-Dreifuss muscular dystrophy mutations on nuclear morphology and nuclear protein distribution, as well as myogenic cell function such as proliferation and differentiation in overexpression studies, and (**3**) to explore the possibility of using antisense oligonucleotide (AON)-mediated exon skipping as a therapy for laminopathies in a proof-of principle study.

Chapter 2

Material and Methods

2.1 Material and reagents

2.1.1 Chemicals and Plasticware

Details of chemicals such as their concentration and manufacturer are given in each subsection of this chapter when first mentioned. Plasticware used for cell culture and assays were Nunc tissue culture plates (ThermoScientific), LabTek 8well Chamber slides (Permanox/Glass) from Nunc (ThermoScientific), sterile 15mL and 50mL tubes (Falcon) as well as sterile tissue culture pipettes (Falcon). Sterile filters of 0.45µm and 0.22µm pore size were obtained from Millipore.

2.1.2 Antibodies

Details of primary antibodies including the concentration they were used at are listed in table 2.1 below. Details of secondary antibodies are listed in table 2.2.

Table 2.1 Primary antibodies used in this study

Antigen	Clone	Host	Supplier	Cat. Number	Conc. Used
Emerin (AP8)		Rabbit	Generous gift from Juliet Ellis	(Ellis et al., 1998) & ImmuQuest	IF/WB 1:100
Erk 1/2 (MAPK)		Rabbit	Upstate	06-182	WB 1:1000
pErk 1/2		Rabbit	Cell Signalling	9101S	WB 1:1000
GFP		Rabbit	Invitrogen	A11122	IF 1:500 WB 1:2000
GFP		Chicken	Abcam	Ab13970	IF 1:2000
Lamin A	C20	Goat	Santa Cruz	sc-6214	IF 1:100
Lamin A/C	N18	Goat	Santa Cruz	sc-6215	IF 1:200 WB 1:1000
Lamin A/C	131C3	Mouse	Abcam	ab8984	IF 1:250
Lamin B	M20	Goat	Santa Cruz	sc-6217	IF 1:200
Lamin B1		Rabbit	Abcam	ab16048	IF/WB 1:2000
Lap2α		Rabbit	Novus Biologicals	NB 100-676	WB 1:2000
Myogenin	F5D	Mouse	DSHB		IF 1:10
Myosin Heavy Chain	MF20	Mouse	DSHB		IF 1:500
PCNA	PC10	Mouse	Dako	M0879	WB 1:1000
pRb		Mouse	BD Biosciences	554136	WB 1:1000
β-Tubulin	E7	Mouse	DSHB		WB 1:5000
V5		Mouse	Invitrogen	46-0705	IF 1:1000 WB 1:5000
BrdU	BU1/75	Rat	Abcam	ab6326-250	IF 1:50

Table 2.2 Secondary antibodies used in this study

Type	Conjugation	Host	Supplier	Cat. Number	Conc. Used
Mouse IgG	488	Goat	Invitrogen	A11029	1:500
	488	Donkey	Invitrogen	A21202	1:500
	555	Goat	Invitrogen	A21424	1:500
	594	Goat	Invitrogen	A11032	1:500
	594	Donkey	Invitrogen	A21203	1:500
	633	Goat	Invitrogen	A21052	1:500
Rabbit IgG	488	Goat	Invitrogen	A11034	1:500
	488	Donkey	Invitrogen	A21206	1:500
	555	Goat	Invitrogen	A21429	1:500
	594	Goat	Invitrogen	A11037	1:500
	594	Donkey	Invitrogen	A21207	1:500
	633	Goat	Invitrogen	A21071	1:500
Goat	488	Donkey	Invitrogen	A11055	1:500
	594	Donkey	Invitrogen	A11058	1:500
Chicken	488	Goat	Invitrogen	A11039	1:500
Rat	594	Goat	Invitrogen	A11007	1:500
Mouse IgG	HRP	Donkey	GE Healthcare	NA931V	1:5000
Rabbit IgG	HRP	Sheep	GE Healthcare	NA934V	1:5000
Goat IgG	HRP	Donkey	Abcam	ab19 (old)	1:5000
Goat IgG	HRP	Rabbit	Abcam	ab6741	1:50,000

2.1.3 Buffers and Solutions

1M Tris Buffer

To prepare 1M Tris buffer, 60.6g of Trizma-base (Sigma) were dissolved in 500mL ddH_2O before adjusting the pH with 5M HCl (pH7.4 or 8.0 depending on the application) and autoclaving.

EDTA solution

For a 500mM stock solution of EDTA, 14.6g of EDTA (Sigma) were dissolved in 100mL ddH_2O and sterile filtered.

TE-buffer

To prepare TE-buffer, 10mM Tris-HCl (Sigma) and 1mM EDTA (Sigma) were dissolved in ddH_2O. The pH was adjusted to pH8 with 1M HCl.

TAE buffer

A 50x concentrated stock of TAE (Tris-acetate-EDTA) agarose gel electrophoresis buffer was prepared by dissolving 242g Tris base in water, adding 57.1mL glacial acetic acid, and 100mL of 500mM EDTA (pH8.0) solution, and bringing the final volume up to 1 litre.

Phosphate buffered saline (PBS)

The PBS working solution was prepared by dissolving 1 PBS-tablet (Oxoid) in 100mL ddH_2O and was autoclaved subsequently. Each tablet contained 0.8g NaCl, 0.02g KCl, 0.115g Na_2HPO_4 and 0.02g KH_2PO_4.

PBST

To make PBST, 0.1% (v/v) Tween20 was added to 1x PBS.

Paraformaldehyde Solution (4% PFA)

To prepare 4% (w/v) PFA, 4g of paraformaldehyde (Sigma) were dissolved in 80mL ddH_2O at 65°C under constant stirring in a fume hood. After adding a few drops of 1M NaOH to raise the pH and dissolve the PFA completely, the solution was immediately cooled down to room temperature on ice. One PBS tablet (Oxoid) was added and the pH was adjusted to 7.4 with 1M HCl before topping up to 100mL with ddH_2O. The PFA was stored frozen at -20°C.

Cell suspension buffer

Cell suspension buffer contains 10mL of 5M NaCl (Sigma), 5mL of 1M Tris-HCl (pH 7.5) and 1mL of 500mM EDTA (pH 8.0) made up with ddH_2O to 500mL and was autoclaved before use. The suspension buffer was stored at 4°C.

Gel loading buffer (2x)

Double concentrated (2x) gel loading buffer (Laemmli, 1970) contains 2ml 10% (w/v) SDS, 1mL Glycerol, 0.625mL 1M Tris-HCl (pH6.8) and 1.375mL ddH_2O and was stored at room temperature (RT).

Suspension buffer P1

The suspension buffer contains 50mM Tris (pH8.0), 10mM EDTA (pH8.0) and 100µg/mL RNAseA (Roche) and was stored at 4°C

Alkaline lysis buffer P2

Alkaline lysis buffer contains 200mM NaOH (BDH) and 1% (w/v) SDS (Sigma) and was stored at RT.

Neutralisation buffer P3

The neutralisation buffer is a 3M potassium acetate solution adjusted to pH5.5 and was stored at RT.

2.2 Methods and Protocols

2.2.1 Mouse work

2.2.1.1 Maintenance of *Lmna* mouse colony

Mice were kept and maintained by the Biological Services Unit (BSU) at King's College London under project license PPL70/7092 and according to standard regulations and guidelines as prescribed in the Animals (Scientific Procedures) Act 1986. The *Lmna*-mice on a C57BL/6 backround (Sullivan et al., 1999) were a kind gift from Carlos Lopez-Otin (University of Oviedo, Spain).

2.2.1.2 Genotyping by PCR

Adult *Lmna* mice were tagged for identification by ear punching and a piece of tail was collected for genotyping as wild-type, heterozygotes or homozygotes for the null allele. To genotype embryos, a piece of the yolk sac was used. Total genomic DNA was extracted by digesting the tissue samples in 100µL DNA extraction buffer (Direct PCR Tail or Direct PCR Yolk Sac; Viagen) supplemented with 20µg proteinase K (Roche) at 55°C overnight. The samples were heat inactivated at 85°C for 45min and spun down. For the PCR, 1µL of the supernatant was mixed with 4µL 5x GoTaq buffer (Promega), 0.5µL dNTPs (10mM; Fermentas), 0.5µL of each primer (P1, P2 and P3, see table 2.3), 0.1µL Taq Polymerase (Promega) and 13µL ddH_2O.

Table 2.3 Genotypeing primers used in this study. All listed oligonucleotides were obtained from Sigma.

ID	Primer Name	Primer sequence (5'>3')
Genotyping Primers		
P1	*Lmna* wild type-Fwd	CGATGAAGAGGGAAAGTTCG
P2	*Lmna* wild type-Rev	GCCGAATATCATGGTGGAAA
P3	*Lmna* mutant-Rev	CCATGGACTGGTCCTGAAGT

The DNA was amplified on a Techne TC-512 thermocycler under following conditions: Initial denaturation for 5min at 95°C, followed by 35 cycles of 95°C/15sec, 58°C/30sec, 72°C/1min and 5min extension at 72°C. The PCR products together with a 10kb DNA ladder (SmartLadder; Eurogentech) were separated by gel electrophoresis on a 1% (w/v) agarose gel (Fisher Scientific) supplemented with 0.5µg/mL Ethidium Bromide (Sigma) and visualised under UV-light.

The PCR reaction yields 2 different amplicons depending on the genotype of the animal. The shorter band at approx. 520bp corresponds to wild-type *Lmna* allele, a larger band of 750bp corresponds to the mutant null *Lmna* allele.

2.2.2 Cloning of construct used in this thesis

2.2.2.1 General Cloning method

Constructs were generally cloned by PCR amplification of the cDNA with primers containing recognition sites for restriction enzymes. Upon digest of the vector and insert with the restriction enzyme under conditions recommended by the supplier (NEB and Promega), the DNA fragments were either purified using spin columns (Qiagen) or extracted from the agarose gel using a gel extraction kit (Qiagen). The DNA concentration was measured using a Nanodrop spectrophotometer. Vector and insert were then incubated in the presence of T4 ligase (NEB) over night at 16°C at a molar ratio of 1:3 (Vector:Insert). One microlitre of the ligation reaction was transformed into One Shot TOP10 competent cells (Invitrogen) by a 45sec heat shock. The bacteria were allowed to recovered for one hour at 37°C in SOC medium (Invitrogen) and plated on selective agar plates containing 100µg/mL ampicillin or kanamycin as appropriate. Colonies were grown in 2mL LB-broth under selection conditions before extracting plasmid DNA by miniprep. Positive colonies were identified by restriction mapping and grown for 16hrs in 100mL selective LB medium. Plasmid DNA was extracted using a midiprep kit (Qiagen) and sent for sequencing.

2.2.2.2 Plasmid DNA miniprep

To extract plasmid DNA, 1mL of bacteria culture was transferred into a 1.5mL Eppendorf tube and spun at 10,000g for 1min to pellet the cells. The pellet was resuspended in 100µL suspension buffer P1 and lysed by adding 100µL alkaline lysis buffer buffer P2. Protein together with genomic DNA was precipitated by adding 100µL neutralisation buffer P3 and spun down at 13.000g for 5min. The supernatant was transferred into a new Eppendorf tube and the plasmid DNA was precipitated by adding 0.7 volumes of Isopropanol (VWR). After pelleting the DNA by centrifugation (13,000g for 5min) it was washed with 70% ethanol, dried, and resuspended in 100µL TE-buffer. For sequencing, plasmid DNA obtained by miniprep was purified on a spin column (Qiagen) and eluted with ddH_2O.

2.2.2.3 pMSCV-IRES-eGFP

All constructs used in this study were cloned into the pMSCV-IRES-eGFP (MIG) retroviral expression vector, described by Zammit et al. (2006b). Briefly, an internal ribosomal entry site (IRES) together with eGFP and an SV40 polyadenylation signal was cloned into the murine stem cell viral vector (pMSCV; Clonetech) to create a bicistronic retroviral expression system. The original viral vector is ecotropic and replication incompetent for safety reasons. A map of this vector is shown in figure 2.1.

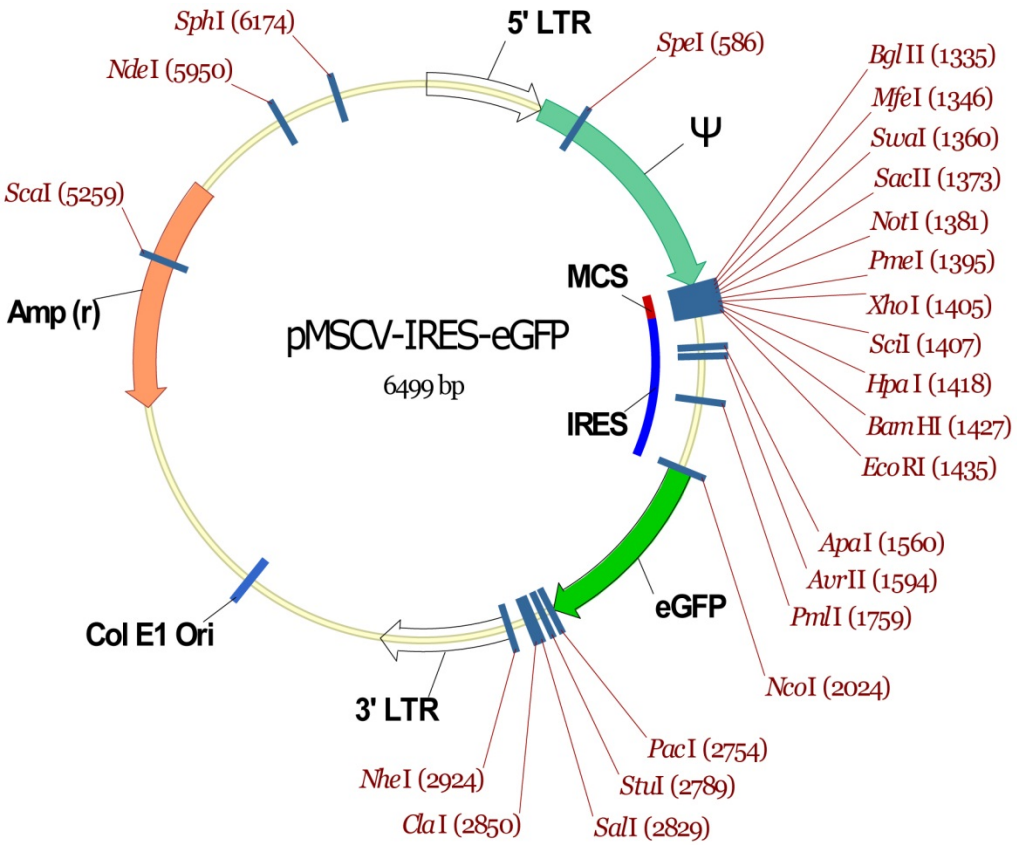

Figure 2.1 Map of the *pMSCV-IRES-eGFP* vector. Unique restriction enzymes and main features of the vector are indicated. LTR, Long terminal repeat; Ψ, Psi packaging signal; MCS, Multiple cloning site; IRES, Internal ribosomal entry site; Col E1 Ori, Origin of replication; Amp (r), Ampicillin resistance gene.

2.2.2.4 Wild-type lamin A and mutant lamin A variants in MIG

Wild-type lamin A (Motsch et al., 2005) and mutant lamin A (R25P, R190dup, R249W, S295P, S303P, N496I and R541P, kindly provided by Juliet Ellis) were amplified using lamin A specific primers with restriction enzyme sites XhoI and BamHI (primers P9 and P10, table 2.4) under following conditions: 200ng (diluted in 2µL) plasmid DNA template was mixed with 5µL 10x Pfx Amplification buffer (Invitrogen), 1.5µL dNTPs (10mM; Fermentas), 1µL $MgSO_4$ (50mM; Invitrogen), 1.5µL of each primer (P9 and P10, see table 2.4), 0.5uL Platinum Pfx DNA Polymerase (Invitrogen) and 37µL ddH_2O.

The DNA was amplified on a Techne TC-512 thermocycler under following conditions: Initial denaturation for 5min at 95°C, followed by 35 cycles of 95°C/15sec, 55°C/30sec, 68°C/2min and 5min extension at 68°C. The PCR products together with a 10kb DNA ladder (SmartLadder; Eurogentech) were separated by gel electrophoresis on a 1% agarose gel (Fisher Scientific) supplemented with 0.5µg/mL ethidium bromide (Sigma) and visualised under UV-light.

PCR fragments were purified on a spin column (Qiagen) and digested using restriction enzymes XhoI and BamHI under standard conditions before they were ligated with the digested MIG-vector (see above).

Table 2.4 Cloning primers used in this study. All listed oligonucleotides were obtained from Sigma.

P3	*Lmna* mutant-Rev	CCATGGACTGGTCCTGAAGT
Lamin A Sequencing Primers		
P4	Lamin A-cDNAseq 1 Fwd	CCGAGTCTGAAGAGGTGGTC
P5	Lamin A-cDNAseq 2 Rev	CACGCAGCTCCTCACTGTAG
P6	Lamin A-cDNAseq 3 Fwd	TCTGCTGAGAGGAACAGCAA
P7	Lamin A-cDNAseq 4 Fwd	GTGGAAGGCACAGAACACCT
P8	Lamin A-cDNAseq 5 Fwd	GAAGCTTCGAGACCTGGAGG
PCR Cloning Primers		
P9	XhoI-lamin A-exon 1 Fwd	TATCTCGAGCAAC**ATG**GAGAC (start codon in bold)
P10	Lamin A-exon 12-BamHI Rev	TTCTAGGATCC**TTA**CATGATGC (stop codon in bold)
P11	Lamin A-Δexon 3 Rev	CTTGGCCACCTGGCCCC
P12	Lamin A-Δexon 5 Rev	CTTGGCAGAATAAGTCTTCTC
P13	Lamin A-Δexon 3 Fwd	GAGCTGCGTGAGACCAAGC
P14	Lamin A-Δexon 5 Fwd	CTGGCAGCCAAGGAGGCG
Mutagenesis Primers		
P15	N195K-Fwd	GGTGGATGCTGAGAAGAGGCTGCAGACCATGAAGG
P16	N195K-Rev	CCTTCATGGTCTGCAGCCTCTTCTCAGCATCCACC

2.2.2.5 Creation of lamin A-N195K by site directed mutagenesis

To create lamin A-N195K, wild-type lamin A was mutated using the QuickChange Site-Directed mutagenesis kit (Agilent) according to manufacture's instructions. In principle, the plasmid to be mutated (lamin A-wt in MIG) was amplified by two complementary primers containing the mutation (lamin A-N195K mutagenesis primers P15 and 16, table 2.4) resulting in nicked circular strands. The non-mutated parental plasmid was then digested with DpnI (target sequence: 5´-Gm^6ATC-3´) which is specific for methylated and hemimethylated DNA. DNA isolated from almost all E. coli strains is dam methylated and therefore susceptible to Dpn I digestion which allows the selection for mutation-containing synthesised DNA. The nicked vector containing the mutation was then transformed into XL1-Blue supercompetent cells (Agilent) and sent for sequencing to confirm the mutation.

2.2.2.6 Creation of lamin A constructs with internal deletions

The deletion of 48 amino acid fragments corresponding to exons 3 and 5 was carried out as follows (illustrated in Fig. 2.2 below): lamin A was amplified with 2 primer pairs (see table 2.4) amplifying 2 lamin A fragments on either side of the sequence to be removed. The fragments were purified on a spin column (Qiagen) and analysed on an agarose gel to confirm their correct size. The two

corresponding fragments were then phosphorylated with T4 polynucleotide kinase (Sigma) in presence of 0.1mM ATP (Sigma) and blunt ligated with T4 ligase (NEB). The ligation reaction was purified with a spin column (Qiagen) and digested with both enzymes introduced with primers P9 (XhoI) and P10 (BamHI). The digest was separated on an agarose gel and the band with the correct size (1885bp) was cut. After extraction of the DNA with a gel extraction kit (Qiagen), it was re-amplified under the same conditions as above, using primer P9 and P10. The amplicon was purified on a spin column, digested and ligated with the MIG backbone under standard conditions (see above). The presence and accuracy of the deletion was confirmed by sequencing.

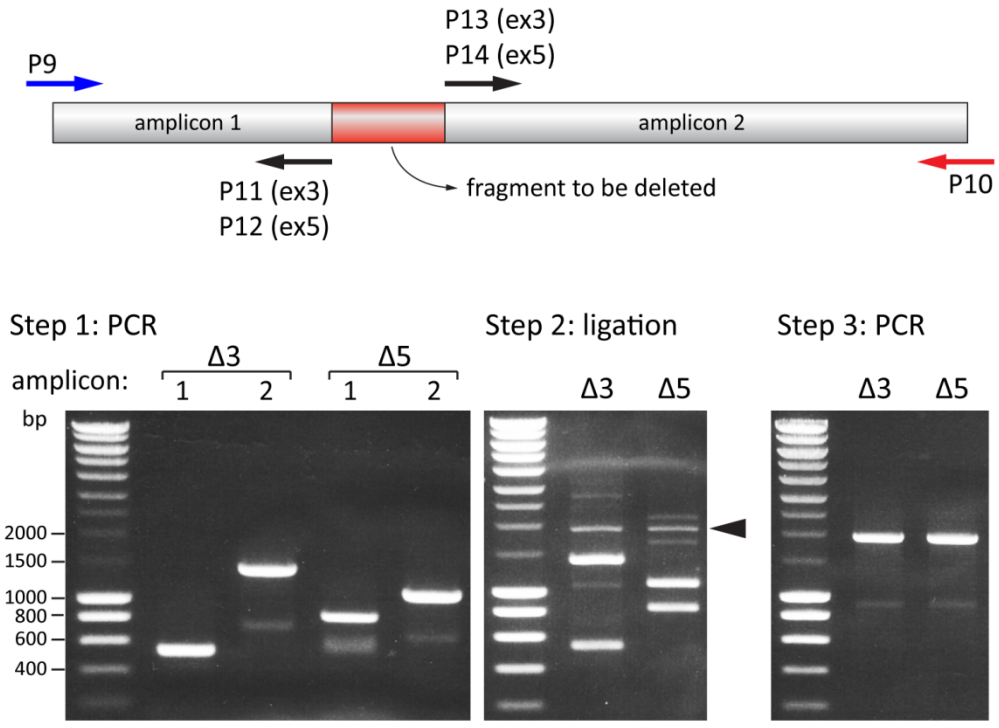

Figure 2.1 Cloning strategy to create lamin A-Δ3 and Δ5 by PCR. The fragment to be deleted (exon 3 or 5) is shown in red. Primers are indicated by arrows (see table 2.3) Coloured primers contain restriction sites XhoI (blue) and BamHI (red). Step1: Two sequences excluding exons 3 or 5 were amplified. Step 2: The amplicons were phosphorylated, blunt ligated and digested with XhoI and BamH1. The black arrowhead indicates the correct ligation product (1885bp) which was excised from the gel. Step 3: Excised DNA bands were re-amplified using primer pair P9/P10 and cut with XhoI and BamHI before ligation with the MIG vector.

2.2.3 Cell culture protocols

2.2.3.1 Single Fibre Isolation and Culture

Single fibres were isolated as per protocol by (Collins and Zammit, 2009; Rosenblatt et al., 1995). The extensor digitorum longus (EDL) of young adult mice (6-8 weeks of age) in a Bl-6 background was isolated intact and incubated in 0.2% (w/v) collagenase (Sigma) in DMEM-Glutamax (Gibco) supplemented with 1% (v/v) Penicillin/Streptomycin (Sigma) for 1hr 30min at 37°C. Muscles were

transferred into deep plastic dishes treated with 5% (w/v) BSA (in ddH_2O; Sigma) to prevent attachment. Single fibres were liberated by trituration with heat polished Pasteur pipettes and incubated in plating medium (DMEM-Glutamax supplemented with 10% horse serum (PAA), 0.25% (v/v) chick embryo extract (MP Biomedicals) and 1% (v/v) Penicillin/Streptomycin) for 24hrs. At T24 (24 hours after isolation), once satellite cells have been activated and entered cell cycle, fibres were exposed to viral particles (without polybrene) and fixed at 48hrs and 72hrs respectively (24hrs and 48hrs post infection respectively).

2.2.3.2 Isolation and culture of plated satellite cells

To prepare satellite cells, single fibres were isolated as described above. Debris from damaged fibres, tendons and connective tissue were removed through three washing steps by transferring intact fibres into new culture dishes. Clean fibres were then transferred into 10cm dishes (coated with 0.5mg/mL matrigel (BD Biosciences) for 45min at 37°C) filled with satellite cell medium consisting of DMEM (Gibco), 20% (v/v) FBS Gold (PAA), 10% (v/v) horse serum (Gibco), 1% (v/v) chicken embryo extract (MP Biomedicals), 1% (v/v) Penicillin/Streptomycin (Sigma), 2mM L-glutamine (Sigma) and 10ng fibroblast growth factor (PeproTech). After 3 days satellite cells have migrated off the fibres and started to proliferate. At this point the fibres are removed by repeatedly flushing medium across them with a sterile pipette tip and the satellite cells are subcultured into 6-well plates for retroviral infection. To infect plated satellite cells, they are subjected to retroviral particles for 6hrs in presence of 4μg/mL polybrene (Sigma). Infected cells were subcultured into matrigel coated chamber slides and analysed 24-72hrs post infection. To assay the myogenic potential, satellite cells were induced to differentiate by changing to differentiation medim (2% (v/v) horse serum in DMEM) and analysed 24-48hrs later.

2.2.3.3 Isolation and Culture of primary Mouse Embryonic Fibroblasts (pMEFs)

Primary MEFs were isolated according to Xu (2005). Lamin A/C heterozygous female mice were set up for mating with a Lamin A/C heterozygous male and sacrificed 13.5 days post coitum (dpc) to collect E13.5 embryos. The embryos were dissected under a stereomicroscope in the laminar flow hood and transferred into a new dish containing ice cold sterile PBS. At the same time part of the yolk sack was collected for genotyping (for genotyping protocol see section 1.2.1.2). After removing the brain and internal organs, the body of the embryo was minced in 1mL ice cold Trypsin-EDTA (Gibco) and transferred into a 15mL sterile Falcon tube. The minced embryos were kept on ice for 1hr to allow the Trypsin-EDTA to penetrate the tissue pieces before incubating them at 37°C for 20min. The digested embryonic tissue was then triturated to obtain a single cell suspension and filtered through a 100μm cell strainer to remove larger, undigested tissue pieces. The cells of one embryo were resuspended in 30mL MEF medium and plated into three 10cm cell culture dishes to allow attachment of embryonic fibroblasts overnight. Cells at this stage were designated passage number P0. On the next day, unbound cells were removed by rinsing the plates 3 times with PBS. The remaining cells were left in culture for an additional day to reach confluence.

Cells were then trypsinised, counted and frozen for future use. MEFs were cultured in DMEM (Gibco) supplemented with 10% FBS Gold (PAA), 1% (v/v) Penicillin/Streptomysin (Sigma), 2mM L-glutamine (Sigma) and 0.1mM β-Mercaptoethanol (Sigma). The cells were frozen in DMEM supplemented with 30% (v/v) FBS, 1% (v/v) Penicillin/Streptomycin, 2mM L-glutamine and 10% (v/v) DMSO (Sigma) and stored in liquid N_2.

2.2.3.4 Production of Retrovirus

Non-replicating viral particles were produced in HEK-293T (maintained in DMEM/10%FBS) cells by transiently co-transfecting 4µg of the retroviral constructs, together with 4µg of an ecotropic packaging plasmid. To do so, plasmid DNA was diluted in 1.8mL OptiMEM medium (Gibco) together with 8µL Plus-Reagent (Invitrogen) and 24µL Lipofectamine LTX (Invitrogen). After 30min incubation at RT the transfection mixture was added to subconfluent (approx. 70%) HEK-293T cells, grown in a T75cm² flask. No penicillin was added to the medium at this stage. After 12-16hrs the medium was changed and the supernatant (5mL at each time point) was harvested 48, 60 and 72 hours after transfection.

2.2.3.5 C2C12 myoblast culture

The C2C12 myoblast cell line (Blau et al., 1983; Yaffe and Saxel, 1977) was grown and maintained in DMEM (Gibco) supplemented with 10% FBS Gold (PAA) 1% (v/v) Penicillin/Streptomycin (Sigma) and 2mM L-Glutamine (Sigma). For viral infection, cells were incubated in growth medium supplemented with 4µg/mL polybrene to support viral uptake. To induce differentiation by serum withdrawal, cells were washed with PBS before exposing them to DMEM supplemented with 2% horse serum (Gibco) 1% Penicillin/Streptomycin and 2mM L-Glutamine.

2.2.3.6 Cell Cycle analysis by Flow Cytometry

Cells were grown in 6 well plates and harvested by trypsinization 48 hours after infection. After fixation in 70% ethanol, cells were incubated with 40µg/mL propidium iodide (PI) (Sigma), 40µg/mL RNAseA (Roche) and 0.1% NP40 (Sigma) in TE buffer pH8.0 for 30 minutes at 37°C. Cells were then stored at 4°C protected from light until analysis by flow cytometry. To determine the proportion of GFP positive cells, cells were fixed with 4% PFA, washed twice with PBS and stored at 4°C protected from light until analysis by flow cytometry.

2.2.3.7 BrdU Incorporation

To label cells in S-phase, they were pulsed with 10µM BrdU (Sigma) for 2hrs prior fixation with 4% PFA.

2.2.3.8 Immunocytochemistry

Myofibers were collected from growth plates with a fire polished Pasteur pipette and transferred into a 2mL Eppendorf tube. They were washed with PBS, fixed with 4% PFA (10min at RT) and

transferred into shallow plastic dishes (4cm diameter). After permeabilisation with 0.5% (v/v) Triton X-100 (Sigma) in PBS (10 min at RT), they were blocked with 5% (v/v) normal goat serum (Dako) and 5% normal swine serum (Dako) for 1hr at RT. Fibres were incubated with primary antibodies (diluted in PBS containing 0.025% (v/v) Tween-20 and 0.5% (v/v) serum; see table 2.1) overnight at 4°C, washed three times with PBS+0.025% (v/v) Tween-20 and incubated with the secondary antibody (diluted in PBS+0.025% Tween-20; see table 2.2) for 1hr at RT protected from light. After a further washing of the fibres, they were transferred onto glass slides, mounted with Vectashield mounting medium containing DAPI to mark all nucei (Vector Labs) and stored at 4°C in the dark.

Plated cells were processed in the chamber slides. They were washed with PBS, fixed with 4% PFA (10min at RT) and permeabilised with 0.5% (v/v) Triton X-100 (Sigma) in PBS (10 min at RT) and blocked with 2.5% (v/v) normal goat serum (Dako) and 2.5% (v/v) normal swine serum (Dako) for 1hr at RT. Where a primary antibody raised in goat was used, cells were blocked with 5% (v/v) normal swine serum. Subsequently, cells were incubated with primary antibodies (diluted in PBS containing 0.025% (v/v) Tween-20 and 0.5% (v/v) serum; see table 2.1) overnight at 4°C, washed three times with PBS+0.025% (v/v) Tween-20 and incubated with the secondary antibody (diluted in PBS+0.025% (v/v) Tween-20; see table 2.2) for 1hr at RT protected from light. To stain the DNA, cells were exposed to 300nM DAPI (Sigma) for 10min at RT, washed, mounted with FluoromountG (Southern Biotech) and stored at 4°C in the dark.

To stain for BrdU, cells were fixed and permeabilised as above. To unmask the BrdU epitope, cells were treated with 3M HCl diluted in ddH_2O for 10mins, rinsed with 0.5% (w/v) BSA/PBS and neutralised by rinsing them twice with 100mM Borate (pH8.5). After two washes with PBS+0.025% (v/v) Tween-20, the primary anti-BrdU antibody was applied diluted in PBS containing 0.025% (v/v) Tween-20 and 0.5% (w/v) BSA and incubated over night at 4°C. After 3 washes with PBS+0.025% (v/v) Tween-20, cells were incubated with the secondary antibody (diluted in PBS+0.025% (v/v) Tween-20) for 1hr at RT. The finished slides were stained for DNA and mounted as above.

2.2.4 Immunoblotting protocol

2.2.4.1 Total protein extraction

Cells were rinsed with PBS, scraped off and harvested in an Eppendorf tube by centrifugation at 13.000 rpm for 1 min. The cell pellet was resuspended in 40-100µL of suspension buffer (depending on the pellet size) and lysed by adding an equal amount of 2x gel loading buffer. The suspension buffer was supplemented with protease and phosphatase inhibitors just before use: complete Mini Protease Inhibitor Cocktail (Roche), 10mM Sodium Orthovandate (Sigma), 10mM Sodium pyrophosphate (Sigma) and 50mM Sodium Fluoride (Sigma). The samples were heated to

100°C on a heat block and boiled for 10min before they were sonicated two times for 10sec (10µm amplitude) by inserting a probe directly into the sample. Insoluble compounds were spun down at 13.500 rpm for 5min. The supernatant was transferred into a new tube and stored at -20°C after a small aliquot for protein estimation was taken.

2.2.4.2 Protein estimation

The protein concentration was estimated using the photometric Bio-Rad Dc Protein Assay according to the manufacturer's instructions. Briefly, each protein sample was diluted 1:2 to 1:20 (depending on the pellet size) in ddH_2O and analysed in triplicates in a flat bottom 96-well plate. After adding 25µL Reagent A and 200µL Reagent B (BioRad Dc protein Assay solution) to each well containing 5µL sample, the plate was incubated for 20min in the dark at RT. The absorbance at 620nm was measured with a Multiskan Ex spectrophotometer (Thermo) and the concentration was determined using a BSA (Promega) standard curve in the range of 0.2 - 1.0mg/mL, which was processed in parallel. After determining the total protein concentration, samples were diluted to 0.5-2µg/µL protein in 1x gel loading buffer. To each sample 150mM Dithiothreitol (Sigma), and 1x RunBlue loading buffer (Expedeon) was added and then stored at -20°C.

2.2.4.3 SDS-Polyacrylamide Gel Electrophoresis

Samples were separated on RunBlue precast denaturing gels (Expedeon) by 1D SDS Polyacrylamide Gel Electrophoresis (SDS-PAGE) using the RunBlue Electrophoresis system (Expedeon). Samples were boiled for 2min before they were loaded onto the gel at a range between 5 and 50µg total protein per lane. The protein size was determined by a standard protein ladder (RunBlue 2-Color SDS Marker (Expedeon)). The electrophoresis was carried out with 1x Tris-Glycine Electrophoresis buffer (Expedeon) at a constant voltage of 120V. Once the samples have entered the separation gel, the voltage was increased to 180V and left running until the colour indicator had migrated off the gel.

2.2.4.4 Immunoblotting

To transfer the protein bands onto a PVDF membrane, the semidry iBlot system (Invitrogen) was used. Membranes were then washed in PBS, blocked with 5% (w/v) BSA (Sigma) in PBST for 1 hour at RT before the primary antibody was added and incubated over night at 4°C on a laboratory shaker. Subsequently, the membranes were washed 3 times for at least 10 min. with PBST and incubated with the corresponding HRP conjugated secondary antibody diluted in 1% BSA/PBST for 1 hour at room temperature. All primary and secondary antibodies used are listed in tables 2.1 and 2.2. After a further three washes with PBST and a final rinse with PBS, the membranes were incubated for 5 minutes with ECL Western Blotting Detection Reagents (GE Healthcare). In the darkroom, an X-ray film was exposed for several seconds up to 5min, and developed using an automated film processor. Films were labelled and scanned for permanent recording.

2.2.5 Microscopy and picture analysis

Micrographs of single fibres were taken on a Zeiss Axiovert 200M using the Zeiss Axiovision software. Micrographs of plated cells were captured with a Zeiss Axioplan 2 using Openlab v3.1.7. Pictures were exported to .tiff files and compiled using Adobe Photoshop CS4. The Cell Counter plugin for Image J v.1.43 (http://rsbweb.nih.gov/ij/) was used to quantify cells and/or nuclei.

To quantify the morphological abnormalities of nuclei such as elongation or lobulation, I measured the perimeter and the area of lamin B stained nuclei and calculated the nuclear roundness or contour ratio (4π area/ circumference^2) (Goldman et al., 2004). The contour ratio (CR) of a circle is 1, and the value gets smaller with an increased degree of lobulation. To calculate the perimeter and area of the nuclei, they were outlined using the polygon selection tool and measured with ImageJ.

Confocal micrographs were taken at the Zeiss LSM at 63x magnification. Laser voltage and gain was adjusted for each fluorophore. Pictures were converted using the LSM Toolbox plugin (Image J) and the fluorescence intensity was measured using the Plot Profile tool (Image J).

2.2.6 Bioinformatics analysis

2.2.6.1 Structure representation and visualisation

Structures of the central rod domain (PDB# 1X8Y, (Kapinos et al., 2011)) and Ig-fold doamin (PDB# 1IVT (Krimm et al., 2002)) were visualised with the molecular visualisation system PyMOL version 1.3.

2.2.6.2 Calculation and visualisation of electric surface potential

To visualise the electrostatic surface potential of the Ig-fold structure, it had to be converted to allow the inclusion of parameters such as charge and radius information. This was done with the online server PDB2PQR available at http://kryptonite.nbcr.net/pdb2pqr/ (Dolinsky et al., 2007). The forcefield chosen was PARSE which has been optimised for solvent calculation and is therefore the best choice for visualization of protein electrostatics. To assign the charge to the structure electrostatics calculation was performed using the Adaptive Poisson-Boltzmann Solver (APBS) software package (Baker et al., 2001) which is integrated into the PyMOL software package. Once completed, the electrostatic surface potential was visualised with PyMOL with the trajectory colour range (colour intensity) for the electrostatic potentials set from -5000 (red, negative charge) to +5000 (blue, positive charge).

2.2.6.3 In silico mutagenesis

To perform *in silico* mutagenesis the corresponding mutagenesis plugin in PyMOL was used. The plugin can be used to replace any residue in the structure. Once the residue to be mutated and the new amino acid are selected, a choice of rotamers is presented. Rotamers are permitted different configurations of the new amino acid within the structure (residue side-chains can only take a

specified series of preferred conformations with respect to the peptide bond). Since the 3D orientation of amino acids in the rest of the structure is not changed, mutated residues might physically interfere with neighbouring residues, especially if the new residue is physically larger than the original amino acid. PyMOL displayed the points of contact between the new residue and remaining structure for each rotamer. In this analysis the least disruptive rotamer (the rotamer with the least number of contact points with the rest of the structure) was chosen because it is the orientation likely to be found in the structure. The isoelectric surface potential of each new Ig-fold mutated isoform was calculated and visualised as described above.

2.2.7 Statistical analysis and graph representation

Curves and bar charts were created using Microsoft Excel, figures were created and arranged with Adobe Illustrator CS4. Chi-square statistics and Student's t-test were used to determine a significant statistical difference between samples whereby $p<0.05$ was considered significant (*) and $p<0.01$ was considered highly significant (**).

Chapter 3

Genotype-Phenotype Correlations in Laminopathies

3.1 Introduction

As of December 2010, the universal mutation database (www.umd.be/*LMNA*) lists 303 different mutations in the *LMNA* gene in 1560 patients. However, there are only a handful of mutations where the genotype-phenotype link is consistent and well understood. For the vast majority of mutations in the *LMNA* gene the correlation with the resulting phenotype remains a mystery (Scharner et al., 2010).

According to the current understanding, the proposed pathological mechanisms of *LMNA* mutations can be classified according to the protein modification/functional consequence the mutations result in, which is (1) protein degradation (2) lamin A filament formation (3) function/integrity of lamin A interacting proteins (4) accumulation of farnesylated lamin A (Worman and Bonne, 2007). However, for the majority of mutations it is unknown how exactly they affect the protein structure or function.

Clinical phenotypes resulting from *LMNA* mutations include a large spectrum of disorders ranging from cardiomyopathy to premature ageing. However, upon careful inspection, the clinical disorders can be grouped according to the tissue they affect, which is either striated muscle, adipose tissue, peripheral nerve or multiple systems with signs of accelerated ageing. This classification is for the most part robust although other and overlapping phenotypes have been described (Worman, 2012) (section 1.4.1).

The majority of mutations seem to be randomly distributed throughout the protein with no clear association between the type of mutation, its location and the resulting phenotype. This is highlighted in figure 3.1, which illustrates mutations associated with a range of phenotypes and their location in the lamin A protein (www.umd.be/LMNA). However, each disease category has one or more mutations with a good correlation between the genotype and the resulting phenotype.

I will introduce mutations where the genotype-phenotype link is very consistent for a large number of patients and mutations where we have a clear understanding about the effects these mutations have on the protein and the resulting phenotype. I will then highlight what is known about mutations with no obvious correlation with the phenotype and summarise attempts by fellow researchers to elucidate genotype-phenotype correlations in laminopathies.

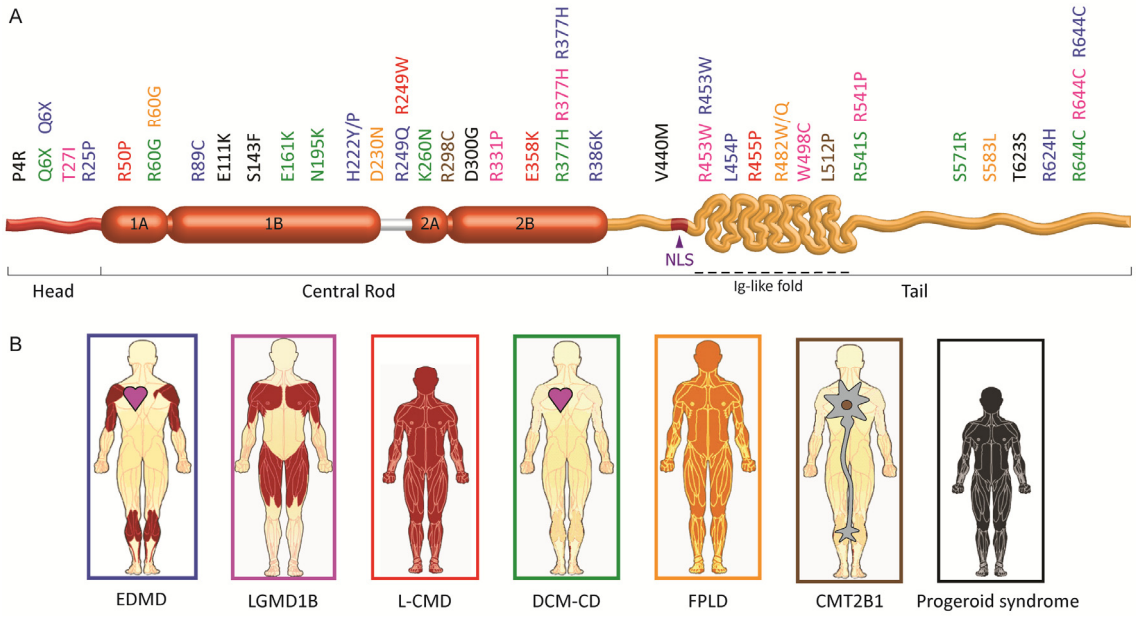

Figure 3.1 Mutations reported in the *LMNA* gene and their associated phenotype. A schematic of the lamin A protein and selected mutations resulting in EDMD (blue), LGMD1B (purple), L-CMD (red), DCM-CD (green), FPLD (gold), ARCMT2 (brown) and progeroid syndrome (black) are shown.

3.1.1 *LMNA* mutations with a predictive genotype-phenotype link

A small number of *LMNA* mutations are at mutation 'hot-spots' and almost always result in the same phenotype in a large number of cases. One such example is the de novo mutation c.1824C>T/p.G608G which is always associated with HGPS. The mutation results in a cryptic splice donor site in the lamin A-specific exon 11, and deletion of the last 50 codons of exon 11 (De Sandre-Giovannoli et al., 2003; Eriksson et al., 2003). The resulting truncated protein (termed progerin) retains the CAAX box but lacks the endoproteolytic cleavage site so cannot be processed by Zmpste24, and is incorporated into the nuclear lamina carrying the C-terminal farnesyl group. Two unrelated patients with severe forms of HGPS have recently been reported carrying two new mutations (c.1968+1G>A and c.1821G>A), but both cause a more frequent use of the splice donor site that is activated in typical HGPS patients (Moulson et al., 2007). Other splice defects leading to the loss of *LMNA* exon 11 also result in the accumulation of farnesylated prelamin A and severe progeroid syndrome (Navarro et al., 2004). Hence, mutations resulting in prelamin A accumulation have a strong predictive character and novel mutations that result in similar defects are likely to produce a premature ageing phenotype. However, not all patients with a premature ageing phenotypes show signs of farnesylated prelamin A accumulation (Agarwal et al., 2008; Verstraeten et al., 2006), suggesting that there are other mechanisms involved (Fig. 3.1).

There are other mutations that also have a very strong predictive character, however without a clear understanding of the underlying pathogenic mechanism. For example the missense mutation p.R482W is reported in 141 individuals, 125 (88.7%) of these suffers from FPLD, 10 (7.1%) suffer

from FPLD with a skeletal muscle involvement and 29 relatives of affected individuals are asymptomatic. Although SREBP1, a dual role transcription factor regulating cholesterol biosynthesis and adipogenesis has been shown to bind to lamin A, it remains unknown if an alteration of this interaction by R482W is the underlying mechanism of FPLD (Lloyd et al., 2002).

Two other mutations with a strong predictive character are p.R453W which causes EDMD in 44/45 individuals who carry this mutation and p.S143P causing DCM-CD in 20/30 individuals who carry this mutation (10 asymptomatic relatives with p.S143P are described). For some mutations with a high predictive character and a large number of patients a founder effect is evident. For example the p.S143P mutation is common among Finnish DCM patients and haplotype analysis strongly suggests a founder effect for this mutation (Karkkainen et al., 2004).

Another example is the *LMNA* mutation p.R298C which is found in 44 (55%) patients who suffer from autosomal recessive Charcot-Marie-Tooth disease type 2A (AR-CMT2A) and 29 (36.3%) unaffected relatives (www.umd.be/LMNA). All of these individuals belong to large consanguineous families in northwest Algeria and east Morocco and form the only population in the world with this particular *LMNA* mutation. The identification of a common ancestral haplotype in 21 unrelated families in this region supports the idea of a founder mechanism (De Sandre-Giovannoli et al., 2002; Tazir et al., 2004).

3.1.2 *LMNA* mutations with an non-predictive genotype-phenotype link

Out of 206 missense mutations reported in the UMD database, only 20 (9.7%) mutations have been reported in more than 10 individuals, generally as a result of screening large families of patients with *LMNA* mutations (Garg et al., 2002; Jakobs et al., 2001; van Tintelen et al., 2007). The other 186 mutations have each been found in less than 10 individuals (often in only one or two), mainly due to mutation screening of specific patient cohorts (Brown et al., 2001; Perrot et al., 2009; Pethig et al., 2005; Scharner et al., 2011). Pathologies associated with these mutations mainly affect striated muscle (AD-EDMD, LGMD1B and DCM-CD) and adipose tissue (FPLD2). Mutations associated with each of the pathologies are distributed throughout the gene (Fig. 3.1) although mutational 'hot spots' have been described such as the Ig-fold domain for FPLD2 mutations and the central rod domain for DCM-CD mutations (Perrot et al., 2009; van der Kooi et al., 2002; Worman and Bonne, 2007).

3.1.3 Proposed genotype-phenotype links

So far there have been several suggestions for a genotype-phenotype link in laminopathies. However some of these correlations are based on a very small number of mutations and therefore merely indicate certain trends or are only valid for a subset of mutations. Below is a summary of proposed correlations between mutations in the *LMNA* gene and the resulting disease phenotype.

3.1.3.1 Mutations resulting in a premature translation termination codon (PTC) are associated with cardiomyopathy and late onset neuromuscular disease

Bonne et al. first attempted a genotype-phenotype correlation by mutation-type in *LMNA* (Bonne et al., 2000). Of the 53 patients analysed, all 12 with isolated heart involvement carried a nonsense mutation in p.Q6X of the head domain, indicating a link between lamin A/C haploinsufficiency and cardiac disease. In the remaining 41 patients with muscle weakness though, attempts to correlate disease severity with the protein domain affected by the missense mutations, proved inconclusive. Interestingly Lamin A/C haploinsufficiency also causes dilated cardiomyopathy in mouse. Wolf et al. (2008) reported early-onset programmed cell death of atrio-ventricular (AV) nodal myocytes, cardiac dilation and progressive electrophysiological disease in aged *lmna*$^{+/-}$ mice.

Whether haploinsufficiency is the primary cause for cardiomyopathy remains controversial. Geiger et al. (2008) have shown that truncated lamin A/C protein with a nonsense mutation in *LMNA* exon 6 (p.R321X) is detectable after proteasome inhibition and conclude that small amounts of truncated protein may interfere with normal lamin A function. Truncated lamin protein was also found in patients diagnosed with Heart-hand syndrome who suffer primarily from cardiac disease (Renou et al., 2008). Here, the inclusion of the last 11 nucleotides of intron *LMNA* intron 9 resulted in a frameshift and a PTC. Nuclei from patient fibroblasts displayed an abnormal morphology and intranuclear lamin A foci while lamin B and emerin was localised normally (Renou et al., 2008). In contrast, cardiac biopsies from DCM-CD patients with a heterozygous nonsense mutation in *LMNA* (p.E111X) showed reduced lamin A/C expression by Western blot. Truncated form of the protein was not detected, supporting haploinsufficiency as a probable disease mechanism (Arbustini et al., 2002).

Davies et al. proposed another theory of how *LMNA* mutations result in cardiomyopathy which supports haploinsufficiency as the disease mechanism in principle (Davies et al., 2011). Interestingly, mice homozygous for nonfarnesylated premature lamin A only (*lmna*$^{nPLAO/nPLAO}$) also develop cardiomyopathy (Davies et al., 2010). These mice express lamin A where the cysteine of the CAAX box is mutated to a serine. As a result, prelamin A is not farnesylated and does not undergo the first or second cleavage step while lamin C is not expressed. To demonstrate if the cardiomyopathy is caused by a toxic protein or a less active protein, *lmna*$^{nPLAO/-}$ mice were generated (Davies et al., 2011). If a toxic protein is the cause of the disease, the phenotype should be reduced in these mice. However, if the cardiomyopathy in *lmna*$^{nPLAO/nPLAO}$ mice was caused by a hypoactive protein, the phenotype is expected to be more severe. The results were very clear; *lmna*$^{nPLAO/-}$ had a greatly shortened survival, demonstrating that the cardiomyopathy is caused by the presence of non-functional lamin A protein. The authors therefore conclude that *LMNA* mutations can be divided into two categories – those yielding a toxic lamin and those yielding a functionally hypoactive lamin. Why the presence of non-functional lamin protein does not affect other tissues remains to be answered (Davies et al., 2011).

In human, Benedetti et al. separated neuromuscular patients according to the age of disease onset (Benedetti et al., 2007). The type of *LMNA* mutation differed, such that 89% (17/19) early-onset patients carried missense mutations and in-frame deletions, while only 63% (5/8) of late-onset patients did. The remaining three late-onset patients had frameshift mutations. Interestingly, variants associated with early-onset were primarily found in the Ig-like-fold (35%) and in coil 2A (24%) while variants associated with late-onset mainly occurred in coil 2B (60%) (Benedetti et al., 2007). These results indicate that the underlying disease mechanism may be more associated with the functional properties of the affected protein domain, rather than the type of mutation.

3.1.3.2 Mutations in the Ig-fold have different consequences at a molecular level

In 2002 the 3D structure of the Ig-fold domain was solved independently by Krimm et al. (2002) and Dhe-Paganon et al. (2002). In the more extensive study of the two, Krimm et al. characterised a number of mutations located on the Ig-fold domain and found that mutations associated with muscle-specific diseases are found in conserved hydrophobic and buried polar residues. In contrast, mutations associated with FPLD are located on three residues close in space, solvent accessible and lead to a diminution of the conserved positively charged character of a site defined by the three mutated residues (Krimm et al., 2002). They concluded that mutations located in the centre of the Ig-fold domain (which are more likely to destabilize the entire structure) are associated with a skeletal muscle phenotype while mutations associated with FPLD are located on the surface of the Ig-fold domain and destroy the positive charge of a potential interaction site. The structure of the Ig-fold with the FPLD mutation p.R482W was solved in 2009 (Magracheva et al., 2009). Superposition of wild-type and mutated molecules showed that the two structures are very similar. The mutant protein however forms intercalated dimers by interchanging their β-strand g'. Although not seen by others, this allosteric effect might point towards a different mechanism by which R482W results in disease.

Mutations associated with progeroid phenotypes located in the Ig-fold domain have also been shown to cluster in a 'hot-spot' (Verstraeten et al., 2006). Importantly, the authors highlight the fact that the progeria hot spot is physically separated from the FPLD hot spot identified by (Krimm et al., 2002). The authors hypothesise that progeria mutations in the Ig-fold destabilise the nuclear lamina, leading to pathology (Verstraeten et al., 2006), although the effects of the mutations on the surface charge of the Ig-fold were not analysed.

3.1.3.3 Mutations in Lamin A vs. mutations in Lamin A/C

Since *LMNA* is alternatively spliced, another way to classify *LMNA* mutations is whether they affect both lamin A and lamin C or just one protein. Of the 12 exons in *LMNA*, exons 11 and 12 are specific to lamin A, which is produced by alternative splicing of exon 10. The lamin C protein ends at exon 10 and has six unique C-terminal residues (Lin and Worman, 1993) (Fig. 1.4). Lamin C function is not well understood. Lamin A has been shown to required for the nuclear localisation of

lamin C, and has therefore been interpreted as being the more important protein (Vaughan et al., 2001). However, the apparent normal phenotype of the *lmna*$^{LCO/LCO}$ mouse, where lamin C is the only A-type lamin present, suggests that prelamin A and lamin A are dispensable (Fong et al., 2006b). Similarly, mice expressing only lamin A (mature form or pre-form) are also normal, which confirms a redundancy between A-type lamins (Coffinier et al., 2010; Davies et al., 2010).

Expectedly given its size, only 2 mutations, p.R571S causing DCM (Fatkin et al., 1999) and p.R571C causing muscular dystrophy with axonal neuropathy (Benedetti et al., 2005) have been associated with the lamin C-specific tail. Exon 12 encodes 8 amino acids that are cleaved during posttranslational modification of prelamin A, so unless mutations affect prelamin A processing, they would not be expected to effect lamin A function. Interestingly, few mutations occur in lamin A-specific exon 11 and those that do are less associated with skeletal muscle involvement and more with lipodystrophy, premature ageing and neuropathy (www.umd.be/LMNA).

3.1.4 Effect of modifying genes and single nucleotide polymorphisms on phenotypic variability in laminopathies

A large number of *LMNA* mutations show a high degree of inter- and intra-familial variability (Bonne et al., 2000). For example, patients carrying the p.R644C mutation have a range of clinical conditions incuding DCM, LGMD1B, atypical HGPS, lipodystrophy etc. which suggests that the genetic background contributed to disease phenotype (Brown et al., 2001; Csoka et al., 2004; Mercuri et al., 2005; Rankin et al., 2008).

The *LMNA* gene contains many single nucleotide polymorphisms (SNPs) with no pathologic phenotype: of 40 on the Leiden Open Variation Database (www.dmd.nl/lmna_seqvar.html), 75% (30/40) are silent mutations, and the rest are missense mutations affecting the head (one), central rod (three) or tail (six) domains. Depending on the context however, these mutations can cause disease: p.T528M or p.M540T alone appear non-pathogenic, but when inherited together, they result in HGPS but without prelamin A accumulation (Verstraeten et al., 2006). SNPs can also alter the clinical condition diagnosed: while the mutation p.S583L normally causes FPLD2, when present with T528M it results in FPLD1 (Savage et al., 2004).

In some patients, mutations in modifying genes such as emerin or desmin have been shown alter the EDMD phenotype caused by the *LMNA* mutation, providing evidence for epistasis (Muntoni et al., 2006). Furthermore, approx. 60% of all EDMD patients have no mutations in *LMNA, EMD* or *FHL1* which suggests that there are additional genes involved in EDMD pathology (Gueneau et al., 2009; Meinke et al., 2011). Mutations in nesprins for example have been found in patients with an EDMD phenotype (Zhang et al., 2007). However, it has not been excluded that the missense mutations are in fact polymorphisms in these patients and thus not EDMD-causing.

In summary, an influence of the genetic backround and modifying mutations on the phenotypic outcome is likely to explain the inconclusive attempts to associate mutation with laminopathy.

3.2 Aim

The aim of this chapter is to investigate genotype-phenotype links in laminopathies applying a very general approach including all mutations listed in the UMD database. By grouping mutations according to the resulting phenotype and statistically analysing general characteristics of mutations in these groups (such as the severity of the amino acid change or the position of these mutations within the protein structure) I aim to identify commonalities within each group. This will allow me to make predictions about the phenotypic outcome of a novel mutation and perhaps propose novel mechanisms through which mutations in the *LMNA* gene might cause a phenotype.

3.3 Results

3.3.1 The *LMNA* mutation dataset

The *LMNA* mutation dataset used for this meta-analysis was obtained from the Universal Mutation Database (www.umd.be/LMNA) last updated on 20.12.2010. The dataset lists 303 different *LMNA* mutations and 1560 patients (probands initially screened for mutations in *LMNA* and their and relatives) and provides genetic and clinical information for each patient. Unfortunately the dataset was not complete and contained errors so I added, removed, changed and combined data. Below are examples of changes made to the dataset I generated for my study, to illustrate what kind of errors were found and corrected.

I removed one patient entry from the database because the nucleotide change c.1073T>A did not match the protein modification reported (p.M358K). The missense mutation p.R343Q was not included in the analysis because none of the four entries with this mutation (1 proband and 3 relatives) was reported to have a phenotype. According to the original publication by Vytopil et al., the *LMNA* mutation p.R343Q was found in a group that served as negative controls for their study (Vytopil et al., 2002). Similarly the frameshift mutation p.A170PfsX7 was not included in this study because both patient entries reported with this mutation did not display a phenotype (Doh et al., 2009). Entries with different nucleotide changes that result in the same protein modification were combined in the analysis.

The clinical information available for each patient reported in the database varies. It ranges from a general diagnosis to very detailed description of the phenotype. To standardise the patient information available and prepare it in the context of genotype-phenotype correlations, I grouped patients into six phenotype categories based on the tissue affected: (1) 'skeletal muscle', (2) 'cardiac-only', (3) 'premature ageing', (4) 'lipodystrophy' and (5) 'neuropathy'. For a list of diseases belonging to each category refer to table 1.1. Patients that suffer from more than one disease or any other disease that does not fall in categories 1-5 are grouped into category (6) 'Other/Combined'.

3.3.2 Normalising the data entries

More than half (56.1%) of the mutations listed in the UMD dataset have multiple patient entries. Although in most cases, entries for a specific mutation are reported to have the same phenotype, there are other cases where one mutation is associated with multiple phenotypes likely due to genetic background or modifying mutations. To explore genotype-phenotype correlations, each mutation needs to be associated with a phenotype. In order to avoid artificial errors by assigning every mutation against a single phenotype, I have devised a phenotype weighing method to normalise the data. Each mutation was assigned a Phenotype Outcome Index (POI^{mut}) which represents the association of a mutation with a specific phenotype. Similarly, each amino acid residue was assigned a Phenotype Outcome Index (POI^{res}), which represents to what extent a given

residue is associated with a phenotype. This normalising method is described in detail below and is illustrated in figure 3.2.

3.3.2.1 Mutation Phenotype Outcome Index (POI^{mut})

To accurately represent the number of mutations that cause a specific phenotype, I have assigned a phenotype outcome index to each mutation. The index represents the percentage of patients with this phenotype for each mutation (it is therefore a numerical representation of the fraction of that mutation that contributes to a particular phenotype). **The total phenotype outcome index for each mutation will always add up to one and is defined as the normalised number of mutations (hereafter mutations^N) associated with that phenotype.** If more than one patient is reported for a given mutation, the mutation can contribute to multiple groups of phenotypes.

This is best explained by giving the following example (illustrated in Fig. 3.2): There are 3 patients reported with missense mutation p.Y45C. Out of these 3 patients, 2 patients have been diagnosed with EDMD (EDMD is classified as a 'skeletal muscle' phenotype). The third patient has been diagnosed with DCM-CD (DCM-CD is classified as a 'cardiac-only' phenotype). The missense mutation p.Y45C therefore was assigned: (i) a 'skeletal muscle' POI^{mut} of 0.67 (2/3 patient entries with this mutation) and (ii) a 'cardiac-only' POI^{mut} of 0.33 (1/3 patient entries with this mutation). Therefore, the p.Y45C mutation is associated with both a skeletal muscle phenotype and a cardiac-only phenotype to various degrees represented by the POI^{mut}.

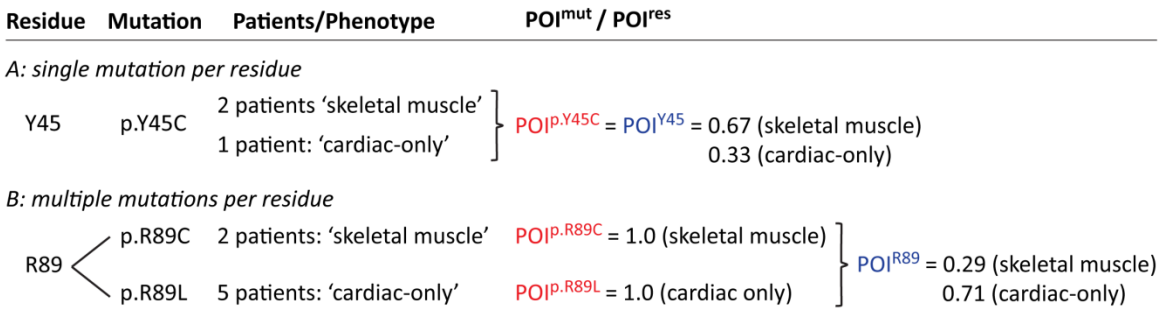

Figure 3.2 Calculation of the Phenotype Outcome Index for mutations (POI^{mut}) and residues (POI^{res}). (**A**) For residues with a single reported mutation the POI^{mut} (red) is the same as the POI^{res} (blue) and represents to what degree a mutation is associated with a phenotype. (**B**) For residues with more than one reported mutation, the POI^{res} reflects the phenotype outcome of all patients reported on that residue and gives an indication to what degree that the residue is associated with a phenotype.

3.3.2.2 Residue Phenotype Outcome Index (POI^{res})

Most of the data presented here are based on individual mutations and therefore uses POI^{mut} to weigh the phenotype. However some data are based on the properties of specific amino acid residues such as the heptad repeat position of residues in the central rod domain or the surface

exposure of residues in the Ig-fold domain. Because a number of residues in lamin A/C harbour multiple mutations, the phenotype was weighed by assigning each residue with a POI (POI^{res}). If there is only one mutation reported on a residue the POI^{res} is the same as the POI^{mut} (Fig. 3.2A). However, if multiple mutations occur on the same residue, their phenotype outcome is combined to calculate the POI^{res} for this residue (Fig. 3.1B). **The total POI^{res} for a single residue is always one and defined as the normalised number of unique residues associated with that phenotype (hereafter residues^{N})**.

Following is an example of calculating the POI^{res} for a unique residue with multiple mutations (illustrated in Fig. 3.2B): for residue R89, 2 patients are listed where the arginine is mutated to a cysteine (p.R89C). Both patients are reported to have a 'skeletal muscle' phenotype. In 5 other patients however, the arginine is mutated to a leucine (p.R89L), resulting in a 'cardiac-only' phenotype in all these 5 patients. When these two mutations are considered individually, their POI^{mut} would be 1.0 for (a) the 'skeletal muscle' phenotype and (b) the 'cardiac-only' phenotype, respectively. The POI^{res} for residue R89 however takes all seven patients with mutations on that residue into account, resulting in a 'skeletal muscle' POI^{res} of 0.29 (2/7 patient entries with mutations on this residue) and a 'cardiac-only' POI^{res} of 0.71 (5/7 patient entries with mutations on this residue).

3.3.3 Breakdown of the *LMNA* mutations from the UMD dataset

All together 1560 patients with 303 different pathogenic protein modifications, intronic mutations and silent mutations have been reported so far and are listed in the UMD dataset. I have sorted the data according to the type of mutation and the resulting phenotype and the results are summarised in figure 3.3.

The types of mutation have been classified into 5 different categories (Fig. 3.3A):

1. Missense mutations (206 or 67.9%) resulting in a single amino acid change.
2. Nonsense mutations (45 or 15.1%) resulting in a premature stop codon at the mutated amino acid or after a frame shift of various length. This group also contains mutations or deletion of the start codon (p.M1?) which is likely to result in a non-coding mRNA.
3. Intronic mutations (23 or 7.5%) represent the third largest group.
4. In-frame insertions and deletions of one or more amino acids (18 or 5.9%)
5. Silent mutations (11 or 3.6%) form the smallest category

Out of 1560 patients only 1338 were reported to have a clinical phenotype. The remaining 222 patients (exclusively relatives of probands) were asymptomatic at the point of data entry. In this study asymptomatic cases were not included for the following reason. Being relatives of probands they were usually tested either together with the symptomatic proband or shortly after the pathogenic mutation was discovered. It is therefore very likely that most, if not all of the asymptomatic cases had not yet developed a phenotype at the time of testing. It could also be that

the genetic background of relatives protected/delayed onset of the relevant laminopathy symptoms. It is important to note, that it is not possible to predict the phenotype these cases might develop solely based on the probands phenotype. Assigning asymptomatic cases with a hypothetic or predicted phenotype would therefore artificially inflate the strength of the dataset. Furthermore, including asymptomatic relatives would incorporate the risk of reducing the statistical power of the dataset by diluting the phenotypic value for each mutation.

The majority of *LMNA* mutations^N result in a skeletal muscle phenotype (137.4 or 42.5%) closely followed by a cardiac only phenotype (96.5 or 34.7%). The third most common phenotypic group includes the premature ageing disorders caused by 30.0 (9.9%) mutations^N. Lipodystrophy disorders are caused by 17.4 (5.7%) mutations^N while only 3.0 (1.0%) mutations^N cause neuropathy. The remaining 18.8 mutations^N (6.2%) cause other or combined phenotypes such as Insulin Resistance Syndrome (IRS) or a combination of FPLD and DCM-CD etc. (Fig. 3.3B).

In general, all phenotypic groups are predominantly caused by missense mutations. When analysing the different phenotypic categories for mutational biases I observed an interesting correlation in the 'cardiac-only' phenotype (Fig. 3.3C and D). When the proportions of the different types of mutations which cause the 'cardiac-only' phenotype is compared to the distribution of all mutations in the UMD dataset, it is significantly different. In total 395 'cardiac-only' patients with 96.5 different mutations^N are listed in the UMD dataset. Out of those 96.5 mutations^N 27.2 (28.1%) led to protein truncations, which is twice as many as would be expected statistically if they were randomly distributed. In contrast, when mutations resulting in a 'skeletal muscle' or 'premature ageing' phenotype are broken down into mutation type, an expected number of missense mutations, truncations, etc. is found. In other words, I have shown that patients who have an *LMNA* mutation that results in the truncation of the protein are more likely to develop DCM-CD compared to patients with missense mutations. In fact, when truncation mutations are considered only, the vast majority (60.4%) result in a 'cardiac-only' which confirms results obtained by others (Benedetti et al., 2007; Bonne et al., 2000) suggesting that mutations resulting in lamin A truncation primarily cause DCM-CD. However, if the truncation mutations result in protein expression which interferes with lamin A function or a loss of lamin A expression from the affected allele remains to be determined for the majority of the mutations (Geiger et al., 2008; Renou et al., 2008).

Although this analysis gives a good overview about the type of mutation that results in a certain phenotype, this correlation is very general. In order to allow more detailed predictions about the phenotypic outcome of a particular mutation, the mutations need to be examined in the context of the effects on specific protein/functional domains of the lamin A protein.

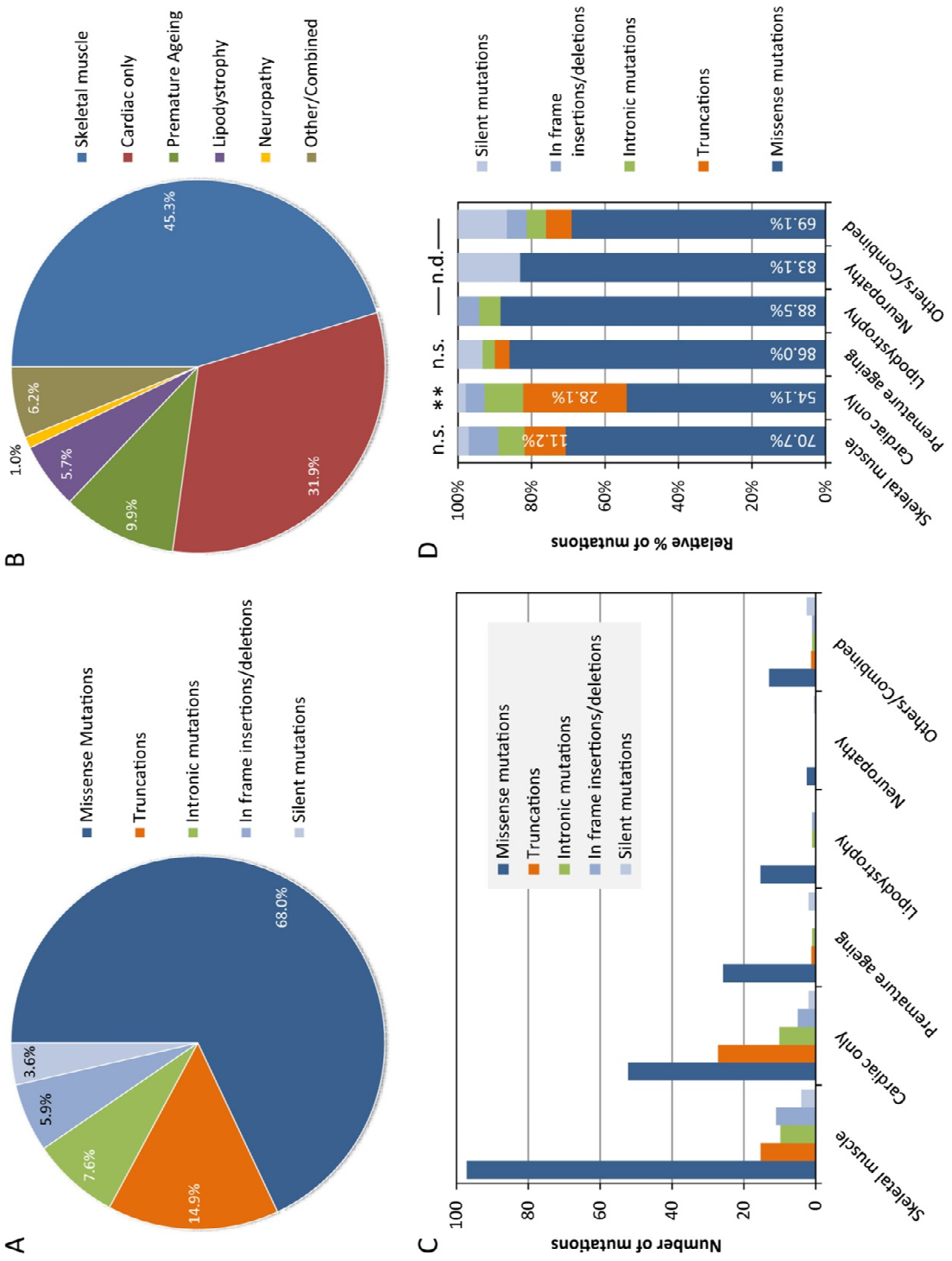

Figure 3.3 Breakdown of *LMNA* mutations from the UMD dataset. A total of 303 mutations are included in this study. (**A**) Breakdown of the dataset according to the type of mutation reported. (**B**) Breakdown of the dataset according to the clinical phenotype. (**C**) Number of mutations^{N} resulting in a specific laminopathy. The vast majority of mutations result in either a skeletal muscle phenotype or a cardiac-only phenotype. The next most common group of diseases are the premature ageing syndromes followed by lipodystrophy and neuropathy. (**D**) Relative percentages of mutations^{N} resulting in a specific phenotypic group. The proportion of different mutation types resulting in a 'cardiac-only' phenotype is significantly different to the global distribution with protein truncations being over-represented in this category. n.d. not determined; n.s. not significant; **p<0.01 (Chi-Square statistics)

3.3.4 Folded regions of the lamin A protein harbour more pathogenic missense mutations than unstructured regions

A large portion of the lamin A protein is folded into defined secondary and tertiary structures, including alpha-helices, and beta-sheets. To determine if mutations in these folded regions are statistically more likely to result in a pathogenic phenotype, I separated the protein into two regions: (1) one I termed the 'unstructured region', which includes the loosely organised globular head domain and the globular tail domain excluding the Ig-fold domain and is formed by 193 amino acids (2) and the second, the 'folded region', which includes the α-helices of the central rod domain, the linker and hinge regions of the central rod domain as well as the Ig-fold of the tail domain and consists of 471 amino acids (Fig. 3.4A).

Once I specified the different regions of the lamin A protein, I grouped all 206 missense mutations according to their location to either unstructured or folded regions (Fig. 3.4B and C). Out of 206 missense mutations, 169 (82.0%) are located in the folded regions while only 37 (18.0%) are located in the unstructured regions of the lamin A protein. The 206 different missense mutations affect 154 unique residues. When the data was normalised for unique residues (eliminating mutations located on the same residue) the distribution remained almost the same with 124 (80.5%) residues located in the folded region and 30 (19.5%) residues located in the unstructured region. If these values are compared to the expected values (assuming random mutational events approx. 71% would be found in the folded region), I found that a significantly larger proportion of missense mutations are located in folded regions even after normalising the data for unique residues.

Since it is statistically more likely that an amino acid change in the folded region results in a pathogenic phenotype, this result suggests that the folded domains of the lamin A protein play a more important role in lamin A function than unstructured region. This however, does not take into consideration mutations that have never been described due to embryonic lethality (which might be located in the unstructured region of the protein). In terms of total numbers of missense mutations and unique residues, both mutations in the central rod domain and the Ig-fold domain are equally likely to result in a pathogenic phenotype. So although folded domains are more affected, the central rod domain and Ig-fold domain contribute equally to this result.

To find out if mutations resulting in a certain phenotype are randomly distributed throughout the lamin A protein, the observed frequencies of phenotypes have been compared to the frequencies of phenotypes of all reported missense mutations. The result shows that mutations in the unstructured region of the lamin A protein result in a significantly different distribution of phenotypes when compared to all missense mutations. This is due to a reduced number of mutations resulting in a 'skeletal muscle' and 'cardiac-only' phenotype. Mutations resulting in 'lipodystrophy' and 'other/combined' phenotypes however, were overrepresented in the unstructured region of the lamin A protein. In contrast, mutations in the central rod domain or Ig-fold domain (analysed separately or combined), result in a statistically expected proportion of phenotypes (Fig. 3.4D).

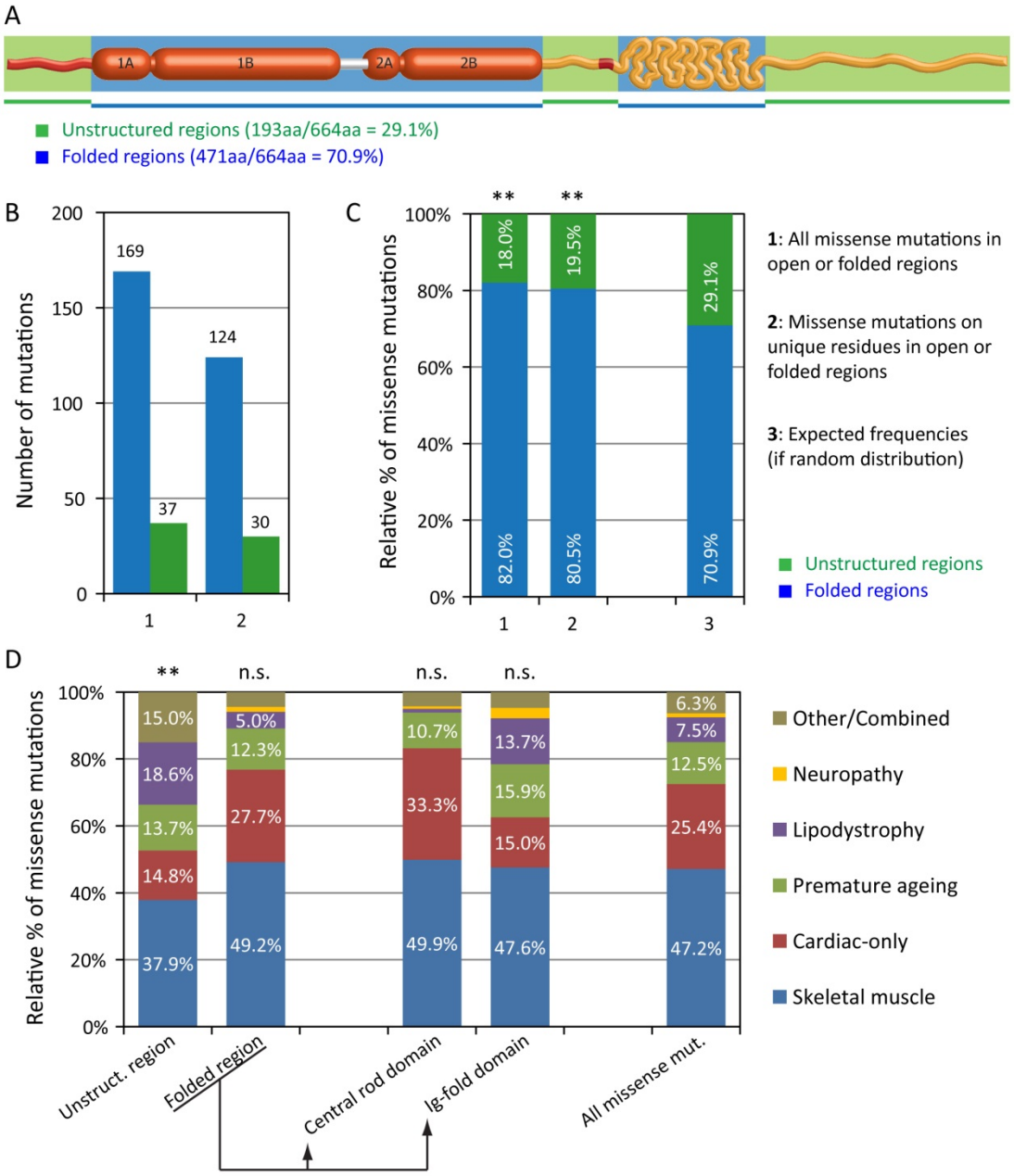

Figure 3.4 Separation of unstructured regions and folded domains in lamin A. (**A**) Schematic diagram of the lamin A protein with unstructred regions highlighted in green and folded regions highlighted in blue. The folded region includes the central rod domain and the Ig-fold domain while the unstructured region includes the head and tail domain and an unfolded region between the central rod and Ig-fold domain. (**B**) Absolute number of missense mutations located in unstructured or folded domains of the protein before and after removing mutations on residues with multiple reported mutations. (**C**) Relative percentage of missense mutations in unstructured regions or folded domains of the protein showing significantly more mutations located in the folded domains of the protein (before and after the removal of residues with multiple reported mutations). (**D**) Distribution of phenotypes caused by missense mutations located in unstructured region and folded domains of the lamin A protein compared to all reported missense mutations. The central rod domain and Ig-fold domain are analysed individually. Only mutations located in the unstructured region of the lamin A protein result in a phenotype distribution that is significantly different from the distribution of all reported missense mutations combined. ** p<0.01 (Chi-square statistics)

Interestingly, the proportion of mutations resulting in a cardiac phenoptype is slightly elevated in the central rod domain (when compared to the Ig-fold domain and all missense mutations combined) which confirms results by others who suggest that the central rod domain is a hot-spot for DCM mutations (Perrot et al., 2009).

A possible explanation could be that DCM mutations differentially affect lamin A binding partners such as c-Fos and Erk1/2 which have been shown to bind to the central rod domain (Gonzalez et al., 2008). Further evidence for this hypothesis is provided by lamin A mouse model where upregulation of the Erk1/2 signalling cascade has been shown to be involved in the development of cardiomyopathy (Muchir et al., 2007b; Muchir et al., 2009).

In summary, folded domains of the lamin A protein (the central rod domain and Ig-fold domain) harbour significantly more missense mutations than the unstructured region suggesting that these domains play a more important role in lamin A function/interaction with binding partners. At the same time, the proportion of mutations that cause a 'skeletal muscle' and 'cardiac-only' phenotype is reduced and 'lipodystrophy' and 'other/combined' phenotypes are overrepresented in unstructured regions of lamin A for reasons that are yet unclear.

3.3.5 Classification of the type of amino acid change

Even though all the mutations analysed are missense mutations, some result in amino acid changes in which the new amino acid is structurally/chemically similar to the original, while others introduce amino acids that confer quite different chemical side chains compared to the original residue. Amino acids can be classified into 4 groups according to the polarity of their side chain: (a) amino acids with nonpolar aliphatic and aromatic side chains (Gly, Ala, Val, Leu, Ile, Met, Phe, Trp); (b) amino acids with uncharged polar side chains (Ser, Thr, Asn, Gln, Tyr, Cys); (c) amino acids with positively charged side chains (Lys, Arg, His) and (d) amino acids with negatively charged side chains (Asp, Glu). Proline with its cyclic structure is generally considered a special amino acid (for amino acid structures see appendix 3).

To address the question of whether a larger number of pathogenic missense mutations arise from more drastic changes in the residue properties, I classified the missense mutations into 2 categories according to the chemical and physical properties of the amino acid change. 1) 'Drastic changes' of amino acid side chain characteristics are changes from nonpolar to charged or vice versa, a change of charge and changes to/from proline. 2) 'Moderate changes' of amino acid side chain characteristics are all other changes and include nonpolar to nonpolar, nonpolar to polar, charged to the same charge etc. (Fig. 3.5A).

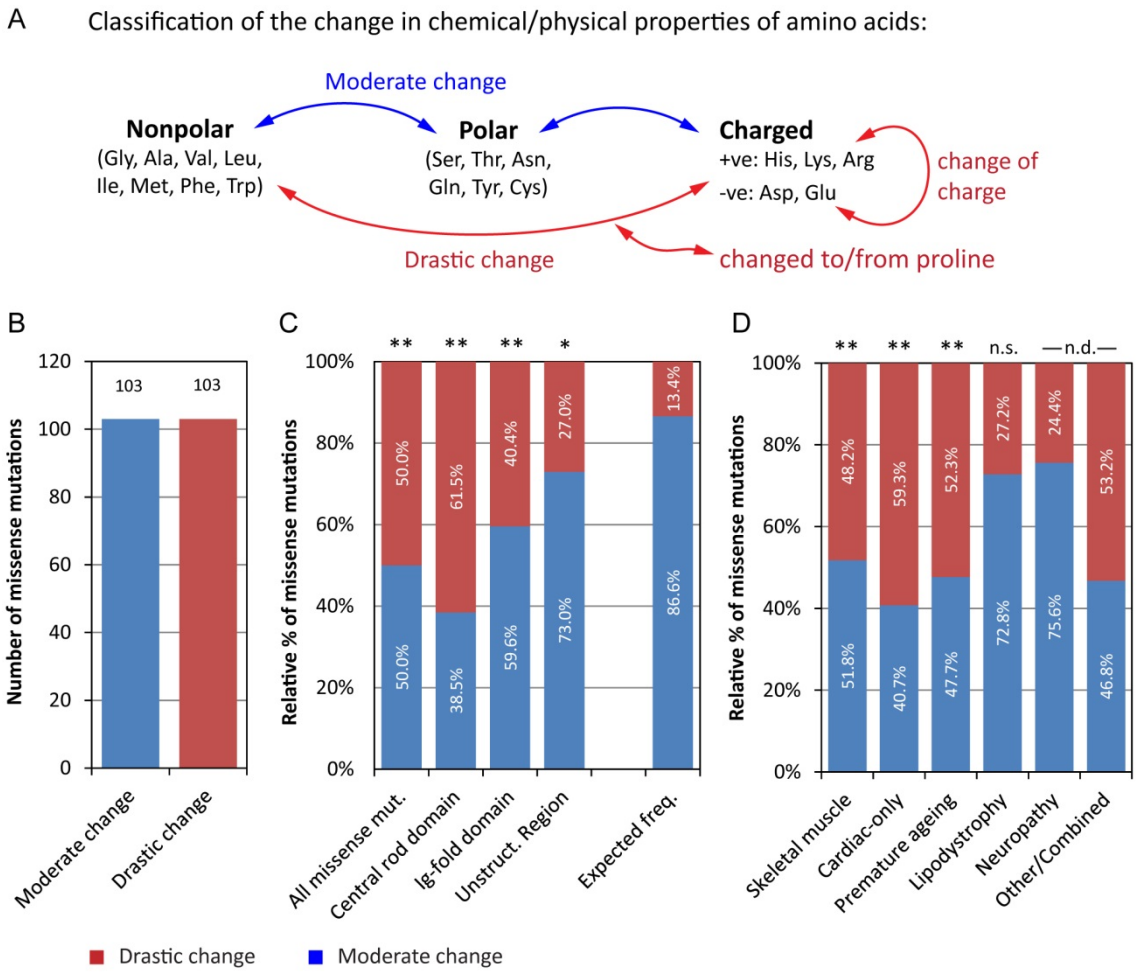

Figure 3.5 Classification of all missense mutations by the type of amino acid change. (**A**) Classification of the amino acid changes into 2 groups according to their chemical and physical properties. 'Drastic' amino acid changes are changes from hydrophobic to charged or vice versa, a change of charge and changes to/from proline. 'Moderate' amino acid changes are all other possible mutations. (**B**) Number of 'drastic' and 'moderate' missense mutations reported in the UMD database. Half of all missense mutations are classified as 'drastic'. (**C**) Relative percentages of 'drastic' and 'moderate' missense mutations reported along the entire lamin A protein or on specific protein domains. Taking all reported missense mutations into consideration, there are significantly more classified 'drastic' than would be expected statistically. (**D**) Relative percentages of 'drastic' and 'moderate' missense mutations for each phenotypic group. All three major phenotypic groups (skeletal muscle, cardiac-only and premature ageing) are caused by a significantly larger proportion of 'drastic' amino acid changes than expected. Expected frequencies represent relative percentages of all possible missense mutations (157 in total). n.d. not determined; n.s. not significant; ** $p<0.01$ (Chi-square statistics)

To determine if the number of drastic missense mutations found in the UMD dataset can be expected by chance, I compared it to the proportion of drastic amino acid changes of possible missense mutations. In theory any of the 20 standard amino acids can be mutated to any of the remaining 19 to qualify as a missense mutation, equating to a total of 380 different mutations. However, virtually all *LMNA* missense mutations listed in the UMD dataset arise from single nucleotide changes. This study therefore considers only those missense mutations that can arise from a single nucleotide change. For example the codons UAU and UAC encode for Tyr while the codons AAA and AAG encode for Lys. If only a single nucleotide is changed, a Tyr residue cannot be mutated to a Lys residue and vice versa. Excluding such mutations results in a total of 157 missense mutations, that can be caused by a single nucleotide change. Out of those 157, 21 (13.4%) missense mutations cause a drastic change in amino acid property while the remaining 136 (86.6%) missense mutations result in a moderate change in amino acid property (Fig. 3.5A).

If 'drastic' and 'moderate' amino acid changes are equally likely to cause a phenotype (assuming random mutational events) one would expect the proportion of 'drastic' missense mutations in the UMD dataset to be close to 13.4%. However, out of 206 missense mutations 103 (50%) classify as 'drastic' and 103 (50%) classify as 'moderate' amino acid changes (Fig. 3.5B). A significantly larger proportion of drastic amino acid changes is also found in each of the three sub-regions of the lamin A protein (Fig. 3.4C) which shows, not surprisingly, that 'drastic' amino acid changes are more likely to result in a phenotype than 'moderate' amino acid changes.

The question remains if all phenotypic groups arise equally from a larger proportion of 'drastic' mutations. To address this, I calculated the relative percentages of all reported 'drastic' and 'moderate' missense mutations grouped by phenotype (Fig. 3.5D). The result shows that three major phenotypic groups (skeletal muscle, cardiac-only and premature ageing syndromes) but not lipodystrophy, are caused by a significantly larger proportion of missense mutations classified as 'drastic' than what we would expect if we assume the occurrence of random mutational events. The number of mutations resulting in 'neuropathy' and 'other/combined' phenotypes is too small for statistical analysis.

3.3.6 Missense mutations in the central rod domain

The central rod domain of lamin A is formed of four α-helices two linker regions and one hinge region all of which engage in a coiled-coil dimerization with a second lamin A protein (see section 1.3.4.1). Sequences of α-helical coiled-coils display a periodicity of seven amino acids (heptad repeats) with nonpolar amino acids occupying heptad positions a and d. These hydrophobic residues form a hydrophobic seam running along the centre of the coils, stabilising the interaction (Parry et al., 2008). A typical example of a heptad repeat sequence (taken from the lamin A central rod domain) is illustrated in figure 3.6. If mutations on hydrophobic residues do destabilize α-helical coiled-coils, it can be hypothesised that the residues lining the inner surface of the coiled-coil

(a and d) are likely to be more sensitive to changes than those located on the outside of the coiled-coil. The lamin A central rod domain contains a total of 42 heptad repeat units. If pathogenic mutations would be distributed randomly throughout the central rod domain, we would expect approximately 2/7 (28.8%) of all mutations to fall on hydrophobic residues (a and d).

To test if this is true, all missense mutations and unique residues located within the 4 α-helices of the central rod domain were sorted according to their corresponding heptad repeat position and were plotted on a graph (Fig. 3.7A). Interestingly, missense mutations are not over-represented on hydrophobic heptad positions (a and d). When the proportion of mutation^N and unique residues^N on the seven heptad repeat positions were compared to the expected numbers, no significant difference was found (Fig. 3.7B). This might suggest that (a) either the stability of the α-helical coiled coil is not affected by mutations on hydrophobic heptad positions or (b) that destabilizing the α-helical coiled coils are not the underlying mechanism of phenotypes arising from mutations in the central rod domain.

Although the global analysis did not point to hydrophobic residues as being more susceptible to changes it was unclear if this is true for each individual phenotype. The next step was therefore to find out if all the major disease phenotypes are caused by an expected number of mutations on hydrophobic (a and d) or other (b, c, e, f and g) heptad repeat residues or if any of the phenotypes is caused by mutations that favour a specific heptad repeat position. Because of the low number of mutations in each category, hydrophobic (a and d) and other (b, c, e, f and g) heptad positions have been combined and were analysed together (Fig. 3.7C).

The result however, shows that none of the phenotypes are caused by a larger number of hydrophobic residues as statistically expected, although a trend was observed for mutations resulting in a skeletal muscle phenotype where one third of all mutations are located on heptad position a or d. Unfortuantely, the number of known mutations is currently not large enough to yield a conclusive result. However, the result indicates that for skeletal muscle laminopathies, heptad repeat positions might be affected to a larger extent, which could potentially lead to defective lamin dimerization or filament assembly.

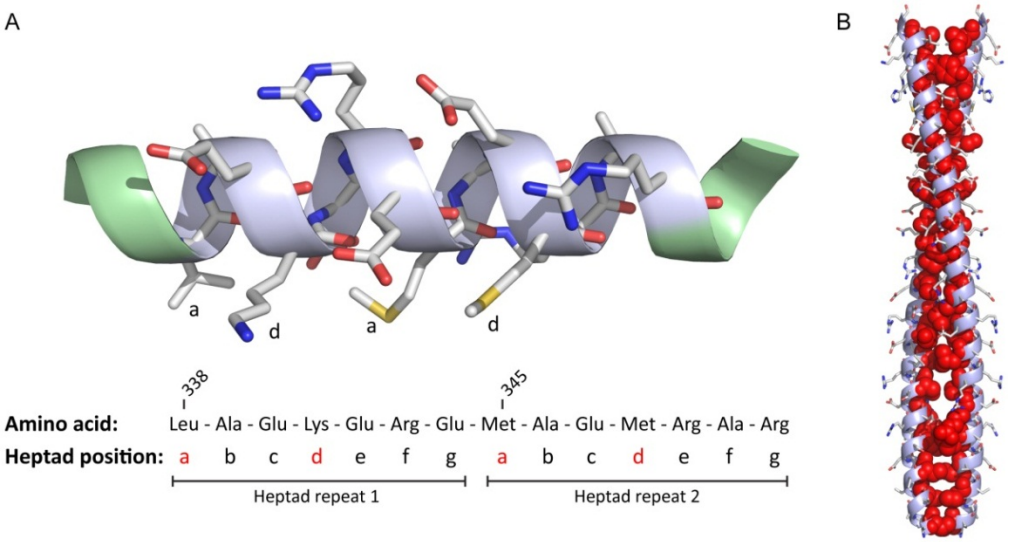

Figure 3.6 Heptad repeat sequence of the lamin A central rod domain. (**A**) Two consecutive heptad repeats (residues 338-351) from the human lamin A central rod domain are shown with nonpolar amino acids occupying heptad positions a and d. Occasionally charged amino acids are located on position a or d such as lysine 341. In this case, lysine 341 forms a salt bridge with a glutamate residue of the neighbouring α-helix, reinforcing the coiled-coil (Kapinos et al., 2011). (**B**) Structural representation of a coiled coil α-helix. Residues located on heptad positions a and d are shown in space fill (highlighted in red) and form a seam along the interface of both a α-helices.

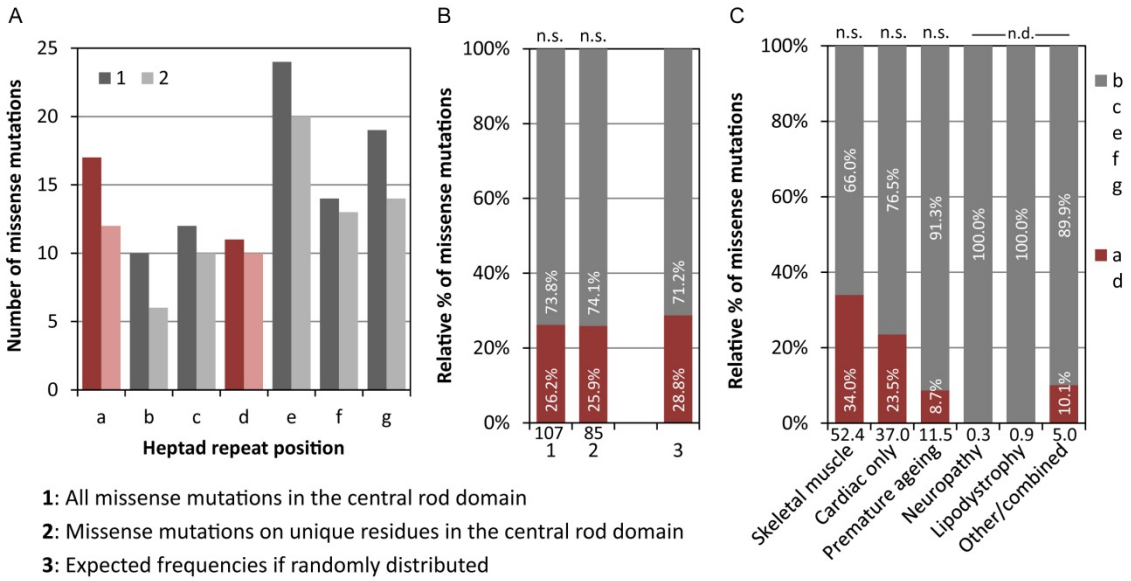

Figure 3.7 Occurrence of missense mutations on specific heptad repeat positions. (**A**) Absolute numbers of missense mutations (1) and numbers of unique residues with pathogenic missense mutations (2) located on hydrophobic (red) and other (grey) heptad repeat positions. (**B**) Relative percentage of missense mutations located on hydrophobic (a and d) and other (b, c e, f and g) heptad positions. Hydrophobic residues (a and d) are marked in red in all 3 panels. (**C**) Relative percentage of missense mutations resulting in a specific phenotype located on hydrophobic (a and d) and other (b, c e, f and g) heptad positions. For all major disease phenotypes a statistically expected number of mutations is found on both, hydrophobic and other heptad positions; The number of mutations in each category is indicated on the x-axes; n.d. not determined; n.s. not significant

3.3.7 Missense mutations in the Ig-fold domain

3.3.7.1 Surface exposure as a potential link between genotype and phenotype

The Ig-fold domain stretches from residue 428-547 of the lamin A protein and encodes two β-sheets which fold to form a β-sandwich (see section 1.3.4.2). The 3D structure of the Ig-fold domain has been solved independently by Krimm et al. (2002) and Dhe-Paganon et al. (2002). For this study, the NMR structure from Krimm et al. (PDB ID 1IVT) was used since it covers a longer length of the Ig-fold domain and is thus likely to present a more accurate structure. For a detailed description of structure manipulation and graphical representation refer to section 2.2.6.

My results described above show that in the Ig-fold, the severity of the amino acid change cannot be used to predict the phenotypic outcome of the mutation. The question here is, if the spatial position of the residues within the Ig-fold, i.e. buried or exposed, can be statistically associated with certain phenotypes, which was first proposed by Krimm et al. (2002) for lipodystrophy disorders.

In order to address the question, I first calculated the Solvent Accessible Surface Area (SASA) for each amino acid residue in the protein model of the Ig-fold domain with the Parameter Optimised Surfaces (POPS) program (Cavallo et al., 2003; Fraternali and Cavallo, 2002). The SASA of the amino acid in the Ig-fold was then compared to the SASA of the same amino acid in the tripeptide Ala-Xxx-Ala (isolated form) which was considered to be the maximum SASA (Fraternali F., personal communication). Residues are defined as buried when its SASA in the protein is lower than 20% of its SASA in the tripeptide Ala-Xxx-Ala. The relative values of surface exposure for residues of the Ig-fold are visualised graphically in figure 3.8A with the 20% cut-off indicated as a red line.

In total 38 residues (31.7%) in the Ig-fold domain have a relative surface exposure of less than 20% and are therefore considered buried. If mutations on buried and other residues are equally likely to result in a phenotype we would expect approximately 32% of all residues that are associated with disease to be buried residues. However, out of the 34 residues that cause a phenotype when mutated, 17 (50%) are found on buried residues which is significantly more than statistically expected (p=0.0215, Chi-square statistics).

Next, the residues were sorted according to the phenotype they are associated with to analyse if buried or exposed residues are more likely to result in a certain phenotype when mutated. According to the numbers shown in figure 3.8B the distribution of residues resulting in 'skeletal muscle' disorders when mutated is significantly different from expected numbers of buried, intermediate and exposed residues. Here 10.1 residues^N (61.4%) instead of the expected 5.1 residues^N (i.e. twice the number) fall within the buried amino acid category. In contrast, a lower proportion of residues associated with other phenotypic groups seem to be located on buried residues. Unfortunately, the number of residues associated with the other phenotypic groups was not large enough to apply Chi-square statistics. In the entire Ig-fold there are 16.5 residues^N

associated with a skeletal muscle phenotype. The other phenotypic groups are associated with considerably less residues, in descending order: 'premature ageing' (5.3 residues^{N}), 'cardiac phenotype' (4.5 residues^{N}), 'lipodystrophy' (4.4 residues^{N}) and 'neuropathy' (1.6 residues^{N}).

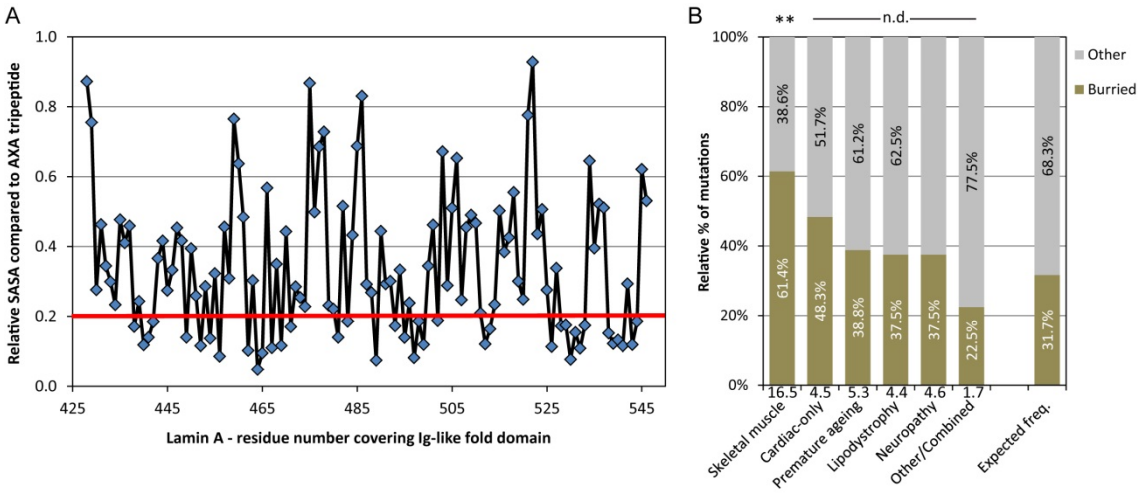

Figure 3.8 Parameter Optimises Surfaces (POPS) analysis of the Ig-fold domain. (**A**) POPS analysis on the lamin A Ig-fold domain (PDB ID 1IVT) was performed using the online server available at http://mathbio.nimr.mrc.ac.uk/wiki/POPS (Cavallo et al., 2003). The graph displays the relative solvent accessible surface area (SASA) of each amino acid residue in the Ig-fold domain (residues 428-547) compared to the SASA of the same amino acid in the Ala-X-Ala tripeptide. Residues with less than 20% exposure (indicated by the red line) are considered buried. (**B**) Relative percentages of mutations located on buried/other residues (identified in A) associated with a specific phenotype. The results show that mutations causing a skeletal muscle phenotype are significantly more likely to fall on a buried residue. Number of mutations in each category is indicated on the x-axes; n.d. not determined; ** p<0.01 (Chi-square statistics)

3.3.7.2 Visualising mutations in a spatial context reveals that they cluster for specific phenotypic groups

Since most disease categories are only caused by mutations on a small number of residues in the Ig-fold, I have chosen a more direct approach to find a correlation between mutation/residue and the phenotype. The 3D structure of the lamin A Ig-fold is freely available and can be manipulated in a number of ways using different molecular visualisation tools such as PyMOL. The strategy employed here was to bring residues that are strongly associated with a certain phenotype into a spatial context by highlighting them on the 3D structure of the Ig-fold (Fig. 3.9). The advantages of doing this are threefold: 1) By looking at every residue change individually, even a small number of mutations can yield strong correlation. 2) Residues that would not be associated with each other by looking at the primary sequence are brought into a spatial proximity and this might highlight regions of special interest. 3) Amino acids can be mutated *in silico* to predict chemical and physical changes they might cause to the structure.

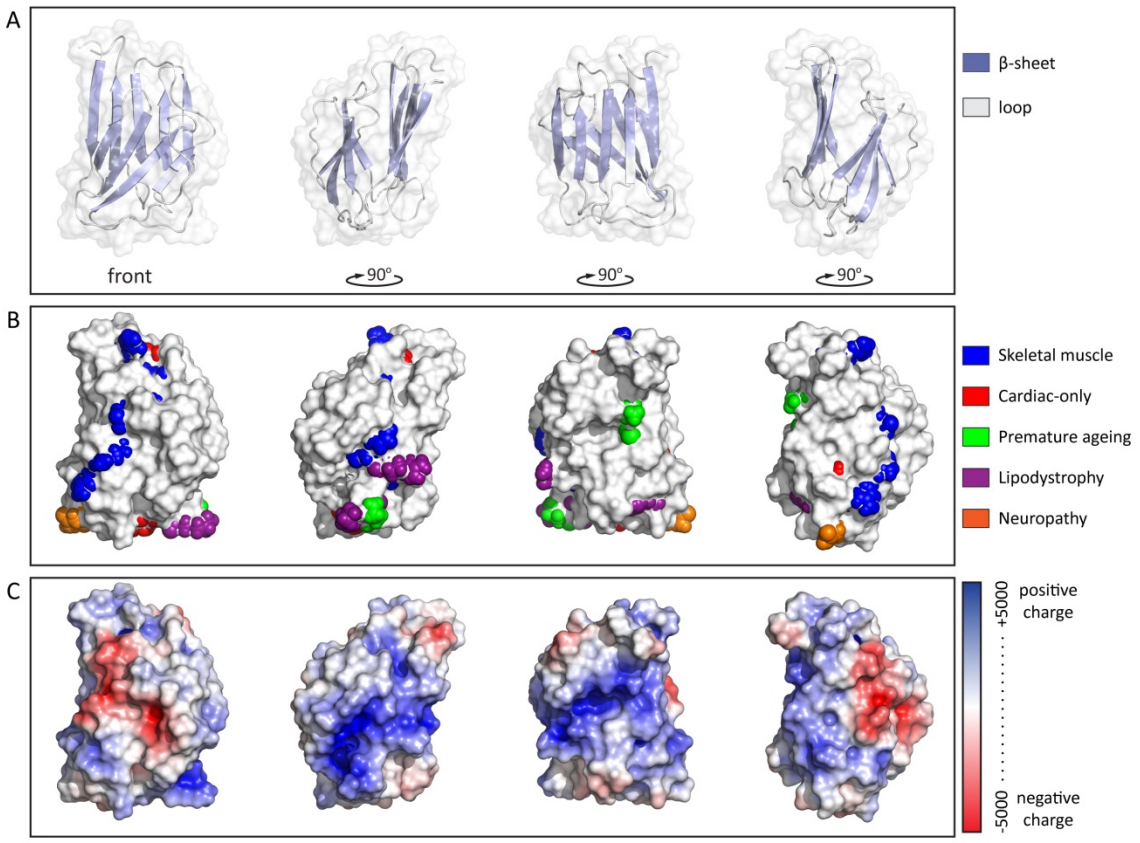

Figure 3.9 Location of residues associated with a specific phenotype (when mutated) on the 3D structure of the wild-type lamin A Ig-fold domain. (**A**) Backbone of the wild-type lamin A Ig-fold domain viewed from 4 different angles, rotated by 90°. The β-sheets forming the β-sandwich are indicated in blue, loops are indicated in grey. (**B**) Representation of the surface of the Ig-fold (white). Amino acid residues associated with a certain phenotype (when mutated) are highlighted in colour: skeletal muscle (blue), cardiac-only (red), premature ageing (green), lipodystrophy (purple) and neuropathy (orange). (**C**) Electrostatic surface potential of the Ig-fold. Blue areas indicate a positive surface potential while red areas represent negative surface charge of the protein.

Figure 3.9A shows the backbone structure of the Ig-fold in four orthographic views to help with the three dimensional orientation. Figure 3.9B shows the surface representation of the Ig-fold in the same orientation as the backbone structure above. In addition, residues showing a strong association with a certain phenotype are highlighted in different colours. In figure 3.9C the electrostatic surface potential of the Ig-fold is shown.

Residues visualised in figure 3.9B are those with a very high association (phenotype outcome index >0.9) with particular phenotype. The result clearly shows that residues that do cause a certain phenotype when mutated cluster together on the surface of the 3D structure of the Ig-fold which confirms results obtained by others (Krimm et al., 2002; Verstraeten et al., 2006). Residues in blue are associated with a skeletal muscle phenotype and are mainly located on a negatively charged phase of the β-fold. Residues associated with premature ageing (green) and lipodystrophy (purple)

are located in regions on the opposite phase of the structure. For residues associated with a 'cardiac only' phenotype (red) no specific region could be identified and only one residue located on a loop was strongly associated with neuropathy (orange).

Another interesting observation is that all regions that contain mutations carry either a strong negative charge or a strong positive charge while regions with a neutral electrostatic surface potential seem to be free of pathogenic amino acid changes (Fig. 3.9B and C).

From previous results (Fig. 3.4) we saw that mutations causing 'premature ageing' and 'lipodystrophy' syndromes are over-represented in the Ig-fold. This, and the fact that mutations causing these phenotypes cluster together in specific regions of the 3D structure of the Ig-fold strongly suggests that there is a specific interaction at this point (either with lamin A itself or other proteins) that if disrupted, leads to a certain phenotype. To analyse this finding in greater detail, I took all of the mutations that are both partially exposed at the surface and fall within a contained region of the Ig-fold causing the same phenotype, and re-analysed them on an individual basis.

3.3.7.3 In silico mutagenesis of the lamin A Ig-fold identifies consistent changes of surface charge for some laminopathies

After the identification of specific regions that seem to be associated with a certain phenotype, the question arose if mutations in these regions all cause the same change to the surface charge of the Ig-fold. To answer this, I applied *in silico* the mutagenesis plug-in of the visualisation software PyMOL to mimic mutational changes to amino acid residues in the Ig-fold domain.

After mutating residues in the Ig-fold with PyMOL (see section 2.2.6 for details) the surface potential of each isoform was compared to the wild-type structure to establish if mutations in the region analysed (for a specific phenotype) alter the surface potential of the Ig-fold in the same way. Four regions of the Ig-fold were analysed this way: the skeletal muscle regions 1 and 2 (Fig. 3.10), the premature ageing region (Fig. 3.11) and the lipodystrophy region (Fig. 3.12). The summary of the findings are summarised in table 3.1.

<u>Mutations resulting in a skeletal muscle phenotype</u>

Residues resulting in a skeletal muscle phenotype when mutated cluster to 2 main regions on the Ig-fold. The first region is located along the front of the Ig-fold and forms a negatively charged ridge. The second region clusters between both β-sheets around residue Y481 forming a positively charged area (Fig. 3.10). When the electrostatic surface potential of each mutation in cluster 1 is compared to wild-type, it becomes obvious that these changes are not consistent among different mutations.

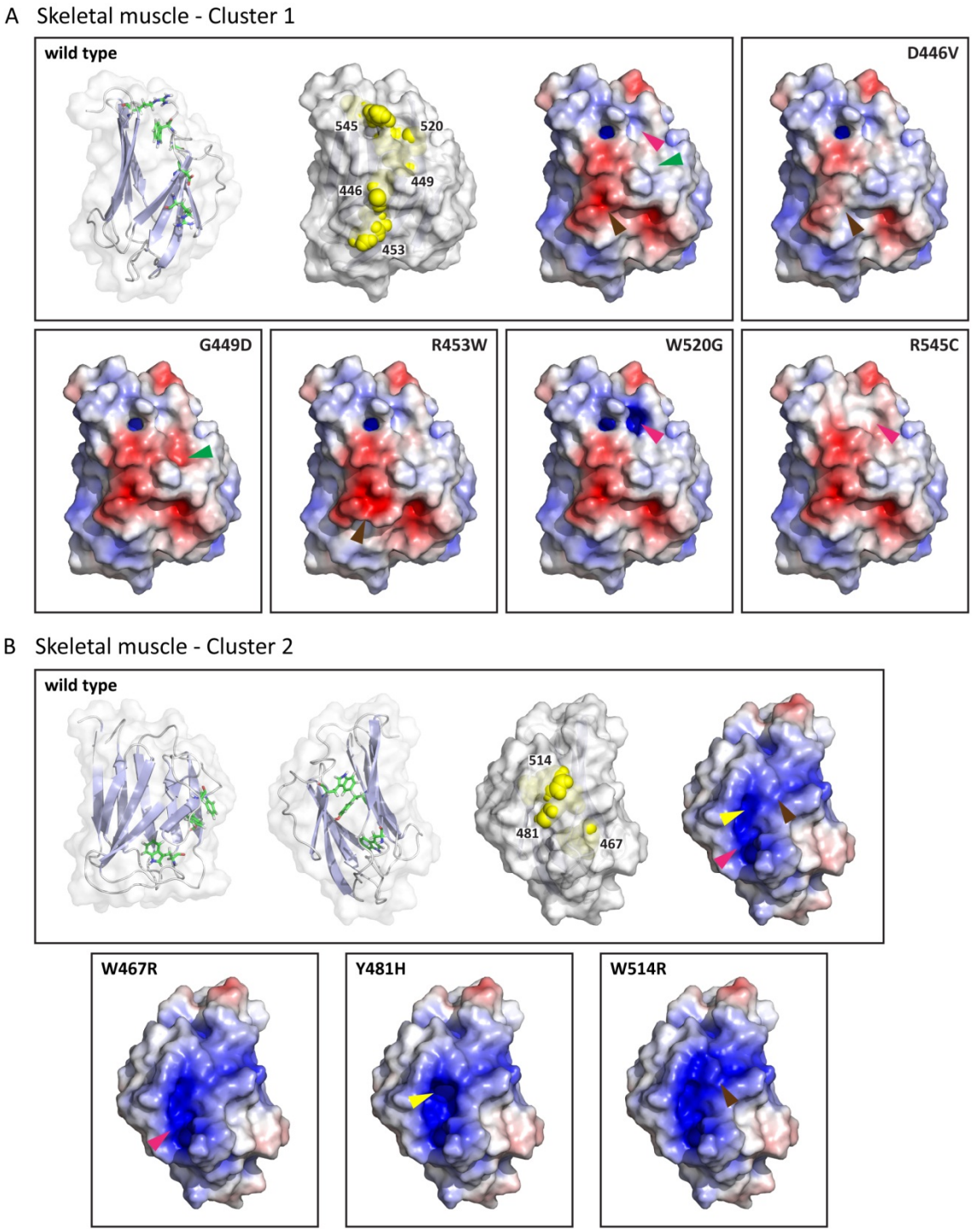

Figure 3.10 Change in the electrostatic potential with mutations causing a skeletal muscle phenotype. Shown are the Ig-fold backbone, positions of residues subjected to *in silico* mutagenesis (in yellow) and the electrostatic surface potential of wild-type as well as mutated structures. I have identified two main clusters of residues on the Ig-fold that result in a skeletal muscle phenotype when mutated. Cluster 1 is located on one side of the β-sandwich and involves residues. D446, G449, R453, W520 and R545 while cluster 2, located on the opposite β-sheet and involves residues W467, Y481 and W514. Coloured arrows indicate areas of the mutated Ig-fold that are affected by each amino acid change.

Three out of six mutations located in this region cause an increase of positive charge (p.D446V, p.W520G and p.W520S), two mutations result in an increase in negative charge (p.G449D and p.R453W) and one mutation causes a reduction in the positive charge (p.R545C).

Mutations in the second cluster identified on the other hand, lead to a very consistent surface charge change in this area. All three mutations (p.W467R, p.Y481H and p.W514R) substantially increase the positive charge already present in this area (Fig. 3.10, summarised in table 3.1).

The fact that mutations resulting in a 'skeletal muscle' phenotype in region 1 do show such large variations in terms of the change to the surface potential they cause is not surprising. As shown above, residues associated with a skeletal muscle phenotype are statistically more likely to be buried. Notably, a number of residues (including residues G449, W467 and Y481) are buried entirely. This result supports the theory proposed by others (Krimm et al., 2002) that mutations giving rise to a skeletal muscle phenotype are more likely to disrupt the structural core of the Ig-fold. So instead of just disrupting the surface charge, mutations of buried residues might also lead to a destabilisation of the overall Ig-fold structure. This however does not mean that all mutations resulting in a skeletal muscle phenotype do so by the same mechanism. Here I present strong evidence that there are skeletal muscle mutations on the Ig-fold that, although on buried residues, do seem to affect the surface charge of region 2 in a very specific way, increasing the positive charge of a potential interaction site.

Mutations resulting in a premature ageing phenotype

The premature ageing phenotype is currently associated with eight different missense mutations affecting residues clustering around residue R527, which is part of positive surface charge patch on the back side of the Ig-fold. Six mutations (p.R435C, p.R471C, p.R527C, p.R527H, p.A529T, and p.K542N) result in a reduction of the positive charge within this region (Fig. 3.11, summarised in table 3.1).

Two mutations located in the same cluster (p.T528M/p.M540T) have been shown to cause HGPS when inherited together, whereas alone, they appear to be non-pathogenic (Verstraeten et al., 2006). Interestingly, p.M540T results in a slight increase in the positive charge in this region of the Ig-fold which is inconsistent with the other five mutations. In contrast, the second mutation (p.T528M) does not affect the surface charge of the Ig-fold domain (not depicted in Fig. 3.11).

Importantly, all patients with progeroid phenotypes (MADA or HGPS) who carry mutations in this cluster have been shown to be homozygous for that mutation (Agarwal et al., 2008; Kosho et al., 2007; Novelli et al., 2002; Plasilova et al., 2004; Simha et al., 2003; Youn et al., 2010). One further patient is compound heterozygous for two mutations located in the cluster (p.R471C/R527C) (Cao and Hegele, 2003), both resulting in a reduction of the positive charge in the domain surface. Unfortunately, most studies did not test patient cells for prelamin A accumulation. However, those

that did test for it found no evidence of prelamin A accumulation (Agarwal et al., 2008; Verstraeten et al., 2006).

Together, this provides strong evidence for a very consistent genotype-phenotype where homozygous or compound heterozygous mutations located in a small cluster on the Ig-fold domain all result in progeroid phenotypes.

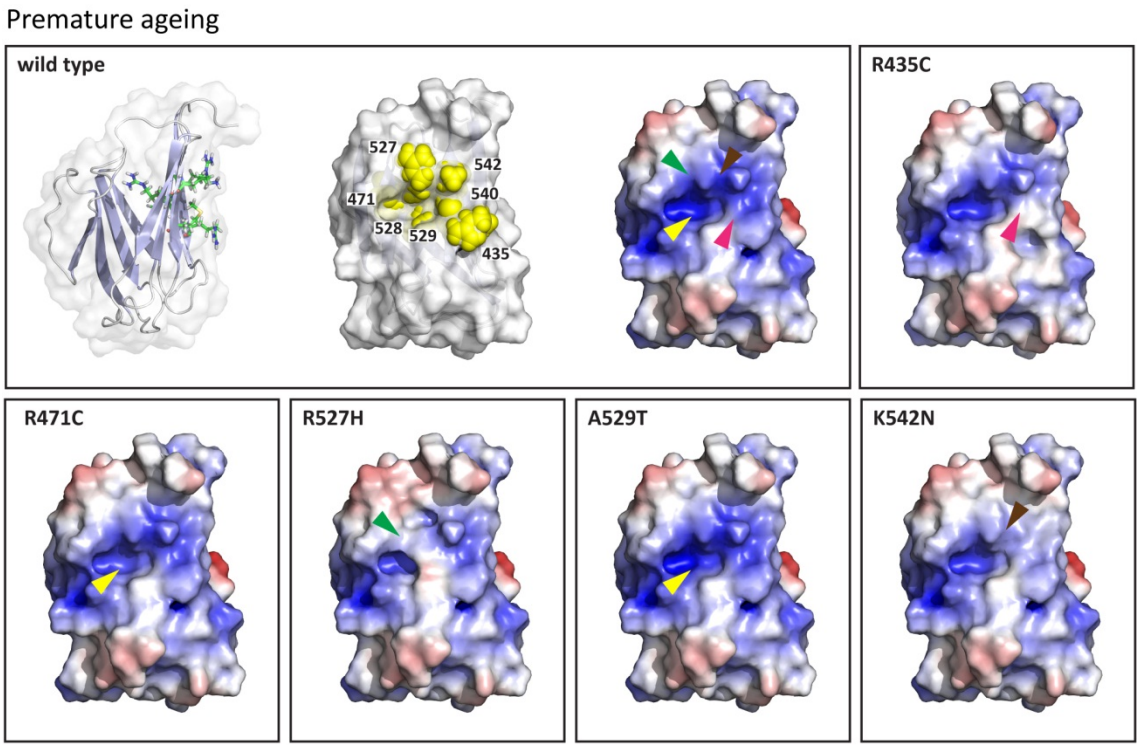

Figure 3.11 Change in the electrostatic potential with mutations causing premature ageing syndromes. Shown are the Ig-fold backbone, positions of residues subjected to *in silico* mutagenesis (in yellow) and the electrostatic surface potential of wild-type as well as mutated structures Coloured arrows indicate areas of the mutated Ig-fold that are affected by each amino acid change.

Mutations resulting in a lipodystrophy phenotype

The last cluster I analysed includes mutations that lead to a lipodystrophy phenotype. It is located in a region at the back of the Ig-fold, adjacent to the skeletal muscle cluster 2 and includes residues R439, G465, R482 and K486 forming a negatively charged patch in this area. Five of the six mutations found in this region (p.R439C, p.G465D, p.R482W, p.R482Q and p.K486N) result in an increase of the negative charge while one mutation (p.R482L, not shown) results in a reduction of the positive charge surrounding the area of interest (Fig. 3.12, summarised in table 1.1).

Lipodystrophy

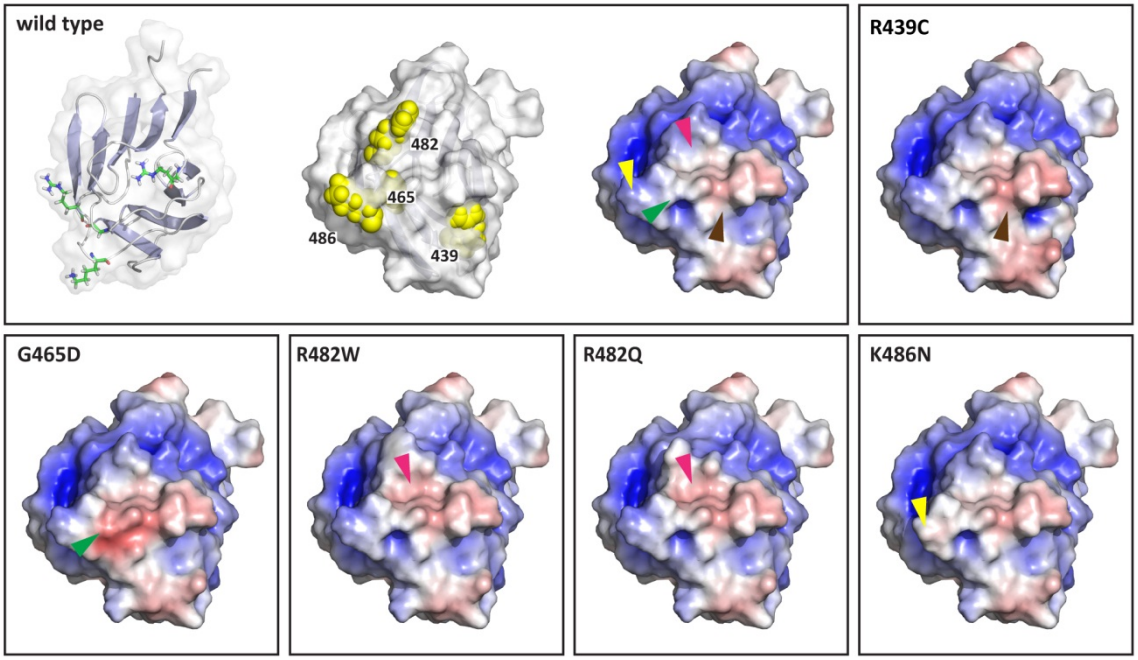

Figure 3.12 Change in the electrostatic potential with mutations causing a lipodystrophy phenotype. Shown are the Ig-fold backbone, positions of residues subjected to *in silico* mutagenesis (in yellow) and the electrostatic surface potential of wild-type as well as mutated structures. Coloured arrows indicate areas of the mutated Ig-fold that are affected by each amino acid change.

Table 3.1 Summary of the effects of amino acid changes on the electrostatic surface potential of the Ig-fold.

Phenotypic group	Mutation	Relative SASA	Effect on electrostatic surface potential	Correlation
Skeletal muscle (cluster 1)	p.D446V	0.33	Increase of positive charge (mod)	
	p.G449D	0.14 (b)	Increase of negative charge (strong)	
	p.R453W	0.29	Increase of negative charge	
	p.W520G	0.25	Increase of positive charge	Not consistent
	p.W520S*	0.25	Increase of positive charge	
	p.R545C	0.62	Reduction of positive charge	
Skeletal muscle (cluster 2)	p.W467R	0.11 (b)	Increase of positive charge (strong)	
	p.Y481H	0.14 (b)	Increase of positive charge (strong)	Consistent
	p.W514R	0.23	Increase of positive charge (mod)	
Premature ageing	p.R435C	0.48	Reduction of positive charge (strong)	
	p.R471C	0.17 (b)	Reduction of positive charge (mod)	
	p.R527C*	0.34	Reduction of positive charge (strong)	Consistent
	p.R527H	0.34	Reduction of positive charge (strong)	
	p.A529T	0.18 (b)	Reduction of positive charge (mod)	
	p.K542N	0.29	Reduction of positive charge (strong)	
	p.T528M*/	0.17 (b)	No change in charge observed	(not consistent with
	p.M540T*	0.13 (b)	Increase of positive charge (slight)	other mutations)
Lipodystrophy	p.R439C	0.24	Increase of negative charge (strong)	
	p.G465D	0.09 (b)	Increase of negative charge (strong)	
	p.R482W	0.52	Increase of negative charge (mod)	
	p.R482Q	0.52	Increase of negative charge (mod)	Consistent
	p.R482L*	0.52	Increase of negative charge (mod)	
	p.K486N	0.83	Increase of negative charge (mod)	

abbreviations: SASA, solvent accessible surface area; b, buried; * not shown in figures 10-12; The effect on electrostatic surface potential was estimated viasually.

To summarise the findings above, all the changes identified in the *in silico* mutagenesis analysis for each mutation together with the SASA information has been listed in table 3.1. The results suggest that there are defined regions in the Ig-fold that, when mutated, cause a specific change in charge that results in either a premature ageing, or lipodystrophy phenotype.

3.3.7.4 Comparison of mutations on the same/adjacent residue resulting in different phenotypes

Although the clusters of mutations that result in a specific phenotype are in distinct regions of the Ig-fold, some residues within or nearby these clusters have been reported to cause a different phenotype. For example, direct comparison of two neighbouring mutations (p.R527H, resulting in a premature ageing phenotype with p.T528R, resulting in a skeletal muscle phenotype) revealed opposing effects on the surface charge in the region. When the Arg527 is substituted with a histidine, the positive charge in the region is decreased. When the neighbouring Thr528 however is substituted with an arginine, the positive charge is increased (Fig. 3.13A). Another mutation reported on Thr528, p.T528K, is also predicted to increase the positive charge and also results in a skeletal muscle phenotype. This result suggests that a potential interaction site is affect by opposite charge changes which may explains why mutations located on neighbouring residues result in different phenotypes.

However, there are two other crucial differences between these mutations/residues: (1) progeroid patients are homozygous for p.R527H (Novelli et al., 2002; Simha et al., 2003) while patients with a skeletal muscle phenotype are heterozygous for p.T528R (Vytopil et al., 2003) and p.T528K (Bonne et al., 2000; Raffaele Di Barletta et al., 2000). (2) Arg527 is exposed (rel. SASA=0.34) while Thr528 is buried (rel. SASA=0.17).

Taken together this supports the hypothesis that buried residues are associated with a skeletal muscle phenotype (Krimm et al., 2002). However, it also raises the possibility of a new pathogenic mechanism for progeroid phenotypes associated with mutations in the Ig-fold, potentially involving lamin A interacting proteins.

The second example involves neighbouring residues located in 2 different disease regions of the Ig-fold, the skeletal muscle region 2 and the lipodystrophy region. Residue Y481 is located in the positively charged pocket; residue R482 on the other hand is located in the negatively charged area adjacent to it. Interestingly, mutations on the two residues result in opposite charge changes that are constrained to their respective region. Mutation p.Y481H increases the charge of the positively charged pocket and always results in a skeletal muscle phenotype (POI 1.0). Mutation p.R482W however increases the negative charge in the adjacent region without affecting the positively charged pocket and mainly results in lipodystrophy disorder (POI 0.93) (Fig. 3.13B). This result supports the hypothesis that there are specific regions of the Ig-fold that are particularly sensitive and result in a certain phenotype when altered. Again, this can also provide an explanation of how mutations on residues located next to each other result in a different phenotype.

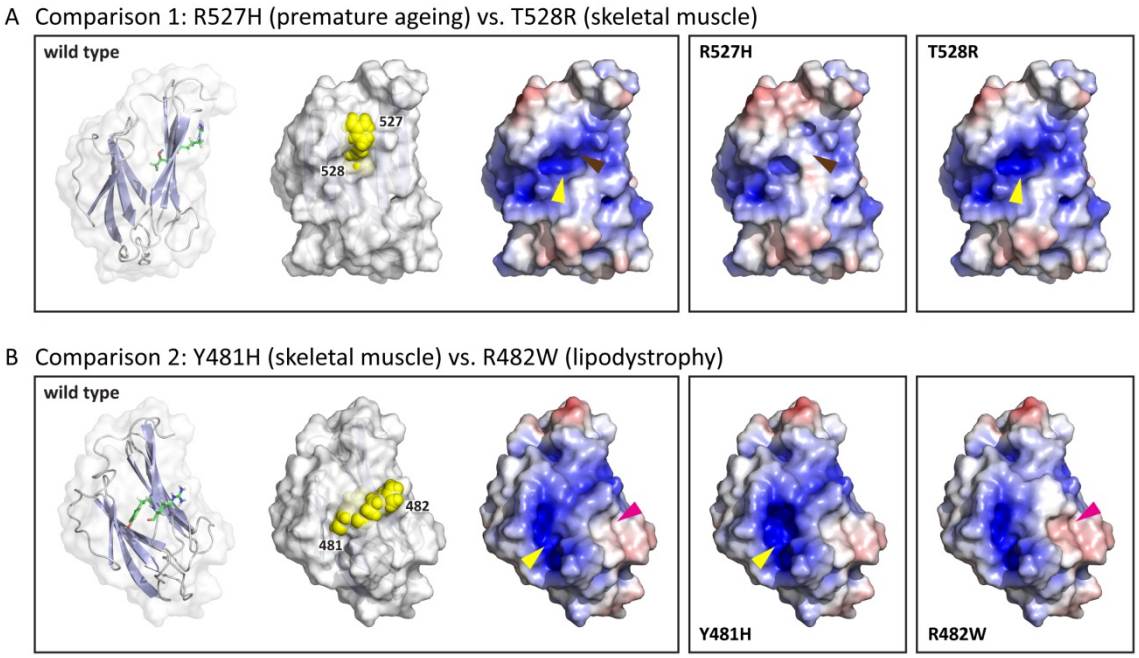

Figure 3.13 Comparison of mutations on adjacent residues that result in a different phenotype (**A**) Mutations on neighbouring residues R527 and T528 (both located in the premature ageing cluster) are associated with 2 different phenotypes. Mutation p.R527H strongly reduces the positive charge in this area and causes a premature ageing phenotype (POI 1.0). Mutation p.T528R however increases the positive charge in this area and causes a skeletal muscle phenotype (POI 1.0). (**B**) Mutations on neighbouring residues Y481 and R482 are associated with two different phenotypes. Mutation p.Y481H increases the charge of a positively charged pocket and always results in a skeletal muscle phenotype (POI 1.0). Mutation p.R482W however increases the negative charge in the region without affecting the positively charged pocket next to Y481 and mainly results in lipodystrophy disorder (POI 0.93). Coloured arrows indicate areas of the mutated Ig-fold that are affected by each amino acid change.

3.4 Discussion

Genotype-phenotype correlations in laminopathies are not well understood for the majority of *LMNA* mutations, although some mutation hot-spots (i.e. p.R482W which is associated with lipodystrophy disorders) and specific protein modifications (i.e. retention of the farnesyl group which is associated with premature ageing disorders) have been shown to result in consistent phenotypes (Worman and Bonne, 2007). The aim of this chapter was to identify genotype-phenotype links in laminopathies by grouping mutations according to the resulting phenotype and statistically analysing general characteristics of mutations in these groups.

I have shown that a significant proportion (60.4%) of patients with nonsense mutations in *LMNA* develop cardiomyopathy. Nonsense mutations generally result in a premature termination codon (PTC) and as a consequence, mRNAs containing PTCs are usually subject to nonsense mediated decay, which serves as a quality control mechanism to prevent the accumulation of truncated, potentially harmful protein or products of faulty splicing (Maquat, 2005; Rebbapragada and Lykke-Andersen, 2009). A loss of lamin A/C expression from one *LMNA* allele would mean that haploinsufficiency is a likely explanation for the phenotype.

Evidence supporting haploinsufficiency was provided by Arbustini et al. (2002), who found reduced levels but no truncated form of lamin A/C in cardiac tissue of DCM-CD patients with the nonsense mutation p.E111X. Truncated lamin protein was also absent in patient fibroblasts heterozygous or homozygous for the nonsense mutation p.Y259X (Muchir et al., 2003). Further, lamin A/C heterozygous mice also express reduced levels of lamin A/C which results in cardiac dilation and progressive electrophysiological disease (Wolf et al., 2008).

Whether DCM is caused by lamin A/C haploinsufficiency in man, remains controversial. Geiger et al. (2008) found reduced lamin A mRNA levels in explanted myocardial tissue and cultured fibroblasts from DCM patients with the nonsense mutation p.R321X. However, protein levels were unchanged when compared to wild-type control samples and truncated lamin protein were only detected in presence of a proteasome inhibitor. The authors concluded that low amounts of truncated protein could interfere with normal lamin A/C function, before it is degraded by the proteasome (Geiger et al., 2008). Truncated protein was also found in patients diagnosed with Heart-hand syndrome carrying a splice site mutation in *LMNA* intron 9, indicating that haploinsufficiency does not occur for all nonsense mutations (Renou et al., 2008). Importantly this could explain why nonsense mutations in different parts of the protein result in different phenotypes. Truncated lamin protein of various lengths could have different effects on normal lamin A function, or lamin A interacting proteins resulting in a range of phenotypes.

Although haploinsufficiency appears to be a likely cause in some cardiomyopathy cases, there are a number of missense mutations that also result in cardiomyopathy. My result shows that one third of all missense mutation in the central rod domain result in cardiomyopathy (Fig. 3.4). This supports results by others suggesting that the central rod domain is a hot-spot for DCM-CD

mutations (Perrot et al., 2009). Interestingly, c-Fos and Erk1/2 bind to the central rod domain (Gonzalez et al., 2008) and upregulation of the Erk1/2 signalling cascade has been shown to be involved in the development of cardiomyopathy in mice (Muchir et al., 2007b; Muchir et al., 2009; Wu et al., 2011).

Different pathogenic mechanisms are also evident in other mouse models for cardiomyopathy. Mice homozygous for p.N195K develop cardiomyopathy and have a maximum survival time of 17 weeks (Mounkes et al., 2005). Desmin staining revealed a loss of organisation at sarcomeres and gap junction proteins connexin 40 and 43 were mislocalised in *lmna*$^{N195K/N195K}$ hearts. In contrast, *lmna*$^{+/-}$ and *lmna*$^{nPLAO/nPLAO}$ mice have a much longer maximum survival time of up to two years and disorganisation of sarcomeres or misocalisation of gap junction proteins was not reported (Davies et al., 2010; Wolf et al., 2008). Interestingly, in *lmna*$^{nPLAO/-}$ mice, the phenotype worsened which led to the conclusion that for a subset of mutations, loss of function is the underlying disease mechanism for cardiomyopathy (Davies et al., 2011).

An interesting observation I made was that domains in the lamin protein with defined tertiary structures (central rod domain and Ig-fold domain) harbour significantly more mutations than unstructured regions. Sequence alignment of lamin A from human, mouse and frog (all 664 or 665 amino acids long) shows a very high sequence homology especially in the central rod domain and the Ig-fold domain (Appendix 2). There are only 33/471 residues (7.0%) in folded regions of lamin A (22 in the central rod domain and 11 in the Ig-fold domain) which are partly conserved or not conserved (Appendix 2). Out of those, only 2 residues (Gly125 and Ser268) are associated with a phenotype in human when mutated, both causing muscular dystrophy (Astejada et al., 2007; Scharner et al., 2011). In contrast, unstructured regions allow for larger variation in the sequence. Here, 44/193 residues (22.8%) are only partly conserved or not conserved, suggesting that folded regions are more important to lamin A function.

It is therefore unsurprising that structured regions of the lamin A protein appear to be more sensitive to amino acid changes and are more likely to result in a phenotype (Fig. 3.4). Furthermore, 65.5% of all missense mutations in the central rod domain and 40.4% of all missense mutations in the Ig-fold domain resulted in a drastic change in the amino acid side chain characteristics. Both domains are important in filament formations and mutations disrupting the central rod domain or Ig-fold domain potentially interfere with filament formation.

The question of whether all lamin mutations, or only those that cause a certain phenotype affect lamin filament formation was addressed by Yosef Gruenbaum and his team in 2008 (Wiesel et al., 2008). The ability of lamins to form higher filaments can be assayed *in vitro*. Wild-type lamins form paracrystals when dialysed from urea into a Tris-HCl buffer containing $CaCl_2$ (Karabinos et al., 2003) or assemble into 10nm branched filaments when diluted in assembly buffer (Foeger et al., 2006). Analysis of the ability of 14 Ce-lamin mutations (resulting in EDMD, HGPS, DCM and FPLD in human) to form paracrystals and filaments in vitro revealed that some of the mutants did

not affect paracrystal or filament assembly, some affected either paracrystal or filament assembly and some affected both. However, none of these characteristics associated with a specific phenotype (Wiesel et al., 2008). Even when I applied my own more detailed analysis to these 14 mutations and tried to link their inability to form paracrystals or filaments with the severity of the amino acid change, the heptad repeat position (residues in the central rod domain) or the surface exposure (residues in the Ig-fold domain), I could not detect any obvious correlation. This is very interesting and may suggest that the ability or inability to form filaments *in vitro* does not provide common ground for a pathogenic mechanism of lamin mutations. In fact, even proteins with severe deletions in the central rod domain (Schirmer et al., 2003), deletion of the entire tail domain (Moir et al., 1991) and progerin with its farnesyl group, are able to form paracrystals *in vitro* (Taimen et al., 2009).

Recently, crystal structures of lamin A coil 2B, harbouring missense mutations associated with DCM-CD (p.R335W or p.E347K) have been solved. However, the amino acid substitutions did not affect the overall structure of the α-helix, which provides additional evidence that lamin dimerisation not affected by these mutations. Although an effect on higher filament assembly or protein protein interaction cannot be ruled out; although an effect on higher filament assembly or protein protein interaction cannot be ruled out (Bollati et al., 2012).

The possibility that mutations destabilise the 3D structure of the Ig-fold was first proposed by Krimm et al. (2002). I have shown that more than 60% of all residues associated with a skeletal muscle phenotype are buried which is significantly different from what would be expected in case of a random distribution. However we also know that there are a large number of mutations in the Ig-fold that are located on buried residues but do not cause a skeletal muscle phenotype. All Ig-like domains have a common 2-plus-2 stranded structural core (strands b, c, e, f, Fig. 1.6) which is surrounded by structurally more variable strands (Bork et al., 1994). In the Ig-fold of A-type lamins the structural core corresponds to residues number 451-455 (strand b), 468-473 (strand c), 494-499 (strand e) and 525-531 (strand f) (Krimm et al., 2002). Mutations that disrupt the structural core are therefore more likely to destabilize the Ig-fold domain than mutations located in peripheral β-strands. This could also explain why not all buried residues result in a skeletal muscle phenotype.

Indeed, out of nine buried residues in the Ig-fold associated with a skeletal muscle phenotype (phenotype score ≥0.75) six are located on strands b, c, e and f. One residue (N456) is located at the border to strand b. In total 17 buried residues were found to be associated with a phenotype. A large number (8/17) buried residues does not cause a skeletal muscle phenotype. Interestingly, six of these eight residues are not located on one of the four core strands. Taken together, these results confirm the hypothesis stated in 2002, and demonstrate the importance of the location of the residue in a spatial context in the 3D structure, while the type of amino acid change does not seem to have an important influence on the pathogenicity in this domain.

Unfortunately, crystal structures for the Ig-fold domain with mutations on buried core residues are not yet available. However, there is in vitro evidence in *Xenopus* suggesting that the Ig-fold domain is involved in lamin polymerisation, and that this function is modified by the presence of an EDMD mutation (equivalent to p.R453W in human) (Shumaker et al., 2005).

For other disease phenotypes caused by missense mutations in the Ig-fold, altered protein interaction is a far more likely explanation. Clusters in the Ig-fold associated with a specific phenotype have been described before for lipodystrophy disorders (Krimm et al., 2002) and progeria disorders (Verstraeten et al., 2006).

Importantly, my analysis of mutations in the Ig-fold domain also revealed, that mutations located in these clusters result in a similar change of charge (section 3.3.7). Mutations in a cluster associated with lipodytrophy disorders generally result in an increase in negative charge while mutations in a second cluster (located on a different phase of the 3D domain) result in a loss of positive charge suggesting the involvement of specific protein interactions for each disease phenotype.

To date, numerous interaction partners have been described that bind to the tail domain of lamin A including emerin, actin, PCNA, SREBP1, etc. (Fig. 1.8). However, none of these interactions has been mapped to specific regions of the Ig-fold. One could use docking simulations to try to map interaction sites. To do so however, requires the 3D structure of the Ig-fold in presence of different mutations and to date, only one Ig-fold structure with a mutation (p.R482W) has been solved (Magracheva et al., 2009). The transcription factor SREBP1, involved in lipid homeostasis and adipogenesis, has been shown to directly interact with the lamin A tail domain and is a promising candidate for FPLD pathology (Capanni et al., 2005; Lloyd et al., 2002).

Using *in silico* docking analysis, Rajendran et al. (2011) have attempted to measure the binding energy of emerin and SREBP1 bound to the wild-type Ig-fold and compare it to the binding energy when bound to the Ig-fold containing the p.R482W mutation. Their results show that both emerin and SREBP1 are bound tighter to the mutant Ig-fold than they are to the wild-type Ig-fold. Unfortunately the interaction site was restricted to a very narrow region on both binding partners to speed up the docking simulation. In addition, this data is contradictory to *in vitro* data which shows a reduced lamin A-SREBP1 interaction in presence of p.R482W as well as other FPLD causing missense mutations (Lloyd et al., 2002).

The by far most striking correlation was seen in a small cluster of mutations resulting in premature ageing syndromes (MADA and HGPS). Interestingly, all reported patients with mutations in this cluster had one thing in common: both their *LMNA* alleles were affected by either homozygous mutations (Agarwal et al., 2008; Kosho et al., 2007; Novelli et al., 2002; Plasilova et al., 2004; Simha et al., 2003; Youn et al., 2010) or compound heterozygous mutations for two mutations (Cao and Hegele, 2003; Verstraeten et al., 2006) located within this specific region of the Ig-fold. Furthermore, 6/8 mutations resulted in a moderate/strong reduction of a positive charge found in this region (Fig. 3.11).

A mechanism, similar to that proposed for skeletal muscle disorders involving the destabilisation of the structure by these mutations is unlikely, because heterozygous relatives (of homozygous patients) are unaffected. Similarly, individuals who carry either p.T528M or p.M540T alone are unaffected, but together, they result in HGPS (Verstraeten et al., 2006). Additional evidence is provided by analysing Thr528 in more detail. A substitution of Thr528, which is a buried hydrophobic residue (rel. SASA=0.17) with methionine, does not result in a drastic change in the amino acid characteristic and is therefore less likely to dirupt the structure (table 3.1). However, replacing Thr528 with a positively charged and very large arginine residue will have more severe consequences on the Ig-fold stability. Indeed, p.T528R has been shown to cause EDMD in all six reported patients (www.umd.be/LMNA).

A common molecular feature of HGPS patients is the accumulation of farnesylated prelamin A (Davies et al., 2009). However, prelamin A accumulation was not evident in homozygous (Agarwal et al., 2008), and compound heterozygous (Verstraeten et al., 2006) patients, which suggests that a different underlying mechanism is involved. The consistent change in charge suggests that a protein interaction is involved. Since many of progeroid patients also show lipodystrophy syndromes the molecular mechanism might be smililar to that of FPLD. Another potential mechanism could involve the accumulation of SUN1, shown to be pathogenic in phenotypes caused by farnesylated lamin A and loss of lamin A alike (Chen et al., 2012).

Although I could identify potential genotype-phenotype links for mutations in the central rod domain and Ig-fold domain, a large number of mutations in other parts of the protein do not show a clear correlation. For example mutations in unstructured regions result in a larger number of lipodystrophy disorders and overlapping phenotypes while the number of striated muscle phenotypes ('skeletal muscle' and 'cardiac-only') is reduced. Unfortunately the functional role of the tail domain beyond the Ig-fold domain, apart from its role in the posttranslational processing of lamin A, is not well understood. Lamin C lacks the tail domain completely and mice expressing lamin C (but not lamin A) are apparently normal, suggesting that the tail region bears no specific function (Fong et al., 2006b). Mutations in the tail domain could modulate lamin A processing, which was shown for residue R644 (Barrowman et al., 2012), and therby affect the phenotypic outcome.

Another possible explanation is that some of the mutations in the database are not the cause of pathogenesis for the diagnosed disease. The *LMNA* gene contains many single nucleotide polymorphisms (SNPs) with no pathologic phenotype (www.dmd.nl/lmna_seqvar.html). Further, approx. 60% of all EDMD patients have no mutations in *LMNA, EMD* or *FHL1* which suggests that there are additional genes involved in EDMD pathology (Gueneau et al., 2009). Examples are mutations in emerin and desmin which have been shown to modulate the disease severity of *LMNA* mutations (Muntoni et al., 2006). Further, mutations in nesprins have been found in patients with EDMD phenotype (Zhang et al., 2007). It can therefore not be ruled out that some of

the mutations in the database are non-pathogenic SNPs (that may or may not contribute to the pathology), especially for mutations where only one patient is reported.

3.5 Conclusion

In this chapter I set out to find correlations between mutations in the *LMNA* gene and the resulting phenotype by grouping mutations according to the resulting phenotype and statistically analysing general characteristics of mutations in these groups. My results confirm hypotheses postulated by others such as a correlation between truncation mutations and a cardiomyopathy phenotype or that buried residues in the Ig-fold are more likely to result in a skeletal muscle phenotype. However my results also show novel correlations such as the spatial clustering of mutations resulting in a specific phenotype on the Ig-fold domain which correlates with a similar change in charge. Further I could show that pathogenic missense mutations in the central rod domain generally result in a drastic change in side chain characteristics while pathogenic missense mutations in the Ig-fold and the unstructured region of the protein result in a moderate change in side chain characteristics.

In future, well established genotype phenotype correlations in combination with perinatal genetic screening for mutations in *LMNA* may be used to monitor the health status of the patient well before the first symptoms arise. That such an approach would be hugely beneficial for patients is already evident. The analysis of familial and sporadic DCM cases shows that DCM patients with mutations in the *LMNA* gene have a significantly poorer cumulative survival rate compared to non-carriers (Taylor et al., 2003). The most frequent cause of death in patients with DCM is sudden cardiac arrest which is usually prevented by implanting a pacemaker. If genetic screening becomes more widely available, individuals with *LMNA* mutations likely to cause DCM could be monitored for cardiac defects before symptoms arise, providing them with a better quality of life.

Similarly, once treatment for other types of laminopathies becomes available, and the phenotypic outcome of a specific mutation can be predicted, treatment can start early and again improve life expectancy and/or quality of life of patients. Until we reach that point a lot more work has to be done to understand the functions of lamins and how mutant lamins affect cell structure and function. The latter is part of the next chapter of this thesis.

Chapter 4

Novel *LMNA* Mutations in Patients with Emery-Dreifuss Muscular Dystrophy and Functional Characterisation of Four *LMNA* Mutations

4.1 Introduction

As shown in the previous chapter, a lot of mutations have been described on the *LMNA* gene so far and novel pathogenic mutations continue to get published and are collated on a regular basis on the Universal Mutation Database (UMD) which can be accessed online at www.umd.be/LMNA. The latest novel *LMNA* mutation is an autosomal recessive EDMD mutation (p.R225Q) located on exon 4 in the linker region L12 of the central rod domain, published in April this year (Jimenez-Escrig et al., 2012). In a collaborative effort with Dr. Charlotte A. Brown formally of Carolinas Medical Center in North Carolina (USA) (present address Director, Clinical and Scientific Affairs BD Diagnostics, Women's Health and Cancer 4025 Stirrup Creek Dr., Suite 400, Durham, NC 27703 USA) we have analysed a large cohort of patients from North America with skeletal muscle dystrophy and identified 15 novel *LMNA* mutations (reported in this chapter).

An increasing number of mutations known on the *LMNA* gene will help analysis to understand the relationship between the type of mutation, their location and the resulting phenotype as discussed in chapter 3. However, we also need to understand the effects that different lamin A mutations have on cellular and nuclear structure and in cell function.

Cells isolated from patients with a laminopathy and mice carrying *lmna* mutations often display abnormalities, such as minor deformations, lobulations and herneations. A-type and B-type lamins are frequently mislocalised in such nuclei and aggregate in coarse meshworks known as honeycomb structures, intranuclear lamin foci or a combination of both (Agarwal et al., 2008; Kandert et al., 2009; Mounkes et al., 2005; Muchir et al., 2004; Muchir et al., 2003; Vigouroux et al., 2001). The reason why certain mutations cause these phenotypes, while other mutations apparently do not result in any abnormalities remains a mystery.

To advance the understanding of the effect of *LMNA*-mutations on cells, I chose four pathogenic *LMNA* mutations from our study, located on conserved residues throughout the lamin A/C protein that can each cause a skeletal muscle phenotype. Because of the observed muscle phenotype in patients where these mutations have been found, I have chosen to use C2C12 myoblasts to express mutant lamins and study their structural and functional effects on the cells.

The first mutation analysed in this study was p.R25P which results in a drastic amino acid change because of the cyclic structure of proline and the loss of a positive charge (see section 3.3.5 for details). Residue R25 is conserved down to *D. melanogaster* and located in the head domain of lamin

A/C. To date three pathogenic mutations (p.R25G, p.R25C, p.R25P) in a total of 11 patients have been found on residue R25. All patients were diagnosed with a skeletal muscle phenotype (Brown et al., 2001; Fokkema et al., 2005; van Tintelen et al., 2007).

The second mutation used in this study was the severe amino acid substitution p.R249W. The mutation eliminates a positive charge and is located in a heptad repeat (position e) on coil 2A in the central rod domain of lamin A/C. One further pathogenic mutation, p.R249Q, has been described on this residue (Benedetti et al., 2007; Bonne et al., 2000). All patients with mutations on residue R249, 28 in total, were diagnosed with a skeletal muscle phenotype. Recently, p.R249W has also been found in patients with lamin associated congenital muscular dystrophy (Quijano-Roy et al., 2008).

Mutation p.N456I, the third mutation in this study was a severe mutation located on a loop connecting strands b and c in the Ig-fold domain. It is a buried residue (rel. SASA=0.09; see section 3.3.7 for a detailed explanation) and is associated with a skeletal muscle phenotype. There are three further pathogenic amino acid substitutions reported on residue N456: p.N456H, p.N456D and p.N456K. All four mutations have been shown to cause a skeletal muscle phenotype in a total of 7 patients (Astejada et al., 2007; Bonne et al., 2000; Quijano-Roy et al., 2008).

The last mutation included in this study was p.R541P, a severe amino acid change located on strand f of the Ig-fold domain. The residue is buried (rel. SASA=0.12) and was found in two patients, one diagnosed with a skeletal muscle phenotype (this study) and one diagnosed with DCM (van Tintelen et al., 2007). Residue R541 is conserved to Amphioxus and has been shown to be pathogenic if mutated to three other amino acids (p.R541S p.R541C p.R541H). All four mutations have been diagnosed in a total of 19 patients, 5 (26%) diagnosed with a skeletal mucle phenotype, 12 (63%) diagnosed with a cardiac-only phenotype and 2 (11%) diagnosed with other phenotypes.

The effects of these four LMNA mutations on nuclear structure and lamin distribution in myogenic cells are the subject of this chapter. Since these results were recently published in the journal Human Mutation (Scharner et al., 2011), I have included the paper as a results section of this chapter (as permitted under current regulations).

Figure and table numbers in this chapter remain as in the published manuscript (figure 1, figure 2, table 1, etc.). However for clarity and consistency, in the list of figures and tables for the thesis and when referred to in other parts of the thesis, figures and tables in this chapter will receive the chapter number as a prefix. Thus, figure 1 will then be referred to as figure 3.1, table 1 as table 3.1 etc.

4.2 Authors contributions

I co-authored the publication with Charlotte A. Brown who was a geneticist at Carolinas Medical Center in North Carolina at the time of data collection. Charlotte sequenced DNA samples from patients and compiled a list of genetic and clinical information for each patient from patient samples and information supplied by co-authors Matthew Bower, Susan T. Iannaccone, Ismail A. Khatri, Diana Escolar, Erynn Gordon, Kevin Felice, Carol A. Crowe, Carla Grosmann, Matthew N. Meriggioli, Alexander Asamoah and Ora Gordon.

I selected four different *LMNA* mutations, cloned them into a retroviral expression vector and analysed their effects on nuclei of the myogenic C2C12 cell line. I also produced the figures and tables and wrote a draft of the manuscript, which was edited and reviewed by co-authors Viola F. Gnocchi, Juliet A. Ellis and Peter S. Zammit.

4.3 Aim

The aim of this chapter was to identify and compare the effects of four different pathogenic lamin A mutations on nuclear morphology and the localisation of nuclear envelope proteins. The chosen mutations (p.R25P, p.R249W, p.N456I and p.R541P) were all identified in patients with skeletal muscle dystrophy. Since defective myoblasts might play a role in the pathology of these mutations, I have chosen C2C12 myoblasts to study these mutations. It was also important to create conditions that closely resemble a physiological environment. I therefore utilised a retroviral expression system to achieve high infection efficiency and moderate expression levels of the mutant protein.

RESEARCH ARTICLE

Human Mutation

OFFICIAL JOURNAL
HGVS
HUMAN GENOME VARIATION SOCIETY
www.hgvs.org

Novel *LMNA* Mutations in Patients With Emery-Dreifuss Muscular Dystrophy and Functional Characterization of Four *LMNA* Mutations

Juergen Scharner,[1†] Charlotte A. Brown,[2†] Matthew Bower,[3] Susan T. Iannaccone,[4] Ismail A. Khatri,[5] Diana Escolar,[6] Erynn Gordon,[7] Kevin Felice,[8] Carol A. Crowe,[9] Carla Grosmann,[10] Matthew N. Meriggioli,[11] Alexander Asamoah,[12] Ora Gordon,[13] Viola F. Gnocchi,[1] Juliet A. Ellis,[1] Jerry R. Mendell,[14*‡] and Peter S. Zammit[1*‡]

[1]Randall Division of Cell and Molecular Biophysics, King's College London, United Kingdom; [2]BD Diagnostics, Durham, North Carolina; [3]Department of Pediatrics, Fairview University Medical Center, Minneapolis, Minnesota; [4]Texas Scottish Rite Hospital for Children, UT Southwestern Medical Center, Dallas, Texas; [5]Division of Neurology, Shifa International Hospital, Islamabad, Pakistan; [6]Research Center for Genetic Medicine, Children's National Medical Center, Washington, DC; [7]Coriell Institute for Medical Research, Camden, New Jersey; [8]Department of Neuromuscular Medicine, Hospital for Special Care, New Britain, Connecticut; [9]Department of Pediatrics, MetroHealth Medical Center, Cleveland, Ohio; [10]Department of Neurology, Rady Children's Hospital San Diego, San Diego, California; [11]Department of Neurology and Rehabilitation, University of Illinois, Chicago, Illinois; [12]Department of Pediatrics, Weisskopf Child Evaluation Center, University of Louisville, Kentucky; [13]Medical Genetics Institute, Cedar-Sinai Medical Center, Los Angeles, California; [14]Department of Pediatrics and Neurology, Ohio State University, and the Research Institute at Nationwide Children's Hospital, Columbus, Ohio

Communicated by Arnold Munnich

Received 11 June 2010; accepted revised manuscript 1 September 2010.
Published online 16 September 2010 in Wiley Online Library (wileyonlinelibrary.com). DOI 10.1002/humu.21361

ABSTRACT: Mutations in *LMNA* cause a variety of diseases affecting striated muscle including autosomal Emery-Dreifuss muscular dystrophy (EDMD), *LMNA*-associated congenital muscular dystrophy (L-CMD), and limb-girdle muscular dystrophy type 1B (LGMD1B). Here, we describe novel and recurrent *LMNA* mutations identified in 50 patients from the United States and Canada, which is the first report of the distribution of *LMNA* mutations from a large cohort outside Europe. This augments the number of *LMNA* mutations known to cause EDMD by 16.5%, equating to an increase of 5.9% in the total known *LMNA* mutations. Eight patients presented with either p.R249W/Q or p.E358K mutations and an early onset EDMD phenotype: two mutations recently associated with L-CMD. Importantly, 15 mutations are novel and include eight missense mutations (p.R189P, p.F206L, p.S268P, p.S295P, p.E361K, p.G449D, p.L454P, and p.W467R), three splice site mutations (c.IVS4+1G>A, c.IVS6−2A>G, and c.IVS8+1G>A), one duplication/in frame insertion (p.R190dup), one deletion (p.Q355del), and two silent mutations (p.R119R and p.K270K). Analysis of 4 of our lamin A mutations showed that some caused nuclear deformations and lamin B redistribution in a mutation specific manner. Together, this study significantly augments the number of EDMD patients on the database and describes 15 novel mutations that underlie EDMD, which will contribute to establishing genotype–phenotype correlations.
Hum Mutat 32:152–167, 2011. © 2011 Wiley-Liss, Inc.

KEY WORDS: lamin A; lamin B; emerin; EDMD; LGMD; L-CMD; nuclear envelope; nuclear lamina; laminopathy; skeletal muscle

Introduction

Emery-Dreifuss muscular dystrophy (EDMD) manifests in childhood with slowly progressive muscle weakness with a scapulohumeroperoneal distribution, associated with contractures of the Achilles tendon, neck, and elbow. Cardiac involvement is a consistent feature associated with nearly all patients by the third decade, initially involving arrhythmias, progressing toward complete heart block with a substantial risk of sudden death in middle age [Emery, 1989].

Both X-linked and autosomal forms of EDMD have been described. Mutations in the *EMD* gene (Xq28; MIM# 300384) have been identified in patients with X-linked EDMD (X-EDMD; MIM# 310300) [Bione et al., 1994]. *EMD* encodes emerin, a small integral membrane protein located at the inner nuclear membrane and a member of the LEM domain proteins [Wagner and Krohne, 2007]. Mutations in the *LMNA* gene (1q21.3; MIM# 150330), encoding the A-type lamins, lamin A and C by alternative splicing (Fig. 1A), have been found in patients with autosomal dominant (EDMD2; MIM# 181350) [Bonne et al., 1999] and autosomal recessive (EDMD3; MIM# 604929) [Raffaele Di Barletta et al., 2000] forms of EDMD. *LMNA* mutations are also associated with

†These authors contributed equally to this work.

‡These authors are joint last authors.

*Correspondence to: Peter S. Zammit, King's College London, Randall Division of Cell and Molecular Biophysics, Guy's Campus, London, SE1 1UL, UK. E-mail: peter.zammit@kcl.ac.uk or Jerry R. Mendell, Nationwide Children's Hospital, Neurology, Columbus, Ohio. E-mail: jerry.mendell@nationwidechildrens.org

Contract grant sponsor: The Muscular Dystrophy Association; Contract grant number: A6356678101; Contract grant sponsor: The MYORES Network of Excellence; Contract grant number: 511978; Contract grant sponsor: The Medical Research Council; Contract grant number: G0700307.

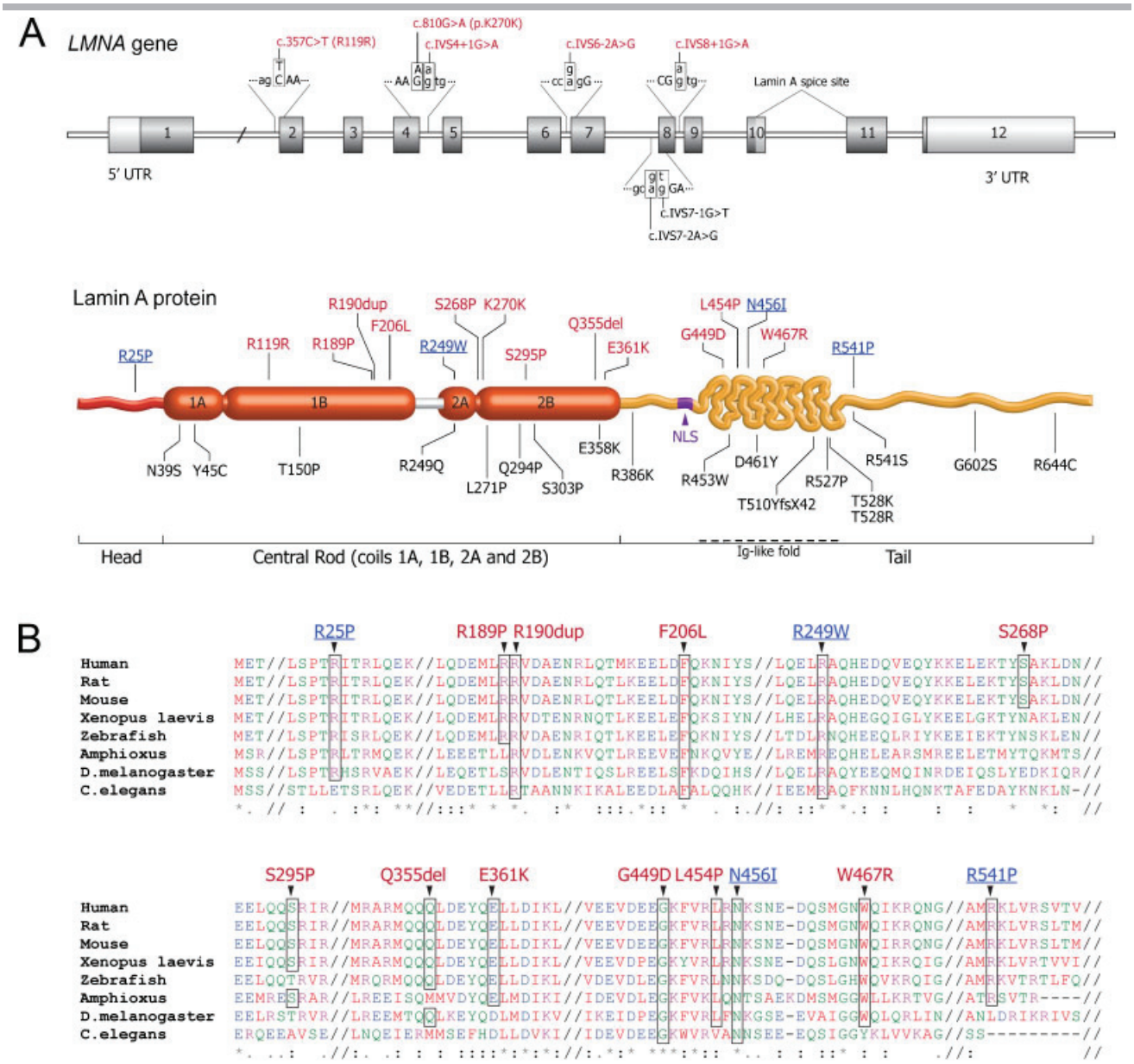

Figure 1. Schematic of the *LMNA* gene and lamin A protein indicating mutations. **A:** Schematic of the *LMNA* gene and lamin A protein. Lamin A is encoded by exons 1–12, whereas lamin C terminates at exon 10 with six unique amino acids at its C-terminal. The alternative splice site for lamin A is indicated. Sequence variations affecting splice donor or acceptor sites that lead to disease are shown for IVS 4, 6, 7, and 8. Missense mutations, insertions, and deletions are indicated on the lamin A protein, where the head, central rod, and tail domain (incorporating the nuclear localization signal [NLS], and Ig-like fold) are indicated. Novel sequence variants are shown above the gene/protein (red) and mutations used for in vitro investigation are underlined (blue), whereas recurring mutations are shown beneath the gene/protein. Table 2 provides a detailed genetic description of the sequence variants. **B:** Illustration of evolutionary conservation of residues associated with novel missense mutations, insertions, and deletions located in the coding region of *LMNA* and those used in our in vitro analysis (blue/underlined). Sequences were obtained from the online databank swissprot (http://expasy.org/sprot/) and aligned with the online tool ClustalW2 (http://www.ebi.ac.uk/clustalw/). Partial sequence only, with // denoting nonconsecutive sequence, *indicating identical residues in all aligned sequences; ":" showing conserved substitutions; and "." marking semiconserved substitutions. If viewed in color: residues with nonpolar side chains are indicated in red, acidic residues are shown in blue, basic residues shown in magenta, and amino acids with uncharged polar side chains are indicated in green.

a congenital muscular dystrophy termed *LMNA*-related congenital muscular dystrophy (L-CMD; MIM♯ 613205) [Quijano-Roy et al., 2008]. Lamins A and C are type V intermediate filament proteins, and together with B-type lamins, are major components of the nuclear lamina: a proteinaceous meshwork underlying the inner nuclear membrane, thought to provide a structural framework for the nuclear envelope and an anchoring site at the nuclear periphery for interphase chromosomes. Recently, it has been shown that mutations in the *FHL1* gene (Xq27.2; MIM♯ 300163) are also associated with EDMD [Gueneau et al., 2009]. *FHL1* encodes a LIM domain protein containing two zinc fingers in tandem, which has been implicated in sarcomere assembly [Gueneau et al., 2009; McGrath et al., 2006].

Emerin and lamin A/C are thought to have a close functional relationship, even though the phenotypes caused by *EMD* and *LMNA* mutations are clinically different [Bonne et al., 2003;

Meune et al., 2006]. In fact, direct interaction between emerin and lamin A has been demonstrated by multiple experimental techniques [Clements et al., 2000; Lee et al., 2001] and emerin localization has been shown to be affected by mutant lamin A [Holt et al., 2003]. *LMNA* mutations have also been detected in patients with autosomal dominant limb-girdle muscular dystrophy with atrioventricular conduction disturbances (LGMD1B; MIM# 159001) [Muchir et al., 2000]. Atlhough the clinical phenotype of LGMD1B overlaps with EDMD, there are differences, for example, LGMD1B is characterized by slowly progressive pelvic girdle weakness, with a sparing of the lower leg muscles. In addition, contractures and cardiac disturbances tend to occur later in life in LGMD1B, compared to EDMD patients [Muchir et al., 2000].

In addition to EDMD, LGMD1B, L-CMD, and isolated dilated cardiomyopathy and conduction-system disease (CMD1A; MIM# 115200) [Fatkin et al., 1999] that primarily affect striated muscle, "laminopathies" also affect other tissues. Such laminopathies include Dunningan-type familial partial lipodystrophy (FPLD; MIM# 151660) [Hegele et al., 2000; Shackleton et al., 2000; Speckman et al., 2000], autosomal recessive Charcot-Marie-Tooth Disorder Type 2B1 (CMT2B1; MIM# 605588) [De Sandre-Giovannoli et al., 2002], mandibuloacral dysplasia (MAD; MIM# 248370) [Novelli et al., 2002; Shen et al., 2003], Hutchinson-Gilford progeria syndrome (HGPS; MIM# 176670) [De Sandre-Giovannoli et al., 2003; Eriksson et al., 2003], and autosomal dominant atypical Werner's syndrome (WRN; MIM# 150330) [Chen et al., 2003]. In addition, both intrafamilial and interfamilial variability of phenotypes associated with *LMNA* mutations is a common feature [Shen et al., 2003; Simha et al., 2003; Speckman et al., 2000; Vytopil et al., 2002].

A clear genotype–phenotype correlation has not been identified for most laminopathies, although HGPS tends to correlate with C-terminal splicing defects, while other conditions (i.e., MAD, WRN, and CMT2B1) result from "hot spot" missense mutations. For other laminopathies including EDMD, the pathogenic *LMNA* mutations are distributed throughout the gene [Scharner et al., 2010]. The *LMNA* gene contains 12 exons and encodes both lamin A and C by alternative splicing, both sharing the first 566 amino acids [Lin and Worman, 1993]. In addition to their role in the nuclear lamina, lamins also interact with numerous integral proteins of the inner nuclear membrane and proteins of nuclear pore complexes [Schirmer and Foisner, 2007], orchestrating a number of cellular and molecular processes including nuclear envelope assembly, maintenance of nuclear architecture, DNA synthesis, chromatin organization, gene transcription, cell cycle progression, cell differentiation, and migration and response to DNA damage [Broers et al., 2006; Prokocimer et al., 2009; Verstraeten et al., 2007], processes that could be differentially affected by specific mutations.

This report describes novel and recurrent *LMNA* mutations identified in 50 patients referred for clinical testing for a suspected diagnosis of EDMD or LGMD in the United States and Canada. This is also the first report of the distribution of *LMNA* mutations from a large patient cohort from outside Europe, and augments the EDMD mutation database by ~6%. Importantly, among these were 15 novel pathogenic *LMNA* mutations that include eight missense mutations (p.R189P, p.F206L, p.S268P, p.S295P, p.E361K, p.G449D, p.L454P, and p.W467R), three splice site mutations (c.IVS4+1G>A, c.IVS6−2A>G, and c.IVS8+1G>A), one duplication/in frame insertion (p.R190dup), one deletion (p.Q355del), and two silent mutations (p.R119R and p.K270K). Examining four of our *LMNA* mutations further, we found that mutations located in various protein domains differentially affect basic nuclear characteristics including nuclear size, shape, and protein distribution. Taken together, we provide clinical and in vitro data to confirm the complex pathogenicity associated with *LMNA* mutations, suggesting that genetic background is also a major player in the severity of the expressed phenotype of autosomal EDMD.

Material and Methods

Patients

The 255 patients reported in this manuscript were referred to either the DNA Diagnostic Laboratory at Carolinas Medical Center (1996–2001) or the Molecular Diagnostics Laboratory at the University of Minnesota (2001–2003) from the United States of America and Canada for mutation analysis of the *LMNA* gene (GenBank Accession Number RefSeq NM_170707.2). The clinical diagnoses of patients referred for testing included muscular dystrophies of the EDMD, LGMD, congenital, Becker (BMD), and fascioscapulohumeral (FSHD) types, as well as spinal muscular atrophy (SMA). This study was approved by the Institutional Review Board at both Carolinas Medical Center and the University of Minnesota.

DNA Isolation and Polymerase Chain Reaction

DNA extracted from peripheral blood by either standard proteinase K/phenol-chloroform extraction procedures on a 341 Nucleic Acid Extractor (Perkin-Elmer, Norwalk, CT) or using a QIamp DNA Blood Mini Kit (Qiagen, Valencia, CA). Exons 1–12 of *LMNA* were amplified by PCR as previously described [Brown et al., 2001]. Primers used for the PCR reaction are listed in Supp. Table S1.

Sequencing

Amplimers were extracted from agarose gel using a Gel Extraction Kit (Qiagen) and each exon sequenced directly from both strands using the Prism Ready Reaction DyeDeoxy Terminator Cycle Sequencing Kit (Applied Biosystems, Foster City, CA) with analysis of sequenced products on either an ABI377 or ABI3100 Genetic Analyzer. Generated sequences were compared to the published *EMD* or *LMNA* gene sequence using the Sequence Navigator (Applied Biosystems) or Sequencher (Gene Codes Corporation, Ann Arbor, MI) software packages. Nucleotide numbering reflects cDNA numbering with +1 corresponding to the A of the ATG translation initiation codon in the reference sequence, according to journal guidelines (www.hgvs.org/mutnomen). The initiation codon is codon 1.

Retroviral Expression Vectors

The retroviral (RV) backbone *pMSCV-puro* (Clontech, Mountain View, CA) was modified to replace the puromycin selection gene with *eGFP*, to create *pMSCV–IRES–eGFP*, which served as the RV control vector [Zammit et al., 2006]. Wild-type [Motsch et al., 2005] and four mutant human lamin A pEGFP-C1 cDNAs (R25P, R249W, N456I, and R541P) were subcloned into pMSCV–IRES–eGFP to generate control *pMSCV–laminA–IRES–eGFP* and *pMSCV–laminA–R25P–IRES–eGFP, pMSCV–laminA–R249W–IRES–eGFP, pMSCV—laminA–N456I–IRES–eGFP,* and *pMSCV–laminA–R541P–IRES–eGFP*, producing either wild-type lamin A

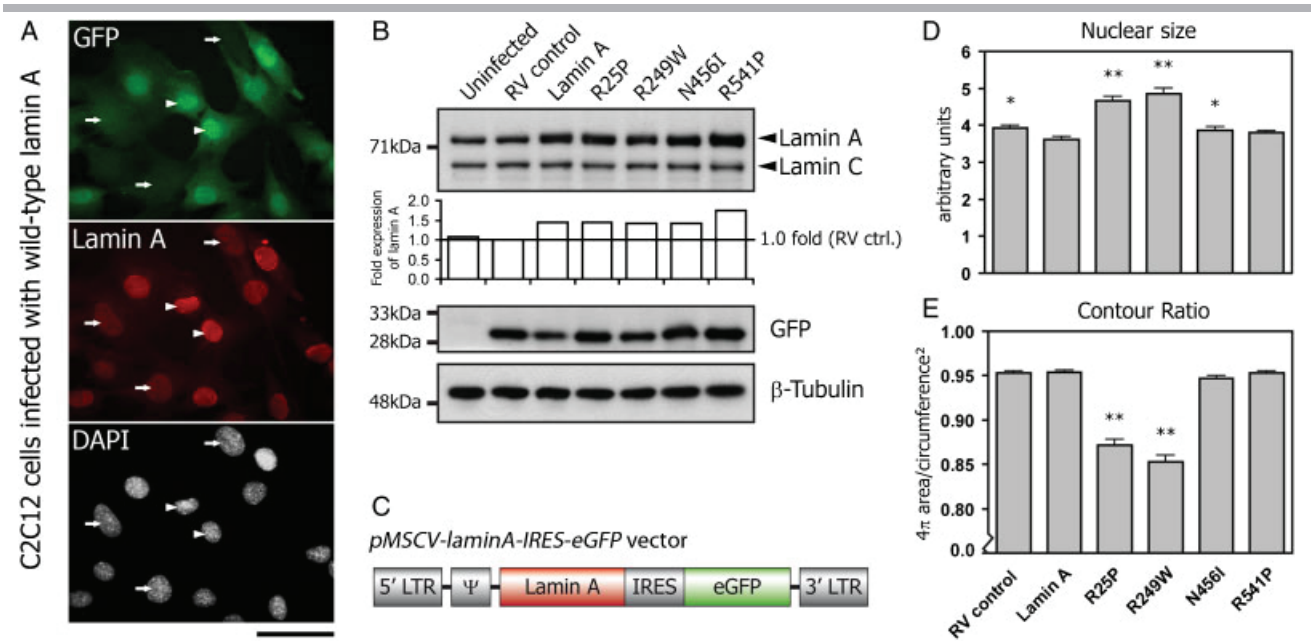

Figure 2. Mutant lamin A species affect nuclear size and shape in myogenic cells. **A:** Proliferating mouse C2C12 cells infected with control pMSCV–laminA–IRES–eGFP encoding wild-type lamin A-IRES–eGFP and immunostained for eGFP and lamin A. Cells expressing high levels of GFP show a increased expression of lamin A wild type (arrowheads) compared to cells expressing low levels of GFP (arrows); Scale bar 100 μm. **B:** Western blot of uninfected C2C12 cells and cells infected with *pMSCV–IRES–eGFP* (RV control), *pMSCV–laminA–IRES–eGFP* (Lamin A), *pMSCV–laminA–R25P–IRES–eGFP* (R25P), *pMSCV–laminA–R249W–IRES–eGFP* (R249W), *pMSCV–laminA–N456I–IRES–eGFP* (N456I) and *pMSCV–laminA–R541P–IRES–eGFP* (R541P). A representative blot probed for lamin A/C (N19) is shown. The relative quantities of lamin A normalized to β-tubulin are shown below, and range from 1.5–1.7-fold endogenous lamin A levels in the RV control sample. The endogenous level of lamin C does not change with constitutive expression of wild-type lamin A or the mutant forms. **C:** Schematic of the *pMSCV–laminA–IRES-EGFP* vector used in this study, indicating the 5′ and 3′ long terminal repeats (LTR), ψ; packaging signal, the lamin A (wild-type or mutant versions) and eGFP cDNAs, separated by an internal ribosome entry site (IRES). **D:** Nuclear size (cross-sectional area) of cells with lamin A-R25P and lamin A-R249W increased by 29 ± 3.3% and 34 ± 4.5%, respectively, compared to lamin A wild-type infected cells. **E:** The contour ratio was significantly decreased in nuclei of cells expressing lamin A-R25P (0.87 ± 0.006) and lamin A-R249W (0.85 ± 0.007), but not with the other two mutant lamin A species. Values represent the mean ± SEM; $^{*}P<0.05$; $^{**}P<0.01$ compared to lamin A wild-type infected cells. [Color figure can be viewed in the online issue, which is available, at wileyonlinelibrary.com]

as a control, or mutant lamin A species, as a bicistronic message with eGFP (Fig. 2C). Retroviral constructs, together with an ecotropic packaging plasmid, were transiently cotransfected into 293T cells to produce nonreplicating retrovirus and the supernatant harvested 48, 60, and 72 hr later.

Cell Culture and Retroviral Infection

C2C12 mouse myoblast cells were grown and maintained in DMEM-Glutamax (Invitrogen, Paisley, UK) supplemented with 10% FBS (PAA, Somerset, UK) and 1% Penicillin/Streptomycin (Sigma, Dorset, UK). A total of 20,000 C2C12 cells were plated into one well of a six-well plate and exposed to retroviral supernatant (diluted 1:5 in growth medium supplemented with 4 μg/mL polybrene) for at least 12 hr, before they were analyzed at least 24 hr later.

Morphometric Analysis

To quantify the morphological abnormalities of nuclei such as elongation or lobulation, we measured the perimeter and the area of at least 120 nuclei from three independent experiments and calculated the nuclear roundness or contour ratio (4π; area/circumference^2) [Goldman et al., 2004]. The contour ratio of a circle is 1, and the value gets smaller with an increased degree of lobulation. Micrographs of infected C2C12 cells stained for lamin B were analyzed using the NIH ImageJ software (http://rsbweb.nih.gov/ij/). To calculate the perimeter and area of the nuclei, they were outlined using the polygon selection tool and measured with ImageJ. A two-tailed Student's *t*-test was used to calculate the statistical significance of the result.

Immunostaining

Cells were fixed with 4% paraformaldehyde (PFA) for 10 min, permeabilized with 0.5% Triton X-100 in PBS for 10 min and blocked with 5% normal goat serum and 5% normal swine serum (or 5% horse serum and 5% normal swine serum when primary antibodies raised in goat were used) in PBS/0.025% Tween20 for 1 hr at room temperature. After incubation with primary antibody in 1% serum (goat anti-lamin A C20 1:100, goat anti-lamin A/C N18 1:200, goat anti-lamin B [recognizes all forms] M20 1:200 [Santa Cruz Biotechnology, Santa Cruz, CA]; rabbit anti-emerin AP8 1:100 [Ellis et al., 1998]; rabbit anti-GFP 1:500 [Molecular Probes, Eugene, OR] and mouse anti-GFP 7.1 and 13.1 1:100 [Roche, Mannheim, Germany]), the cells were washed and exposed to fluorescently coupled secondary antibodies (Alexa Fluor, Molecular Probes) at a concentration of 1:500 and mounted in DAPI containing mounting medium. F-actin was stained by exposing the PFA-fixed cells to Alexa Fluor 633-conjugated phalloidin (Molecular Probes) (diluted 1:50 in PBS + 0.025% Tween20) for 30 min prior washing, and mounting the slides with DAPI containing mounting medium.

Fluorescence Intensity Measurement

Representative nuclei stained for DAPI, lamin A, and lamin B, respectively, were analyzed using the "Plot Profile" tool in ImageJ. The x and y coordinates were imported in MS Excel to compile the histogram.

Western Blot

Harvested cells were resuspended in suspension buffer (100 mM NaCl, 10 mM Tris-HCl pH 7.5, 1 mM EDTA) supplemented with proteinase inhibitors and lysed in loading buffer [Laemmli, 1970]. The protein concentration was determined with the Bio-Rad DC Protein Assay based on the Lowry method [Lowry et al., 1951]. Samples were immunoblotted with the following antibodies: goat antilamin A/C N18 1:1000 (Santa Cruz Biotechnology), rabbit anti-GFP 1:2000 (Molecular Probes), mouse anti-β-tubulin 1:1000 (DSHB, Iowa City, IA), and then probed with HRP-conjugated secondary antibodies (ECL^{TM}; sheep antimouse or rabbit 1:5000, GE Healthcare, Uppsala, Sweden; sheep antigoat SO84 1:5000, Abcam, Cambridge, UK), and developed using ECL from GE Healthcare. Band intensity was quantified using ImageJ.

Results

Clinical and Genetic Information on 50 Patients

This is the first report on the distribution of *LMNA* mutations from a large patient cohort from the United States and Canada. Among the 255 referrals, 23 patients (9.0%) were found to possess *EMD* gene mutations (manuscript in preparation), and 61 individuals (23.9%) were found to have *LMNA* mutations. Clinical and genetic information on 11 of the patients with *LMNA* mutations has been published previously [Brown et al., 2001]. The mutations identified in the remaining 50 patients and their clinical information are presented in Tables 1 and 2.

Among the 50 individuals found to carry a *LMNA* mutation, 37 different mutations (in 36 patients) were detected, scattered throughout the gene (Fig. 1A and Tables 1 and 2). The majority of *LMNA* mutations identified here are missense mutations (27/37; 73.0%), with an additional two mutations being small in-frame insertions or deletions (2/37; 5.4%). Seven mutations were found to be deleterious mutations at conserved donor or acceptor splice site sequences (5/37; 13.5%) or silent mutations (2/37; 5.4%). Importantly, the bases associated with the silent mutations are located on the first or last base of the exon, so could affect splicing efficiency. The final mutation in patient 2974 was the only frame shift mutation, presumably encoding both truncated lamin A and lamin C protein species (1/37; 2.7%). This patient had a predominantly cardiac phenotype with only mild skeletal muscle weakness developing at age 50. These results are consistent with the phenotypes of other patients found to possess truncating mutations [Benedetti et al., 2007]. The most common previously reported *LMNA* mutation, c.1357C>T (p.R453W), was also the most frequent in our study group, being found in six (12.0%) of the patients. Two mutations were found to be confined to the lamin A protein, p.G602S, and p.R644C, suggesting that alterations in the far C-terminus of the lamin A protein alone is sufficient to cause EDMD2. A few of the patients with p.R249W, p.E358K or p.N39S presented at <1–2 years old (Table 1), which is below the average onset age for a severe EDMD2 case (32 months). Interestingly, these mutations have recently been reported to be associated with the congenital muscular dystrophy L-CMD, presenting from birth to 1 year.

Five patients (33, 7975, 1412, 6388, and 2660) had mutations located in noncoding regions at the exon–intron or intron–exon junctions affecting the universally conserved GT and AG dinucleotides. Therefore, these mutations likely affect pre-mRNA splicing although RNA analysis was not performed. These patients with intronic splice-site mutations presented with an EDMD phenotype (Table 1). A further three patients (91, 778, and 2018) had two silent mutations located on either the first or last nucleotides of an exon, which could also modify splicing.

Of the 45 patients for whom a family history was available, there was an approximately even split between cases that appeared to be familial in origin (21/45 [46.7%]) compared to cases that appeared to be sporadic (24/45 [53.3%]). Indeed, for our commonest mutation for which we have information (p.R453W), two cases were familial and three cases were sporadic. DNA analysis was only performed on the family members of three cases classed as sporadic (patients 6537, 3734, and 778), which confirmed the de novo origin of mutations in these individuals. It is possible of course, that apparently sporadic cases may have relatives who are currently asymptomatic gene mutation carriers.

Novel Pathogenic *LMNA* Mutations

Of these 37 *LMNA* mutations, 15 are novel pathogenic *LMNA* mutations (highlighted in red in Fig. 1A and B and Tables 1 and 2), not previously published or listed in any of the following databases: The Universal Mutation Database (UMD) (http://www.umd.be/), Human Intermediate Filament Database (http://www.interfil.org/) [Szeverenyi et al., 2006] and the Leiden Open Variation Database (LOVD) (http://www.dmd.nl/). This augments the number of *LMNA* mutations known to cause EDMD by 16.5%, equating to an increase of 5.9% in the total known *LMNA* mutations. These 15 mutations include eight missense mutations (p.R189P, p.F206L, p.S268P, p.S295P, p.E361K, p.G449D, p.L454P, and p.W467R), three splice site mutations (c.IVS4+1G>A, c.IVS6−2A>G, c.IVS8+1G>A), one duplication/in frame insertion (p.R190dup), one deletion (p.Q355del) and two silent mutations (p.R119R and p.K270K). The majority of patients carrying novel mutations (13/15) show symptoms associated with EDMD, whereas patient 2018 carrying the silent mutation c.810G>A (p.K270K), was initially diagnosed with BMD, prior to screening for *LMNA* mutations. Patient 91 carrying the silent mutation c.357C>T (p.R119R) presented with an LGMD1B phenotype with cardiac involvement. Of the 12 mutations located in the coding region of *LMNA*, four are in coil 1B, five are in coil two of the central rod domain, and the remaining three are located on conserved residues in the Ig-like fold of the tail of the lamin A/C protein (Fig. 1).

The *LMNA* gene is well conserved with 33% homology of the coding region between *Drosophila melanogaster* and *Homo sapiens*. The majority of our novel missense mutations and one insertion (7/10) affect residues highly conserved between species from *Caenorhabditis elegans* to *Homo sapiens*, while the remaining two missense mutations and one deletion (p.R189P, p.S268P, and p.Q355del) are all located in the central rod domain, and affect residues that are less conserved between species (Fig. 1B).

Effects of Lamin A Mutants on Myogenic Cells

Having described pathogenic *LMNA* mutations in patients, we next sought to gain insight into the effects of several mutant

Table 1. Summary of Clinical Description of Patients with *LMNA* Mutations

ID#	LMNA mutation	Gender	Age of onset	Age of diagnosis	Origin	Skeletal muscle involvement	Contractures	Cardiac involvement	Other information
▼Novel mutations									
91	p.R119R	M	Childhood	Died at age 45	Familial	Progressive proximal leg weakness; LGMD phenotype	Heel cord	Mild dilated cardiomyopathy; LVEF, 42% and cardiac conduction disease; pacemaker at age 33; died of heart failure at age 45	Weakness and pacemaker in mother; sudden cardiac death in brother (age 5); cardiac arrest (in 40s) in maternal grandfather, uncle and aunt
3734[c]	p.R189P	M	10	33	Sporadic	Limb-girdle, proximal upper	Neck and elbow (age 14)	Primary AV block and palpitations at age 22	n.a.
2952	p.R190dup	F	n.a.	30	Familial	Generalized	None	Atrial standstill, ventricular arrythmia	n.a.
8542	p.F206L	M	n.a.	57	Familial	Generalized	n.a.	Cardiac conduction defect	n.a.
8434	p.S268P	M	n.a.	17	Familial	Proximal lower weakness	Elbow and achilles tendon	n.a.	n.a.
2018	p.K270K	M	n.a.	24	n.a.	n.a.	n.a.	Cardiomyopathy and conduction disorder	Initially diagnosed with BMD
778[c]	p.K270K	M	5	26	Sporadic	EDMD phenotype; Limb-girdle, proximal upper, distal lower	Elbow and ankle	Cardiac involvement age 25, prolonged PR-interval that slowly lengthened until at age 31 developed atrial fibrillation and cardiomyopathy; pacemaker at age 31	Muscle biopsy age 8—myocyte apoptosis.
33[a]	c.IVS4+1G>A (c.810+1G>A)	M	2	15	Familial	Proximal and distal weakness	Elbow, neck, and rigid spine	n.a.	n.a.
6298	p.S295P	F	n.a.	47	Familial	Proximal weakness	Generalized	Cardiomyopathy with conduction system defects	n.a.
116	p.Q355del	F	n.a.	33	Familial	Atrophy of deltoid, triceps, trapezius and proximal legs muscles and calf hypertrophy	n.a.	First-degree heart block at age 20; mild AV dysfunction on bundle studies	n.a.
2785	p.E361K	F	<5	12	Familial	EDMD phenotype	Ankle, achilles tendon, and elbow	n.a.	Cardiomyopathy in mother who received a heart transplant
7975	c.IVS6-2A>G (c.1159-2A>G)	M	n.a.	41	Sporadic	EDMD phenotype; moderate proximal upper, distal lower and limb-girdle weakness	Elbow (severe), neck, and ankle (minimal)	Cardiac conduction defect, pacemaker fitted	n.a.
342[a]	p.G449D	M	2	9	Familial	Limb-girdle, proximal upper and distal lower weakness	Neck, elbow (age 3) and ankle (age 9)	n.a.	n.a.
9106	p.L454P	F	7	21	Sporadic	Limb-girdle, proximal upper and distal lower weakness	Ankle (age 7), elbow and neck (age 12)	Cardiac involvement at age 22	Non-ambulatory at age 14
7461[a]	p.W467R	F	<3	5	Sporadic	Limb-girdle, proximal upper and distal lower weakness	Ankle (under age 3) and elbow (age 5)	n.a.	Clinical diagnosis of LGMD vs. CMD
2660	c.IVS8+1G>A (c.1488+1G>A)	M	n.a.	17	Sporadic	n.a.	n.a.	Pacemaker at age 24 which was replaced at age 30	Patient needed a cane and a scoot for ambulation; died in his early 30s (death possibly unrelated to EDMD)
▼Recurrent mutations									
6537[a,c]	p.N39S	M	<20 months	Died at age 13	Sporadic	Limb-girdle, proximal upper and distal lower weakness	Ankle (unhder age 4), knee (age 7), neck and elbow (age 9)	Right bundle branch block, AV block, atrial flutter, atrial fibrillation age 7, pacemaker at age 13	In wheelchair at age 4; patient died at age 13 of cardiac failure
5182	p.Y45C	M	n.a.	15	Sporadic	n.a.	n.a.	Severe dilated cardiomyopathy associated with muscular dystrophy, atrial flutter/fibrillation	n.a.
563	p.T150P	F	n.a.	38	Familial	Progressive limb weakness	Neck and elbow	Cardiac arrhythmia at age 22	n.a.
7897	p.R249W	M	n.a.	6	Familial?	Wasting of humeral muscles	Neck	n.a.	n.a.
61[a]	p.R249W	M	1	10	n.a.	Wasting/weakness of biceps, triceps, brachii	Elbow and ankle	n.a.	Initially diagnosed with FSHD; asymptomatic mother, grandfather with cardiac abnormalities

Table 1. Continued

ID#	LMNA mutation	Gender	Age of onset	Age of diagnosis	Origin	Skeletal muscle involvement	Contractures	Cardiac involvement	Other information
8281[a]	p.R249W	F	<1	13	Sporadic	Limb-girdle, proximal upper and distal lower weakness	Ankle (<age 3), elbow (age 6) and neck (age 11)	Primary AV block, prolonged PR-interval (age 6), prolapse of mitral valve with mitral insufficiency	Initially diagnosed with Spinal muscular atrophy
3[b]	p.R249W; p.R644C	F	<2	12	Sporadic	n.a.	Elbow and knee (age 5)	Mild ventricular enlargement with normal function at age 10, no cardiac disease or atrial arrythmias at age 18	Nonambulatory at age 5
9696	p.R249Q	F	n.a.	26	Sporadic	Proximal and distal upper and lower extremity weakness	Neck, elbows and knees	n.a.	n.a.
167[a]	p.R249Q	F	<2	28	Familial	CMD phenotype; distal and upper lower extremity weakness, facial weakness	Elbow	n.a.	Congenital cataracts, nystagmus, glaucoma
1943	p.L271P	M	n.a.	12	Familial	Humeroperoneal weakness	Elbow and tibialis anterior	Cardiomypathy	n.a.
2111	p.Q294P	F	n.a.	33	Familial	EDMD phenotype	n.a.	n.a.	n.a.
149[a]	p.S303P	M	<2	16	Sporadic	Mild proximal upper and lower weakness	n.a.	Normal sinus rhythm borderline prolonged PR-interval with occasional premature supraventricular complexes, poor R-wave progression	n.a.
2570[a]	p.E358K	M	n.a.	13	Sporadic	Proximal upper, distal lower and limb-girdle weakness;	Neck, elbow, ankle, and knee	Dysrhythmia with prolonged PR-interval (age 13)	Wheelchair at age 5
8419[a]	p.E358K	F	n.a.	7	Familial	Severe EDMD phenotype	n.a.	n.a.	n.a.
26[a]	p.E358K	M	2	7	Sporadic	Proximal and distal lower extremity weakness	Elbow, ankle, knee, and hip	n.a.	n.a.
2631	p.R386K	M	n.a.	30	Sporadic	n.a.	n.a.	n.a.	n.a.
5653	p.R386K	F	n.a.	33	n.a.	EDMD phenotype	n.a.	n.a.	n.a.
7309	p.R453W	M	n.a.	24	Familial	Mild proximal weakness;	Neck and heel cord	Echocardiogram shows mildly enlarged left atrium and ventricle, mild global hypokinesis and reduced systolic function, estimated LVEF 45%	CK level 2,607 U/L
565	p.R453W	M	n.a.	36	n.a.	EDMD phenotype	n.a.	First degree heart block	n.a.
2975	p.R453W	M	n.a.	32	Sporadic	Limb-girdle, proximal upper, distal lower	Neck, elbow, ankle, and knee	Beta blockers at age 22, pacemaker at age 32	Wheelchair at age 14
5176	p.R453W	M	<4	19	Sporadic	Limb-girdle, proximal upper, distal lower	Neck, elbow, and ankle	No cardiac involvement	n.a.
1283	p.R453W	F	6	28	Familial	Leg weakness (foot-drop like gait)	Elbow	EMG-diffuse myopathic process; cardiac involvement	Spinal fusion for sever thoracic–lumbar scoliosis (age 20); normal muscle biopsy (age 22), and normal CK level
68	p.R453W	M	3	7	Sporadic	LGMD phenotype; proximal lower extremity weakness	Hip	Normal electrocardiography	Increased CK level (2,012 U/L); muscle biopsy showed scattered hypercontracted fibers often associated with a membrane protein defect
1412	c.IVS7−2A>G (c.1381−2A>G)	M	n.a.	17	Sporadic	EDMD phenotype; muscular atrophy	Neck extensor, elbow flexor and ankle (severe), knee (minimal)	n.a.	Scoliosis requiring surgery
6388[b]	c.IVS7-1G>T (c.1381−1G>T); p.D461Y	F	<1	6	Familial	Proximal upper and limb-girdle weakness	Neck, elbow, ankle and knee	Cardiac catheterization (age 3); suggestive of probably early cardiomyopathy	n.a.
2974	p.T510YfsX42	M	n.a.	51	Sporadic	Mild proximal upper weakness at age 50	Mild elbow contractures	Arrythmia onset in 20s, pacemaker placement recommended at age 29, placed at age 42 when patient experienced incomplete heart block, heart transplant at age 51	n.a.

						Proximal upper and limb-girdle				
7288[a]	p.R527P	M	<3	5	Familial	weakness	None	Right bundle branch block diagnosed <age 4	n.a.	
1527	p.T528K	M	n.a.	11	Sporadic	n.a.	n.a.	n.a.	n.a.	
1200	p.T528R	M	n.a.	12	n.a.	n.a.	n.a.	n.a.	n.a.	
							Bilateral elbow			
						Congenital myopathy phenotype; distal	contractures (age	Normal EMG, myopathic biopsy,		
2257[a]	p.T528R	F	1	12	Sporadic	lower weakness	11), neck, ankle	no cardiac issues at age 11	Progressive arthrogryposis, increased CK level	
								Dilated cardiomyopathy; congestive	Family history of various degrees of DCM and	
2743	p.R541S	M	n.a.	13	Familial	n.a.	n.a.	heart failure requiring transplant	LGMD1B, loss of adipose tissue in females	
						LGMD1B phenotype; proximal upper,				
						limb-girdle, distal lower weakness,			One child with EDMD, the other with	
198	p.R541P	F	Childhood	52	Familial	loss of muscle mass (age 19)	Elbow, knee	Atrial fibrillation	LGMD1B	
							Hamstrings, elbows,			
							neck, and rigid			
853	p.G602S	M	n.a.	6	Sporadic	Limb-girdle weakness (age 11)	spine	Cardiac defect (atrial septal defect)	n.a.	
						Weakness and hypotonia of the				
						proximal musculature of the upper				
						and lower extremities and broad			Progression until age 10, then stabilization; CK	
51[a]	p.R644C	M	Birth	19	Sporadic	based gait (age 3)	Elbow and ankle	n.a.	level 1,400 U/L	

[a]Patients with a severe phenotype and single *LMNA* mutation.
[b]Compound heterozygous patients with a severe phenotype.
[c]Patients confirmed to be sporadic cases of EDMD by molecular analysis of family members including parents and siblings.
n.a., data not available; AV, Atrioventricular; CK, Creatine kinase; EMG, Electromyography; LVEF, left ventricular ejection fraction.

human lamin A species on myogenic cells. We chose four mutations from this (p.R249W and p.R541P) and our previous study (p.R25P and p.N456I) [Brown et al., 2001] that span the *LMNA* gene and affect different domains of the protein. The majority of pathogenic lamin A mutations are dominant, with usually only one allele being affected in patients. This suggests that in cases that are not caused by haploinsufficiency, the amount of mutated protein that is necessary to create a phenotype is relatively small. Importantly, patient myoblasts are not readily available and a commonly used DNA delivery method is cell transfection, which results in dramatic overexpression (up to 25-fold) of mutant lamin A [Bechert et al., 2003].

Retroviral infection is efficient in mouse C2C12 myogenic cells with an infection rate of >98% routinely obtained (data not shown). Retroviral-mediated constitutive expression of wild-type lamin A clearly shows the coexpression of lamin A and eGFP (Fig. 2A–C), with cells with higher levels of eGFP generally also expressing higher levels of lamin A (Fig. 2A). In addition to efficiently targeting >98% cells, retroviral-mediated constitutive expression also has the advantage that the levels of exogenous proteins are generally only moderately elevated compared to endogenous proteins. Western blot analysis confirmed increased levels of exogenous wild-type and mutant lamin A was only on average 1.3–1.7-fold higher than controls (Fig. 2B) resembling a more physiological condition. Endogenous expression level of lamin C was not affected (Fig. 2B).

The Presence of Lamin A-R25P and Lamin A-R249W Results in Abnormal Nuclear Morphology

We observed large differences in nuclear size depending on the lamin variant expressed. Although a small increase in the nuclear cross-sectional area was observed in cells treated with the RV control, the average nuclear size was further significantly increased in the presence of lamin A-R25P (29% increase) and lamin A-R249W (34% increase) compared to lamin A wild-type-infected cells (Fig. 2D). Constitutive expression of lamin A wild type did not have an effect on nuclear size. The dramatic increase in nuclear size coincides with changes in nuclear morphology. Normal ovoid nuclear morphology was observed when cells were infected with RV control (contour ratio 0.95 ± 0.003) or lamin A wild-type (0.95 ± 0.002). The presence of either lamin A-R25P or lamin A-R249W, however, resulted in abnormal nuclear morphology with simple or multiple lobules of the nuclear envelope. The contour ratio was significantly smaller in cells expressing lamin A-R25P (0.87 ± 0.006) and lamin A-R249W (0.85 ± 0.007), reflecting these nuclear distortions (Fig. 2E). Changes in both nuclear size and contour ratio occurred concomitantly. This effect was mutation specific however, because the presence of lamin A-N456I or lamin A-R541P did not alter nuclear size or shape.

Mutant Lamin A Protein Species Are Mislocalised in the Nucleus

Abnormalities in mutant lamin A protein distribution were also observed (Figs. 3 and 4A–C). Although all the mutant lamin A proteins were present to some degree at the nuclear periphery, there was frequent disorganization of the lattice, with evidence of lamin A capping, particularly in lamin A-R25P and lamin A-R249W-expressing nuclei (lamin A mislocalization is shown by arrows in Fig. 3). There were also more lamin A-positive nuclear speckles present, with a greater size distribution compared with cells expressing lamin A wild type. Prominent lamin A speckles distributed throughout the nucleus were particularly

Table 2. Summary of *LMNA* Mutations and Encoded Protein

ID #	*LMNA* mutation	*LMNA* exon/intron	Predicted amino acid change	Mutation type	Protein domain affected	Ref. for published mutations
▼Novel mutations						
91	c.357C>T	2	p.R119R	Silent	Coil 1b	Novel
3734	c.566_567delinsCC	3	p.R189P	Missense	Coil 1b	Novel
2952	c.568_570dup	3	p.R190dup	Duplication (In frame insertion)	Coil 1b	Novel
8542	c.618C>G	3	p.F206L	Missense	Coil 1b	Novel
8434	c.802T>C	4	p.S268P	Missense	Coil 2b	Novel
2018	c.810G>A	4	p.K270K	Silent	Coil 2b	Novel
778	c.810G>A	4	p.K270K	Silent	Coil 2b	Novel
33	c.IVS4+1G>A (c.810+1G>A)	IVS 4		Splice site		Novel
6298	c.883T>C	5	p.S295P	Missense	Coil 2b	Novel
116	c.1064_1066del	6	p.Q355del	In frame deletion	Coil 2b	Novel
2785	c.1081G>A	6	p.E361K	Missense	Coil 2b	Novel
7975	c.IVS6−2A>G (c.1159-2A>G)	IVS 6		Splice site		Novel
342	c.1346G>A	7	p.G449D	Missense	Tail (Ig-fold)	Novel
9106	c.1361T>C	7	p.L454P	Missense	Tail (Ig-fold)	Novel
7461	c.1399T>C	8	p.W467R	Missense	Tail (Ig-fold)	Novel
2660	c.IVS8+1G>A (c.1488+1G>A)	IVS 8		Splice site		Novel
▼Recurrent mutations						
6537	c.116A>G	1	p.N39S	Missense	Coil 1a	[Benedetti et al., 2007; Quijano-Roy et al., 2008]
5182	c.134A>G	1	p.Y45C	Missense	Coil 1a	[Bonne et al., 2000]
563	c.448A>C	2	p.T150P	Missense	Coil 1b	[Felice et al., 2000]
7897	c.745C>T	4	p.R249W	Missense	Coil 2a	[Quijano-Roy et al., 2008]
61	c.745C>T	4	p.R249W	Missense	Coil 2a	same as above
8281	c.745C>T	4	p.R249W	Missense	Coil 2a	same as above
3	c.745C>T; c.1930C>T	4; 11	p.R249W; p.R644C	Missense	Coil 2a; Tail (Lamin A specific)	[Quijano-Roy et al., 2008; Csoka et al., 2004; Genschel et al., 2001; Mercuri et al., 2005; Muntoni et al., 2006; Pasotti et al., 2008; Perrot et al., 2009; Rankin et al., 2008]
9696	c.746G>A	4	p.R249Q	Missense	Coil 2a	[Benedetti et al., 2007; Bonne et al., 2000; Boriani et al., 2003; Brown et al., 2001; Ki et al., 2002; Muchir et al., 2004; Raffaele Di Barletta et al., 2000; Rudenskaya et al., 2008; Vytopil et al., 2003]
167	c.746G>A	4	p.R249Q	Missense	Coil 2a	same as above
1943	c.812T>C	5	p.L271P	Missense	Coil 2b	[Kichuk Chrisant et al., 2004]
2111	c.881A>C	5	p.Q294P	Missense	Coil 2b	[Bonne et al., 2000]
149	c.907T>C	5	p.S303P	Missense	Coil 2b	[Onishi et al., 2002]
2570	c.1072G>A	6	p.E358K	Missense	Coil 2b	[Benedetti et al., 2007; Bonne et al., 2000, 2001; Mercuri et al., 2004; Quijano-Roy et al., 2008]
8419	c.1072G>A	6	p.E358K	Missense	Coil 2b	same as above
26	c.1072G>A	6	p.E358K	Missense	Coil 2b	same as above
2631	c.1157G>A	6	p.R386K	Missense	Coil 2b	[Bonne et al., 2000; Boriani et al., 2003]
5653	c.1157G>A	6	p.R386K	Missense	Coil 2b	same as above
7309	c.1357C>T	7	p.R453W	Missense	Tail (Ig-fold)	[Benedetti et al., 2007; Bonne et al., 1999; Bonne et al., 2000; Brette et al., 2004; Colomer et al., 2002; Fidzianska and Glinka, 2006; Golzio et al., 2007; Muchir et al., 2004; Raffaele Di Barletta et al., 2000; Vytopil et al., 2003]
565	c.1357C>T	7	p.R453W	Missense	Tail (Ig-fold)	same as above
2975	c.1357C>T	7	p.R453W	Missense	Tail (Ig-fold)	same as above
5176	c.1357C>T	7	p.R453W	Missense	Tail (Ig-fold)	same as above
1283	c.1357C>T	7	p.R453W	Missense	Tail (Ig-fold)	same as above
68	c.1357C>T	7	p.R453W	Missense	Tail (Ig-fold)	same as above
1412	c.IVS7−2A>G (c.1381−2A>G)	IVS 7		Splice site		[Quijano-Roy et al., 2008]
6388	c.IVS7−1G>T (c.1381−1G>T); c.1381G>T	IVS 7/exon 8	p.D461Y	Splice site; Missense	Tail (Ig-fold)	[Bakay et al., 2006]
2974	c.1526dup	9	p.T510YfsX42	Frame shift	Tail (Ig-fold)	[Arbustini et al., 2005]
7288	c.1580G>C	9	p.R527P	Missense	Tail (Ig-fold)	[Benedetti et al., 2007; Bonne et al., 1999, 2000; Brown et al., 2001; Raffaele Di Barletta et al., 2000; van der Kooi et al., 2002]

Table 2. Continued

ID #	*LMNA* mutation	*LMNA* exon/intron	Predicted amino acid change	Mutation type	Protein domain affected	Ref. for published mutations
1527	c.1583C>A	9	p.T528K	Missense	Tail (Ig-fold)	[Benedetti et al., 2007; Bonne et al., 2000; Fokkema et al., 2005; Raffaele Di Barletta et al., 2000]
1200	c.1583C>G	9	p.T528R	Missense	Tail (Ig-fold)	[Fokkema et al., 2005; Vytopil et al., 2003]
2257	c.1583C>G	9	p.T528R	Missense	Tail (Ig-fold)	same as above
2743	c.1621C>A	10	p.R541S	Missense	Tail	[Sylvius et al., 2005]
198	c.1622G>C	10	p.R541P	Missense	Tail	[van Tintelen et al., 2007]
853	c.1804G>A	11	p.G602S	Missense	Tail (Lamin A specific)	[Bakay et al., 2006; Young et al., 2005]
51	c.1930C>T	11	p.R644C	Missense	Tail (Lamin A specific)	[Csoka et al., 2004; Genschel et al., 2001; Mercuri et al., 2005; Muntoni et al., 2006; Pasotti et al., 2008; Perrot et al., 2009; Rankin et al., 2008]

LMNA GenBank Accession Number RefSeq NM_170707.2; Nucleotide numbering reflects cDNA numbering with +1 corresponding to the A of the ATG translation initiation codon in the reference sequence, according to journal guidelines (www.hgvs.org/mutnomen). The initiation codon is codon 1.

evident in many cells expressing the lamin A-N456I and lamin A-R541P mutant proteins (lamin A-N456I, 25.9±4.0%; lamin A-R541P, 9.0±3.5%) than with the other mutants (Fig. 4A and C). Lamin A speckles observed in lamin A-N456I infected cells were generally larger in size compared to those observed in lamin A-R541P infected cells (Fig. 4A). When the fluorescence intensity of lamin A together with that of DAPI was plotted on a histogram, lamin A-positive foci did not costain with the chromatin (Fig. 4B). Nuclear lamin A foci were not analyzed in cells infected with RV control because the fixation protocol used to preserve cellular morphology resulted in endogenous mouse lamin A being weakly detected (Fig. 3), compared to the robust immunostaining to the human lamin A species encoded by RVs.

Endogenous Lamin B Mis-localization in the Presence of Lamin A-R25P and R249W

To investigate whether other endogenous nuclear envelope components were mislocalized in the presence of the mutant lamin A proteins, we analyzed the expression of several components of the nuclear envelope by immunocytochemistry (Figs. 3 and 4D–F). Lamin A and C directly bind emerin in vitro [Vaughan et al., 2001] and have been shown to colocalize with mutant lamin A [Ostlund et al., 2001]. We therefore determined if the expression of our constructs had an effect on emerin localization, and if lamin A-N456I, in particular, could cause nuclear foci that strongly immunostain for emerin. However, none of the lamin A mutants induced nuclear foci that contained emerin, confirming previous descriptions [Capanni et al., 2003; Muchir et al., 2004] (Fig. 3). F-actin staining by standard immunofluorescence microscopy appeared normal, except in cells expressing the p.R25P mutation, where fewer stress fibers were observed (Fig. 3).

The localization of lamin B, however, was changed by the expression of two mutant lamins. In nuclei of cells expressing lamin A-R25P and lamin A-R249W, B-type lamins were lost from one or more poles in some cells (Fig. 3, arrowed and Fig. 4D), which was particularly severe with the p.R249W mutant. The DAPI staining pattern implies the nuclei remain intact, but the redistribution of lamin B is suggestive of nuclear membrane herniation. Figure 4D shows a detailed micrograph of lamin B stained cells infected with either lamin A wild-type, lamin A-R25P or lamin A-R249W. Fluorescent intensity profiles of DAPI and B-type lamin staining across a central axis of the nuclei were calculated (Fig. 4E). Whereas the signal for lamin B in cells expressing lamin A wild type (shown by the histogram) remained constant across the nucleus, in the presence of lamin A-R249W, where the central axis bisects one of the poles, the fluorescence intensity gradually reduced to background levels as the pole was approached. Nuclei of cells infected with lamin A-R25P showed an intermediate phenotype between lamin A wild type and lamin A-R249W. Although a mean of less than 6% of nuclei infected with lamin A wild type, lamin A-N456I, and lamin A-R541P were affected, the number of nuclei with a polar loss of lamin B was significantly higher in presence of lamin A-R25P (19.6±2.7%) and especially lamin A-R249W (32.7±3.3%), with cells containing the R249W mutation being the most severely affected (Fig. 4F).

Discussion

In this study we report 16 patients with novel, and 34 patients with recurring *LMNA* mutations, increasing the known *LMNA* mutation database by ~5.9% (The Universal Mutation Database; UMD). Because laminopathies are rare diseases, this significant increase in patient data will hopefully aid genotype–phenotype correlations.

Variable expressivity of the EDMD phenotype is noted in many families illustrating the importance of the genetic background for clinical presentation. One example of highly variable expressivity in EDMD2 is demonstrated by the family of patient 7309, found to be heterozygous for the common p.R453W lamin A/C mutation. The proband was initially diagnosed with a mild form of LGMD1B at age 6, and at age 26, he had mild proximal muscle weakness, contractures, and cardiac involvement. The probands father died of heart failure at age 61, at which time he had neck and elbow contractures, but minimal, if any, muscle weakness. The proband's paternal grandmother was not considered to be affected with EDMD until an autopsy performed at age 88 revealed a skeletal muscle myopathy consistent with this disorder, but a cardiac muscle biopsy exhibited no significant pathology. Another example of the phenomenon of variable expressivity is demonstrated by patient 33, who was found to be heterozygous for an intron 4 splice junction mutation. Although both patient 33 and his sister were known to be affected with EDMD2 upon referral for genetic testing, neither of their parents showed any clinical

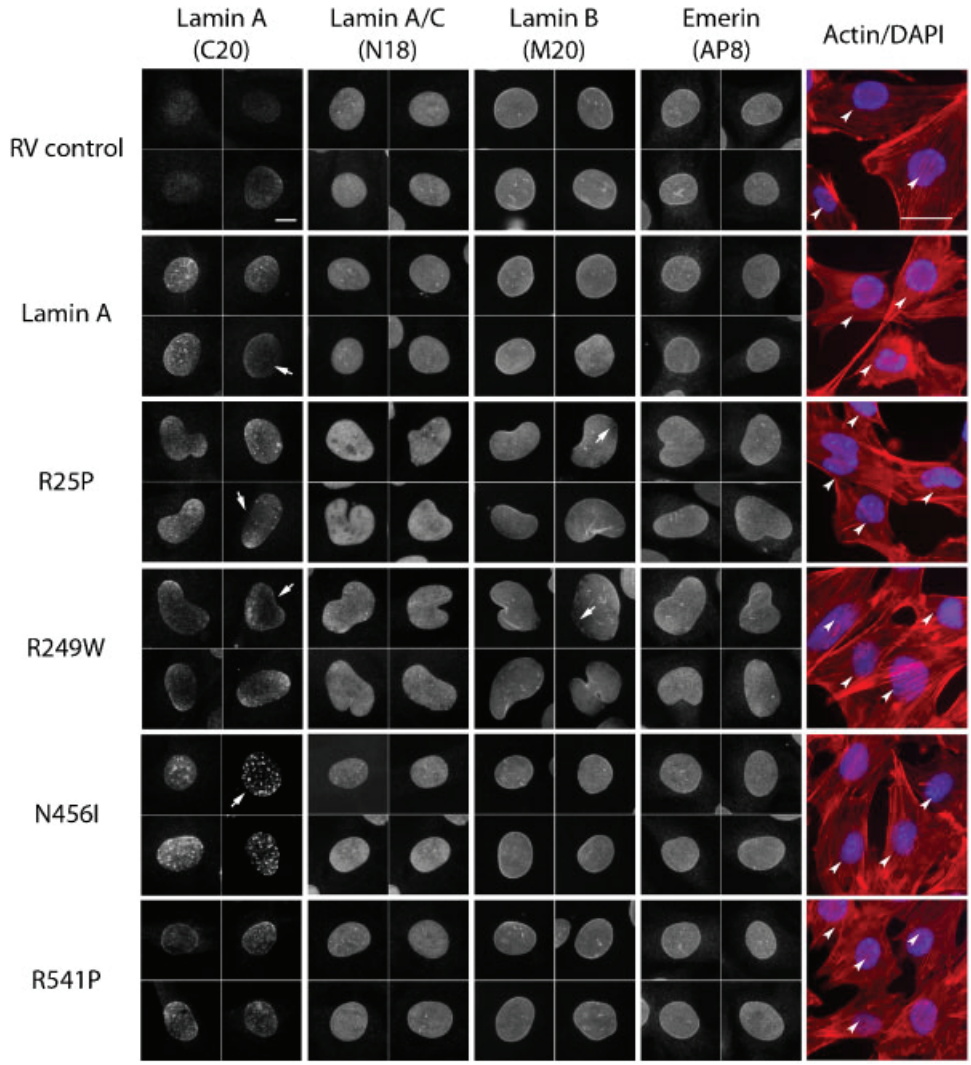

Figure 3. Distribution of nuclear envelope-associated components in myogenic cells infected with mutant lamin A. Cells infected with *pMSCV–IRES–eGFP* (RV control), *pMSCV–laminA–IRES–eGFP* (Lamin A), *pMSCV–laminA–R25P–IRES–eGFP* (R25P), *pMSCV–laminA–R249W–IRES–eGFP* (R249W), *pMSCV–laminA–N456I–IRES–eGFP* (N456I), and *pMSCV–laminA–R541P–IRES–eGFP* (R541P) were immunostained for nuclear envelope components (lamin A, lamin A/C, lamin B, emerin; Scale bar = 10 μm) and F-actin (red) (eGFP-positive infected cells are indicated by arrowheads; Scale bar = 50 μm). A representative selection of nuclei and cells are shown. Lamin A-positive nuclear speckles and lamin A capping (arrows) as well as a loss of lamin B from nuclear poles was evident to varying degrees in a mutant-dependent fashion. The localization of emerin was normal in all instances. [Color figure can be viewed in the online issue, which is available, at wileyonlinelibrary.com]

signs of this disorder. Molecular testing indicated that their father carried the splice junction mutation and shortly after receiving this information, presented with cardiac arrhythmia.

Two patients were found to have a missense mutation within codon 541. Patient 198, with a predicted p.R541P mutation within lamin A/C was diagnosed with LGMD1B. She has two affected children: a daughter diagnosed with mild LGMD1B and a son with a severe form of EDMD. A p.R541S mutation was detected in patient 2743, who required a heart transplant at age 13 due to severe DCM. Other members of this family possessing the p.R541S mutation were diagnosed with either dilated cardiomyopathy or LGMD1B, whereas female mutation carriers had an unusual habitus due to loss of adipose tissue.

We previously reported patient 1325 who is heterozygous for both p.E358K and p.R624H mutations [Brown et al., 2001]. We hypothesized that the compound heterozygous mutations found in this patient may account for her particularly severe phenotype, with the lamin A-specific mutation being either recessive or dominant with incomplete penetrance, as it was detected in her clinically unaffected father. Of note, three other patients in this study were found to be heterozygous for just the p.E358K mutation, and all appear to be severely affected with EDMD, making the role of the second, lamin A-specific mutation, in patient 1325 unclear. In this study, two compound heterozygous patients were found, both presenting with an early onset phenotype (marked by superscript b in Table 1). Patient 6388, with a severe form of EDMD, was compound heterozygous for c.IVS−1G>T and p.D461Y, two mutations that have been described before in a patient with early onset EDMD [Bakay et al., 2006]. A second severely affected patient (patient 3) was also found to be a compound heterozygote carrying p.R249W and p.R644C mutations. Interestingly, our study population included patients carrying each of these sequence alterations individually, with patient 8281 being heterozygous for the p.R249W alteration and patient 51 being heterozygous for the lamin A-specific p.R644C mutation. As the two latter patients with single

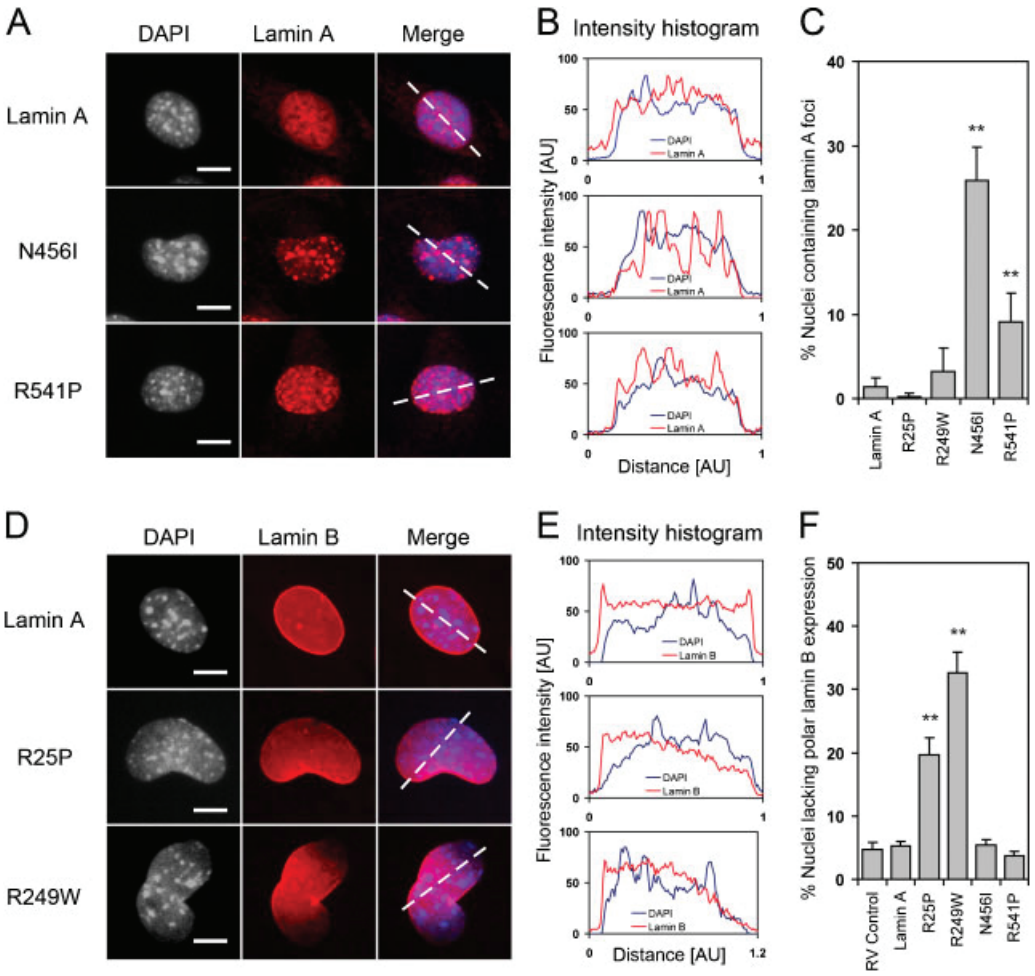

Figure 4. Nuclear abnormalities in myogenic cells infected with mutant lamin A. **A:** Prominent lamin A foci distributed throughout the nucleus were frequently observed in cells infected with lamin A-N456I and lamin A-R541P. Nuclei with representative lamin A foci are shown. Scale bar = 10 μm. **B:** The fluorescence intensity of DAPI and lamin A along the central axis indicated by a dashed line in A is shown in the adjacent histogram. **C:** Quantification of nuclei with prominent lamin A foci distributed throughout the nucleus. Values represent the mean ± SEM; $^{*}P<0.05$, $^{**}P<0.01$ compared to wild-type lamin A infected cells (wild type). **D:** Loss of lamin B expression from one or multiple poles is frequently observed in cells expressing lamin A-R25P and lamin A-R249W. Scale bar = 10 μm. **E:** The fluorescence intensity of DAPI and lamin B along the central axis indicated by a dashed line in D is shown in the histogram. **F:** Quantification of nuclei where a polar loss of lamin B expression was observed. Values represent the mean ± SEM; $^{*}P<0.05$, $^{**}P<0.01$ compared to wild-type lamin A infected cells.

mutations are affected with early age-of-onset disease, both of these mutations appear to act in a dominant fashion. This paradox suggests further studies are required to determine the true reason behind modifying effects, if any, of compound heterozygosity on clinical phenotype.

In 2008, Quijano-Roy et al. reported a new form of congenital muscular dystrophy associated with 11 different mutations in the *LMNA* gene [Quijano-Roy et al., 2008]. Notably, affected patients presented with muscle weakness between birth and the first year of life (rather than at an average age of 32 months as seen for EDMD2). L-CMD patients additionally display a dropped head, also not observed in EDMD2. The muscle weakness in L-CMD expresses as selective axial weakness and wasting of the cervicoaxial muscles with a predominantly proximal upper and distal lower limb involvement. Of 50 patients reported in our study, 14 (marked by superscript a in Table 1) associated with 11 different singular mutations originating from familial and sporadic origin, expressed a severe EDMD-like phenotype characterised by an onset of <3 years of age or early cardiac involvement. Three mutations (p.N39S, p.R249W, and p.E358K) with an early onset were also reported to cause L-CMD [Quijano-Roy et al., 2008]. Three further mutations described here (c.IVS4 +1G>A, p.G449D, and p.W467R) causing early onset EDMD are novel. The remaining five mutations (p.R249Q, p.S303P, p.R527P, p.T528R, and p.R644C) have been previously described as causing EDMD [Benedetti et al., 2007; Bonne et al., 1999, 2000; Boriani et al., 2003; Brown et al., 2001; Fokkema et al., 2005; Muchir et al., 2004; Onishi et al., 2002; Raffaele Di Barletta et al., 2000; van der Kooi et al., 2002; Vytopil et al., 2003] with R644C causing a large variety of phenotypes including EDMD [Brown et al., 2001; Csoka et al., 2004; Mercuri et al., 2005; Rankin et al., 2008]. We conclude that additional mechanisms must contribute to the disease severity at presentation such as modifier genes or digenism. Patients with mutations in both *EMD* and *LMNA* genes present with a more severe phenotype [Ben Yaou et al., 2007], but all our patients were also screened for *EMD* mutations and found to be negative.

Taking the entire lamin A protein, approximately 50% of all pathogenic mutations affect residues that are conserved from man to *C. elegans*. Although mutations in the conserved residues are

more likely to cause a phenotype, to date, no clear genotype–phenotype correlation has been established. Six of eight novel amino acid substitutions described in this report affect highly conserved residues of the lamin A protein. Two affected residues reported to be pathogenic (p.R189 and p.S268) are located in the central rod domain of lamin A and are not conserved in evolution. Interestingly, both nonconserved residues are mutated to a proline and located adjacent to pathogenic residues. These are p.R190, associated with DCM when mutated to Trp or Gln [Perrot et al., 2009; Sylvius et al., 2005], and p.Y267, associated with EDMD and DCM when mutated to His or Cys [Carboni et al., 2008; Vytopil et al., 2003]. Proline is not found in the center of a straight α-helix, due to its helix breaking attributes [Richardson and Richardson, 1988]. Interestingly, 9/30 (30%) of all pathogenic, nonconserved residues in the central rod domain, are substituted to a proline. Eight of these cause either EDMD or DCM, while one (p.A57P) has been reported to cause WRN [Chen et al., 2003]. Our data therefore confirms the assumption that the introduction of a proline is more likely to be pathogenic irrespective of amino acid conservation.

Eight patients were found to have mutations located on the exon–intron or intron–exon junctions, suggesting they may affect pre-mRNA splicing. In five (33, 7975, 1412, 6388, and 2660), the universally conserved GT and AG di-nucleotides are affected. The majority of intronic splice site mutations published so far are associated with DCM or LGMD1B [Chrestian et al., 2008; Muchir et al., 2000; Otomo et al., 2005] while others have been shown to result in EDMD [Bakay et al., 2006]. In our study, however, all patients with intronic splice site mutations presented with an EDMD phenotype (Table 1). We also had three patients with mutations located on either the first nucleotide of exon 2 or the last nucleotide of exon 4. Patient 2018, who presented with DCM, and patient 778, who presented with an EDMD phenotype with cardiac involvement, both had the last nucleotide of exon 4 mutated to an A (c.810G>A; p.K270K). In patient 91, who presented with an LGMD phenotype with cardiac involvement, the first nucleotide in exon 2 is mutated to a T (c.357C>T; p.R119R) (Fig. 1A). Such mutation types are very rare mutational events and only one other such mutation has been described so far in the *LMNA* gene. It is located on the last nucleotide of exon 2 (c.513G>A; p.K171K) and was found in four patients diagnosed with LGMD1B [Todorova et al., 2003]. mRNA analysis on these patients showed that this results in a partial skipping of the canonical 5′ splice site in intron 2 and the alternative use of a cryptic GT donor site within intron 2 leading to an insertion of 15 additional amino acids between exon 2 and 3 [Todorova et al., 2003].

Cells isolated from patients with *LMNA* mutations, or cells overexpressing mutant lamin A, often display aberrant localization of nuclear envelope proteins and changes in nuclear morphology. In our study, we observe both phenomena: constitutive lamin A-R25P and lamin A-R249W expression caused severe changes in nuclear shape and size, while lamin A-N456I and lamin A-R541P resulted in nuclear lamin A-positive foci. Nuclear foci staining for lamin A are frequently described when overexpressing mutant and lamin A wild type in vitro [Bechert et al., 2003; Holt et al., 2001; Ostlund et al., 2001]. In contrast, such foci are not very common in primary cells isolated from patients with *LMNA* mutations [Emerson et al., 2009; Markiewicz et al., 2002; Muchir et al., 2004; Taimen et al., 2009; Vigouroux et al., 2001; Zhang et al., 2007], suggesting that lamin A-positive foci formation can be attributed to lamin A overexpression. Patient fibroblasts that do show lamin A-positive foci usually carry FPLD but also EDMD causing mutations in the Ig-fold domain [Capanni et al., 2003; Muchir et al., 2004]. We see similar effects using mouse C2C12 myogenic cells. Cells expressing lamin A-R25P and lamin A-R249W do not form nuclear foci staining for lamin A. However, constitutive expression of the lamin A variants with a mutation in the Ig-like fold (lamin A-N456I) and adjacent to the Ig-like fold (Lamin A-R541P) induces lamin A foci formation in 25 and 10% of all infected nuclei, respectively. Although nuclear foci appear to be smaller in cells infected with lamin A-R541P, these results may suggest that the molecular mechanism inducing these foci and perhaps the underlying disease mechanism, is similar for the two mutations in the tail domain of lamin A analyzed in this study.

In contrast, constitutive lamin A-R25P and lamin A-R249W expression in mouse myogenic cells caused severe changes in nuclear shape and size. Nuclear blebbing is a type of nuclear distortion commonly found in progeria and other laminopathies [Eriksson et al., 2003; Goldman et al., 2004; Jacob and Garg, 2006; Taimen et al., 2009]. Khatau et al. [2009] report that the nuclear morphology can be regulated by a perinuclear actin cap, which is disrupted in cells from *lmna*$^{-/-}$ and *lmna*$^{L530P/L530P}$ mice. To test if the abnormal nuclear morphology we observed was associated with a misarranged actin-cytoskeleton, we stained infected C2C12 cells for F-actin. However, although there were perturbed F-actin stress fibers with lamin A-R25P, as has been described previously for other mutations in patient fibroblasts [Emerson et al., 2009], confocal imaging did not reveal differences in the perinuclear actin cap associated with this, or any of our other mutant lamin A-species (data not shown). This suggests that there might be other factors involved in nuclear deformation in this case. One possibility of nuclear deformation is a misregulation of nesprin or other members of the LINC complex which physically connects the nuclear lamin with the cytoskeleton [Razafsky and Hodzic, 2009]. The expression pattern of these interaction partners will be the subject of future investigations.

Interestingly, aberrant nuclear morphology in both mutants (lamin A-R25P and lamin A-R249W) is accompanied by a polar loss of lamin B expression in a mean of 20% and 33% of nuclei respectively. The same phenomenon has been observed by others in cells from HGPS patients with the p.E145K mutation [Taimen et al., 2009] and in fibroblasts isolated from FPLD patients [Vigouroux et al., 2001]. Mouse embryonic fibroblasts from mouse embryos homozygous for a truncated, nonfunctional form of lamin B1 show severely misshaped nuclei also, suggesting that the loss of lamin B1 is a causative event for the observed nuclear lobulation [Vergnes et al., 2004]. How mutated lamin A affects lamin B localization is unclear, and if a correction of lamin B expression can restore a normal nuclear morphology remains to be determined. It would also be very interesting to see if there are any *LMNA* single nucleotide polymorphisms (SNPs) that can affect lamin B localization and nuclear morphology.

Generally, patient fibroblasts with mutations associated with severe forms of laminopathies such as MAD (p.L59R, p.R527C, and p.R527H) [Agarwal et al., 2008; Nguyen et al., 2007; Novelli et al., 2002], WRN (p.R133L, and p.L140R) [Caux et al., 2003; Chen et al., 2003], and FPLD (p.R439C) [Verstraeten et al., 2009] all show the most profound changes in nuclear morphology. Taimen et al. [2009] have shown that nuclei of dermal fibroblast isolated from HGPS patients with the lamin A-E145K mutation show drastic changes in morphology and are severely lobulated. It has been suggested that the underlying mechanism of the pathogenicity of HGPS causing lamin A-E145K is a disrupted filament formation [Taimen et al., 2009]. However, mutant lamin A variants that caused an effect on nuclear morphology in our study result in either typical EDMD2 (lamin A-R25P) or an early

onset/L-CMD phenotype (lamin A-R249W), but whether they affect filament formation to differing degrees is unknown.

A-type lamins are expressed in mouse satellite cells: the resident stem cells of skeletal muscle [Gnocchi et al., 2009]. Therefore, perturbed lamin function does not only affect the myonuclei of muscle fibers, but could also compromise satellite cell-mediated muscle maintenance and repair. A disrupted nuclear morphology is likely to affect basic cellular processes, such as proliferation and differentiation of myoblasts [Gnocchi et al., 2008]. It is generally accepted that mutations in lamin A can affect cell cycle kinetics [Emerson et al., 2009; Johnson et al., 2004]. Fibroblasts from HGPS patients demonstrate a decreased cell growth rate [Goldman et al., 2004] and fibroblasts isolated from EDMD but not DCM patients have been shown to have an increase in cell proliferation [Emerson et al., 2009]. However, it has also been reported that cell cycle progression is dependent on nuclear size [Roca-Cusachs et al., 2008; Yen and Pardee, 1979]. It is therefore likely that cells expressing lamin A-R25P and lamin A-R249W show altered cell cycle progression and proliferation.

In conclusion, we describe 15 novel *LMNA* mutations that underlie a striated muscle phenotype, increasing the LMNA mutation spectrum by ~6%. These will contribute toward formulating more accurate genotype–phenotype correlations in the laminopathies. Our analysis of 4 LMNA mutations shows that mutations located in the head and central rod domain perturb lamin B polarization and nuclear morphology, while the two mutations in the Ig-fold domain and adjacent to the Ig-fold domain, increase the incidence of lamin A-positive nuclear foci. We conclude that although the molecular mechanisms underlying the *LMNA*-generated pathogenic cascade in a particular tissue, with respect to intrinsic cellular processes such as cell cycle, cell signalling, etc., may be similar for a given laminopathy, the disease penetrance and clinical variability within a phenotype may arise from the combined contribution of genetic background, digenism and environmental factors.

Acknowledgments

The laboratory of PSZ is also supported by The Muscular Dystrophy Campaign, the Association of International Cancer Research, Association Française contre les Myopathies, The Wellcome Trust, and OPTISTEM (contract 223098), through the European Union 7th Framework Programme.

References

Agarwal AK, Kazachkova I, Ten S, Garg A. 2008. Severe mandibuloacral dysplasia-associated lipodystrophy and progeria in a young girl with a novel homozygous Arg527Cys LMNA mutation. J Clin Endocrinol Metab 93:4617–4623.

Arbustini EA, Pasotti M, Pilotto A, Repetto A, Grasso M, Diegoli M. 2005. Gene symbol: CMD1A. Disease: dilated cardiomyopathy associated with conduction system disease. Hum Genet 117:295.

Bakay M, Wang Z, Melcon G, Schiltz L, Xuan J, Zhao P, Sartorelli V, Seo J, Pegoraro E, Angelini C, Shneiderman B, Escolar D, Chen YW, Winokur ST, Pachman LM, Fan C, Mandler R, Nevo Y, Gordon E, Zhu Y, Dong Y, Wang Y, Hoffman EP. 2006. Nuclear envelope dystrophies show a transcriptional fingerprint suggesting disruption of Rb-MyoD pathways in muscle regeneration. Brain 129(Pt 4):996–1013.

Bechert K, Lagos-Quintana M, Harborth J, Weber K, Osborn M. 2003. Effects of expressing lamin A mutant protein causing Emery-Dreifuss muscular dystrophy and familial partial lipodystrophy in HeLa cells. Exp Cell Res 286:75–86.

Ben Yaou R, Toutain A, Arimura T, Demay L, Massart C, Peccate C, Muchir A, Llense S, Deburgrave N, Leturcq F and others. 2007. Multitissular involvement in a family with LMNA and EMD mutations: Role of digenic mechanism? Neurology 68: 1883–1894.

Benedetti S, Menditto I, Degano M, Rodolico C, Merlini L, D'Amico A, Palmucci L, Berardinelli A, Pegoraro E, Trevisan CP and others. 2007. Phenotypic clustering of lamin A/C mutations in neuromuscular patients. Neurology 69:1285–1292.

Bione S, Maestrini E, Rivella S, Mancini M, Regis S, Romeo G, Toniolo D. 1994. Identification of a novel X-linked gene responsible for Emery-Dreifuss muscular dystrophy. Nat Genet 8:323–3237.

Bonne G, Di Barletta MR, Varnous S, Becane HM, Hammouda EH, Merlini L, Muntoni F, Greenberg CR, Gary F, Urtizberea JA, Duboc D, Fardeau M, Toniolo D, Schwartz K. 1999. Mutations in the gene encoding lamin A/C cause autosomal dominant Emery-Dreifuss muscular dystrophy. Nat Genet 21: 285–288.

Bonne G, Mercuri E, Muchir A, Urtizberea A, Becane HM, Recan D, Merlini L, Wehnert M, Boor R, Reuner U, Vorgerd M, Wicklein EM, Eymard B, Duboc D, Penisson-Besnier I, Cuisset JM, Ferrer X, Desguerre I, Lacombe D, Bushby K, Pollitt C, Toniolo D, Fardeau M, Schwartz K, Muntoni F. 2000. Clinical and molecular genetic spectrum of autosomal dominant Emery-Dreifuss muscular dystrophy due to mutations of the lamin A/C gene. Ann Neurol 48:170–180.

Bonne G, Yaou RB, Beroud C, Boriani G, Brown S, de Visser M, Duboc D, Ellis J, Hausmanowa-Petrusewicz I, Lattanzi G, Merlini L, Morris G, Muntoni F, Opolski G, Pinto YM, Sangiuolo F, Toniolo D, Trembath R, van Berlo JH, van der Kooi AJ, Wehnert M. 2003. 108th ENMC International Workshop, 3rd Workshop of the MYO-CLUSTER project: EUROMEN, 7th International Emery-Dreifuss Muscular Dystrophy (EDMD) Workshop, 13–15 September 2002, Naarden, The Netherlands. Neuromuscul Disord 13:508–515.

Boriani G, Gallina M, Merlini L, Bonne G, Toniolo D, Amati S, Biffi M, Martignani C, Frabetti L, Bonvicini M, Rapezzi C, Branzi A. 2003. Clinical relevance of atrial fibrillation/flutter, stroke, pacemaker implant, and heart failure in Emery-Dreifuss muscular dystrophy: a long-term longitudinal study. Stroke 34:901–908.

Brette S, Penisson-Besnier I, Dupuis JM, Bonne G, Victor J. 2004. [Cardiac manifestations of laminopathies]. Arch Mal Coeur Vaiss 97:973–977.

Broers JL, Ramaekers FC, Bonne G, Yaou RB, Hutchison CJ. 2006. Nuclear lamins: laminopathies and their role in premature ageing. Physiol Rev 86:967–1008.

Brown CA, Lanning RW, McKinney KQ, Salvino AR, Cherniske E, Crowe CA, Darras BT, Gominak S, Greenberg CR, Grosmann C, Heydemann P, Mendell JR, Pober BR, Sasaki T, Shapiro F, Simpson DA, Suchowersky O, Spence JE. 2001. Novel and recurrent mutations in lamin A/C in patients with Emery-Dreifuss muscular dystrophy. Am J Med Genet 102:359–367.

Capanni C, Cenni V, Mattioli E, Sabatelli P, Ognibene A, Columbaro M, Parnaik VK, Wehnert M, Maraldi NM, Squarzoni S, Lattanzi G. 2003. Failure of lamin A/C to functionally assemble in R482L mutated familial partial lipodystrophy fibroblasts: altered intermolecular interaction with emerin and implications for gene transcription. Exp Cell Res 291:122–134.

Carboni N, Mura M, Marrosu G, Cocco E, Ahmad M, Solla E, Mateddu A, Maioli MA, Marini S, Nissardi V, Frau J, Mallarini G, Mercuro G, Marrosu MG. 2008. Muscle MRI findings in patients with an apparently exclusive cardiac phenotype due to a novel LMNA gene mutation. Neuromuscul Disord 18: 291–298.

Caux F, Dubosclard E, Lascols O, Buendia B, Chazouilleres O, Cohen A, Courvalin JC, Laroche L, Capeau J, Vigouroux C, Christin-Maitre S. 2003. A new clinical condition linked to a novel mutation in lamins A and C with generalized lipoatrophy, insulin-resistant diabetes, disseminated leukomelanodermic papules, liver steatosis, and cardiomyopathy. J Clin Endocrinol Metab 88:1006–1013.

Chen L, Lee L, Kudlow BA, Dos Santos HG, Sletvold O, Shafeghati Y, Botha EG, Garg A, Hanson NB, Martin GM, Mian IS, Kennedy BK, Oshima J. 2003. LMNA mutations in atypical Werner's syndrome. Lancet 362:440–445.

Chrestian N, Valdmanis PN, Echahidi N, Brunet D, Bouchard JP, Gould P, Rouleau GA, Champagne J, Dupre N. 2008. A novel mutation in a large French–Canadian family with LGMD1B. Can J Neurol Sci 35:331–334.

Clements L, Manilal S, Love DR, Morris GE. 2000. Direct interaction between emerin and lamin A. Biochem Biophys Res Commun 267:709–714.

Colomer J, Iturriaga C, Bonne G, Schwartz K, Manilal S, Morris GE, Puche M, Fernandez-Alvarez E. 2002. Autosomal dominant Emery-Dreifuss muscular dystrophy: a new family with late diagnosis. Neuromuscul Disord 12:19–25.

Csoka AB, Cao H, Sammak PJ, Constantinescu D, Schatten GP, Hegele RA. 2004. Novel lamin A/C gene (LMNA) mutations in atypical progeroid syndromes. J Med Genet 41:304–308.

De Sandre-Giovannoli A, Bernard R, Cau P, Navarro C, Amiel J, Boccaccio I, Lyonnet S, Stewart CL, Munnich A, Le Merrer M, Lévy N. 2003. Lamin a truncation in Hutchinson-Gilford progeria. Science 300:2055.

De Sandre-Giovannoli A, Chaouch M, Kozlov S, Vallat JM, Tazir M, Kassouri N, Szepetowski P, Hammadouche T, Vandenberghe A, Stewart CL, Grid D, Lévy N. 2002. Homozygous defects in LMNA, encoding lamin A/C nuclear-envelope proteins, cause autosomal recessive axonal neuropathy in human (Charcot-Marie-Tooth disorder type 2) and mouse. Am J Hum Genet 70:726–736.

Ellis JA, Craxton M, Yates JR, Kendrick-Jones J. 1998. Aberrant intracellular targeting and cell cycle-dependent phosphorylation of emerin contribute to the Emery-Dreifuss muscular dystrophy phenotype. J Cell Sci 111(Pt 6):781–792.

Emerson LJ, Holt MR, Wheeler MA, Wehnert M, Parsons M, Ellis JA. 2009. Defects in cell spreading and ERK1/2 activation in fibroblasts with lamin A/C mutations. Biochim Biophys Acta 1792:810–821.

Emery AE. 1989. Emery-Dreifuss syndrome. J Med Genet 26:637–641.

Eriksson M, Brown WT, Gordon LB, Glynn MW, Singer J, Scott L, Erdos MR, Robbins CM, Moses TY, Berglund P, Dutra A, Pak E, Durkin S, Csoka AB, Boehnke M, Glover TW, Collins FS. 2003. Recurrent de novo point mutations in lamin A cause Hutchinson-Gilford progeria syndrome. Nature 423:293–298.

Fatkin D, MacRae C, Sasaki T, Wolff MR, Porcu M, Frenneaux M, Atherton J, Vidaillet Jr HJ, Spudich S, De Girolami U, Seidman JG, Seidman C, Muntoni F, Müehle G, Johnson W, McDonough B. 1999. Missense mutations in the rod domain of the lamin A/C gene as causes of dilated cardiomyopathy and conduction-system disease. N Engl J Med 341:1715–1724.

Felice KJ, Schwartz RC, Brown CA, Leicher CR, Grunnet ML. 2000. Autosomal dominant Emery-Dreifuss dystrophy due to mutations in rod domain of the lamin A/C gene. Neurology 55:275–280.

Fidzianska A, Glinka Z. 2006. Rimmed vacuoles with beta-amyloid and tau protein deposits in the muscle of children with hereditary myopathy. Acta Neuropathol 112:185–193.

Fokkema IF, den Dunnen JT, Taschner PE. 2005. LOVD: easy creation of a locus-specific sequence variation database using an "LSDB-in-a-box" approach. Hum Mutat 26:63–68.

Genschel J, Bochow B, Kuepferling S, Ewert R, Hetzer R, Lochs H, Schmidt H. 2001. A R644C mutation within lamin A extends the mutations causing dilated cardiomyopathy. Hum Mutat 17:154.

Gnocchi VF, Ellis JA, Zammit PS. 2008. Does satellite cell dysfunction contribute to disease progression in Emery-Dreifuss muscular dystrophy? Biochem Soc Trans 36(Pt 6):1344–1349.

Gnocchi VF, White RB, Ono Y, Ellis JA, Zammit PS. 2009. Further characterisation of the molecular signature of quiescent and activated mouse muscle satellite cells. PLoS One 4:e5205.

Goldman RD, Shumaker DK, Erdos MR, Eriksson M, Goldman AE, Gordon LB, Gruenbaum Y, Khuon S, Mendez M, Varga R, Collins FS. 2004. Accumulation of mutant lamin A causes progressive changes in nuclear architecture in Hutchinson-Gilford progeria syndrome. Proc Natl Acad Sci USA 101:8963–8968.

Golzio PG, Chiribiri A, Gaita F. 2007. "Unexpected" sudden death avoided by implantable cardioverter defibrillator in Emery Dreifuss patient. Europace 9: 1158–1160.

Gueneau L, Bertrand AT, Jais JP, Salih MA, Stojkovic T, Wehnert M, Hoeltzenbein M, Spuler S, Saitoh S, Verschueren A, Tranchant C, Beuvin M, Lacene E, Romero NB, Heath S, Zelenika D, Voit T, Eymard B, Ben Yaou R, Bonne G. 2009. Mutations of the FHL1 gene cause Emery-Dreifuss muscular dystrophy. Am J Hum Genet 85:338–353.

Hegele RA, Anderson CM, Cao H. 2000. Lamin A/C mutation in a woman and her two daughters with Dunnigan-type partial lipodystrophy and insulin resistance. Diabetes Care 23:258–259.

Holt I, Clements L, Manilal S, Brown SC, Morris GE. 2001. The R482Q lamin A/C mutation that causes lipodystrophy does not prevent nuclear targeting of lamin A in adipocytes or its interaction with emerin. Eur J Hum Genet 9:204–208.

Holt I, Ostlund C, Stewart CL, Man N, Worman HJ, Morris GE. 2003. Effect of pathogenic mis-sense mutations in lamin A on its interaction with emerin in vivo. J Cell Sci 116(Pt 14):3027–3035.

Jacob KN, Garg A. 2006. Laminopathies: multisystem dystrophy syndromes. Mol Genet Metab 87:289–302.

Johnson BR, Nitta RT, Frock RL, Mounkes L, Barbie DA, Stewart CL, Harlow E, Kennedy BK. 2004. A-type lamins regulate retinoblastoma protein function by promoting subnuclear localization and preventing proteasomal degradation. Proc Natl Acad Sci USA 101:9677–9682.

Khatau SB, Hale CM, Stewart-Hutchinson PJ, Patel MS, Stewart CL, Searson PC, Hodzic D, Wirtz D. 2009. A perinuclear actin cap regulates nuclear shape. Proc Natl Acad Sci USA 106:19017–19022.

Ki CS, Hong JS, Jeong GY, Ahn KJ, Choi KM, Kim DK, Kim JW. 2002. Identification of lamin A/C (LMNA) gene mutations in Korean patients with autosomal dominant Emery-Dreifuss muscular dystrophy and limb-girdle muscular dystrophy 1B. J Hum Genet 47:225–228.

Kichuk Chrisant MR, Drummond-Webb J, Hallowell S, Friedman NR. 2004. Cardiac transplantation in twins with autosomal dominant Emery-Dreifuss muscular dystrophy. J Heart Lung Transplant 23:496–498.

Laemmli UK. 1970. Cleavage of structural proteins during the assembly of the head of bacteriophage T4. Nature 227:680–685.

Lee KK, Haraguchi T, Lee RS, Koujin T, Hiraoka Y, Wilson KL. 2001. Distinct functional domains in emerin bind lamin A and DNA-bridging protein BAF. J Cell Sci 114(Pt 24):4567–4673.

Lin F, Worman HJ. 1993. Structural organization of the human gene encoding nuclear lamin A and nuclear lamin C. J Biol Chem 268:16321–16326.

Lowry OH, Rosebrough NJ, Farr AL, Randall RJ. 1951. Protein measurement with the Folin phenol reagent. J Biol Chem 193:265–275.

Markiewicz E, Venables R, Mauricio Alvarez R, Quinlan R, Dorobek M, Hausmanowa-Petrucewicz I, Hutchison C. 2002. Increased solubility of lamins and redistribution of lamin C in X-linked Emery-Dreifuss muscular dystrophy fibroblasts. J Struct Biol 140:241–253.

McGrath MJ, Cottle DL, Nguyen MA, Dyson JM, Coghill ID, Robinson PA, Holdsworth M, Cowling BS, Hardeman EC, Mitchell CA, Brown S. 2006. Four and a half LIM protein 1 binds myosin-binding protein C and regulates myosin filament formation and sarcomere assembly. J Biol Chem 281:7666–7683.

Mercuri E, Brown SC, Nihoyannopoulos P, Poulton J, Kinali M, Richard P, Piercy RJ, Messina S, Sewry C, Burke MM, McKenna W, Bonne G, Muntoni F. 2005. Extreme variability of skeletal and cardiac muscle involvement in patients with mutations in exon 11 of the lamin A/C gene. Muscle Nerve 31:602–609.

Mercuri E, Poppe M, Quinlivan R, Messina S, Kinali M, Demay L, Bourke J, Richard P, Sewry C, Pike M, Bonne G, Muntoni F, Bushby K. 2004. Extreme variability of phenotype in patients with an identical missense mutation in the lamin A/C gene: from congenital onset with severe phenotype to milder classic Emery-Dreifuss variant. Arch Neurol 61:690–694.

Meune C, Van Berlo JH, Anselme F, Bonne G, Pinto YM, Duboc D. 2006. Primary prevention of sudden death in patients with lamin A/C gene mutations. N Engl J Med 354:209–210.

Motsch I, Kaluarachchi M, Emerson LJ, Brown CA, Brown SC, Dabauvalle MC, Ellis JA. 2005. Lamins A and C are differentially dysfunctional in autosomal dominant Emery-Dreifuss muscular dystrophy. Eur J Cell Biol 84:765–781.

Muchir A, Bonne G, van der Kooi AJ, van Meegen M, Baas F, Bolhuis PA, de Visser M, Schwartz K. 2000. Identification of mutations in the gene encoding lamins A/C in autosomal dominant limb girdle muscular dystrophy with atrioventricular conduction disturbances (LGMD1B). Hum Mol Genet 9:1453–1459.

Muchir A, Medioni J, Laluc M, Massart C, Arimura T, van der Kooi AJ, Desguerre I, Mayer M, Ferrer X, Briault S, Hirano M, Worman HJ, Mallet A, Wehnert M, Schwartz K, Bonne G. 2004. Nuclear envelope alterations in fibroblasts from patients with muscular dystrophy, cardiomyopathy, and partial lipodystrophy carrying lamin A/C gene mutations. Muscle Nerve 30:444–450.

Muntoni F, Bonne G, Goldfarb LG, Mercuri E, Piercy RJ, Burke M, Yaou RB, Richard P, Recan D, Shatunov A, Sewry CA, Brown SC. 2006. Disease severity in dominant Emery Dreifuss is increased by mutations in both emerin and desmin proteins. Brain 129(Pt 5):126012608.

Nguyen D, Leistritz DF, Turner L, MacGregor D, Ohson K, Dancey P, Martin GM, Oshima J. 2007. Collagen expression in fibroblasts with a novel LMNA mutation. Biochem Biophys Res Commun 352:603–608.

Novelli G, Muchir A, Sangiuolo F, Helbling-Leclerc A, D'Apice MR, Massart C, Capon F, Sbraccia P, Federici M, Lauro R, Tudisco C, Pallotta R, Scarano G, Dallapiccola B, Merlini L, Bonne G. 2002. Mandibuloacral dysplasia is caused by a mutation in LMNA-encoding lamin A/C. Am J Hum Genet 71:426–431.

Onishi Y, Higuchi J, Ogawa T, Namekawa A, Hayashi H, Odakura H, Goto K, Hayashi YK. 2002. [The first Japanese case of autosomal dominant Emery-Dreifuss muscular dystrophy with a novel mutation in the lamin A/C gene]. Rinsho Shinkeigaku 42:140–144.

Ostlund C, Bonne G, Schwartz K, Worman HJ. 2001. Properties of lamin A mutants found in Emery-Dreifuss muscular dystrophy, cardiomyopathy and Dunnigan-type partial lipodystrophy. J Cell Sci 114(Pt 24):4435–4445.

Otomo J, Kure S, Shiba T, Karibe A, Shinozaki T, Yagi T, Naganuma H, Tezuka F, Miura M, Ito M, Otomo J, Kure S, Shiba T, Karibe A, Shinozaki T, Yagi T, Naganuma H, Tezuka F, Miura M. 2005. Electrophysiological and histopathological characteristics of progressive atrioventricular block accompanied by familial dilated cardiomyopathy caused by a novel mutation of lamin A/C gene. J Cardiovasc Electrophysiol 16:137–145.

Pasotti M, Klersy C, Pilotto A, Marziliano N, Rapezzi C, Serio A, Mannarino S, Gambarin F, Favalli V, Grasso M, Febo O, Marini M, Landolina M, Mortara A, Piccolo G, Viganò M, Tavazzi L, Arbustini E. 2008. Long-term outcome and risk stratification in dilated cardiolaminopathies. J Am Coll Cardiol 52:1250–1260.

Perrot A, Hussein S, Ruppert V, Schmidt HH, Wehnert MS, Duong NT, Posch MG, Panek A, Dietz R, Kindermann I, Böhm M, Michalewska-Wludarczyk A, Richter A, Maisch B, Pankuweit S, Ozcelik C. 2009. Identification of mutational hot spots in LMNA encoding lamin A/C in patients with familial dilated cardiomyopathy. Basic Res Cardiol 104:90–99.

Prokocimer M, Davidovich M, Nissim-Rafinia M, Wiesel-Motiuk N, Bar D, Barkan R, Meshorer E, Gruenbaum Y. 2009. Nuclear lamins: key regulators of nuclear structure and activities. J Cell Mol Med 13:1059–1085.

Quijano-Roy S, Mbieleu B, Bonnemann CG, Jeannet PY, Colomer J, Clarke NF, Cuisset JM, Roper H, De Meirleir L, D'Amico A, Ben Yaou R, Nascimento A, Barois A, Demay L, Bertini E, Ferreiro A, Sewry CA, Romero NB, Ryan M, Muntoni F, Guicheney P, Richard P, Bonne G, Estournet B. 2008. De novo LMNA mutations cause a new form of congenital muscular dystrophy. Ann Neurol 64:177–186.

Raffaele Di Barletta M, Ricci E, Galluzzi G, Tonali P, Mora M, Morandi L, Romorini A, Voit T, Orstavik KH, Merlini L, Trevisan C, Biancalana V, Housmanowa-Petrusewicz I, Bione S, Ricotti R, Schwartz K, Bonne G, Toniolo D. 2000. Different mutations in the LMNA gene cause autosomal dominant and autosomal recessive Emery-Dreifuss muscular dystrophy. Am J Hum Genet 66:1407–1412.

Rankin J, Auer-Grumbach M, Bagg W, Colclough K, Nguyen TD, Fenton-May J, Hattersley A, Hudson J, Jardine P, Josifova D, Longman C, McWilliam R, Owen K, Walker M, Wehnert M, Ellard S. 2008. Extreme phenotypic diversity and nonpenetrance in families with the LMNA gene mutation R644C. Am J Med Genet A 146A:1530–1542.

Razafsky D, Hodzic D. 2009. Bringing KASH under the SUN: the many faces of nucleo-cytoskeletal connections. J Cell Biol 186:461–472.

Richardson JS, Richardson DC. 1988. Amino acid preferences for specific locations at the ends of alpha helices. Science 240:1648–1652.

Roca-Cusachs P, Alcaraz J, Sunyer R, Samitier J, Farre R, Navajas D. 2008. Micropatterning of single endothelial cell shape reveals a tight coupling between nuclear volume in G1 and proliferation. Biophys J 94:4984–4995.

Rudenskaya GE, Polyakov AV, Tverskaya SM, Zaklyazminskaya EV, Chukhrova AL, Groznova OE, Ginter EK. 2008. Laminopathies in Russian families. Clin Genet 74:127–133.

Scharner J, Gnocchi VF, Ellis JA, Zammit PS. 2010. Genotype-phenotype correlations in laminopathies: how does fate translate? Biochem Soc Trans 38(Pt 1):257–262.

Schirmer EC, Foisner R. 2007. Proteins that associate with lamins: many faces, many functions. Exp Cell Res 313:2167–2179.

Shackleton S, Lloyd DJ, Jackson SN, Evans R, Niermeijer MF, Singh BM, Schmidt H, Brabant G, Kumar S, Durrington PN, Gregory S, O'Rahilly S, Trembath RC. 2000. LMNA, encoding lamin A/C, is mutated in partial lipodystrophy. Nat Genet 24:153–156.

Shen JJ, Brown CA, Lupski JR, Potocki L. 2003. Mandibuloacral dysplasia caused by homozygosity for the R527H mutation in lamin A/C. J Med Genet 40:854–857.

Simha V, Agarwal AK, Oral EA, Fryns JP, Garg A. 2003. Genetic and phenotypic heterogeneity in patients with mandibuloacral dysplasia-associated lipodystrophy. J Clin Endocrinol Metab 88:2821–2924.

Speckman RA, Garg A, Du F, Bennett L, Veile R, Arioglu E, Taylor SI, Lovett M, Bowcock AM. 2000. Mutational and haplotype analyses of families with familial partial lipodystrophy (Dunnigan variety) reveal recurrent missense mutations in the globular C-terminal domain of lamin A/C. Am J Hum Genet 66:1192–1198.

Sylvius N, Bilinska ZT, Veinot JP, Fidzianska A, Bolongo PM, Poon S, McKeown P, Davies RA, Chan KL, Tang AS, Dyack S, Grzybowski J, Ruzyllo W, McBride H, Tesson F. 2005. In vivo and in vitro examination of the functional significances of novel lamin gene mutations in heart failure patients. J Med Genet 42:639–647.

Szeverenyi I, Ramamoorthy R, Teo ZW, Luan HF, Ma ZG, Ramachandran S. 2006. Large-scale systematic study on stability of the Ds element and timing of transposition in rice. Plant Cell Physiol 47:84–95.

Taimen P, Pfleghaar K, Shimi T, Moller D, Ben-Harush K, Erdos MR, Adam SA, Herrmann H, Medalia O, Collins FS, Goldman AE, Goldman RD. 2009. A progeria mutation reveals functions for lamin A in nuclear assembly, architecture, and chromosome organization. Proc Natl Acad Sci USA 106: 20788–20793.

Todorova A, Halliger-Keller B, Walter MC, Dabauvalle MC, Lochmuller H, Muller CR. 2003. A synonymous codon change in the LMNA gene alters mRNA splicing and causes limb girdle muscular dystrophy type 1B. J Med Genet 40:e115.

van der Kooi AJ, Bonne G, Eymard B, Duboc D, Talim B, Van der Valk M, Reiss P, Richard P, Demay L, Merlini L, Schwartz K, Busch HF, de Visser M. 2002. Lamin A/C mutations with lipodystrophy, cardiac abnormalities, and muscular dystrophy. Neurology 59:620–623.

van Tintelen JP, Hofstra RM, Katerberg H, Rossenbacker T, Wiesfeld AC, du Marchie Sarvaas GJ, Wilde AA, van Langen IM, Nannenberg EA, van der Kooi AJ, Kraak M, van Gelder IC, van Veldhuisen DJ, Vos Y, van den Berg MP, Working Group on Inherited Cardiac Disorders, line 27/50, Interuniversity Cardiology Institute of The Netherlands. 2007. High yield of LMNA mutations in patients with dilated cardiomyopathy and/or conduction disease referred to cardiogenetics outpatient clinics. Am Heart J 154:1130–1139.

Vaughan A, Alvarez-Reyes M, Bridger JM, Broers JL, Ramaekers FC, Wehnert M, Morris GE, Whitfield WGF, Hutchison CJ. 2001. Both emerin and lamin C depend on lamin A for localization at the nuclear envelope. J Cell Sci 114(Pt 14): 2577–2590.

Vergnes L, Peterfy M, Bergo MO, Young SG, Reue K. 2004. Lamin B1 is required for mouse development and nuclear integrity. Proc Natl Acad Sci USA 101: 10428–10433.

Verstraeten VL, Broers JL, Ramaekers FC, van Steensel MA. 2007. The nuclear envelope, a key structure in cellular integrity and gene expression. Curr Med Chem 14:1231–1248.

Verstraeten VL, Caputo S, van Steensel MA, Duband-Goulet I, Zinn-Justin S, Kamps M, Kuijpers HJ, Ostlund C, Worman HJ, Briede JJ, Le Dour C, Marcelis CL, van Geel M, Steijlen PM, van den Wijngaard A, Ramaekers FC, Broers JL. 2009. The R439C mutation in LMNA causes lamin oligomerization and susceptibility to oxidative stress. J Cell Mol Med 13:959–971.

Vigouroux C, Auclair M, Dubosclard E, Pouchelet M, Capeau J, Courvalin JC, Buendia B. 2001. Nuclear envelope disorganization in fibroblasts from lipodystrophic patients with heterozygous R482Q/W mutations in the lamin A/C gene. J Cell Sci 114(Pt 24):4459–4468.

Vytopil M, Benedetti S, Ricci E, Galluzzi G, Dello Russo A, Merlini L, Boriani G, Gallina M, Morandi L, Politano L, Moggio M, Chiveri L, Hausmanova-Petrusewicz I, Ricotti R, Vohanka S, Toman J, Toniolo D. 2003. Mutation analysis of the lamin A/C gene (LMNA) among patients with different cardiomuscular phenotypes. J Med Genet 40:e132.

Vytopil M, Ricci E, Dello Russo A, Hanisch F, Neudecker S, Zierz S, Ricotti R, Demay L, Richard P, Wehnert M, Bonne G, Merlini L, Toniolo D. 2002. Frequent low penetrance mutations in the Lamin A/C gene, causing Emery Dreifuss muscular dystrophy. Neuromuscul Disord 12:958–963.

Wagner N, Krohne G. 2007. LEM-Domain proteins: new insights into lamin-interacting proteins. Int Rev Cytol 261:1–46.

Yen A, Pardee AB. 1979. Role of nuclear size in cell growth initiation. Science 204: 1315–1317.

Young J, Morbois-Trabut L, Couzinet B, Lascols O, Dion E, Bereziat V, Feve B, Richard I, Capeau J, Chanson P, Vigouroux C. 2005. Type A insulin resistance syndrome revealing a novel lamin A mutation. Diabetes 54:1873–1878.

Zammit PS, Relaix F, Nagata Y, Ruiz AP, Collins CA, Partridge TA, Beauchamp JR. 2006. Pax7 and myogenic progression in skeletal muscle satellite cells. J Cell Sci 119(Pt 9):1824–1832.

Zhang Q, Bethmann C, Worth NF, Davies JD, Wasner C, Feuer A, Ragnauth CD, Yi Q, Mellad JA, Warren DT, Wheeler MA, Ellis JA, Skepper JN, Vorgerd M, Schlotter-Weigel B, Weissberg PL, Roberts RG, Wehnert M, Shanahan CM. 2007. Nesprin-1 and -2 are involved in the pathogenesis of Emery Dreifuss muscular dystrophy and are critical for nuclear envelope integrity. Hum Mol Genet 16: 2816–2833.

Supplementary Table S1: List of primers used for PCR and sequencing

Exon	Primer Name	Sequence (5'-3')
1	1F*†	TCTCTGTCCTTCGACCCGAG
	1R*†	CCTCTCCACTCCCCGCCA
2	2F*†	ACAGACTCCTTCTCTTAAATCTAC
	2R*†	GTAGAAGAGTGAGTGTACATGTG
3	3F*†	ACCTCTCAGCTTCCTTCAAGTT
	3R†	CTAGCCCAGCCCAAGTCTGT
4	4F†	GCCTCCCAGGAACTAATTCTG
	4R*†	CGTGGGTAAGGGTAGGGCTG
5	5F*†	ATGCCCAACTCAGGCCTGTG
	5R†	CGTTCCAGCCTGCATCCGG
6	6F†	TCCCTCCTTCCCCATACTTAG
	6R†	CCAGTTGCCGGGCCAGAG
7	7F†	CCCCACTTGGTCTCCCTCTCC
	7R*†	CCCTGATGCAGCTGTATCCCC
8/9	8F*†	CAAGATACACCCAAGAGCCTG
	9R†	CTCGTCCAGCAAGCAGCCAG
10	10F†	TCTTGTACAACCCTTCCCTGG
	10R*†	GGGTTCCCTGTTCAAGGTATA
11	11F*†	GTTGGGCCTGAGTGGTCAG
	11R*†	CACCTCGTCCTACCCCTCG
12	12F*†	GGCTGGAGTGTGGAGGGATG
	12R*†	CCTCCCATGACGTGCAGGG

* Primer used for PCR; † Primer used for sequencing

4.4 Conclusion

In this chapter I set out to study the effects of four pathogenic lamin A mutations on C2C12 myoblasts. I have found that even moderate expression levels achieved by the retroviral expression system used, induce an obvious but variable phenotype in presence of all four mutations. In presence of missense mutations located in the head (p.R25P) and central rod domain (p.R249W) nuclei were severely dysmorphic and showed mislocalised lamin B expression. In contrast, mutations located in the Ig-fold domain (p.N456I and p.R541P) resulted in lamin A positive nuclear foci, while the nuclear morphology in their presence was not affected. Together, these results demonstrate that mutations manifesting in similar phenotypes can have very different effects on a cellular level, suggesting that different pathogenic mechanisms are at play. To pinpoint potential mechanisms, the effects of mutant lamin on functional aspects of myoblasts such as proliferation and differentiation must be investigated, which will be covered in the next chapter of this thesis.

Chapter 5

Functional Effects of Four Mutant Lamin A Variants on the Proliferation and Differentiation Capacity of Myogenic Cells

5.1 Introduction

The vast majority of all reported *LMNA* mutations (77.2%) result in disease phenotypes affecting skeletal and/or cardiac muscle (www.umd.be/LMNA). The most common disease is Emery-Dreifuss muscular dystrophy (EDMD), characterised by the clinical triad consisting of joint contractures (primarily of elbow and Achilles tendons), slowly progressive muscle weakness of the upper proximal and lower distal musculature (humero-peroneal distribution) and cardiac involvement (see section 1.1.3 for details). However, how mutations in *LMNA* cause muscle dystrophy is largely unknown.

Ever since *LMNA* mutations have been described to cause EDMD, research has been conducted to elucidate the pathogenic mechanism. From this research three non-mutually exclusive hypotheses emerged: the 'mechanical stress' hypothesis and the 'gene expression' hypothesis and the 'cell proliferation/differentiation' hypothesis (Broers et al., 2006; Worman, 2012) (refer to section 1.4.2 for details).

Abnormalities in nuclear structure, caused by lamin mutations, could lead to an increased susceptibility to cellular damage by physical stress. Muscle is especially subject to high forces and constant mechanical stress. Some of the force transmitted through the cytoskeleton could directly affect the nuclear envelope via the LINC (linker of nucleoskeleton and cytoskeleton, see section 1.2.2) complex (Mellad et al., 2011; Padmakumar et al., 2005). This could potentially result in damage of a nuclear envelope compromised by the presence of mutant lamin or the absence of emerin. Indeed, ultrastructural analysis of skeletal muscle from patients with autosomal dominant EDMD and X-linked EDMD reveals widespread damage of nuclear envelopes and leakage of chromatin into the cytoplasm (Fidzianska and Hausmanowa-Petrusewicz, 2003; Fidzianska et al., 1998), providing evidence in favour of this as a potential pathogenic mechanism for certain *LMNA* mutations.

Lamins are able to directly and indirectly interact with chromatin and transcription factors and might therefore affect cell/tissue function by indirectly modulating gene expression and regulation (Wilson and Foisner, 2010; Zastrow et al., 2004). One such example is the regulation of Erk1/2 signalling. Upon extracellular stimulation, Erk1/2 is phosphorylated and activates c-Fos which stimulated cell cycle entry and the transition to S-phase. Lamin A binds to both Erk1/2 and c-Fos (Gonzalez et al., 2008) and mutant lamin A has been shown to affect Erk1/2 phosphorylation and proliferation (Emerson et al., 2009).

Lamins have also been shown to directly interact with the cell cycle regulator pRb in complex with Lap2α, tethering pRb to the nucleoskeleton (Dechat et al., 2000; Markiewicz et al., 2002). Mutant lamins that disrupt this complex potentially affect cell cycle exit: a necessary step for myogenic differentiation (Markiewicz et al., 2005).

Functional tissue of skeletal muscle, the muscle fibre, is post-mitotic, however muscle retains a well-characterized stem cell compartment (satellite cells) responsible for homoeostatic myonuclear turnover, hypertrophy and repair (Zammit, 2008). Thus, next to mutations that weaken the structural support of myonuclei and satellite cells, skeletal muscle may additionally be vulnerable to mutations that also affect cell cycle and/or differentiation of myogenic stem cells. Genetic ablation using Cre-lox technology of satellite cells in adult mice has been shown to completely block regenerative myogenesis demonstrating their absolute requirement to regenerate muscle damaged after acute injury (Lepper et al., 2011). A defective satellite cell pool can therefore potentially contribute to the disease pathology or accelerate disease progression (Gnocchi et al., 2008; Morgan and Zammit, 2010).

One example where defective satellite cells have been shown to play an indirect role in disease progression is Duchenne muscular dystrophy (DMD). Excessive myofibre damage caused by the lack of dystrophin protein induces chronic rounds of degeneration and repair, eventually leading to a decline in the regenerative capacity of muscle (Webster and Blau, 1990). In likely combination with an increasingly hostile microenvironment, this constant demand for a large number of satellite cells ultimately leads to their exhaustion, resulting in a progression of the dystrophic phenotype. Indeed the dystrophic phenotype is worse in mice where telomerase is inactivated, presumably largely due to its effects to limit satellite cell proliferation (Sacco et al., 2010). EDMD patients do not show these repeated rounds of degeneration-regeneration, and so if lamin mutations affect satellite cell function it is likely by affecting muscle homeostasis and repair.

In general, mutant lamins could affect satellite cells on multiple levels (intrinsic and extrinsic) leading to an impaired proliferation or differentiation capacity. For example, satellite cell derived myoblasts from mice lacking A-type lamins display decreased pRb and MyoD protein levels as well as reduced differentiation potential in vitro (Frock et al., 2006). Cells isolated from EDMD patients carrying various *LMNA* mutations show a delayed cell cycle progression by prolonging S-phase (Emerson et al., 2009). Myogenic differentiation also requires a timely exit from the cell cycle which involves remodelling of the nucleoskeleton and the relocation of nucleoplasmic A-type lamins to the nuclear envelope, a process disrupted by mutant lamin A-W520S (Markiewicz et al., 2005). Similarly, C2C12 cells fail to dephosphorylate pRb and exit cell cycle in the presence of lamin A-R453W and as a consequence do not fuse to form myotubes (Favreau et al., 2004).

Evidence that satellite cells are affected *in vivo* is provided by ultrastructural studies. Recently, Park et al. (2009) have analysed muscle sections from EDMD and LGMD1B patients and found that 50% of all satellite cell nuclei and 90% of all myonuclei displayed abnormal chromatin organisation.

Interestingly, abnormalities in nuclear morphology were only detected in approx. 20% of all myonuclei but not in satellite cells (Park et al., 2009).

Taken together, the important role of satellite cells in muscle homeostasis and repair makes them an attractive target to contribute to the pathology of EDMD. In the previous chapter, I examined the effects of four mutations on nuclear structure and localisation of proteins including lamin B. Here I investigated whether these structural defects had effects on myogenic cell function. The effects on myoblast proliferation and differentiation of the four lamin A mutations described in chapter 4 (lamin A-R25P, R249W, N456I and R541P compared to wild-type lamin A as a control) will be addressed in this chapter.

5.2 Aim

In chapter 4, I overexpressed four mutant lamin A variants (lamin A-R25P, R249W, N456I and R541P) found in patients with a skeletal muscle phenotype. Given the vastly different nuclear abnormalities these four mutant lamin A variants caused in C2C12 myoblasts, I also sought to investigate their effects on functional properties of myogenic cells including proliferation and differentiation.

I hypothesise that the muscle phenotype observed in EDMD patients is, in part, caused by dysfunctional satellite cell pool that either fails to efficiently expand due to proliferation/cell cycle defects or to differentiate and form myotubes. This leads to a significant failure in muscle homeostasis and repair in response to the muscle wasting caused by the effects of the mutation in myonuclei, and so exaggeration of the dystrophic phenotype.

Testing this hypothesis, required the analysis of myogenic cells in the presence of mutant lamin A. However, EDMD is a rare disease and patient myoblasts are not readily available. I therefore again overexpressed the same four mutant lamin A proteins in mouse immortalised satellite cell-derived myoblasts (C2C12 cells) by retroviral infection to examine how the nuclear structural changes affect proliferation and differentiation. In addition, I also used primary mouse satellite cells to confirm observations made using C2C12 myoblasts on primary cells.

5.3 Results

5.3.1 Colony Growth is reduced in cells expressing lamin A-R25P and R249W

The first functional analysis performed was to test the effects of mutant lamin A variants on cell proliferation and cell cycle in C2C12 myoblasts. To analyse the proliferative capacity of C2C12 cells I first performed a colony growth assay. The constructs used in this study (see section 2.2.2 for details) express full length human lamin A as well as eGFP from the IRES-eGFP in the retroviral backbone. Infected cells were seeded at low density 24 hours post infection which allowed the formation of individual colonies. The number of cells per eGFP positive colony was counted 24, 48 and 72hrs in culture and is shown for each mutation in figure 5.1.

Retroviral overexpression of wild-type lamin A in C2C12 did not have an effect on colony growth. The colony size is similar to that of cells infected with the control RV at all three time points. After 24 hours in culture none of the mutant lamin A variants resulted in a significant change in colony size. However, at the two later time points (48hrs and 72hrs after seeding) colony size was significantly smaller in the presence of lamin A-R25P and R249W, indicating a lower proliferative potential as compared to wild-type lamin A infected cells. In contrast, the presence of lamin A-N456I and R541P did not have an effect on colony growth at any of the time points analysed.

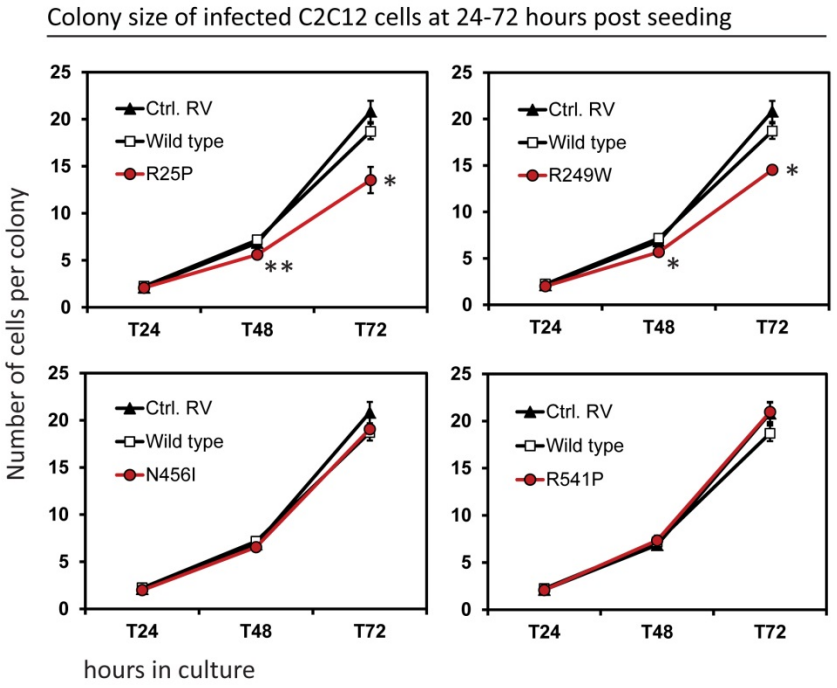

Figure 5.1 Colony growth is reduced in C2C12 myoblasts infected with lamin A-R25P and R249W. Colony size is significantly smaller in the presence of lamin A-R25P and R249W at 48hrs and 72hrs after passaging. Numbers represent the average number of cells/colony from 3 independent infections (at least 35 colonies were counted in total per time point), error bars show S.E.M where an asterisk denotes significant difference (* $p<0.05$, ** $p<0.01$) from wild-type lamin A infected cells using a student's t-test.

To test if the reduced colony growth is associated with a reduced proliferation rate, C2C12 cells were pulsed with bromodeoxyuridine (BrdU) for 2 hours to quantify the number of cells in S-phase (Fig. 5.2A). The proportion of infected cells (eGFP positive) that immunostained for BrdU in presence of each lamin A-variant is shown in figure 5.2B. However, the number of BrdU positive cells was not statistically different in the presence of lamin A-R25P and R249W when compared to wild-type lamin A infected cells, despite the decreased number of cells in the colony assay (Fig. 5.1). Similarly, lamin A-N456I and R541P do not have a significant effect on the number of BrdU positive cells.

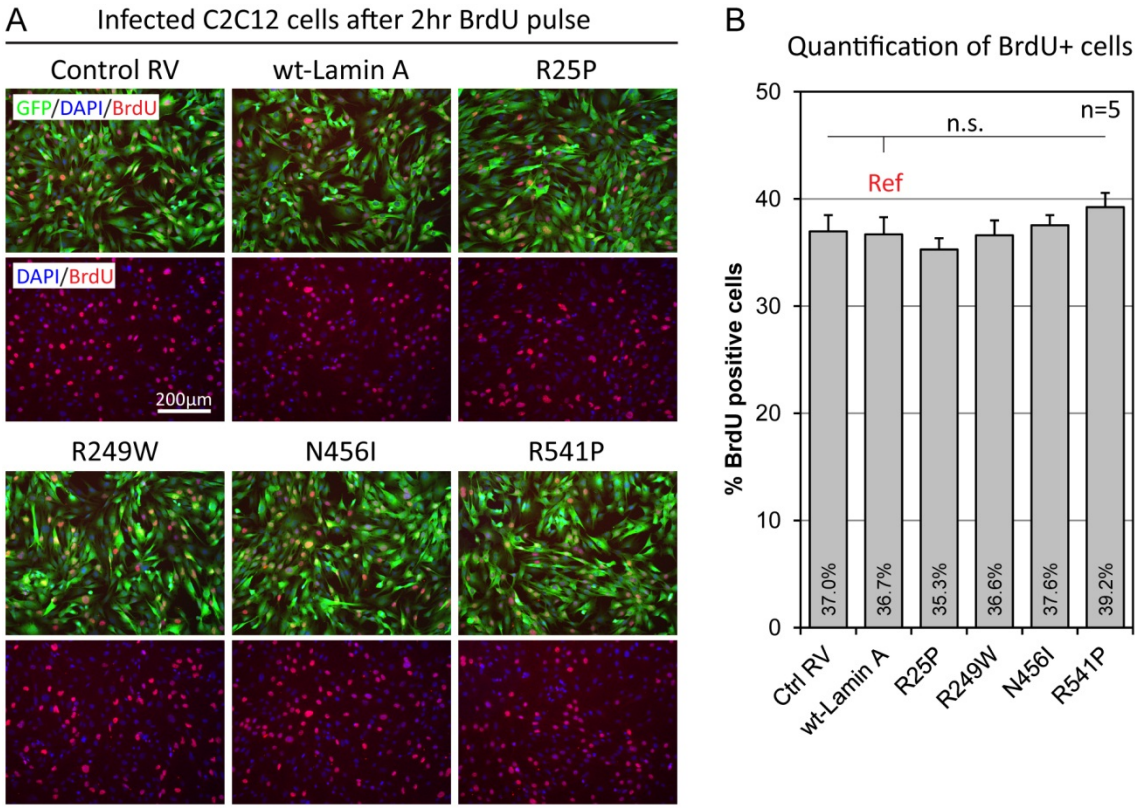

Figure 5.2 BrdU incorporation in proliferating C2C12 cells is not affected in the presence of different lamin A mutants. (**A**) Proliferating C2C12 cells stained for BrdU after a 2hr pulse 72 hours post infection. A representative picture for each construct is shown. (**B**) Quantification of the proportion of infected cells (eGFP positive) that immunostained for BrdU in the presence of mutant lamin A variants from 5 independent experiments. n.s. not significant compared to wild-type lamin A infected cells using a student's t-test.

Overexpression of HGPS causing missense mutations (R133L and L140R) in human fibroblasts has been shown to increase replicative senescence by telomere shortening (Huang et al., 2008). Similarly, signs of premature senescence have been found in patient myoblasts harbouring the EDMD mutation p.R545C (Kandert et al., 2009). To test if senescence is the cause of the reduced colony growth in the presence of lamin A-R25P and R249W, cells were stained for senescence associated (SA) β-gal. However, none of the C2C12 cells infected with any of the four lamin A

variants stained positive for SA β-gal, ruling out senescence as the cause for the discrepancy seen between the colony growth assay and BrdU staining (data not shown).

5.3.2 Mutant lamin A-variants do not affect the cell cycle in C2C12 cells

BrdU is a marker of DNA synthesis and allows visualising cells currently in S-phase. However the number of cells in S-phase does not reveal potential defects in other parts of the cell cycle such as G1 or G2/M. In order to find out if other elements of the cell cycle are affected by any of the four mutant lamin A variants tested in this study, I performed cell cycle analysis by flow cytometry. To do so, proliferating C2C12 cells infected with mutant lamin variants were stained with propidium iodine (PI) and fixed with ethanol before flow cytometry. Unfortunately ethanol fixation cannot be used for the analysis of GFP expression as it allows GFP to leak out of the cell resulting in reduced fluorescence intensity. Therefore all cells stained with PI were included in the cell cycle analysis (50,000 cells per sample). To assess the potential influence of non-infected cells on the result, the infection efficiency was quantified for each of the samples by fixing half the cells with 4% PFA and processing them in parallel. On average 99.8% of the cells were GFP positive (Fig. 5.3) ruling out any influence of non-infected cells on the result.

The results show that little debris (fragmented cells) was present in the sample (as judged by the number of events in the bottom left corner of figure 5.3A and 5.4A respectively) and that the majority of C2C12 cells infected with the control RV are single cells (Fig. 5.4B, gated subset). The same result was obtained with all other samples (data not shown). Cell cycle distributions of cells infected with the control RV and different lamin A variants are shown in figure 5.4C. The proportion of cells in each phase of the cell cycle was quantified using the FlowJo software using the Watson model (Watson et al., 1987) and is summarised in table 5.1. On average, 37.9% of all cells infected with wild-type lamin A were found in G1-phase, 43.3% were found in S-phase and 15.9% were found in G2/M-phase. When these values were compared to other samples, no significant difference was found. The Root Mean Square (RMS) value which is a measure of how well the chosen model fits the curve is similar for all samples.

Table 5.1 Proportion of infected C2C12 cells in different phases of the cell cycle.

	RMS	**% G1**	**p-value**	**% S**	***p*-value**	**% G2/M**	***p*-value**
Control RV	11.2 (2.3)	39.5 (2.67)	*0.44*	41.5 (2.12)	*0.29*	15.7 (1.00)	*0.85*
Lamin A-wt	9.2 (0.1)	37.9 (1.87)	*Ref*	43.3 (1.38)	*Ref*	15.9 (0.61)	*Ref*
R25P	9.8 (1.6)	37.1 (1.01)	*0.53*	43.3 (0.76)	*1.00*	16.4 (0.59)	*0.31*
R249W	10.4 (1.0)	37.1 (2.29)	*0.66*	43.5 (1.48)	*0.91*	16.0 (0.23)	*0.80*
N456I	9.7 (1.2)	37.7 (2.08)	*0.92*	43.7 (1.65)	*0.78*	15.6 (0.35)	*0.55*
R541P	8.9 (0.3)	38.3 (0.81)	*0.77*	42.2 (1.99)	*0.68*	16.0 (0.40)	*0.77*

Values represent the mean (S.E.M.) from 3 independent experiments. The Root Mean Square (RMS) is a measure of how well the chosen model fits the curve; p-values were calculated using a student's t-test.

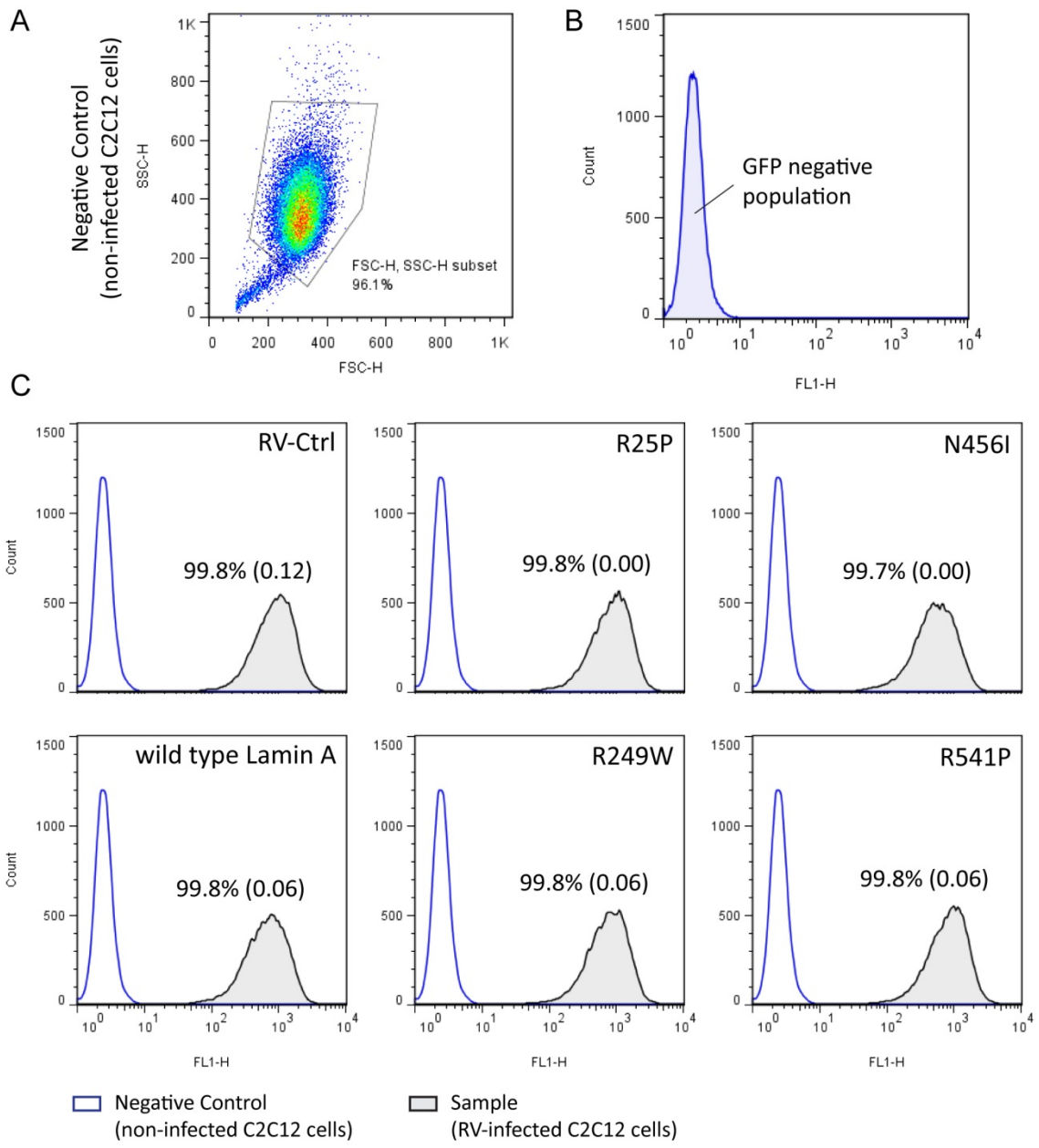

Figure 5.3 Quantification of eGFP positive C2C12 cells after retroviral infection with mutant lamin A variants demonstrates very high infection efficiencies. (**A**) Forward scatter (FSC) vs. side scatter (SSC) plot of non-infected C2C12 cells. (B) GFP intensity (FL1) of non-infected cells gated in panel A which served as a negative control. (**C**) Histograms of infected cells (grey curve) compared to non-infected cells (white curve). Percentages of eGFP positive cells are given for each infection. Values represent the mean±SEM of 3 independent experiments.

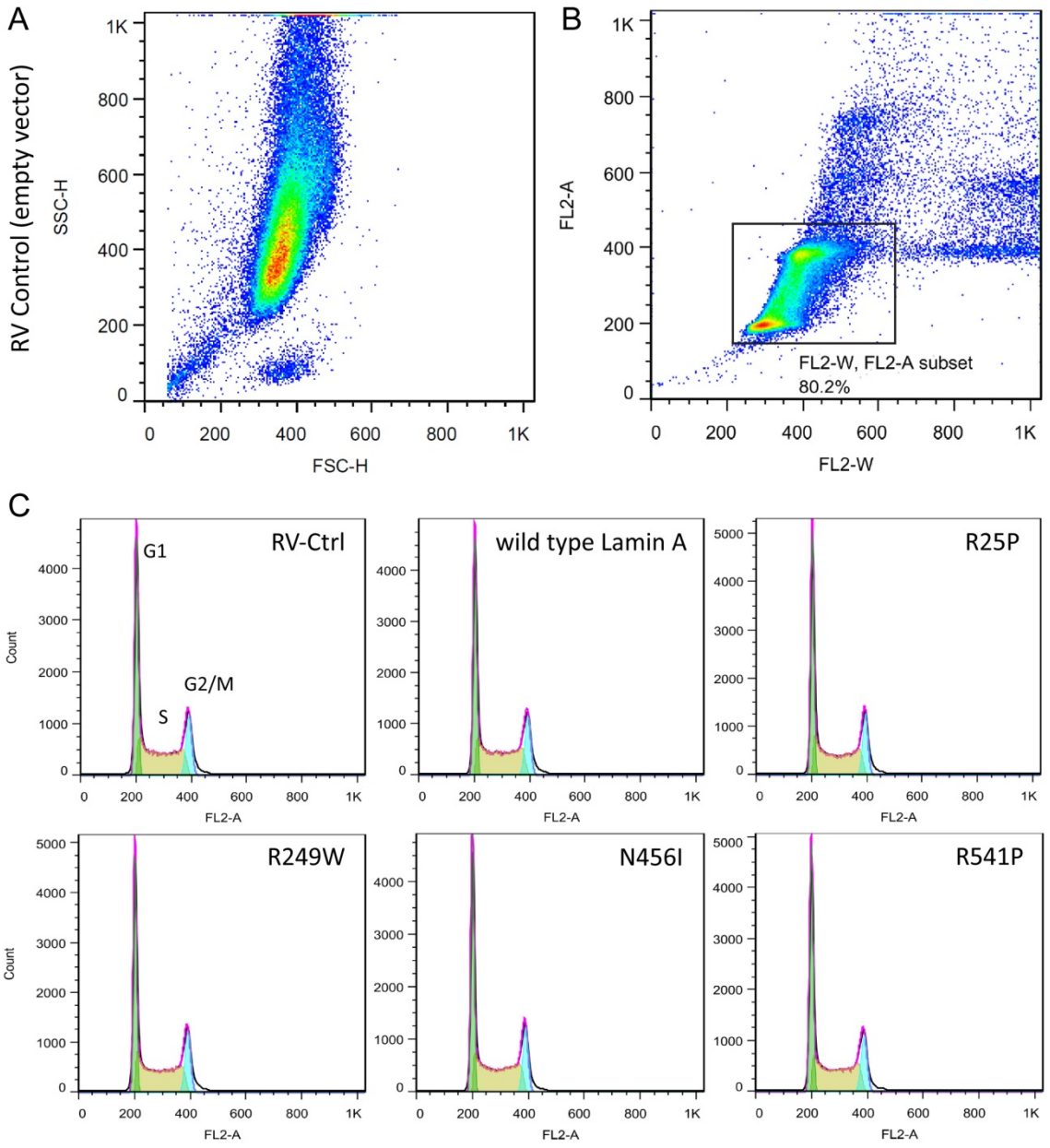

Figure 5.4 Cell cycle analysis of C2C12 cells infected with mutant lamin A variants. (**A**) Side-scatter/Forward Scatter plot to identify debris which would be located in the bottom left corner. (**B**) FL2-A (peak area) vs. FL2-W (peak width) plot indicates cells in different phases of the cell cycle (amount of DNA). Single cell population is gated and was used for cell cycle analysis. (**C**) Cell cycle analysis of infected C2C12 cells by flow cytometry. The DNA content was stained with propidium iodine and the percentages of G1, G2/M and S-phase was determined using FlowJo. 50,000 events of each sample were analysed.

To substantiate the lack of phenotype in C2C12 cells infected with pathogenic lamin A variants, I also analysed the expression of a number of cell cycle markers shown to be mis-regulated in *Lmna*-null cells or presence of mutant lamin A (Fig. 5.5). Sub-confluent C2C12 cells were infected over-night, sub-cultured and harvested while in proliferation 72hrs post infection. Total protein extracts were prepared as described in section 2.2.4 in the presence of protease and phosphatase inhibitors and separated on a 4-20% denaturing gradient gel. The gel was blotted onto a PVDF membrane using the Invitrogen iBlot system and probed with antibodies against pRb, p21, PCNA, Erk1/2 and pErk1/2. Antibody details can be found in tables 2.1 and 2.2. β-tubulin served as a loading control and a standard 2-colour protein ladder (Expedeon) was used to estimate the size of the bands.

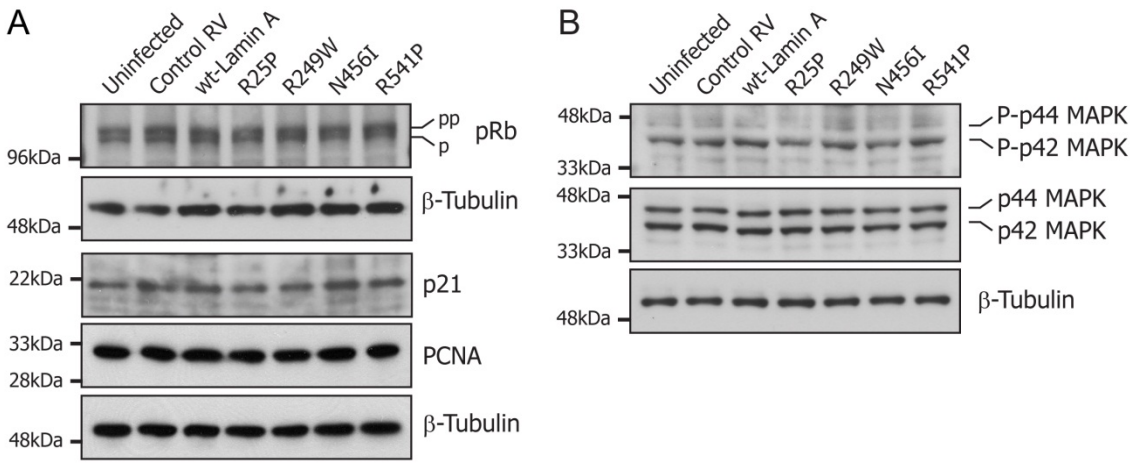

Figure 5.5 Western blot analysis of cell cycle markers in proliferating C2C12 cells expressing mutant lamin A proteins. (**A**) Western blot analysis of proliferating C2C12 cells infected for 72hrs with either control-RV, wild-type lamin A or mutant lamin A variants. A non-infected control sample (lane 1) was also included. Levels of cell cycle regulators pRb (110-116kDa), p21 (21kDa) and the DNA replication elongation factor PCNA (29kDa) did not obviously change in presence of mutant lamin A. (**B**) Total Erk1 (p44 MAPK, 44kDa) and Erk2 (p42 MAPK, 42kDa) as well as phosphorylated pERK1/2 in proliferating C2C12 cells. The expression level of phosphorylated p42 MAPK (Erk1) appears to be slightly reduced in the presence of lamin A-R25P.

The retinoblastoma protein (pRb) forms a complex with nucleoplasmic lamin A and Lap2α which has been shown to be disrupted in presence of mutant lamin A affecting cell cycle dynamic (Markiewicz et al., 2002; Markiewicz et al., 2005). When the cell receives cues to exit cell cycle, the cdk inhibitor p21 is up-regulated and pRb is rapidly hypophosphorylated which inactivates E2F transcription factors, leading to cell cycle arrest (Guo et al., 1995). Hence, if cells exit the cell cycle in the presence of any of the four mutants, pRb as well as p21 levels would be expected to increase. However, there was no obvious change in pRb levels and p21 levels in the presence of all four lamin A mutants which confirms results obtained by cell cycle analysis. Similarly, levels of the DNA replication elongation factor PCNA, which is involved in DNA repair and cell cycle control, and

has been shown to bind the Ig-fold of lamin A (Shumaker et al., 2008), was not obviously altered by any of the mutations.

Erk1/2 activation has been shown to be misregulated during cell cycle entry in human fibroblasts from EDMD patients carrying mutations in *LMNA* (Emerson et al., 2009). Upon serum stimulation, Erk1/2 phosphorylation was initially delayed followed by hyperphosphorylation. Phosphorylated Erk1/2 is necessary to activate the transcription factor c-Fos which initiates cell cycle dependent genes and promotes S-phase progression (Gonzalez et al., 2008). In proliferating asynchronous C2C12 cells infected with mutant lamin A variants, p42/p44 MAPK (Erk1/2) levels as well as phosphorylated p42/p44 (pErk1/2) levels are similar to those in wild-type lamin A infected cells (Fig. 5.5B). In all cases, levels were very similar by eye and the band intensity was therefore not quantified. Although in cells expressing lamin A-R25P, a slight decrease of p42 MAPK (Erk2) expression level was noted.

5.3.3 Myogenic commitment is increased in C2C12 cells in presence of Lamin A-N456I

Next to analysing proliferation and cell cycle, I assayed the effect of pathogenic lamin A mutants on the differentiation potential of myogenic cells. Myogenic differentiation can be separated into multiple different stages (see Fig. 1.2). Two of these stages were analysed in the presence of mutant lamin A namely, myogenic commitment (marked by the expression of myogenin) and sarcomeric assembly (marked by the expression of myosin heavy chain) during myotube formation.

To study myogenic differentiation, I have used C2C12 myoblasts which are maintained in a proliferative state in serum containing medium and at sub-confluency. Differentiation of C2C12 cells is induced by contact inhibition and/or serum deprivation (Blau et al., 1983; Yaffe and Saxel, 1977). To analyse the effect of mutant lamin A on myogenic commitment in C2C12 cells, cells were infected and seeded into chamber slides. When they reached 80-90% confluence (usually 72hrs post infection) they were induced to differentiate by serum deprivation with culture medium containing 2% (v/v) horse serum. By doing so, C2C12 are induced all at the same time which makes this is a very precise and sensitive method to detect potential alterations in myogenic progression caused by mutant lamin A.

Results summarised in figure 5.6 show that 43.5% of all infected cells (wt-lamin A) express myogenin. This is statistically similar to cells infected with control RV (43.1%), lamin A-R25P (43.9%), R249W (45.6%) and R541P (42.3%). The only lamin A variant resulting a statistically significant change was lamin A-N456I. The pathogenic mutation located in the Ig-fold significantly increased (+5.7%, p=0.0099) the proportion of myogenin positive cells after 24 hours in differentiation medium when compared to wild-type lamin A infected cells (Fig. 5.6D). This is consistent with results obtained in primary satellite cells on single fibres.

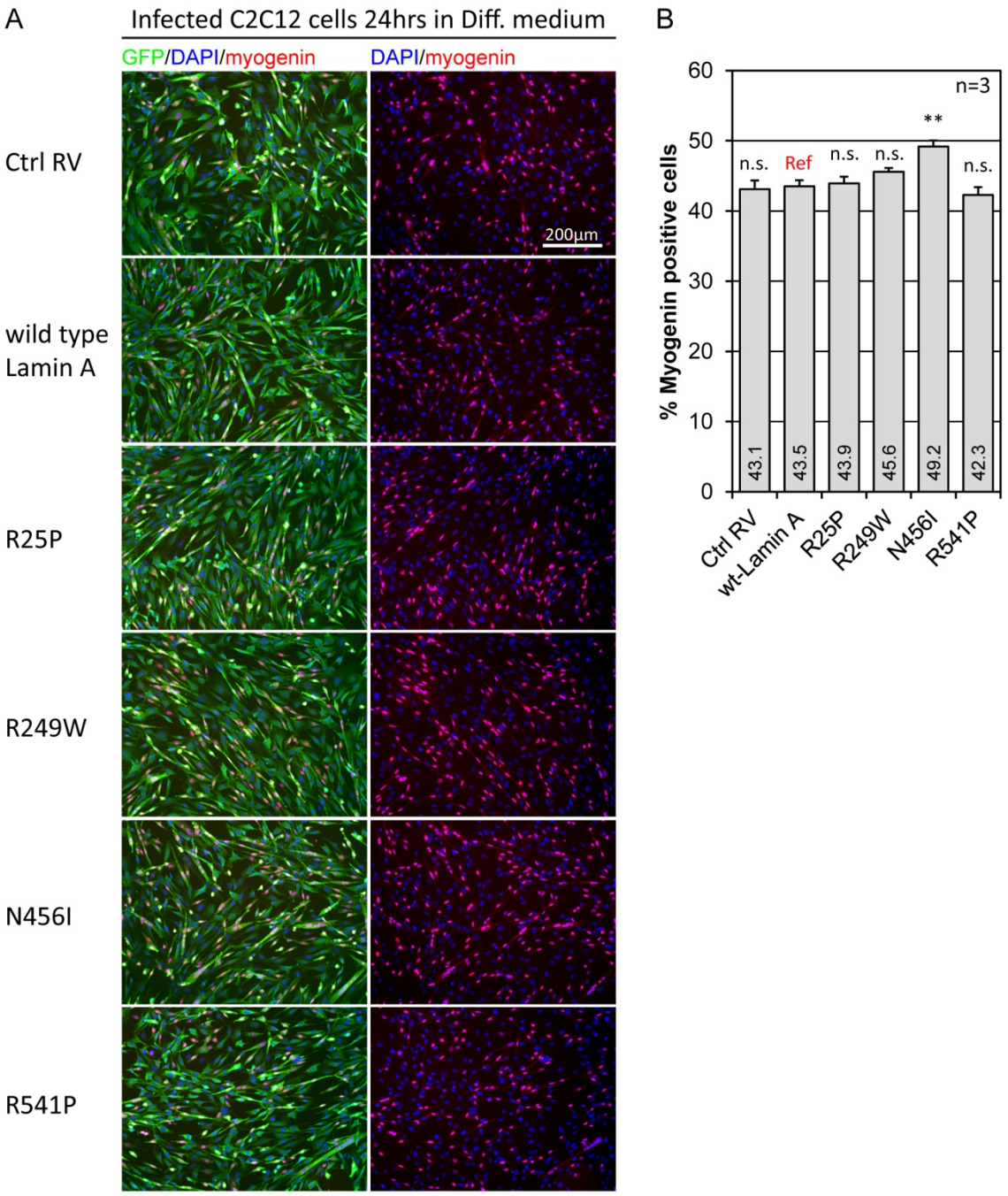

Figure 5.6 C2C12 myoblasts commitment to differentiation is increased in the presence of lamin A-N456I. (**A**) Representative images showing infected C2C12 cells after 24hrs in differentiation medium co-immunostained for eGFP and myogenin. (**B**) Quantification of the proportion of infected (eGFP positive) cells which are positive for myogenin. Values represent the average of three separate experiments. A total of at least 3000 cells (in 3 field of views) were counted for each replicate. Error bars represent he S.E.M.; * $p<0.05$, ** $p<0.01$ when compared to wild-type lamin A infected cells using a student's t-test.

5.3.4 Myogenic differentiation in C2C12 cells is unaffected by Lamin A-mutants

As described above, C2C12 cells are a well-established murine satellite cell-derived myoblast line used to study myogenesis in vitro. When induced to differentiate by serum deprivation, C2C12 cells exit the cell cycle and express myogenin. They then continue to fuse to form multinucleated myotubes and start to express myosin heavy chain, a marker for sarcomere assembly and terminal differentiation (Fig. 5.7A). To see if the accelerated myogenic commitment of cells infected with lamin A-N456I affects later stages of myogenic differentiation, C2C12 cells were infected and 48 hours later switched to differentiation medium and further cultured for 48 hours before fixation and co-immunostaining for MyHC, a marker for terminal differentiation and eGFP.

In addition to serum deprivation C2C12 cells are also induced to differentiate by contact inhibition. A small difference in cell density at the start of the experiment or variability in proliferation might therefore affect the onset of differentiation and skew the result. To assess a potential influence of cell density on my result, I performed a statistical analysis to see whether the average number of cells per picture analysed was significantly different between different samples. However, no difference was found, ruling out an influence of cell density on the obtained result (data not shown). Furthermore, immunostaining showed that cells did not express myogenin at the time that they were induced to differentiate by switching to differentiation medium.

The differentiation index (defined as the proportion of nuclei in MyHC positive cells) of cells infected with wild-type lamin A was 44.0% after 48 hours in differentiation medium. When compared to cells infected with control RV or other lamin A variants, no significant changes were found. The only noticeable although non-significant increase was caused by lamin A-N456I which resulted in a differentiation index 3.6% higher (p=0.085) than that of cells infected with wild-type lamin A (Fig. 5.7B). Similarly the fusion index (defined as the proportion of nuclei in myotubes with 2 or more nuclei) was slightly (but again not significantly) raised in presence of lamin A-N456I (+4.0%, p=0.084) compared to wild-type lamin A infected cells. All other lamin variants and the control RV did not have a noticeable effect on the fusion index (Fig. 5.7C).

Interestingly, examination of myonuclei at higher magnification revealed small differences in nuclear morphology across different constructs (Fig. 5.8). Myonuclei in myotubes formed by cells infected with control RV and wild-type lamin A have a round/ovoid appearance and are aligned in a bead-like fashion. Similarly lamin A-N456I and R541P does not seem to cause drastic changes in nuclear morphology in myotubes. In contrast, abnormal myonuclear positioning is evident in presence of lamin A-R25P and R249W which suggests that there are different mechanisms involved for mutations analysed here.

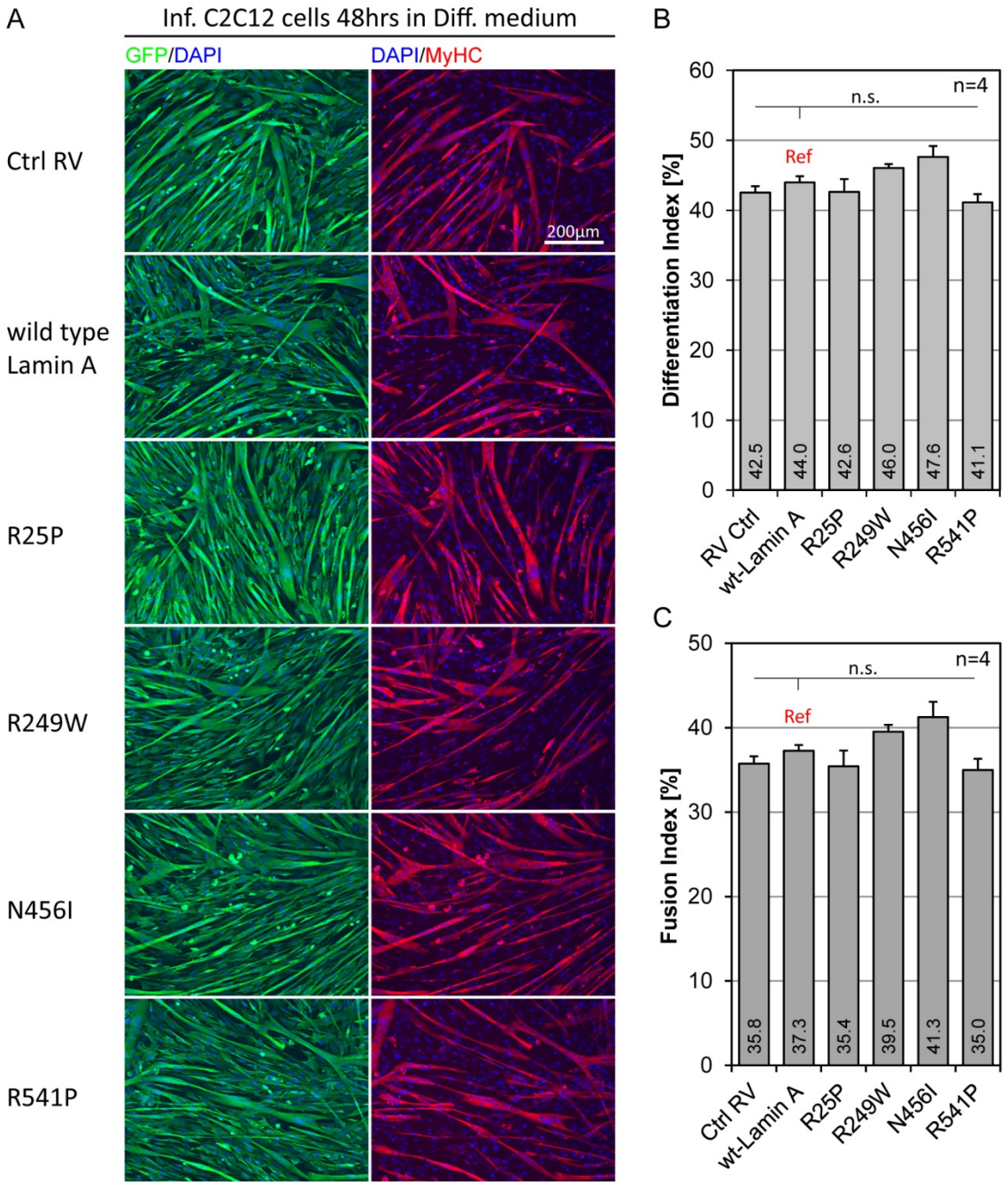

Figure 5.7 Quantification of Differentiation index and Fusion index in C2C12 cells expressing different lamin A mutants. (**A**) Representative images showing infected C2C12 cells after 48hrs in differentiation medium. A significant proportion of cells have fused into large multinucleated myotubes expressing myosin heavy chain. (**B**) Average Differentiation index (%) representing the proportion of nuclei in MyHC positive cells. (**C**) Average fusion index (%) representing the proportion of nuclei in multinucleated (≥2 nuclei) myotubes. Values represent average indices obtained from 4 independent experiments, error bars represent the S.E.M.; A total of at least 2800 cells (in 2 field of views) were counted for each replicate; n.s. not significant when compared to wild-type lamin A infected cells using a student's t-test.

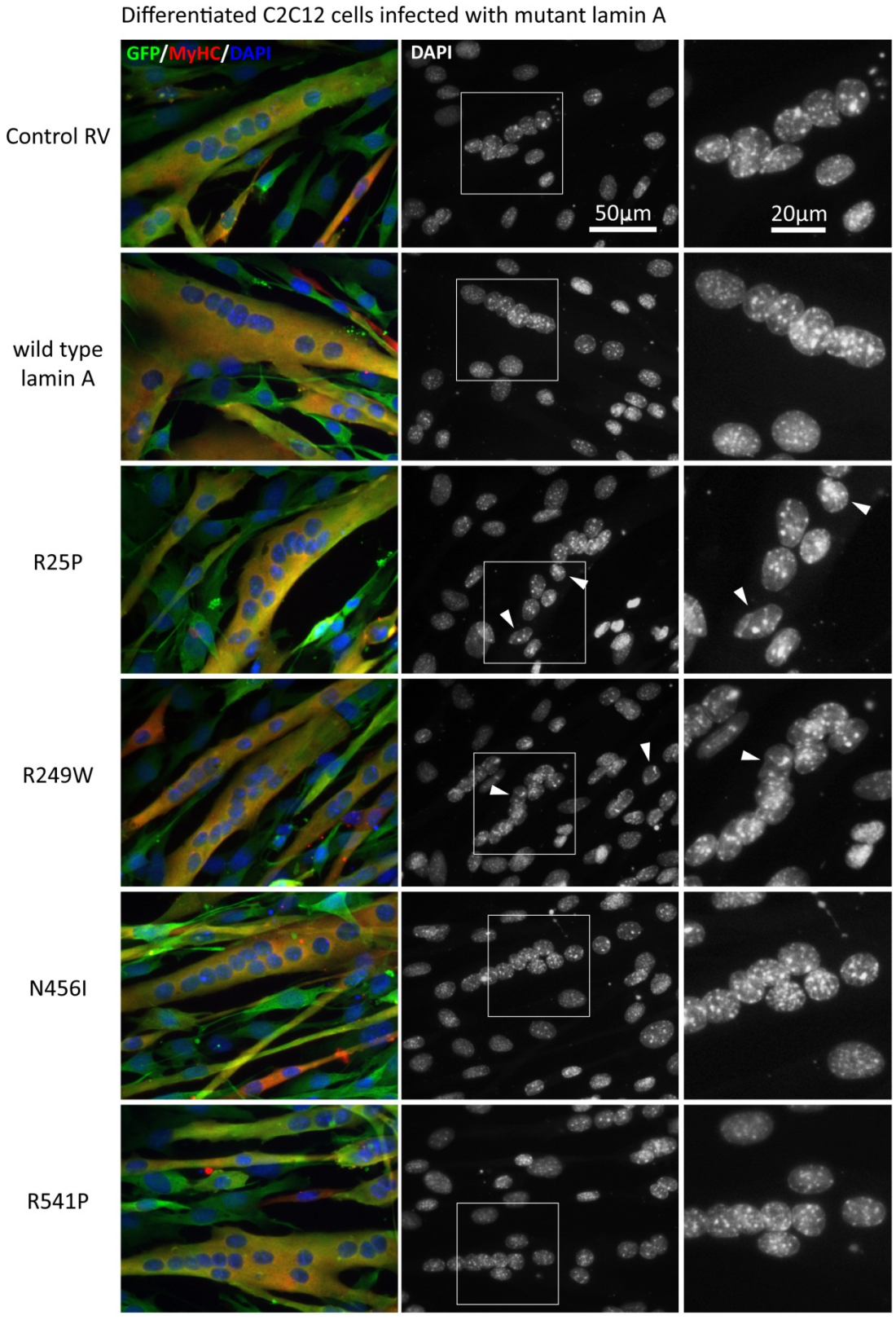

Figure 5.8 Morphological abnormalities are evident in myonuclei of C2C12 cells infected with lamin A-R25P and R249W. Representative selection of pictures showing infected C2C12 cells after 48hrs in differentiation medium. White arrowheads indicate nuclei where morphological abnormalities are evident in presence of lamin A-R25P and R249W. In presence of control RV, lamin A-wt, N456I and R541P, myonuclei generally have a round appearance and are arranged in a bead-like fashion.

The arrangement of nuclei is irregular with a less well defined boundary between individual nuclei and some of the nuclei show signs of deformation. It is likely that these abnormal myonuclei are characterised by mislocalisation of lamin B and therefore more susceptible to physical damage which would support the 'mechanical stress' hypothesis. However, lamin A and lamin B staining is not available for these cells because the antibodies used at the time the experiments were conducted (lamin A/C N18 and Lamin B M20, both goat polyclonal Abs from Santa Cruz) highly cross reacted with a sarcomeric protein, interfering with nuclear staining.

5.3.5 Myogenic commitment is also increased in satellite cells in presence of lamin A-N456I

Myogenic commitment was also assayed in primary mouse satellite cells cultured on single myofibres (Collins and Zammit, 2009; Zammit et al., 2004). This model allows the analysis of satellite cells in their niche as they activate, enter cell cycle and commit to differentiation. Quiescent satellite cells express Pax7, and induce MyoD as they activate. Satellite cells first co-express myogenic markers Pax7 and MyoD while proliferating and later diverge where some down-regulate MyoD and enter quiescence (self-renewal) while others commit to differentiation and start to express myogenin (Zammit et al., 2004; Zammit et al., 2006b). In contrast to C2C12 cells which are polyploid cells which express very low levels of the satellite cell marker Pax7, primary satellite cells provide a much better and physiologically relevant system to study lamin mutations.

To test the effects of lamin A variants on the myogenic commitment in satellite cells, single myofibres were isolated from hind limbs of adult wild-type C57BL/6 mice using standard procedures, entailing careful dissection of extensor digitorum longus (EDL), digestion in collagenase and gentle trituration to separate myofibres (Collins and Zammit, 2009; Rosenblatt et al., 1995). Single floating myofibres were incubated in growth medium for 72 hours (Fig. 5.9A). During the isolation process, satellite cells present underneath the basal lamina are activated. Medium used to culture single fibres is enriched with growth factors, pushing satellite cells to proliferate before spontaneously committing to differentiation by inducing the expression of myogenin. To analyse myogenin expression in presence of mutant lamin A, satellite cells were infected using retroviral particles after 24 hours in culture and further cultured for another 48 hours. After 72 hours in culture (48 hours post infection, p.i.) the myofibres with their associated satellite cells still attached were fixed and co-immunostained for eGFP and myogenin (Fig. 5.9B).

The results show that there was some variation in the total number of GFP positive cells/myofibre 48hrs post infection (Fig. 5.9C). This could be due to infection efficiency or loss of satellite cells during the staining procedure. Importantly, no significant difference was found when fibres exposed to wt-lamin A are compared to the number of GFP positive cells on fibres exposed to other lamin A variants.

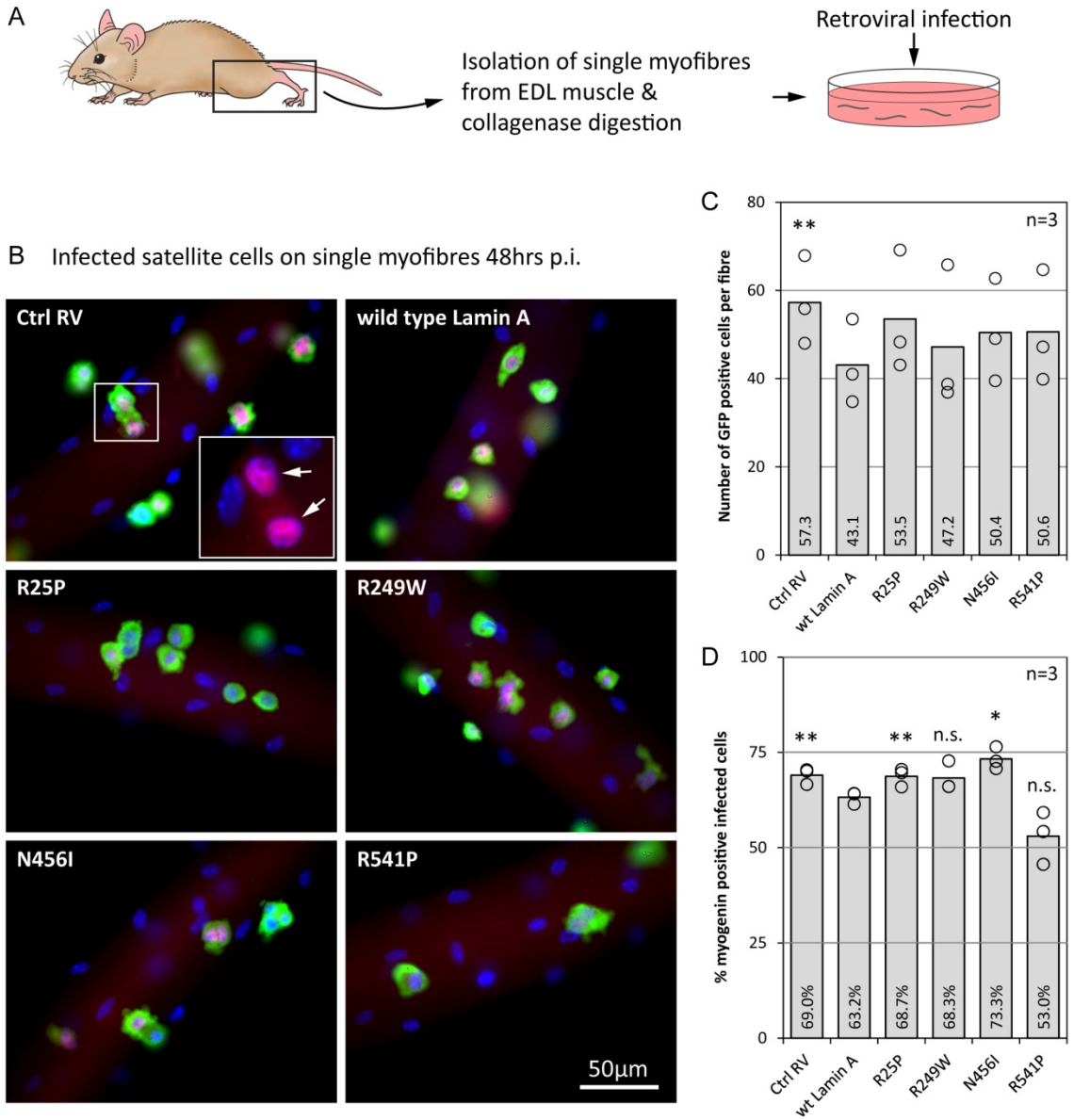

Figure 5.9 Satellite cell commitment to differentiation is increased in the presence of lamin A-N456I (**A**) Schematic representation of the single fibre model. Myofibres were isolated from EDL muscle of adult C57BL/6 mice and the satellite cells infected in a floating culture. (**B**) Myogenin expression (red) in infected wild-type satellite cells (green) in single EDL fibre cultures. The insert shows two infected satellite cells that are positive for myogenin. (**C**) Quantification of the number of eGFP positive cells per myofibre. Open circles represent the average of each of the three independent mice. (**D**) Quantification of the proportion of eGFP positive infected cells that co-expressed myogenin. For the statistical analysis, samples were compared to wild-type lamin A infected satellite cells; for each construct a total of at least 30 myofibres were analysed in three independent mice; * $p<0.05$, ** $p<0.01$ using a student's t-test.

The proportion of myogenin positive (committed) satellite cells infected with control RV was 69.0%. Interestingly, introducing wild-type lamin A significantly reduced the number of myogenin positive cells by 5.8%. The number of myogenin positive cells infected with lamin A-R25P and R249W is 68.7% and 68.3% respectively. This is similar to proportions found with control RV and slightly higher compared to wild-type lamin A infected cells. Introduction of lamin A-N456I resulted in the largest increase of myogenin positive cells (+10.1%, p=0.014) when compared to wild-type lamin A. In contrast, lamin A-R541P resulted in the largest although non-significant decrease (-10.2%, p=0.17) of myogenin positive cells when compared to wild-type lamin A (Fig. 5.9D).

5.3.6 Lamin A-N456I and R541P induce nuclear abnormalities in myotubes but do not result obvious effect on the differentiation capacity of primary *lmna*-null myoblasts

Examination of satellite cells on isolated myofibres is an excellent model to study the early events of satellite cell activation, proliferation and commitment to differentiation. However, a drawback of the single fibre culture is the short time fibres can be kept alive. Three to four days after isolation, fibres hypercontract and can not be analysed. Further, satellite cells do not fuse on the fibre which makes it difficult to analyse later stages of differentiation.

To overcome these issues, fibres are plated on matrigel, a substrate containing a mixture of extracellular matrix components such as laminin and collagen, which supports the growth of satellite cells which migrate off the myofibre (Rosenblatt et al., 1995). These plated satellite cells have been removed from the satellite cell niche and are therefore referred to as satellite cell derived myoblasts or primary myoblasts. In serum rich medium supplemented with fibroblast growth factor (FGF), primary myoblasts are maintained in a proliferative state. Upon serum withdrawal, cells exit cell cycle, express myogenin and start to fuse to form multinucleated myotubes, very similar to C2C12 myoblasts used above.

My results show that the effects of lamin A variants on myogenic commitment in wild-type satellite cells is very minimal and somewhat variable. One reason could be that mouse cells are less sensitive to mutations in the *lmna* gene. This has been shown in knock-in mouse models with dominant *LMNA* mutations such as N195K (Mounkes et al., 2005) and H222P (Arimura et al., 2005) which require homozygous expression of the mutant lamin to elicit a phenotype.

To induce a stronger phenotype I have expressed mutant lamin variants in *lmna*-null satellite cell derived myoblasts which mimicks a homozygous state. Unfortunately, myofibres from *lmna*-null mice do not survive long enough in culture for infection studies so I used the plated satellite cell model. Satellite cells are difficult to obtain in large numbers, especially from *lmna*-null mice. I have therefore only chosen the two mutations that showed the strongest change in the single fibre culture, lamin A-N456I and R541P. *Lmna*-null primary myoblasts infected with control RV and wild-type lamin A served as a control.

Immunostaining confirmed the lack of lamin A/C expression in *lmna*-null myoblasts infected with the control RV while cells infected with wild-type lamin A are labelled by the lamin A/C antibody (Fig. 5.10A). Futher, all single cells express the satellite cell marker Pax7 confirming their identity as shown in figure 5.10B. Interestingly, the lamin A/C antibody used here (mouse monoclonal 131C3, Abcam) did not pick up the mutant forms of lamin which could be due to epitope masking. Degradation of the mutant protein is unlikely, as other cells infected with the RV vector express moderate levels of mutant protein shown by western blot (Fig. 4.1). Further, satellite cell derived myoblasts have robust eGFP expression which is driven by the IRES in the *lamin A-IRES-eGFP* construct, confirming the presence and active translation of the mRNA.

When infected *lmna*-null primary myoblasts were differentiated for 48hrs and immunostained for myosin heavy chain, no obvious defects in differentiation were found. Cells infected with control RV, wild-type lamin A as well as the two mutant lamin A constructs (lamin A-N456I and R541P) formed large myotubes (Fig. 5.10C).

Lmna-null fibroblasts are characterised by abnormal nuclear morphology and mislocalisation of lamin B (Fig. 6.6, and (Sullivan et al., 1999)). However, proliferating *lmna*-null satellite cell derived myoblasts did not show abnormalities in nuclear morphology. Furthermore, lamin B1 localisation was normal in *lmna*-null cells, which was unexpected (indicated by yellow arrowheads in Fig. 5.11A). Interestingly, nuclear herneations together with aberrant lamin B1 localisation were evident in nuclei of differentiated myotubes (indicated by white arrowheads in Fig. 5.11A). In contrast, nuclear abnormalities were not found in wild-type lamin A infected myoblasts or myonuclei in differentiated myotubes (Fig. 5.11B).

Single, proliferating cells infected with lamin A-N456I and R541P also did not show any evidence of nuclear abnormalities (Fig. 5.11B and C). However, nuclei in myotubes demonstrate obvious nuclear abnormalities including herneations, and mislocalisation of lamin B1. Whether these mutations also induce similar nuclear alterations in differentiated wild-type satellite cells remains to be determined.

Taken together, results obtained in *lmna*-null satellite cell-derived myoblasts suggests that mutant lamin A variants (N456I and R541P) do not affect the differentiation potential. Furthermore nuclear alterations are only induced after the formation of myotubes which might result in an increased susceptibility to mechanical force and contribute to the EDMD pathology.

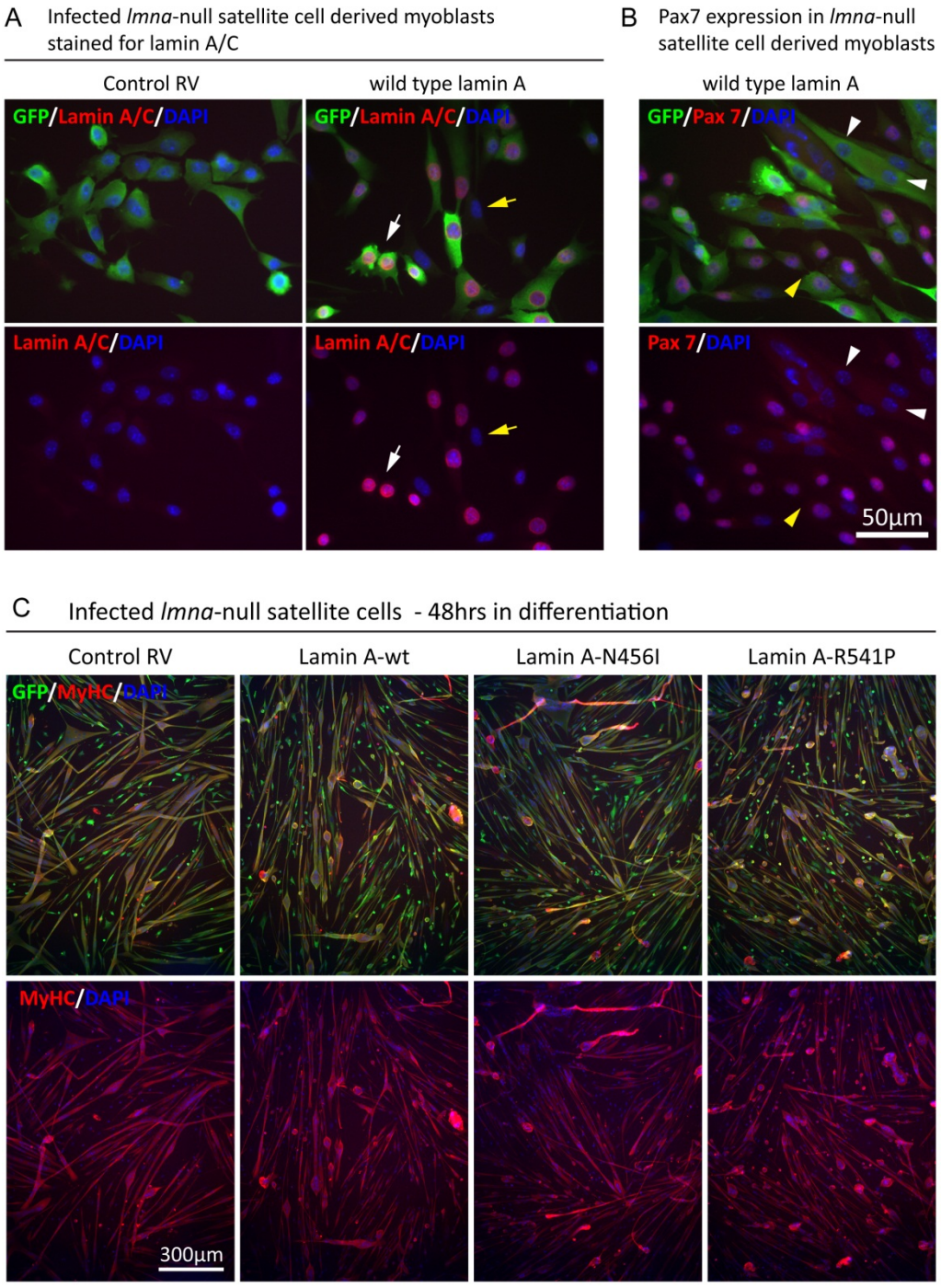

Figure 5.10 Expression of mutant lamin A variants in *lmna*-null satellite cell derived myoblasts does not affect their differentiation potential. (**A**) *Lmna*-null cells (left panel as well as non-infected cells (yellow arrow) lack lamin A/C expression while cells infected with wild-type lamin A (white arrow) are labelled by the lamin A/C antibody. (**B**) Both infected and non-infected single cells (yellow arrowhead) but not myotubes (white arrowhead) express the satellite cell marker Pax7. (**C**) *Lmna*-null satellite cell derived myoblasts infected with mutant lamin A, 48 hours after the induction of differentiation. No obvious difference in the differentiation potential is observed.

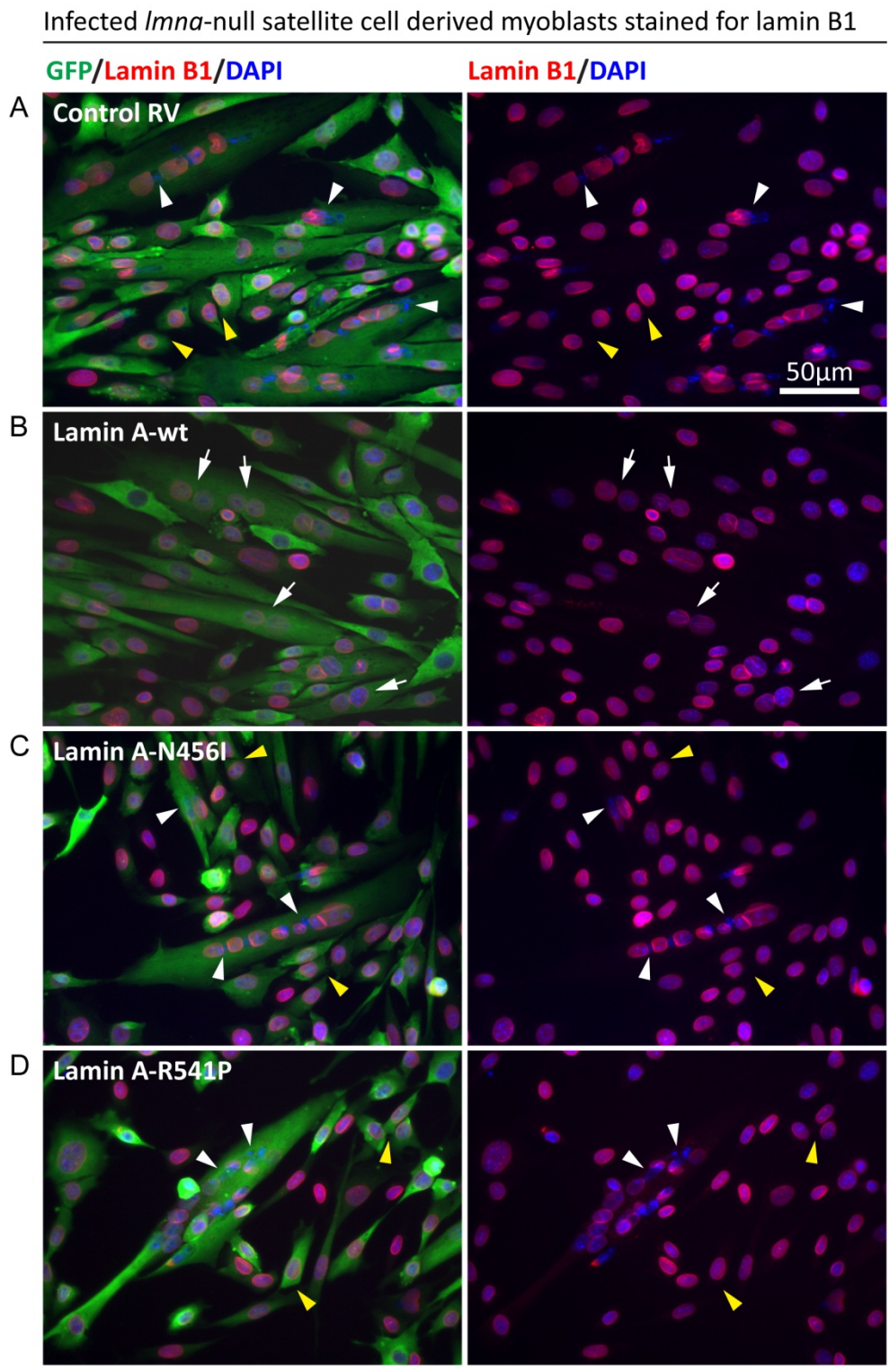

Figure 5.11 Lamin B1 is mislocalised in nuclei of differentiated myotubes but not in proliferating myoblast of *lmna*-null control cells and cells expressing lamin A-N456I and R541P. Pictures show infected *lmna*-null satellite cell derived myoblasts infected with control RV (**A**), lamin A-wt (**B**), N456I (**C**) and R541P (**D**) immunostained for eGFP (marking infected cells expressing the transgene) and lamin B1 (abcam). Single cells with no obvious abnormalities in morphology or lamin B1 localisation are indicated by yellow arrowheads. Nuclei in myotubes show marked herneations and lamin B1 mislocalisation (indicated by white arrowheads) while myonuclei of lamin A-wt infected cells show normal nuclear morphology and lamin B1 localistion (indicated by white arrows).

5.4 Discussion

In this chapter I set out to test the effects of four mutant lamin A variants (lamin A-R25P, R249W, N456I and R541P) on proliferation and differentiation of myogenic cells. Patients with these mutations suffer from a skeletal muscle phenotype, being diagnosed with EDMD (table 4.1). Satellite cells are essential for adult muscle homeostasis and repair and defective satellite cell function could potentially contribute to the pathology of EDMD (Gnocchi et al., 2008; Morgan and Zammit, 2010).

To find out if a dysfunctional muscle stem cell pool does indeed contribute to the skeletal muscle phenotype in EDMD and other skeletal muscle laminopathies, it is crucial to pinpoint what aspect of cell function is affected. To address this question, I have overexpressed mutant lamin variants in primary mouse satellite cells and C2C12 myoblasts. EDMD is a rare disease thus it is difficult to obtain patient myoblasts for functional studies. However the four chosen mutations (like almost all *LMNA* mutations) are autosomal dominant and expression of dominant lamin mutants in wild-type myogenic cells is an accepted approach (Favreau et al., 2004; Hakelien et al., 2008; Ostlund et al., 2001). Usually transfection is used to express mutant lamin A protein in cell culture. However transfection efficiencies are generally low in myoblasts and clonal selection of stable cell lines can lead to a bias in the analysis (Favreau et al., 2004). I have instead chosen to use a retroviral expression system because it results in moderate protein expression level across a large proportion of cells (>98% in C2C12 cells). Furthermore, no epitope tag, which could potentially interfere with lamin function, was used. Mutant lamin A protein was expressed using a bicistronic vector and infected cells were identified by eGFP expression via an IRES sequence.

As described in chapter 4, lamin A-R25P and R249W, located in the head and central rod domain of A-type lamins respectively, result in severe nuclear deformations as well as mislocalisation of lamin B. Interestingly, these cells also demonstrate a reduced colony growth when seeded at low density (Fig. 5.1A). There is evidence that lamin B provides a matrix for spindle assembly during M-phase (Tsai et al., 2006). Abnormalities in the interaction of lamin A and B caused by mutant lamin A could therefore affect cell cycle progression. The cell cycle however was not affected in these cells infected with lamin A-R25P and R249W when analysed by multiple techniques including BrdU incorporation, flow cytometry to analyse cell cycle progression and Western blot to test for abnormal expression/phosphorylation of cell cycle regulators shown to interact with lamin A. The discrepancy seen between colony growth and cell cycle could still be due to delayed cell cycle entry upon seeding or prolonged cell cycle maintaining the proportion of G1, S and G2/M cells. EDMD patient fibroblasts with *LMNA* mutations display reduced cell spreading and delayed Erk1/2 phosphorylation upon seeding (Emerson et al., 2009).

In cells analysed in this study, Erk1/2 and phospho-Erk1/2 levels were not obviously different between the samples and when compared to wild-type lamin A. However, the cells analysed were a heterogeneous population of proliferating asynchronous C2C12 cells potentially masking an effect

on Erk phosphorylation. Synchronisation of cells, which can be achieved by either serum starvation (Emerson et al., 2009), or a combination of drugs that block mitosis (nocodazole) and/or S-phase progression (thymidine) (Dechat et al., 1998), and subsequent induction of the cells, may lead to a more conclusive result.

Cells infected with lamin A-R25P and R249W also stained negative for senescence associated (SA) β-galactisodase, ruling this out as a contribution to cell-cycle exit. However, I did not test for molecular markers of apoptosis which might influence the number of cells/colony as has in fact been shown in C2C12 cells expressing the EDMD mutation p.R453W (Favreau et al., 2004). Although apoptotic nuclei were not observed in C2C12 expressing any of the mutant lamin A variants. Cells infected with lamin A-N456I and R541P did not display a phenotype in colony growth, S-Phase or other parts of the cell cycle. However, these mutants result in lamin A-foci within the nucleus in more than 20% of all cells (Fig. 4.4). Nucleoplasmic lamin A positive foci could potentially immobilise Lap2α affecting cell cycle in a pRb dependent manner (Markiewicz et al., 2002; Pekovic et al., 2007). I therefore tested if mutant lamin A affects localisation and expression levels of Lap2α. However, abnormal Lap2α localisation such as nuclear aggregates was not evident in cells infected with lamin A-N456I and R541P and altered expression levels were not detected by Western blot (data not shown).

If defective satellite cells are involved in the pathology of EDMD, but do not affect myoblasts proliferation, myogenic differentiation must be affected. I therefore also studied the effects of all four lamin A mutations on myogenic commitment and differentiation in C2C12 cells and primary satellite cells. The results show that the missense mutation p.N456I increases myogenic commitment in C2C12 cells and to a greater extent in satellite cells. In later stages of myogenic progression, this trend towards enhanced differentiation was still evident but not statistically significant (p=0.085). Interestingly, increased myogenic differentiation was also found in presence of miR-100, which is specifically upregulated in *LMNA*-associated muscular dystrophy patients (Sylvius et al., 2011).

In general, relatively little information is available on the effects of mutant lamin A on myogenic differentiation but other results published so far, lead to the general conclusion that *LMNA* mutations reduce the myogenic differentiation potential when expressed in cell lines (Favreau et al., 2004; Markiewicz et al., 2005), or in human myoblasts (Kandert et al., 2009). However, the lack of data might be evidence in itself, in that the majority of *LMNA* mutations might not have an effect on myogenic differentiation. Myoblasts used for overexpression studies are generally derived from mouse, which could be less sensitive to mutations in the *lmna* gene. This has been shown in knock-in mouse models with dominant *LMNA* mutations such as N195K (Mounkes et al., 2005) and H222P (Arimura et al., 2005) which require homozygous expression of the mutant lamin to elicit a phenotype. However, even when mutations associated with changes in myogenic commitment (p.N456I and p.R541P) are expressed in *lmna*-null cells, which mimics a homozygous state, no obvious phenotype is observed (Fig. 5.10).

A closer inspection of lamin B1 localisation however reveals a striking difference: proliferating, primary *lmna*-null myoblasts have no overt phenotype while differentiated, multinucleated myotubes show abnormal nuclear morphology and mislocalisation of lamin B1. Importantly, both mutations, which had no effect on lamin B localisation in proliferating C2C12 cells, showed similar abnormalities. In contrast, myonuclei in wild-type lamin A infected cells are normal. The absence of a nuclear phenotype in primary myoblasts could be related to the fact that they are more stem cell like as compared to C2C12 cells. Embryonic stem cells do not express A-type lamins (Constantinescu et al., 2006) and induced pluripotent cells from HGPS fibroblasts have been shown to lose nuclear abnormalities which is related to a loss in A-type lamins (Liu et al., 2011; Zhang et al., 2011). However, satellite cells in their niche are positive for lamin A/C (Gnocchi et al., 2009; Morgan and Zammit, 2010) and primary myoblasts do express lamin A and C at equal levels (Frock et al., 2006). Why *lmna*-null primary myoblasts are less affected by mutant lamin A protein remains to be determined, however, primary myoblasts and C2C12 cells seem to be affected differently by *LMNA* mutations which is an important point to consider in future studies and data interpretation.

One point to note is that all *LMNA* missense mutations associated with a reduced myogenic potential of myoblasts (p.R453W (Favreau et al., 2004), W520S (Markiewicz et al., 2005) and R545C (Kandert et al., 2009)), including p.R541P used in this study, are located in the Ig-fold domain, and likely to disrupt the structure based on my analysis in chapter 3, although different underlying mechanisms have been suggested such as Erk signalling (Favreau et al., 2008), epigenetic defects (Hakelien et al., 2008), Lap2α/pRb misregulation (Markiewicz et al., 2005) as well as proteasome inhibition (Kandert et al., 2009). In contrast, the second mutation used here (p.N456I, associated with increased myogenic commitment), is located on a loop, and results in a moderate (polar to non-polar) amino acid change. Together this provides evidence that these mutations affect the lamin A structure as well as myoblast function in different ways, which could be related to lamin interacting proteins.

The missense mutation in the head domain (p.R25P) and central rod domain (p.R249W) resulted in severe nuclear abnormalities in proliferating C2C12 cells but did not affect myogenic commitment or differentiation. Interestingly, nuclear defects were also evident in myotubes (Fig. 5.8), supporting the 'mechanical stress' hypothesis which states that the disease is caused by an increased susceptibility of nuclei to physical stress (Worman, 2012). The central rod domain of lamin A interacts with nesprins (Mislow et al., 2002; Zhang et al., 2005) and mutations in the lamin A central rod domain disrupts its binding to SUN-domain proteins (Haque et al., 2010). Both, SUN-domain proteins and nesprins, are main components of the LINC complex, which support the structural integrity of the nucleus (Mellad et al., 2011). Disruption of the LINC complex has been shown to induce defects in nuclear morphology (Khatau et al., 2009) and affect the localisation of skeletal muscle nuclei as well as strain transmission between the cell and nucleus (Zhang et al., 2010), while

mutations in giant nesprins 1 and 2 result in a pathology resembling that of EDMD (Zhang et al., 2007).

If mutations in the central rod domain result in a structural instability of the lamin polymer, affect protein protein interactions, or both, remains to be determined. Photobleaching experiments of fluorescently labeled lamins reveal that most *LMNA* mutations tested, result in increased protein mobility, with the most severe effects seen in mutations in the central rod-domain (Broers et al., 2005; Gilchrist et al., 2004).

The result presented here certainly raises the possibility of a contribution of a defective satellite cell pool in EDMD pathology. However mutant lamins are likely to act on multiple levels affecting structural integrity and chromatin organisation of myonuclei and satellite cells alike. Indeed, ultrastructural analysis of muscle from EDMD patients revealed that only approx. 20% of all myonuclei display irregular membrane contours (Park et al., 2009). However, more than 90% of all myonuclei as well as 50% of all satellite cells have markedly abnormal chromatin organisation including reduced or no heterochromatin and reduced euchromatin density (Park et al., 2009).

5.5 Conclusion

Here I present data of four different lamin A mutations associated with skeletal muscle dystrophy that show no or only minor effects on C2C12 and satellite cell function. Cell infected with lamin A-R25P and R249W demonstrated a reduced proliferation potential however showed no overt cell cycle defects when analysed by the methods used here. Myoblasts infected with lamin A-N456I showed increased differentiation potential in early phases of differentiation.

Muscle satellite cells could still contribute to the pathology of EDMD, however, the result obtained in this and the previous chapter suggests that lamins affect muscle in various different ways which might not necessarily involve satellite cell function.

So far, the effects of mutant lamin A variants on myogenesis has only been studied in a handful of mutations though. To identify the different mechanisms at work, it will be necessary to isolate myoblasts from a large number of EDMD patients and screen them in parallel for common phenotypes. Immortalisation of human myoblasts for patients is an encouraging way to produce large amounts of material for study (Mamchaoui et al., 2011). Since patient fibroblasts are easier to obtain, generation of iPS cells could be an alternative method to study the pathogenic mechanism of large number of different *LMNA* mutations (Liu et al., 2011; Zhang et al., 2011).

This comparative study will allow to associate nuclear abnormalities commonly seen in cells expressing mutant lamin A with ability or inability to form myotubes. Once grouped into several categories, common molecular pathways affected by mutant lamins can be isolated and selected for treatment.

Chapter 6

Exon Skipping as a Potential Therapeutic Intervention for Particular Laminopathies

6.1 Introduction

The vast majority of eukaryotic genes produce primary transcripts (pre-mRNA) that contain introns and exons of various numbers and sizes (Lander et al., 2001). To form mature mRNA, the pre-mRNA undergoes splicing which is a tightly regulated process and crucial for the translation of functional proteins. Splicing is carried out in a defined order by the splicing machinery, which recognises conserved 5' and 3' splice site sequences as well as the branch point adenine, resulting in the removal of introns (Cooper et al., 2009).

Disease causing mutations often affect the splicing mechanism. Out of the 123656 mutations published in the human gene mutation database (as of March 2012) 11525 mutations (9.3%) affect splicing (Stenson et al., 2009). The outcome of the mutation depends on its location. If the consensus 5' or 3' splice site is mutated, an intron might be included in the final transcript. If a new splice site is created, part on an intron might get included or part of an exon excluded in the mature mRNA, leading to insertions, deletions or resulting in a frameshift. Antisense oligonucleotides (AONs) can be used to correct faulty splicing and restore expression of the wild-type protein, or to generate internally truncated version that can fully/partially restore function (Aartsma-Rus and van Ommen, 2007; Hammond and Wood, 2011).

6.1.1 Potential use of exon skipping in laminopathies

Laminopathies are a very heterogeneous group of diseases that affect a range of tissues depending on the *LMNA* mutation and the genetic background of the patient. It is therefore very difficult to develop general therapies for laminopathies. Currently, treatments that target very specific aspects of lamin A processing or signalling are under investigation. Examples of such treatments in mice include farnesytranferase inhibitors (FTIs) to treat HGPS (Yang et al., 2006) and ERK inhibitors to treat cardiomyopathy (Muchir et al., 2009). As a result these treatments will potentially only cover a minority of patients with very specific mutations.

To target a larger number of patients a more general approach is needed. One such treatment would be the use of AONs to eliminate exons harbouring premature translation termination codons (PTCs) similar to the example described in figure 6.1B. A prerequisite for this therapy to work is that the exon eliminated is redundant and that the resulting protein product with the deletion is sufficiently partially functional and non-toxic. If individual *LMNA* exons are indeed

redundant, the removal of a single mutated exon by modulating *LMNA* splicing through AONs could be used as a novel treatment strategy for laminopathies.

To go one step further exons harbouring missense mutations could also be considered as targets in this therapy. Given that the majority of pathogenic *LMNA* mutations are missense mutations, a larger number of patients would potentially benefit. The idea however does sound counter intuitive considering that the elimination of an entire exon is to generate a positive effect. However, if the pathogenic mutation results in a protein with a gain of function, replacing this protein with an inert/partially functional protein could ameliorate the phenotype. It is therefore well worth considering exon skipping as a therapeutic intervention for missense and nonsense mutations in *LMNA*. At present, the efficiency of AONs is low, but this should improve with advances in technology. Since laminopathies are usually dominant however, then exon skipping will also have the negative effect of reducing levels of wild-type protein, so it is important to consider the results of this side effect.

6.1.2 Design and properties of common AON chemistries

AONs are defined as oligonucleotides that are 8-50 nucleotides in length, that bind to RNA through Watson-Crick base pairing and upon binding to RNA, modulate its function (Bennett and Swayze, 2010). AONs can be grouped into two categories depending on the mechanism through which they act on the RNA target: (a) AONs that bind to the target sequence and modify its function without promoting degradation and (b) AONs that do promote degradation of the target RNA either through enzymes such as RNAse H or Argonaute 2, or through cleavage mechanisms designed into the oligonucleotide. AONs that modulate splicing are part of the former group and are designed to form stable dimers with pre-mRNA in the nucleus, and do not induce target degradation (Bennett and Swayze, 2010; Muntoni and Wood, 2011).

The two major challenges in AON therapy are the design of stable oligonucleotides and their delivery to a specific target tissue. AONs that mediate splicing have to reach the nucleus without being degraded, and unlike siRNA, must not degrade the template they bind to. Several chemical modifications are used to achieve these properties. Many AONs carry a neutral charge to aid cell penetration and have either backbone modifications, sugar modifications or both (Bennett and Swayze, 2010). Commonly used AON chemistries include: (a) Morpholino oligonucleotides, where morpholino instead of ribose moieties are linked by an uncharged phosphorodiamidate linkage (Corey and Abrams, 2001) (b) Peptide nucleic acids (PNAs) which have a peptide bond in place of the sugar phosphate backbone but are still able to form Watson-Crick base pairs with complementary DNA and RNA (Egholm et al., 1993; Nielsen et al., 1991) (c) the 2'-O-methoxyethyl (MOE) ribose modification which induces the 3'-*endo* (Northern) conformation and is thought to increase the affinity to RNA (Teplova et al., 1999) and (d) Locked Nucleic Acid (LNA) which have a bridge connecting the 2' oxygen and 4' carbon of the ribose which is "locked" in the

3'-*endo* conformation (Jepsen et al., 2004). All modifications listed above show increased resistance against DNA endo- or exonucleases and do not induce RNAse H activity (Bennett and Swayze, 2010).

In therapeutic applications, AONs are usually delivered systemically to achieve the best possible distribution in the organism. However, tissue uptake is often inefficient and as a result AONs are excreted rapidly (Muntoni and Wood, 2011). To overcome this problem and promote tissue uptake of AONs, they can be conjugated with arginine rich cell-penetrating peptides (CPPs) such as $(RXR)_4$, which results in higher efficacy (Wu et al., 2008; Yin et al., 2008). In some cases AONs need to be delivered to specific target tissues such as muscle which can be achieved by using tissue specific targeting peptides. The B-peptide for example has been proven excellent to target AONs to the heart, while naked oligos fail to do so efficiently (Yin et al., 2009).

6.1.3 The use of antisense oligonucleotides to modulate splicing

AONs can be used to modulate splicing in three different ways: (a) correction of a cryptic splice site in a disease state (b) exon exclusion and (c) exon inclusion. All three are described briefly below and examples for clinical applications for each mechanism are given in the text and in table 6.1.

Table 6.1 Current use of antisense oligonucleotides to modulate splicing (modified from Hammond and Wood (2011))

Mechanism	Disorder	Target	Mode of action	Reference
Correction of active cryptic splice site	β-Thalassemia#	β-Globin	Blocking the recognition of cryptic splice sites	(Lacerra et al., 2000)
	Neurofibromatosis type 1*	*NF1*	Blocking the recognition of cryptic 5' splice site	(Pros et al., 2009)
	HGPS*	*LMNA*	Blocking the recognition of a cryptic splice site which results in the deletion of 50aa in exon 11, producing toxic progerin	(Scaffidi and Misteli, 2005)
Exon exclusion	Duchenne muscular dystrophy†	*DMD*	Skipping of exon 51 to correct reading frame and restore protein expression	(Cirak et al., 2011)
	Dysferlinopathy*	*DYSF*	skipping of exon 32 removes a PTC and restores protein expression	(Aartsma-Rus et al., 2010)
Exclusion of pseudoexon	Propionic academia*	*PCCA*, *PCCB*	blocking the recognition of a pseudoexon	(Rincon et al., 2007)
Exon Inclusion	Spinal muscular atrophy#	*SMN2*	Inclusion of exon 7 to provide same function as SMN1	(Hua et al., 2008)

* shown in vitro, # shown in vivo, † currently in clinical trial

6.1.3.1 Correction of active cryptic splice sites

Cryptic splice sites are potential splice sites, are dormant or used only at low levels in RNA processing unless activated by mutation of nearby authentic or advantageous splice sites (Green, 1986). The first example of how AONs can be used to modulate splicing is the correction of cryptic splice sites. In principle, a cryptic splice site recruits the splicing machinery and competes with a commonly used splice site. This results in the inclusion of part of an intron or in the exclusion of part of an exon, depending on where the new splice site is created (Hammond and Wood, 2011). When the created/deleted fragment is in frame with the rest of the transcript, a disease causing protein product with an insertion or deletion might be expressed. If the insertion/deletion is out of frame, the mRNA is either degraded by nonsense mediated decay (NMD) or results in the expression of a truncated protein resulting in disease (Rebbapragada and Lykke-Andersen, 2009). AONs are used to mask the cryptic splice site and prevent the binding of splicing factors. As a result normal splicing of the gene is restored, with the potential to reduce clinical symptoms of disease. The principle of using AONs to target a cryptic splice site is depicted in figure 6.1A.

One of the first examples where AONs were used to correct a cryptic splice site was to restore normal splicing of the β-globin gene. Several mutations are described in intron 2 of the β-globin gene typically creating novel splice sites resulting in a loss of haemoglobin (Hb) A. Patients carrying such mutations suffer from β-thalassemia which is characterised by severe anaemia and sometimes death (Busslinger et al., 1981). AONs were shown to be able to restore normal Hb-A synthesis in erythrocytes from thallasemic patients using AON mediated masking of cryptic splice sites (Lacerra et al., 2000).

Of relevance to laminopathies, this strategy was also used to explore the treatment of Hutchinson-Gilford progeria syndrome (HGPS) with AONs. HGPS is caused by a silent substitution (c.1824C>T; p.G608G) which creates a cryptic 5' donor splice site in *LMNA* exon 11 and results in the expression of a toxic protein product (progerin) that lacks 50 amino acids in the tail domain (see section 1.4 for details). Fibroblasts from HGPS patients show severly dysmorphic nuclei, and mislocalisation of lamin B and lamin associated proteins as well as reduced levels of HP1α (Eriksson et al., 2003; Paradisi et al., 2005; Scaffidi and Misteli, 2005). Using AONs to mask this novel splice site was shown to restore normal *LMNA* splicing and reverse phenotypes seen in HGPS fibroblasts (Scaffidi and Misteli, 2005).

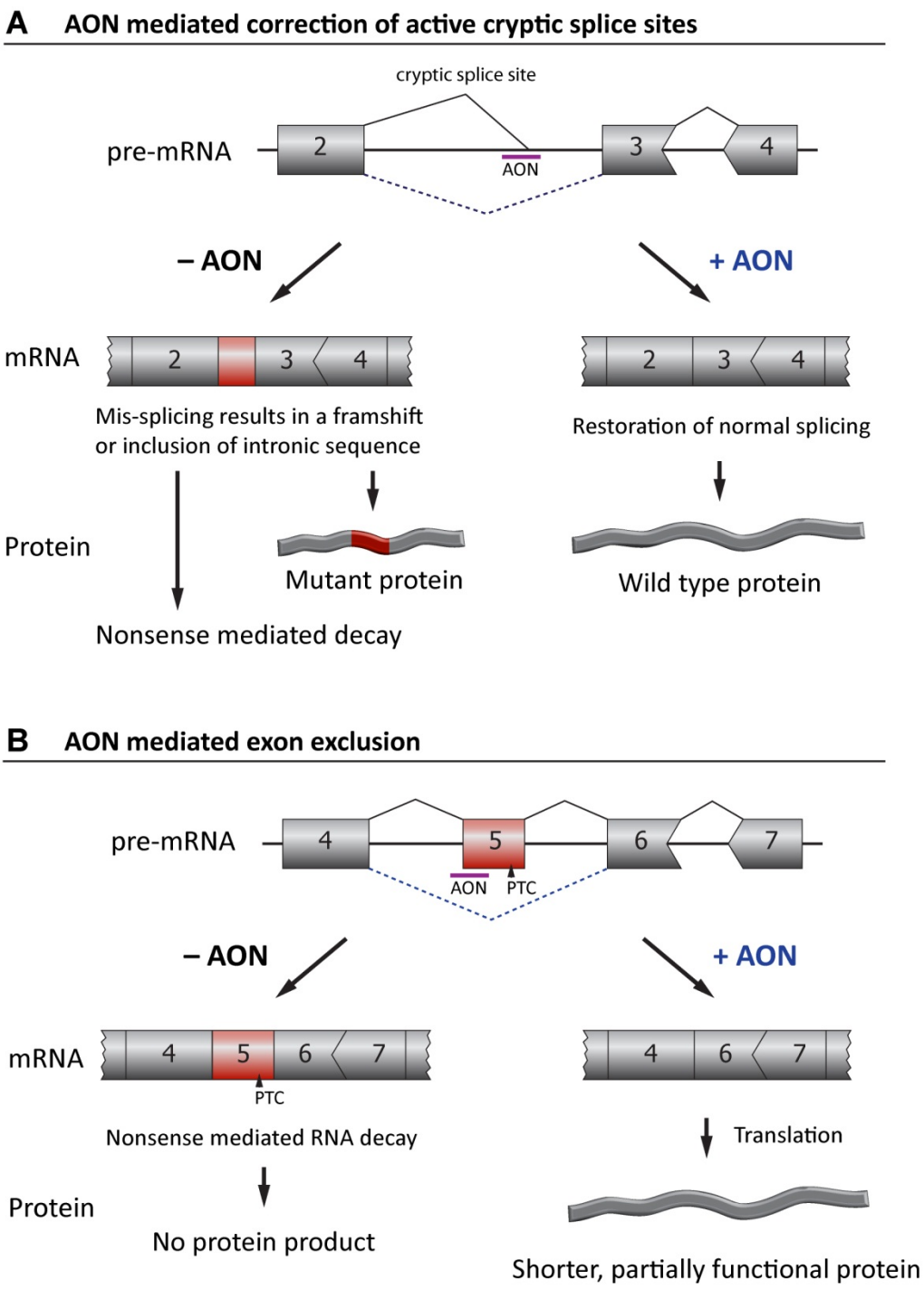

Figure 6.1 The use of antisense oligonucleotides to modulate splicing. (**A**) The introduction of a cryptic splice can disrupt the open reading frame of the mRNA which leads to nonsense mediated decay and loss of protein expression. If the reading frame remains intact, a part of an intron might be included, or a part of an exon removed, resulting in the expression of a mutant protein. Antisense oligonucleotides (AONs) are used to mask cryptic splice sites and to restore the open reading frame of the mRNA and expression of wild-type protein. (**B**) A premature termination codon (PTC) located in an exon results in nonsense mediated decay of the mRNA. The addition of AONs masking splice sites or splice enhancers will result in the exclusion of that exon. Providing that the flanking exons form an in-frame transcript, the AONs are used when the resulting protein product with its deletion is fully or partially functional.

6.1.3.2 Exclusion of an exon

Antisense oligonucleotides are also used to exclude exons (exon skipping) (Aartsma-Rus and van Ommen, 2007). The principle of AON mediated exon skipping is described in figure 6.1B. In this example a gene with multiple exons has a point mutation in exon 5 which results in a PTC. The pre-mRNA gets spliced correctly the transcript however is degraded by nonsense mediated RNA degradation (NMD) and no functional protein is produced. The addition of AONs targeting either the splice donor or the splice acceptor site or exonic splice enhancer sites would lead to the exclusion of that exon and the PTC located in that exon. Providing that the flanking exons form an in-frame transcript, then the resulting transcript would be shorter but serves as a template for a protein with an internal deletion which is potentially beneficial to the organism.

An example is the mouse model for Duchenne Muscular Dystrophy (*mdx*) which lacks dystrophin expression due to a PTC in exon 23. AON mediated skipping of exon 23 restores dystrophin expression and improves the muscle phenotype (Alter et al., 2006; Dunckley et al., 1998). As a result of this and similar work, AON mediated exon skipping is now being tested in clinical trials as a potential therapy for Duchenne muscular dystrophy, and is the most promising therapy so far (Cirak et al., 2011; Goemans et al., 2011). The vast majority of Duchene patients carry deletion mutations within the *DMD* gene, disrupting the reading frame to generate a PTC resulting in no dystrophin expression (www.umd.be/DMD). In human DMD patients, AONs are used to remove adjacent out-of-frame exons which allows for the expression of a shorter but partially functional dystrophin variant.

6.1.3.3 Inclusion of an exon

For some disease interventions AONs are used to include an exon that is typically spliced out. For example Spinal Muscular Atrophy (SMA) is caused by a homozygous loss of the survival of motor neurons 1 (*SMN1*) gene. The severity of the disease is modified by SMN protein encoded by the paralog *SMN2* (Helmken et al., 2003). Although *SMN2* is nearly identical to *SMN1* there is a C to T transition in exon 7 of SMN2 which promotes the exclusion of exon 7 (Lorson et al., 1999). However, only full length SMN protein from the *SMN2* gene is functional so the severity of the SMA disease phenotype is directly correlated with the exclusion of exon 7. An AON therapy that leads to the retention of exon 7 in SMN2 could therefore ameliorate the SMA phenotype which was confirmed in a mouse model (Hua et al., 2010). Hua Y. and colleagues have used AON mediated blocking of an hnRNP A1/A2 intronic splice silencer located in intron 6 to promote the retention of exon 7 in the *SMN2* transcript. This resulted in the production of functional survival of motor neurons 2 protein which could rescue necrosis in the type III mouse model (Hua et al., 2010; Hua et al., 2008).

6.2 Aim

In this chapter I will explore the possibility of using AONs to modulate splicing of the *LMNA* gene to remove mutated exons as a potential therapeutic strategy to treat laminopathies.

Initially, I will identify *LMNA* exons that are potential candidates for exon skipping and then I will construct lamin A cDNAs to test if this works in practice.

I hypothesise that the detrimental effects of missense mutations, insertions and deletions located in some exons of *LMNA* can ameliorated by removing the entire exon. Removing such exons would eliminate the pathogenic mutation resulting in a shortened but functional protein. If successful this would provide proof-of-principle for exon skipping as a novel therapeutic intervention for laminopathies.

6.3 Results

6.3.1 Identification of *LMNA* exon targets for potential therapeutic skipping

Out of 12 exons that form the A-type lamins, not all can be skipped without consequence for lamin function. To select potential target exons I analysed their reading frame and what part of the protein they encode (Fig. 6.2). In general, out of frame exons cannot be skipped as they would result in a disruption of the reading frame and loss of protein expression. A loss of A-type lamins would have severe consequences and has been reported to be lethal in man (Muchir et al., 2003; van Engelen et al., 2005). On this basis exons 2, 6 and 7 as well as the first and last exon were not considered as targets for exon skipping.

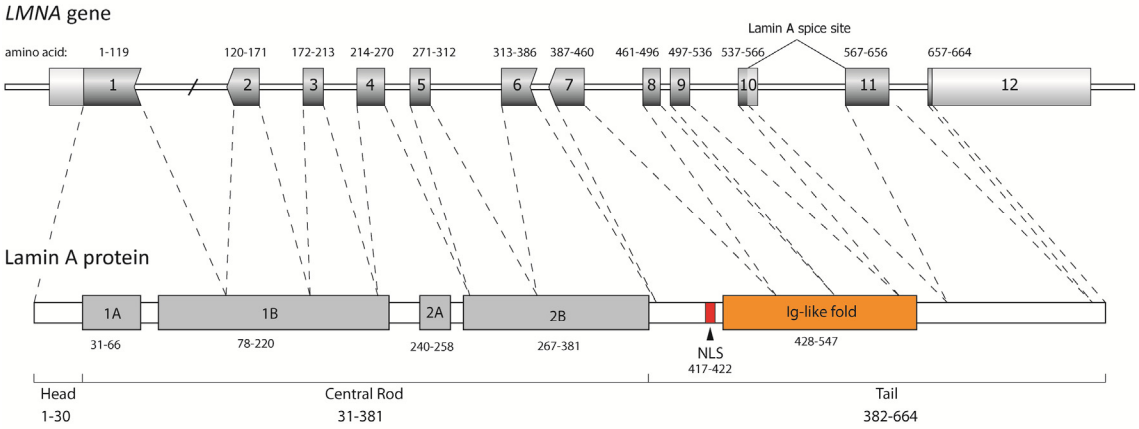

Figure 6.2. Exon structure of the *LMNA* gene. The gene consists of 12 exons, and codes for both lamin A and C. Lamin A is alternatively spliced from exon 10 while lamin C stops in exon 10. All exons except exon 2 can be removed without affecting the open reading frame. Dotted lines indicate the regions of the peptide encoded by each exon.

Exons that encode functional domains important for lamin maturation are further targets which should be excluded for exon skipping. One such exon is exon 11 which encodes the second proteolytic cleavage site necessary to form mature lamin A (Fig. 1.5). Removing exon 11 therefore results in a permanently farnesylated form of lamin A with a deletion similar to that of progerin. The deletion of exon 11 has been found in RD patients and is therefore to be avoided at all costs (Navarro et al., 2004). Similarly, the removal of exon 9 also results in a permanently farnesylated lamin A variant which causes a progeroid phenotype in mice. Lamin A lacking exon 9 most likely undergoes a conformational change which masks the second proteolytic cleavage site and inhibits the maturation of lamin A. In addition, transcripts lacking exon 9 are less stable which results in a reduced lamin A expression while lamin C is not expressed at all (Hernandez et al., 2010; Mounkes

et al., 2003). Given the evidence above, exons 9 and 11 were not considered as suitable candidates for exon skipping.

The remaining exons 3, 4, 5, 8 and 10 can be subdivided into two groups: those that are likely to interfere with lamin A function (providing less suitable but possible targets for exon skipping) and those that are less likely to interfere with lamin function (providing good targets for exon skipping).

Exons 4, 8 and 10 can be considered as potential targets however all three exons encode for important parts of the protein. Exon 4 forms a flexible linker region between coil 1 and 2 (L12) as well as coil 2A of the central rod domain. The removal of this region might reduce the flexibility of the central rod domain and interfere with filament formation.

Exon 8 forms part of the Ig-fold domain and given the importance of this domain in protein interactions (see Fig. 1.8) it was considered to be an unlikely target for exon skipping. Further, the Ig-fold might play an important role in lamin filament assembly. Addition of the Ig-fold motif to Xenopus egg extracts before the introduction of chromatin is sufficient to completely inhibit lamin polymerisation (Shumaker et al., 2005).

Exon 10 codes for part of lamin A Ig-fold as well as the tail of lamin C. Removal of exon 10 will therefore prevent the expression of lamin C. However, mice expressing only lamin A appear to be normal, suggesting lamin C may be redundant (Fong et al., 2006b). Lamin A protein lacking exon 10 has been described as an alternative splice product of the *LMNA* gene, and was found in several carcinoma cell lines (Machiels et al., 1996). It remains to be determined however, if removal of part of the Ig-fold has any detrimental effects on the 3D structure of the Ig-fold and lamin function Carcinoma cells expressing lamin A-Δ10 show lamin A aggregates (Machiels et al., 1995; Machiels et al., 1996) although others have shown that GFP-tagged lamin A-Δ10 localises normally in CHO cells (Broers et al., 1999). Further, a specific role of lamin A-Δ10 in cancer cells can not be ruled out as other expression abnormalities of lamins have been associated with certain types of cancer (Venables et al., 2001; Willis et al., 2008).

The two remaining exons (3 and 5) provide the best targets for initial testing for 2 reasons: Firstly they both encode for 6 complete heptad repeats in coils 1B and 2B respectively which resembles the central rod structure of cytoplasmic IF proteins (Appendix 1, (Herrmann and Aebi, 2004)). As a result their removal is not predicted to disrupt α-helical coiled coils. Secondly, deletion of exons 3 or 5 does not affect any of the linker or hinge regions. Further, Schirmer et al. have shown that 5 heptads on either end of the lamin B1 central rod domain are sufficient to promote filament formation in vitro (Schirmer et al., 2001).

Patients with mutations in exons 3 or 5 would potentially benefit from an exon skipping therapy. Table 6.2 provides a list of mutations that would be targeted by skipping exons 3 and 5, and the number of patients recorded for each mutation. In total, 41 mutations (identified in 244 symptomatic and asymptomatic individuals) have been reported in exons 3 and 5. These are 121 reported cases (7.8%) in exon 3 and 123 reported cases (7.9%) in exon 5. Out of 193 symptomatic

cases (numbers reported in table 6.2), 95 (49.2%) have mutations in exon 3 and 98 (50.8%) have mutations in exon 5.

Table 6.2 Summary of mutations reported in *LMNA* exons 3 and 5 (from www.umd.be/LMNA)

***LMNA* Exon 3**			***LMNA* Exon 5**		
Mutation	**Reports**	**Phenotype**	**Mutation**	**Reports**	**Phenotype**
p.L183P	1	DCM-CD	p.L271P	3	EDMD
p.E186K	1	DCM-CD	p.S277P	1	EDMD
p.R189W	1	DCM-CD	p.A278T	5	LGMD1B (4), DCM-CD (1)
p.R189P	1	DCM-CD	p.E291K	1	DCM-CD
p.R190W	28	DCM-CD	p.L292P	2	LGMD1B (1), L-CMD (1)
p.R190Q	4	DCM-CD	p.Q294P	2	EDMD
p.D192G	1	DCM-CD	p.S295P*****	1	EDMD
p.D192V	2	DCM-CD (1), DCM-CD/FPLD (1)	p.R298C	51	AR-CMT2 (44), Cardiac disease (5), AR-CMT2/EDMD (2)
p.N195D	1	EDMD	p.D300N	3	WRN (2), Progeroid Syndrome (1)
p.N195K*	14	DCM-CD	p.D300G	1	Progeroid Syndrome
p.R196S	1	EDMD	p.L302P**#**	1	L-CMD
p.E203K	15	DCM-CD	p.S303P*****	3	LGMD1B (2), EDMD (1)
p.E203G	6	DCM-CD	p.K311R	1	LGMD1B
p.E203V	1	DCM-CD	p.Q312H	2	LGMD1B (1), DCM-CD (1)
p.F206L	1	EDMD	p.D272AfsX?	2	
p.I210S	1	DCM-CD	p.A287LfsX193	1	LGMD1B
p.R190dup*	1	EDMD	p.A287RfsX44	1	DCM-CD
p.L197_T199del	1	EDMD	p.A287VfsX193	1	DCM-CD
p.K208del	14	LGMD1B	p.H289RfsX190	2	LGMD1B
p.N209TfsX271	3	EDMD	p.S303CfsX27	10	LGMD1B (8), DCM-CD (2)
			c.IVS5+1G>T	1	DCM-CD

6.3.2 Isolation of *lmna*-null and wild-type mouse embryonic fibroblasts

In this proof of principle study, I used a retroviral expression vector (*pMSVC-IRES-eGFP*; see section 2.2.2) to express various lamin A constructs with deletions and missense mutations in *lmna*$^{+/+}$ and *lmna*$^{-/-}$ primary mouse embryonic fibroblasts (pMEFs) (Fig. 6.3). Fibroblasts were chosen because they are easy to isolate and maintain in culture, well characterised and relatively flat which makes it easy to image the nucleus.

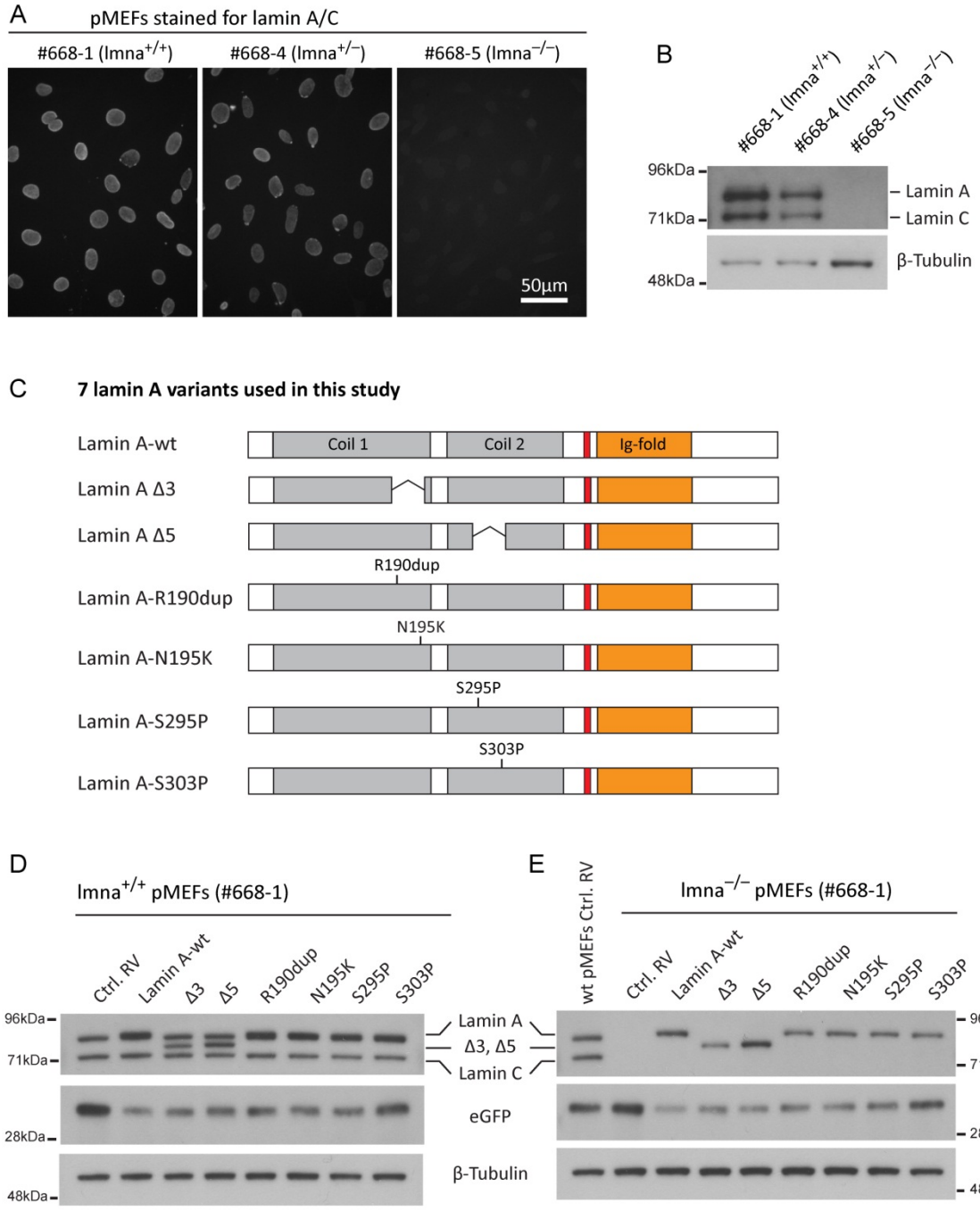

Figure 6.3. Isolation of pMEFs and expression of lamin A variants by retroviral infection. (**A**) Primary MEFs isolated from *lmna* wild-type, heterozygous and null embryos stained for lamin A/C. Scale bar = 50µm (**B**) Western blot of *lmna* wild-type, heterozygous and null pMEFs for lamin A and C confirming the genotypes. (**C**) Constructs used in this study were in the same order as depicted in C: full length wild-type lamin A, lamin A with exon 3 deleted (lamin A-Δ3) and lamin A with exon 5 deleted (lamin A-Δ5) and separate four full length lamin A constructs with mutations in either exon 3 (R190dup or N195K) or exon 5 (S295P or S303P). (**D**) Western blot of wild-type pMEFs infected with retroviruses encoding each of the lamin A constructs to show their successful production. (**E**) *Lmna*-null pMEFs infected with retroviruses encoding each of the lamin A constructs. β-tubulin served as a loading control.

The reason to use wild-type and *lmna*-null cells was twofold. Firstly, the lamin mutations used are dominant and should have a negative effect on wild-type cells. If the Δ3 and Δ5 lamin variants perform like wild-type protein, they should not affect the contour ratio of nuclei or lamin localisation.

Secondly, *lmna*-null cells show severe nuclear defects which can be reversed by re-introducing wild-type lamin A. If lamin A-Δ3 and lamin A-Δ5 act like wild-type lamin A they should also be localised correctly and revert the phenotypes observed in *lmna*-null cells. This is important as exon skipping also reduces the level of wild-type protein. Lamin variants with mutations in exons 3 and 5 on the other hand are expected to mislocalise and have no positive effect on *lmna*-null cells.

Figure 6.3 shows pMEFs isolated from lamin wild-type, heterozygous and null embryos stained for lamin A/C as well as well as Western blot results confirming the genotype of the cells used. A heterogeneous population of primary cells before passage P4 from 3 different embryos for each genotype was used for all experiments.

The lamin A constructs used in this study are depicted in figure 6.3 and listed below.

1 Full length human wild-type lamin A (Lamin A-wt)
2 Lamin A with an internal deletion of 42aa corresponding to exon 3: lamin A-Δ3
3 Lamin A with an internal deletion of 42aa corresponding to exon 5: lamin A-Δ5
4 Lamin A-R190dup (duplication mutation in exon 3)
5 Lamin A-N195K (missense mutations in exon 3)
5 Lamin A-S295P (missense mutation in exon 5)
7 Lamin A-S303P (missense mutation in exon 5)

The constructs were cloned into the pMSCV retroviral construct as described in section 2.2.2 (Fig. 6.3C) where empty vector expressing eGFP served as a control RV. Western blot analysis of infected *lmna*-null pMEFs showed expression levels typically consistent with those found in wild-type cells (Fig. 6.3D). These constructs contained lamin A only, so Lamin C is not expressed in infected *lmna*-null cells.

6.3.3 Lamin A-Δ5, but not lamin A-Δ3 localises correctly to the nuclear envelope

The first question in this study was whether the different lamin variants localise correctly to the nuclear lamina. Since there is no antibody available to discriminate mutant lamins from wild-type lamin A, the localisation of mutant lamin A was assessed in *lmna*-null pMEFs. Cells were infected with lamin A-wt, lamin A-Δ3 and lamin A-Δ5 and four days post infection, were stained for eGFP, Lamin A/C, LaminB1 and DAPI, and imaged with an LSM5 exciter confocal microscope. Figure 6.4 shows single confocal sections of 0.8µm thickness, taken at the centre of infected cells. Wild-type lamin A is shown to be localised at the nuclear lamina and throughout the nucleoplasm as expected. In contrast, the lamin A-Δ3 variant which lacks seven complete heptad repeats (42 amino

acids) in coil 1B, aggregated abnormally into nucleoplasmic foci. The lamin A-Δ3 expressing cells also show prominent lamin A capping, indicated by a yellow arrowhead in figure 6.4. To my surprise, lamin A-Δ5 which also lacks seven complete heptad repeats (42 amino acids), but in coil 2B, had a similar localisation pattern to wild-type lamin A, being evenly localised to the nuclear lamina and nucleoplasm. Notably, lamin B1 mislocalisation found in *lmna*-null cells seems to be normalised by both wild-type lamin A and lamin A-Δ5. In marked contrast, lamin A-Δ3 however did not have a positive effect on lamin B1 localisation which is comparable to non-infected *lmna*-null cells (indicated by white arrowheads in Fig. 6.4).

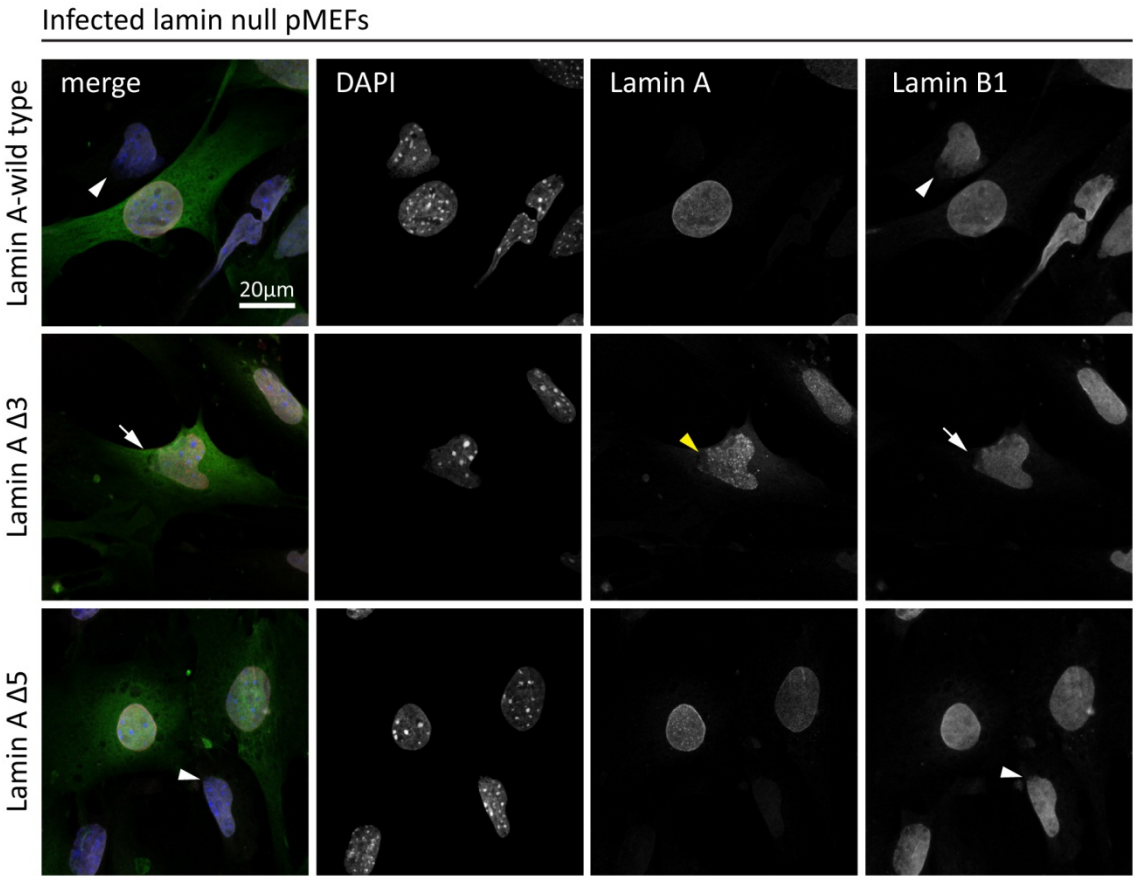

Figure 6.4 Representative confocal images of *lmna*-null pMEFs infected with wild-type lamin A, lamin A-Δ3 and lamin A-Δ5. Micrographs show a single confocal section through the centre of infected cells co-immunostained for eGFP (green), DAPI (blue), lamin A (red) and lamin B1 (grey). DAPI, lamin A and lamin B1 co-immunostaining are shown individually to the right of the merged picture. The yellow arrowhead indicates lamin A capping. White arrowhead indicates lamin B1 mislocalisation in non-infected (eGFP negative) cells. White arrows indicate a lamin A-Δ3 infected cells with lamin B mislocalisation.

To examine if there was a temporal effect, i.e. if the abnormal distribution and localisation of lamin B1 resolved over time, *lmna*-null pMEFs infected with lamin A-wt, lamin A-Δ3 and lamin A-Δ5 were also analysed 5 and 6 days post infection in two separate experiments. The results were very consistent and obvious, in that lamin A-Δ3 aggregates became even more prominent while lamin A-Δ5 remained evenly distributed throughout the nucleus in the majority of cells (data not quantified).

To quantify the number of nuclei that show normal lamin A localisation, lower magnification photographs of infected *lmna*-null pMEFs co-immunostained for eGFP, lamin A and DAPI were taken on a conventional fluorescence microscope 3-4 days post infection (Fig. 6.5A). Here I have included lamin A variants with missense mutations/duplications in exons 3 and 5. The results show that an average of 69.9% of all cells infected with wild-type lamin A demonstrated even lamin A distribution throughout the nuclei. In contrast, lamin A variants with a single amino acid change/insertion lack the potential to localise correctly in *lmna*-null pMEFs. Only 12.2% of cells infected with lamin A-R190dup, 20.2% of cells infected with lamin A-N195K, 12.9% of cells infected with lamin A-S295P and 12.7% of cells infected with lamin A-S303P demonstrate even distribution of lamin A comparable to that in the majority of wild-type lamin A infected cells. All other nuclei in these cells demonstrated abnormalities such as lamin A aggregation, capping and honeycomb structures (Fig. 6.5). Cells infected with lamin A-Δ3 also showed a large proportion of nuclei with lamin A abnormalities and only 8.5% with normal lamin A localisation, which is significantly less than wild-type infected cells. This stands in stark contrast to lamin A-Δ5 which was distributed normally in 66.5% of all infected pMEF nuclei. Importantly this was statistically similar to wild-type lamin A (p=0.17) and significantly different to the number of nuclei in cells expressing missense mutations in exon 5 with normal distribution of lamin A-S295P (p=0.0012) or lamin A-S303P (p=0.0015).

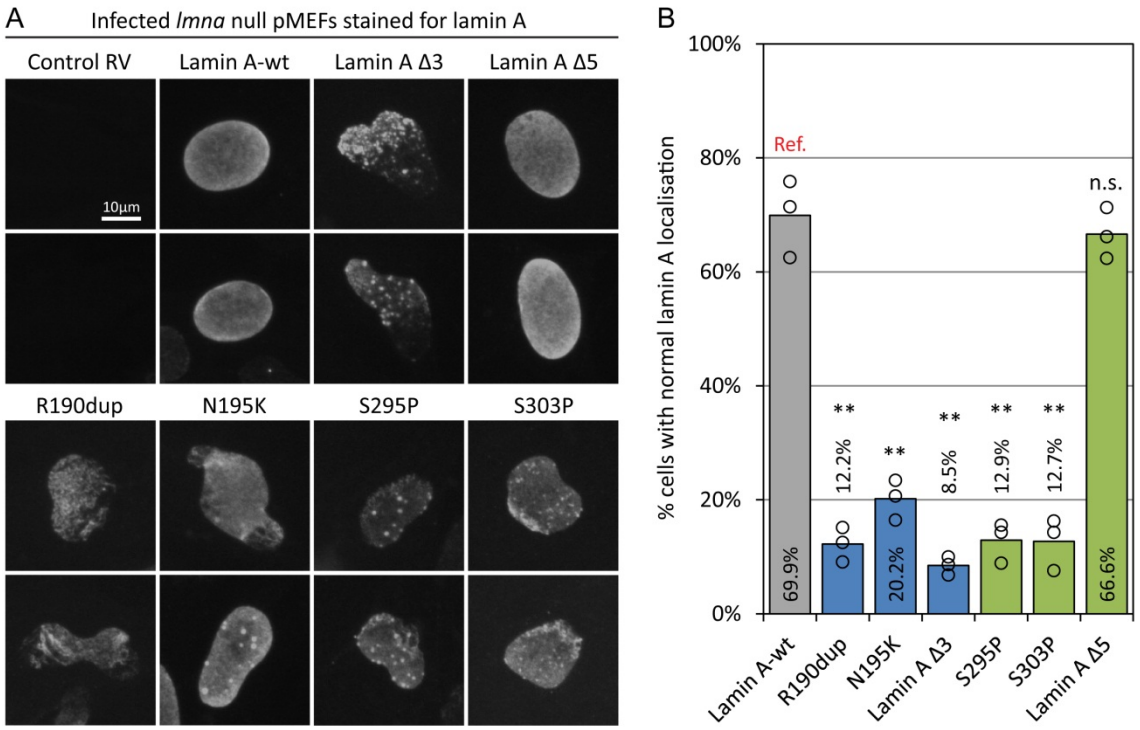

Figure 6.5 Quantification of *lmna*-null pMEFs expressing mutant lamin A species with normal lamin A localisation. (**A**) Representative micrographs of nuclei from cells infected with retroviral constructs encoding different lamin A variants immunostained for lamin A. (**B**) Quantification of cells that show even distribution of lamin A throughout the nucleus and around the nuclear rim, as seen in wild-type cells and *lmna*-null pMEFs expressing native lamin A. Open circles represent values obtained from 3 independent *lmna*-null pMEF lines; A total of at least 230 nuclei were analysed for each sample; ** $p<0.01$, n.s. not significant compared to control-RV infected cells.

6.3.4 Lamin A-Δ5, but not Δ3, can rescue the nuclear abnormalities of *lmna*-null pMEFs

Nuclei of *lmna*-null pMEFs show a range of abnormalities including severe deformations, lamin B capping and loss of emerin localisation from the nuclear rim (Sullivan et al., 1999). Re-introduction of wild-type lamin A into *lmna*-null cells can reverse these abnormalities as shown here and by others (Sullivan et al., 1999). The question was whether lamin variants containing mutations which allow for normal protein localisation can also rescue nuclear structural abnormalities, as expression of wild-type lamin A does.

The first effect analysed was the reversal of lamin B1 capping and honeycomb structures by lamin A variants. In *lmna*-null pMEFs infected with the control RV 71.8% of all nuclei show abnormalities in lamin B1 localisation (Fig. 6.6A and B). In presence of wild-type lamin A, this proportion of cells was reduced to 22.0%, which was statistically significant.

The introduction of lamin A variants with mutations in exons 3 and 5 did not have a positive effect on the abnormal lamin B1 localisation in *lmna*-null pMEFs, which remained in a large proportion of cells infected with lamin A-R190dup (78.1%), lamin A-N195K (75.8%), lamin A-S295P (80.0%) and lamin A-S303P (81.7%). Similarly, in the presence of the lamin A-Δ3 variant, lamin B1 localisation did not improve abnormalities in the majority (76.2%) of cells. In comparison, cells infected with lamin A-Δ5 exhibited a reduction of the proportion of cells with mislocalised lamin B1 to 34.9% which was a significant improvement over control RV infected cells ($p=0.0026$). When this figure is statistically compared to the effect of lamin A variants with point mutations in exon 5 on lamin B1 localisation, a significant improvement had been achieved over the cells infected with lamin A-S295P ($p=0.00094$) or lamin A-S303P ($p=0.0026$) (Fig. 6.6B).

In addition to lamin B1 mislocalisation, *lmna*-null pMEFs also show a large variety of nuclear deformations. The roundness of a nucleus can be numerically represented by its contour ratio (CR). The contour ratio depends on the cross-sectional area and circumference and is 1 for a perfect circle. Normal ovoid nuclei have a contour ratio of approx. 0.9, and the figure decreases the more severe the deformations are. Cartoons of a range of nuclei with different degrees of deformations and their corresponding contour ratio is shown in figure 6.6C to give an indication of how the contour ratio equates to nuclear deformation. *Lmna*-null pMEFs infected with the control RV had an average contour ratio of 0.81 which corresponds to slight deformations. Reintroduction of wild-type lamin A lead to a significant increase of the contour ratio to 0.92 corresponding to a normal ovoid shape, since wild-type pMEFs have an average contour ratio of 0.92 (Fig. 6.9D). Thus, introduction of wild-type lamin A in *lmna*-null cells can completely rescue the abnormal nuclear morphology on *lmna*-null cells.

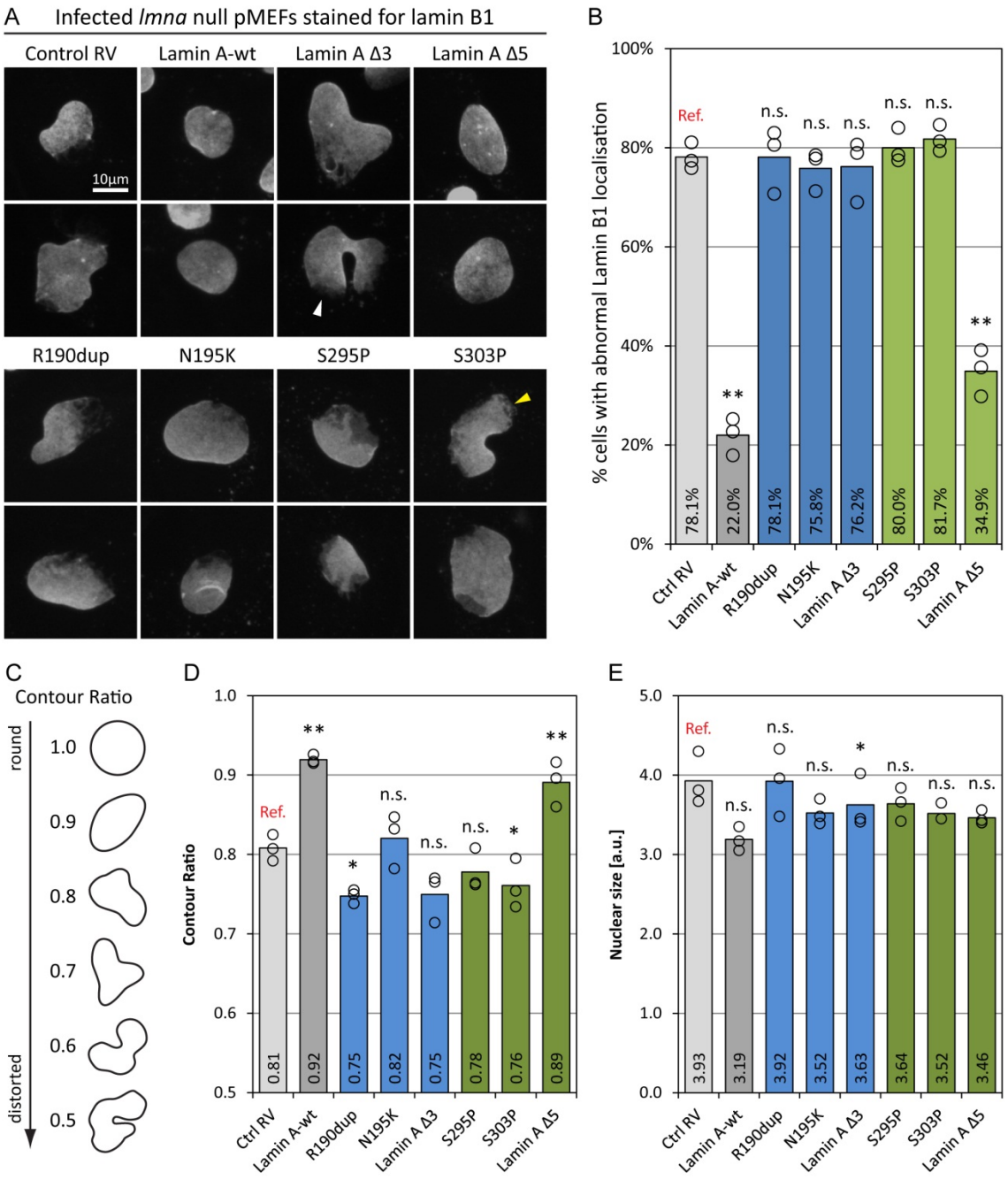

Figure 6.6 Rescue of nuclear abnormalities and lamin B1 localisation in *lmna*-null pMEFs by lamin A-Δ5. (**A**) Representative micrographs of nuclei from cells infected with retroviral constructs encoding different lamin A variants immunostained for lamin B1. Lamin B capping (white arrowhead) and honeycomb structures (yellow arrowhead) are indicated. (**B**) Quantification of cells that show even distribution of lamin B1 throughout the nucleus and around the nuclear rim. A total of at least 280 nuclei were analysed for each sample. (**C**) Range of nuclei found and their respective contour ratio. A perfect circle has a contour ratio of 1.0. If the deformations are more severe, the contour ratio is lower. (**D**) Average contour ratio of nuclei from a total of at least 85 infected cells. (**E**) Quantification of nuclear cross-sectional area of infected cells. Open circles represent values obtained from 3 independent *lmna*-null pMEF lines; * p<0.05; ** p<0.01, n.s. not significant compared to control-RV infected cells.

While wild-type lamin A can rescue nuclear deformations in *lmna*-null cells, two of the four pathogenic lamin A mutations tested (R190dup and S303P) resulted in a more severe phenotype: lamin A-R190dup and lamin A-S303P significantly reduced the contour ratio to 0.75 and 0.76 respectively. Lamin A-N195K (CR 0.82) and lamin A-S295P (CR 0.78) do not have an effect on nuclear morphology when compared to control RV infected cells. Similarly, lamin A-Δ3 (CR 0.75) did not have an effect on nuclear morphology. Importantly, lamin A-Δ5 (CR 0.89) significantly increased the contour ratio of *lmna*-null cells which is consistent with results above (Fig. 6.6C).

As shown in figure 4.2, the introduction of lamin A-R25P and lamin A-R249W results in a decrease of the contour ratio together with an increase in the nuclear cross-sectional area in C2C12 cells. To find out if this is also the case in *lmna*-null pMEFs, the nuclear cross sectional area of cells infected with lamin mutants was calculated and compared to that of control RV infected cells. However as shown in figure 6.6E mutant lamin A variants do not have a significant effect on nuclear cross section area. Only the introduction of wild-type lamin A results in a notable but non-significant decrease (p=0.11). The reduction of the nuclear cross sectional area of lamin A-Δ3 infected compared to control RV infected cells while only small, was statistically significant.

After establishing that the introduction of lamin A-Δ5 results in a significant improvement of the phenotype of *lmna*-null pMEFs, the question remained whether or not this improvement is statistically similar when compared to the effects of the introduction of wild-type lamin A. The proportion of nuclei with abnormal lamin B1 is slightly larger in lamin A-Δ5 infected cells (34.9%) compared to lamin A-wt infected cells (22.0%). However, when the proportion of nuclei with normal lamin B1 localisation in lamin A-wt and lamin A-Δ5 infected cells are directly compared to each other, there is no significant difference between them (p=0.054) (Fig. 6.6B). Similarily, the average contour ratio of lamin A-Δ5 infected pMEFs (0.89) was not significantly different to that of lamin A-Δ5 infected cells (p=0.21) (Fig. 6.6E). These results suggest that lamin A-Δ5 performs very similar to wild-type lamin A in terms of the positive effects on *lmna*-null pMEFs.

The last parameter analysed was the effect wild-type and mutant lamin A variants have on emerin localisation in *lmna*-null pMEFs. As shown in figure 6.7A *lmna*-null cells do stain for emerin, but the majority of the protein is not localised to the nuclear membrane, but was instead mislocalised into the cytoplasm, probably the ER (Vaughan et al., 2001). A similar staining pattern was found when introducing lamin A-Δ3. In contrast, expression of wild-type lamin A and lamin A-Δ5 lead to a redistribution of emerin to the nuclear membrane, as observed in wild-type cells.

The change in emerin localisation was visualised by measuring the fluorescence intensity of the emerin staining across the infected cell and plotting it together with DAPI (Fig. 6.7B and C). To be able to compare different cells with each other, 2.5μm sections through the mid-region of the cells were taken using a confocal microscope.

In both cases (lamin A-wt and lamin A-Δ5) the fluorescence intensity of emerin across an infected cell was directly compared with that of a neighbouring non-infected cell. The DAPI intensity was

used to demarcate the nucleus. The result presented in figure 6.7B (lamin A-wt) and 6.7C (lamin A-Δ5) clearly shows that non infected cells exhibit strong emerin immunostaining beyond the nucleus, which most likely represents emerin localised to the membranes of the endoplasmic reticulum. In cells infected with lamin A-wt and lamin A-Δ5 however, the vast majority of emerin staining was confined to the boundaries of the nucleus. This result supports the fact that lamin A-Δ5 acts in a similar way to wild-type lamin A by also causing emerin to be redistributed to its normal locations.

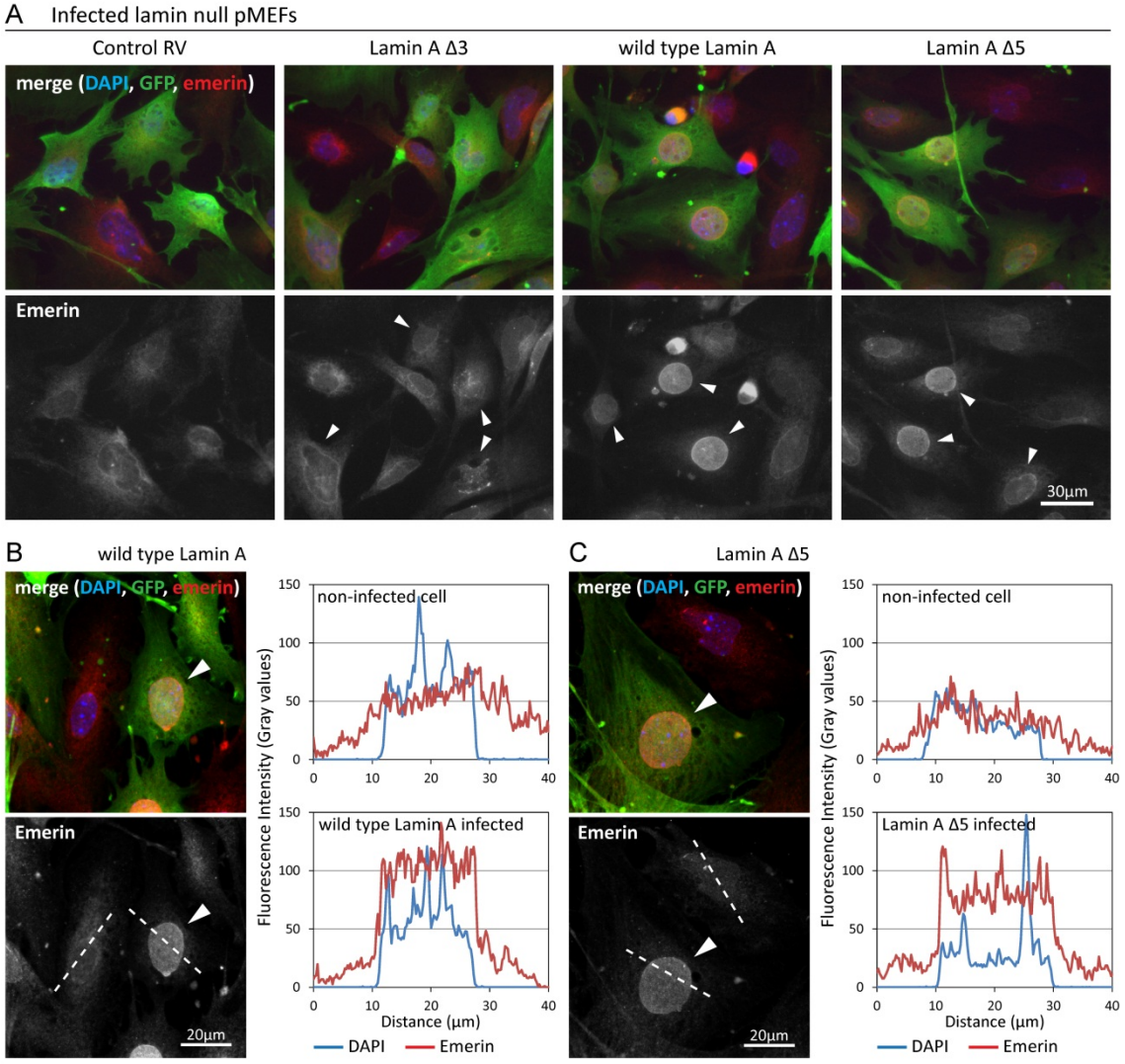

Figure 6.7 Normalisation of emerin localisation in *Imna*-null pMEFs expressing lamin A-Δ5. (**A**) Representative micrographs of Infected *Imna*-null pMEFs co-immuno stained for emerin (red) eGFP (green) and DAPI (blue). The emerin is shown in b/w below the composite. Infected cells are indicated by a white arrowhead. (**B**) Confocal images and fluorescence intensity plots of emerin immunostaining across a lamin A-wt infected and non-infected cell for direct comparison. The fluorescence intensity plot shows emerin (red) as well as DAPI (blue) demarcate the boundaries of the nucleus. The white arrowhead indicates the infected (eGFP positive) cell. (**C**) The same analysis as in B was performed, however, the marked cell (eGFP positive) is infected with lamin A-Δ5.

6.3.5 Deletion of exon 5 does not have a deleterious effect on wild-type pMEFs

Next to having positive effects on *lmna*-null pMEFs which I have shown in the results above, lamin A-Δ5 must not have a negative effect on wild-type cells to qualify as a suitable candidate for exon skipping therapy, since most human laminopathies arise from dominant *LMNA* mutations. To test this pMEFs from three different wild-type embryos were isolated and used to analyse three parameters in presence of lamin A variants: lamin A/C localisation, lamin B1 localisation and abnormalities in nuclear morphology.

Wild-type pMEFs used here show slight abnormalities in lamin A/C localisation in an average of 23.1% of all nuclei (Fig. 6.8). Overexpression of wild-type lamin A did not have a negative effect on lamin A/C localisation. Cells with abnormal lamin A/C localisation were mainly affected by honeycomb structures as indicated by white arrowheads in figure 6.8A. Nuclear aggregations of lamin A such as those seen in *lmna*-null pMEFs were not observed in wild-type pMEFs in the presence of any of the lamin A variants.

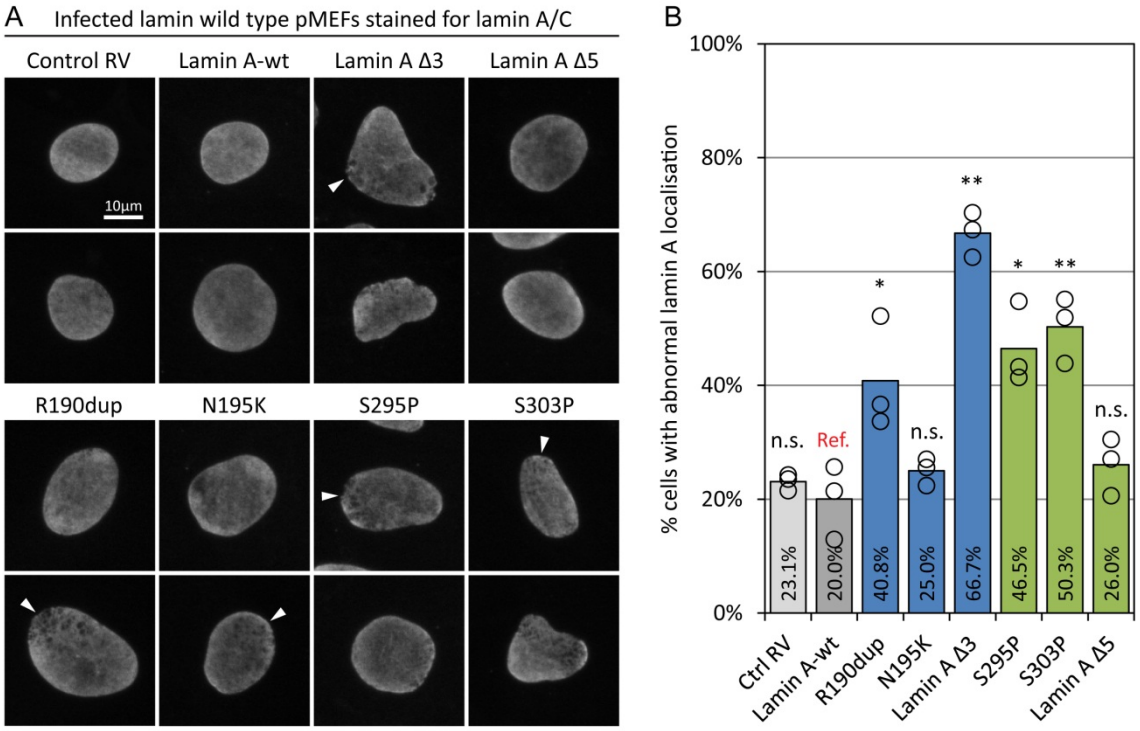

Figure 6.8 Effects of lamin A variants on lamin A/C localisation in wild-type pMEFs. (**A**) Representative micrographs of infected wild-type pMEFs stained for lamin A/C. White arrowheads indicate honeycomb structures found in lamin A-Δ3 infected cells and in cells expressing lamin A variants with mutations in exons 3 and 5 (lamin A-R190dup, N195K, S295P and S303P). (**B**) Quantification of nuclei with abnormalities in lamin A/C localisation. Bar chart shows average percentage of nuclei showing abnormal lamin A/C localisation (mainly honeycomb structures). Open circles represent means of 3 independent experiments; A total of at least 210 nuclei were analysed for each sample; n.s. not significant, * $p<0.05$, ** $p<0.01$ compared to lamin A-wt infected cells.

The proportion of nuclei affected varied between different constructs. Three mutations (R190dup, S295P and S303P) significantly increased the number of nuclei with abnormal lamin A/C localisation when compared to cells infected with lamin A-wt. The presence of lamin A-R190dup increased the proportion of nuclei with abnormal lamin A/C localisation to 40.8%. The expression of lamin A-N195K however did not have an effect on lamin A/C localisation. Lamin A-S295P and lamin A-S303P affected lamin A/C localisation in 46.5% and 50.3% respectively. In the presence of lamin A-Δ3, 66.7% of all nuclei showed mislocalisation of lamin A/C. Crucially, overexpression of lamin A-Δ5 had no effect on lamin A/C localisation when compared to wild-type lamin A infected cells (Fig. 6.8B). The proportion of affected nuclei in cells expressing lamin A species with point mutations in exon 5 was significantly larger when directly compared to pMEFs expressing lamin A-Δ5, which is in line with my previous observations (Fig. 6.5).

Next, I quantified the proportion of nuclei that display abnormal lamin B1 localisation in the presence of the different lamin A variants and calculated their contour ratio. In general two different types of abnormalities were seen: lamin B1 capping (indicated by a white arrowhead in Fig. 6.9A) and lamin B1 honeycomb structures (indicated by a yellow arrowhead in Fig. 6.9A). Cells that display such lamin B1 abnormalities in the presence of lamin A wild-type and mutants were quantified, shown in figure 6.9B. On average 5.6% of wild-type pMEFs infected with control RV and 6.5% of cells infected with lamin A-wt present mislocalisation of lamin B1. Their average contour ratio was 0.92 (control RV) and 0.93 (lamin A-wt). Interestingly, the proportion of nuclei with abnormal lamin B1 localisation is elevated by 9.8% in the presence of lamin A-N195K this however is not significantly different when compared to lamin A-wt infected cells (p=0.054). Similarly the contour ratio is slightly but not significantly reduced in presence of lamin A-N195K.

Mutant lamin A variants lamin A-R190dup, S295P and S303P as well as lamin A-Δ3 significantly increased the proportion of nuclei with abnormal lamin B1 localisation (Fig. 6.9B). They also resulted in a significant reduction of the contour ratio when compared to lamin A-wt infected cells (Fig. 6.9D).

Importantly, lamin A-Δ5 significantly affects neither lamin B1 localisation nor the contour ratio. Both the proportion of cells with abnormal lamin B1 localisation (8.0%) as well as the average contour ratio (0.91) are comparable to that of wild-type lamin A infected cells (Fig. 6.9D). However when directly compared to lamin A-S295P and S303P, the percentage of cells with mislocalised lamin B1 was significantly less and the contour ratio was significantly greater in lamin A-Δ5 infected cells (Fig. 6.9D. This provides yet more evidence that exon 5 is largely dispensable in the lamin A protein for the structural functions of lamin A.

Lastly, none of the lamin A variants significantly affected the average nuclear cross sectional area when compared to wild-type lamin A infected cells (Fig. 6.9E).

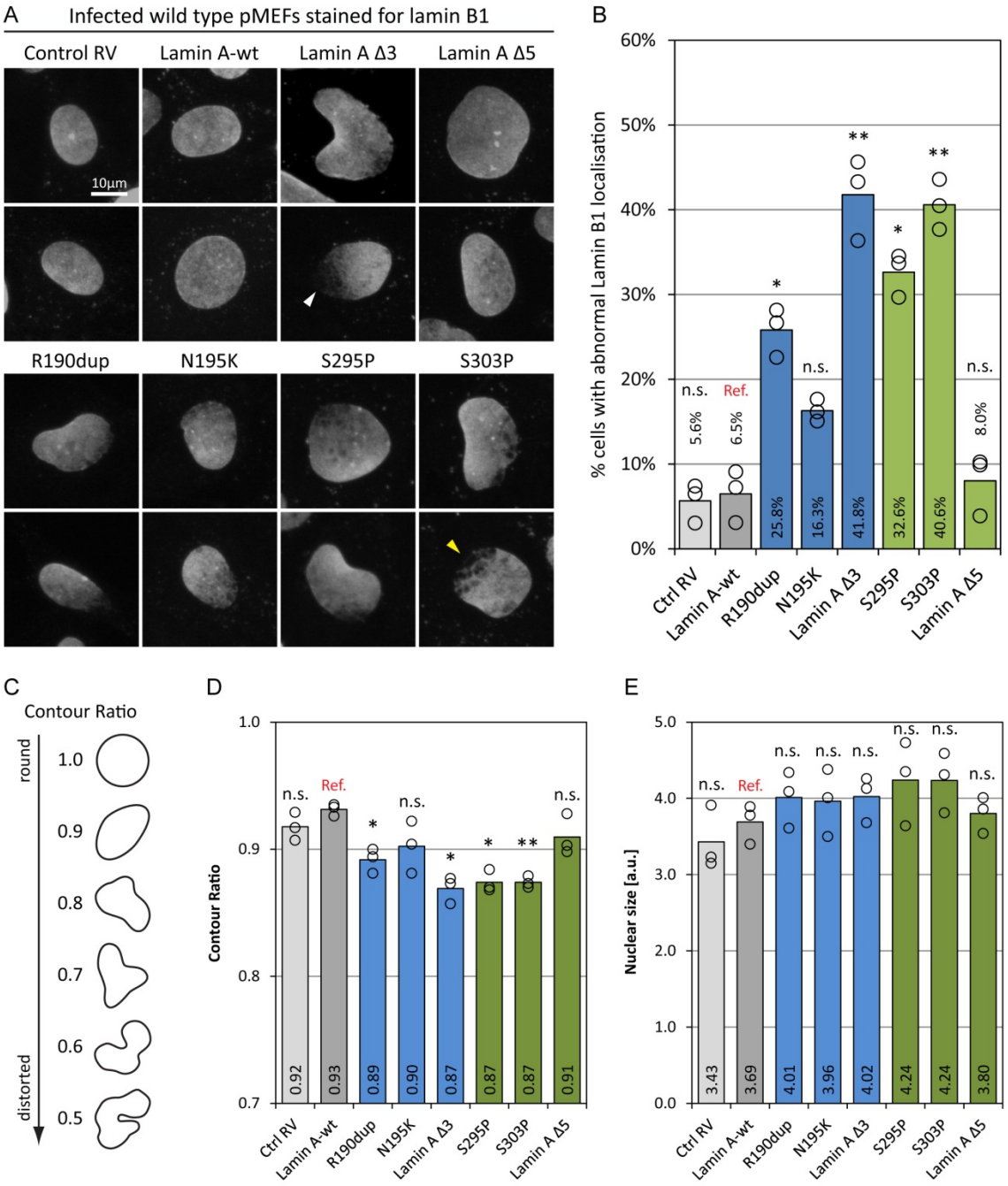

Figure 6.9 Lamin A-Δ5 does not have deleterious effects on lamin B1 localisation and nuclear morphology in wild-type pMEFs. (**A**) Representative micrographs of nuclei from cells infected with retroviral constructs encoding different lamin A variants immunostained for lamin B1. The white arrowhead indicates lamin B1 capping, the yellow arrowhead indicates honeycomb structures. (**B**) Quantification of cells that show abnormalities in lamin B1 localisation such as capping and honeycomb structures. A total of at least 260 nuclei were analysed per sample. (**C**) Range of nuclei found and their respective contour ratio. A perfect circle has a contour ratio of 1.0. If the deformations are more severe, the contour ratio is lower. (**D**) Average contour ratio of nuclei from a total of at least 50 infected cells for each sample. (**E**) Quantification of nuclear cross-sectional area of infected cells. Open circles represent values obtained from 3 independent *Imna*-null pMEF lines; * $p<0.05$; ** $p<0.01$, n.s. not significant compared to lamin A-wt infected cells.

The data presented here is summarised in figure 6.10 and shows that reintroduction of wild-type lamin A and lamin A-Δ5 localise correctly and can normalise aberrant nuclear morphology and abnormal lamin B1 and emerin localisation in *lmna*-null pMEFs. All other lamin A variants mislocalise and do not improve lamin B1 localisation. In addition lamin A-R190dup and S303P significantly decrease the contour ratio of *lmna*-null pMEFs (Fig. 6.10A). Overexpression of wild-type lamin A, lamin A-Δ5 as well as lamin A-N195K do not have a negative effect on wild-type pMEFs. In contrast, lamin A-Δ3, R190dup, S295P and S303P negatively affect nuclear morphology, lamin A/C localisation and lamin B1 localisation in wild-type pMEFs (Fig. 6.10B).

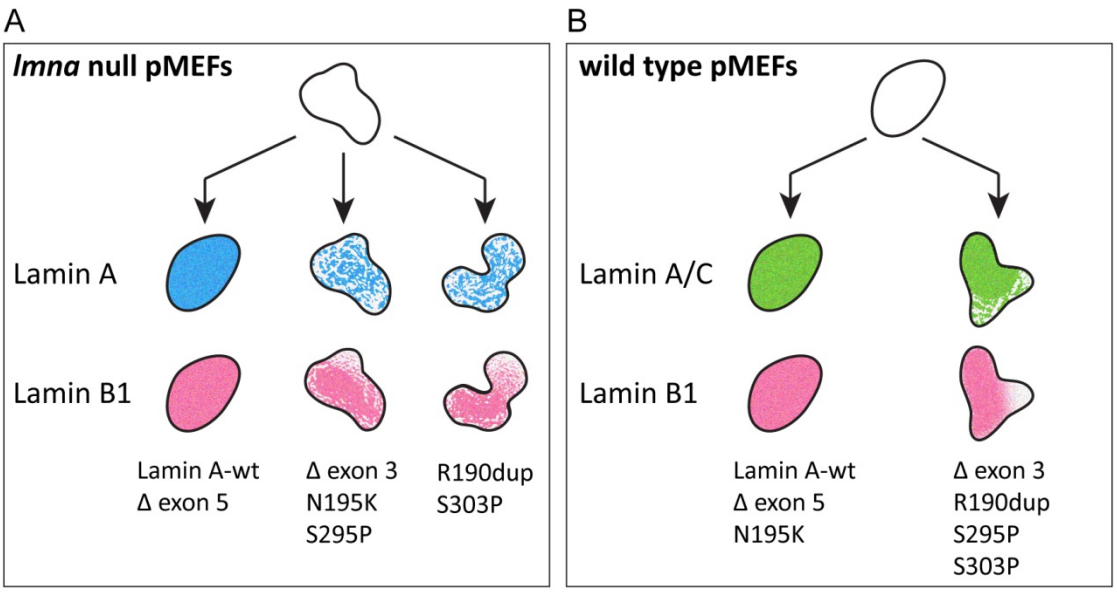

Figure 6.10 Summary of effects of wild-type lamin A, lamin A variants with point/duplication mutations in exon 3 and 5, and lamin A lacking either exon 3 or 5 on *lmna*-null and wild-type pMEFs. (**A**) Effect of lamin A variants on nuclear morphology and lamin B1 distribution of *lmna*-null pMEFs. (**B**) Effect of lamin A variants on wild-type pMEFs. Generally exon 5 is largely dispensable in the lamin A protein for the structural functions of Lamin A.

6.4 Discussion

In this chapter I set out to explore the potential of exon skipping as a therapy for laminopathies by targeting and eliminating exons containing pathogenic mutations with AONs. An initial analysis of the 12 *LMNA* exons revealed exons 3 and 5 as potential candidates, since both exons encode 6 full heptad repeats and are not predicted to severely interfere with lamin A function. To put this theory to the test, lamin A constructs each lacking the 42 amino acids encoded by exons 3 or 5, as well as constructs with pathogenic mutations in exons 3 and 5 were created and expressed in *lmna*-null and wild-type pMEFs. To qualify as a potential target for exon skipping, the candidates had to meet three criteria: (1) they must be able to rescue abnormalities found in *lmna*-null pMEFs, (2) they must not have a negative effect on wild-type pMEFs and (3) they must improve nuclear morphology over lamin A proteins carrying pathogenic mutations in the corresponding exon.

Lamin A-Δ5 turned out to exceed all expectations by fulfilling the three criteria. Even better, when it was compared to lamin A-wt, no significant difference was found. Unexpectedly Lamin A-Δ3 failed in all criteria despite its structural similarity to lamin A-Δ5.

The main difference between lamin A-Δ3 and lamin A-Δ5 is the location of the 6 heptad deletion. Notably, the central rod domain of cytoplasmic IF proteins, also lacks 6 heptad repeats in coil 1B (appendix 1). Moteiro and colleagues aimed to investigate the biological role these additional 6 heptad repeats play in nuclear IF proteins. By swapping various domains between lamin A and the small neurofilament subunit (NF-L) they demonstrated that the lamin A head domain, 6 additional heptad repeats, an NLS and the CAAX motif are necessary to target NF-L to the nuclear membrane (Monteiro et al., 1994). They also showed that the insertion of 6 additional heptad repeats into NF-L affected its co-assembly with vimentin, which led them to speculate that the 42 amino acid insertion in lamins prevent them from association with cytoplasmic IF proteins (Monteiro et al., 1994). In a follow up paper, Mical and Monteiro (1998) investigated the role of domains specific to nuclear IF proteins in nuclear localisation. They showed that removal of 6 heptad repeats from lamin B does not affect lamin B localisation to the nucleus. However, the removal of 6 heptads together with the CAAX motif from lamin B (producing a protein which is similar to lamin A-Δ3) results in the accumulation of nuclear aggregates (Mical and Monteiro, 1998). Interestingly, the deletion was also in coil 1B, which indicates that the additional 6 heptad repeats in coil 1B are not necessary for nuclear targeting of lamins but for their proper nuclear localisation.

Why lamin A-Δ5 does not result in a similar phenotype remains speculative. Importantly, the amino acid composition and therefore the net charge of amino acids in exons 3 and 5 is not the same. Exon 5 harbours 7 positively charged and 10 negatively charged amino acids (net charge -3) while exon 5 harbours 6 positively charged but only 5 negatively charged amino acids (net charge +1). The reason for the discrepancy seen between lamin A-Δ3 and lamin A-Δ5 could therefore be that the loss of three negatives charges has a stronger effect on homodimerisation and/or

heterodimerisation or the interaction with lamin A binding partners. One potential candidate is the lamin interacting protein SUN1 which binds to lamin A (Haque et al., 2006). Deletion of the lamin A binding site in SUN1 has been shown to disrupt lamin A/C localisation in mouse fibroblasts (Haque et al., 2010). Other lamin A interaction partners specifically bind to either coil 1 or coil 2. These are c-Fos, which interacts with coil 1 (Ivorra et al., 2006), and pRb, Erk1/2 and MOK2 which interact with coil 2 (Dreuillet et al., 2002; Gonzalez et al., 2008; Ozaki et al., 1994) (section 1.3.5, Fig. 1.8). However, all of these are involved in cell signalling and therefore unlikely to interfere with lamin filament organisation or localisation.

Another explanation for the observed phenotype could be that lamin A-Δ3 requires a longer time to localise properly. However my results show the opposite; the latest time point analysed was 6 days post infection and instead of normalised lamin A-Δ3 localisation, I found more prominent nuclear aggregates in *lmna*-null pMEFs. Reduced proliferation as a cause for mislocalised lamin A-Δ3 can be ruled out for two reasons. Firstly, cells continue to proliferate in presence of lamin A-Δ3 as confirmed by GFP positive mitotic bodies observed 4 and 6 days post infection. Secondly, it has been shown that the reversal of nuclear abnormalities in HGPS fibroblasts (by introducing wild-type lamin A) does not require the cells to go through a round of cell cycle (Scaffidi and Misteli, 2005). This is likely explained by the dynamic property of the nuclear lamina which has been demonstrated by FRAP experiments (Gilchrist et al., 2004).

Interestingly, lamin A-N195K is the only pathogenic mutation in this study that did not have a negative effect on wild-type pMEFs on the parameters studied. To date 14 patients have been reported with this mutation (www.umd.be/LMNA) all of which suffer from DCM-CD. The other three mutations used here, p.R190dup, p.S295P and p.S303P (reported in chapter 3) all result in a skeletal muscle phenotype.

One of the reasons the p.N195K mutation was chosen for this study was that there is a knock in mouse model available which would have been very useful to test the effects of skipping exon 3 in vivo (Mounkes et al., 2005). Homozygous mutants develop cardiomyopathy and die at the age of 3 months. Homozygous mutant pMEFs show severe nuclear deformationas as well as abnormal lamin A, lamin B, emerin and Nup 154 localisation. Heterozygous mice have a normal life expectancy and show no overt phenotype (Mounkes et al., 2005). This is similar to my results obtained by overexpression of lamin A-N195K in *lmna*-null and wild-type pMEFs. As mentioned in chapter 3, lamin mutations that result in cardiomyopathy are thought to be loss-of-function while other missense mutations might result in a toxic gain-of-function (Davies et al., 2011). My results support this theory, although functional assays (migration, proliferation, differentiation, etc.) are still outstanding, but I would predict that a negative effect of lamin A-N195K on wild-type cells, if any, would be negligible. If cardiomyopathy is indeed caused by loss of function protein, it would be meaningless to delete exon 3 which, in the best case scenario, also results in a loss of function. Unfortunately, the majority of mutations in exon 3 result in cardiomyopathy (table 3.2) wich makes exon 3 a poor target for exon skipping therapy.

Although *LMNA* exon 3 does not seem to be a good candidate for exon skipping therapy, exon 5 remains a valid candidate. Several different types of mutations are located in exon 5 and therefore valid targets for exon skipping therapy. These include 6 nonsense mutations, 13 autosomal dominant missense mutations, 1 autosomal recessive missense mutation and 1 frameshift mutation (table 6.1). AON mediated exon skipping is currently in use to restore the expression of a shorter, partially functional dystrophin protein by targeting nonsense mutations in Duchenne MD patients (Cirak et al., 2011; Goemans et al., 2011). On a first glance it might seem sensible to apply the same logic to the lamin protein. However, as mentioned above and in chapter 3, non-functional or partially functional lamin A protein is thought to result in cardiomyopathy (Davies et al., 2011). So in order to target nonsense mutations which tend to cause cardiomyopathy, the lamin A-Δ5 must have similar functional properties to wild-type lamin A in order to restore the phenotype.

For laminopathies it might therefore be easier to target lamin variants with mutations resulting in a toxic gain-of-function as has been shown for progerin (Scaffidi and Misteli, 2005). Replacing such toxic proteins with a partially functional product might not necessarily eliminate the phenotype completely, but it could alleviate it. One example of a mutation in exon 5 is p.L302P which has been reported to cause congenital muscular dystrophy (CMD) in one patient (Quijano-Roy et al., 2008). If this mutation results in a toxic gain of function (which remains to be determined), removing part of it would shift the phenotype from CMD to a milder, more manageable phenotype such as cardiomyopathy. Although the patient might still suffer from cardiac disease, this would mean a dramatic increase the quality of life for this patient.

AON therapies have a range of limitations, however, the two major hurdles to overcome before AON mediated exon skipping can be considered for laminopathies are improving skipping efficiency, and tissue targeting (Muntoni and Wood, 2011).

The vast majority of missense mutations in *LMNA* are autsosomal dominant (www.umd.be/LMNA). In order to eliminate a phenotype virtually all lamin A protein needs to be skipped. Although to my knowledge the amount of mutant lamin protein necessary to cause a phenotype remains to be determined and likely depends on the type of mutation. With current technology, exon skipping is nowhere near 100% efficient (Yin et al., 2009) and as a result, cells would co-express six different A-type lamin variants: wild-type lamin A and C, mutated lamin A and C and skipped lamin A and C, which at the end might be more detrimental to the cell than higher levels of mutant and wild-type lamins A and C. It is important to note that in this study I only used lamin A-Δ5. Whether lamin C-Δ5 performs in a similar way or is any different to lamin A-Δ5 or wild-type lamin C remains to be determined.

One of the mutations in exon 5 (p.R298C), results in AR-CMT2 (De Sandre-Giovannoli et al., 2002). In this case partial skipping might be enough to ameliorate the phenotype provided that lamin A-Δ5 performs like wild-type lamin A. AR-CMT2 is a peripheral neuropathy characterised by improper myelination and demyelination assumed to originate from defective Schwann cells, which

leads to axonal loss (Bernard et al., 2006). Hence, Schwann cells in peripheral nerve fibres must be targeted in order to treat the phenotype.

This brings me to the second limitation of AON therapies, tissue specific targeting of AONs. AONs to target the *dmd* gene were initially delivered by intra-muscular injections in *mdx*-mice to achieve high concentrations and efficient skipping (Mann et al., 2001). It was later found that systemic delivery of AONs also induces exon skipping in muscle of *mdx*-mice (Alter et al., 2006). However, skeletal muscle in *mdx*-mice and DMD patients undergoes constant regeneration and is inflamed which is thought to make it leaky which promotes AON uptake (Aartsma-Rus and van Ommen, 2007). Skeletal muscle in EDMD patients on the other hand is characterised by mild dystrophic features and does not show overt signs of regeneration (Mittelbronn et al., 2006; Sewry et al., 2001), and so, may not take up AON as easily. Furthermore the primary cause of death in EDMD is cardiac failure and to target heart tissue with AONs is still an issue using current technology.

For laminopathies in general, the tissue that is needed to be targeted depends on the mutation and what phenotype it causes. The disease phenotype of AR-CMT is restricted to peripheral nerve fibres (De Sandre-Giovannoli et al., 2002). Targeting Schwann cells associated with peripheral neurons with AONs, might therefore be sufficient. However, currently there is no technology available to do so (M.J. Wood, personal communication). So far advances have been made in other directions. For example it was shown that oligos conjugated with arginine rich targeting peptides such as the B-peptide are very efficient in penetrating cardiomyocytes (Yin et al., 2009). Hence there may be yet unidentified peptides to specifically target the peripheral nervous system. Other AON delivery methods such as targeted exosomes are being developed to help cross the blood-brain barrier and deliver AONs to the central nervous system, providing novel ways to deliver AONs tissue specifically (Alvarez-Erviti et al., 2011).

6.5 Conclusion

In conclusion *LMNA* exon 5 presents a strong candidate for exon skipping therapy. However before therapies like that can be considered, the properties of lamin A-Δ5 have to be studied in great detail. Some aspects such as the effects of lamin A-Δ5 on cell cycle and migration are currently under investigation and additional experiments addressing the effects of lamin-Δ5 on myogenic differentiation are already planned. It will also be necessary to examine the effects of lamin C-Δ5 on nuclear morphology and cell function. Once these assays have been completed successfully, effective target sites for AONs to skip exon 5 have to be identified. AONs can then be used to skip exon 5 from A-type lamins in wild-type cells, and patient fibroblasts before moving on to testing the idea in mouse models. In summary many challenges lie ahead and with a bit of luck and hard work it will not be too long before AON targeting and delivery technology is advanced enough for it to be considered a serious therapy for certain laminopathies caused by mutations residing in particular *LMNA* exons.

Chapter 7

General Discussion and Conclusion

Laminopathies are a heterogeneous group of diseases associated with defects in A-type lamins. A-type lamins are encoded by the *LMNA* gene and together with B-type lamins, form the nuclear lamina, a proteinaceous network underlying the inner nuclear membrane (Worman et al., 2009). To date more than 300 different mutations have been described in the *LMNA* gene, which are associated with more than 16 different phenotypes (www.umd.be/LMNA). The majority of mutations affect striated muscle and result in Emery-Dreifuss muscular dystrophy or cardiomyopathy while others affect other systems and cause lipodystrophy, neuropathy or premature ageing syndromes.

According to the current understanding, mutations can be classified according to the protein modification/functional consequence they result in, which are (1) mutations resulting in protein degradation (2) mutations affecting lamin A filament formation (3) mutations affecting the function/integrity of lamin A interacting proteins (4) mutations resulting in the accumulation of farnesylated lamin A (Worman and Bonne, 2007). Furthermore, three non-mutually exclusive hypotheses for pathogenic mechanisms underlying the disease phenotypes have been proposed: the 'mechanical stress' hypothesis and the 'gene expression' hypothesis and the 'cell proliferation/differentiation' hypothesis (Broers et al., 2006; Worman, 2012).

Some of these changes are very consistent with the resulting phenotype. Nonsense mutations for example, mainly result in cardiomyopathy (Benedetti et al., 2007; Bonne et al., 2000) which was statistically confirmed in this study. However, the underlying pathogenic mechanism is unclear although different mechanisms including haploinsufficiency (Davies et al., 2011; Wolf et al., 2008), as well as interference of truncated lamin protein with structure or function (Geiger et al., 2008; Renou et al., 2008) have been proposed. Furthermore, missense mutations also result in cardiomyopathy in man (www.umd.be/LMNA) and mouse (Arimura et al., 2005; Mounkes et al., 2005) for which other mechanism might be involved such as mis-regulation of Erk1/2 signalling (Muchir et al., 2007a; Muchir et al., 2009; Wu et al., 2011).

Premature ageing syndromes are primarily caused by the accumulation of farnesylated lamin A, either through mutations in *LMNA* (De Sandre-Giovannoli et al., 2003; Eriksson et al., 2003) or in the lamin A processing enzyme ZMPSTE24 (Navarro et al., 2004). In contrast, skeletal muscle disorders (and to a lesser extent lipodystrophy disorders and peripheral neuropathy), are caused by mutations distributed throughout the protein with no evident genotype-phenotype correlation, although hot-spots have been described for each disorder (reviewed in Scharner et al. (2010))

Correlations between lamin structure and disease

Nuclear lamins are type V intermediate filament proteins and characterised by a tripartite domain organisation formed by the central rod domain flanked by a short N-terminal head domain and a larger C-terminal tail domain (Fuchs and Weber, 1994). The central rod domain is characterised by seven amino acid repeat sequences or heptad repeats $(a\text{-}b\text{-}c\text{-}d\text{-}e\text{-}f\text{-}g)_n$ are characteristic for α-helices engaging in coiled coil formation (Herrmann and Aebi, 2004; Mason and Arndt, 2004; Parry et al., 2008). Mutations of hydrophobic residues (a and d) have been shown to disrupt the dimers and promote tetramer formation in the GCN4 leucine zipper (Harbury et al., 1993), however, similar data for lamins not available. Given that a successful lamin dimerisation via an α-helical coiled-coil interaction is central to higher filament formation, I tested if key residues in the stabilisation of the α-helical coiled-coil are affected at an increased frequency in laminopathies.

Interestingly, heptad positions a and d did not show a higher incidence in pathogenic mutations when compared to other residues (see section 3.3.6). However, lamin dimers form higher filament structures and other residues might be equally likely to destabilise the filament network. Evidence for this hypothesis is provided by photobleaching experiments of fluorescently labelled lamins which reveals that most *LMNA* mutations tested, result in increased protein mobility, with the most severe effects seen in mutations in the central rod-domain (Broers et al., 2005; Gilchrist et al., 2004). Importantly, destabilisation of the nuclear lamina can also be caused by the Ig-fold, which has been shown in *Xenopus*, were the addition of Ig-fold domains prevented the formation of the lamina (Shumaker et al., 2005). The solving of the structure of the Ig-like fold (Krimm et al., 2002) has allowed detailed 3D mapping of the localisation of mutations, revealing associations not clear when analysing the linear sequence. For example mutations associated with a skeletal muscle phenotype are often located on buried residues and likely to destabilise the Ig-fold (first proposed by (Krimm et al., 2002) and supported by my results).

Disruption of lamin A protein interactions (but not necessarily the lamin A structure) has also been suggested to be the underlying mechanism for some laminopathies. For example, a large number of FPLD2 patients carry the missense mutation p.R482W which results in the elimination of a positive charge on the surface of the Ig-fold (Krimm et al., 2002). Interestingly, there are other mutations on the Ig-fold (p.R439C, p.G485D and K486N) which also cause lipodystrophy. By mapping these mutations on the 3D structure of the Ig-fold, I found that they cluster in the same region and cause a similar change in surface charge distribution which strongly suggests that a specific protein interaction is disrupted, providing a unifying theory as to why they all cause the same phenotype (see section 3.3.7). Sterol regulatory element binding protein 1 (SREBP1), a transcription factor involved in adipocyte differentiation, has been shown to bind to the Ig-fold domain, and this interaction was disrupted in presence of p.R482W, p.G485D and p.K486N, suggesting an involvement of SREBP1 in FPLD pathology (Lloyd et al., 2002).

Interestingly, I have uncovered a second cluster of mutations in the Ig-fold that presents a striking correlation with premature ageing phenotypes. All patients are homozygous or compound heterozygous for missense mutations that primarily result in a loss of positive charge in that cluster (Agarwal et al., 2008; Cao and Hegele, 2003; Kosho et al., 2007; Novelli et al., 2002; Plasilova et al., 2004; Simha et al., 2003; Verstraeten et al., 2006; Youn et al., 2010). A mechanism, similar to that proposed for skeletal muscle disorders involving the destabilisation of the structure by these mutations is unlikely, because heterozygous relatives (of homozygous patients) are unaffected. Furthermore, accumulation of farnesylated lamin A, a typical feature in HGPS, was not evident (Agarwal et al., 2008; Verstraeten et al., 2006). It is therefore likely that specific protein interactions are affected by the mutations in this cluster. The Ig-fold interacts with a large array of binding partners involved in cell signalling (SREBP1, MAN1) and cell cycle control (Lap2α, cyclin D3, PCNA) (see section 1.3.5) although which of these might be affected, remains speculation.

Some evidence suggests that the underlying mechanism is similar to that of FPLD patients. Firstly, one mutation in this cluster (p.T528M) which is non-pathogenic when inherited alone, has been shown to modify the lipodystrophy phenotype from FPLD2 to FPLD1 when inherited together with p.S583L (Savage et al., 2004). Secondly, all patients had prominent lipodystrophy. Thus, the explanation may simply be that the mutation is present in a homozygous state, and that the premature ageing phenotype seen in these patients is a severe/modified form of lipodystrophy. Homozygous FPLD or EDMD mutations located in the Ig-fold, would provide further insight into this question, however, such mutations have not been described yet.

Taken together my observations suggest that the modification of specific protein interactions, possibly via the alterations in the charge domains in specific regions of the Ig-fold, is very likely to contribute to the pathology of different phenotypes.

It is important to note that the genetic background can have a big impact on the phenotypic outcome of a mutation which is shown by a large inter- and intra-familial variability seen in laminopathies (Bonne et al., 2000; Granger et al., 2011; Mercuri et al., 2005). 6.2% of all patients reported in the UMD database have overlapping phenotypes or other phenotypes and many mutations have been shown to result in different phenotypes in different patients (www.umd.be/LMNA). In some laminopathy patients with mutations in *LMNA* modifying mutations in desmin or emerin were found to increase the severity of the phenotype (Muntoni et al., 2006). Recently, linkage analysis identified a modifier locus on chromosome 2 (harbouring the genes for desmin and myosin light chain) which is strongly associated with the age of onset of LMNA related myopathy (Granger et al., 2011). Mutations in nesprin and SUN-domain proteins have also been implicated in modulating the disease severity of EDMD patients (Taranum et al., 2012). In one case, a modifying mutation has been shown to reduce the severity of the phenotype. The patient had a homozygous null mutation in ZMPSTE24 together with a heterozygous nonsense mutation in *LMNA*, which lead to the reduction of the amount of farnesylated lamin A, resulting in HGPS rather than RD, which is postnatally lethal (Denecke et al., 2006).

In other cases, patients inherit two non-pathogenic *LMNA* SNPs (one from each parent) which together result in disease (Verstraeten et al., 2006). Significantly, about 60% of patients diagnosed with EDMD have no mutations in *EMD*, *LMNA* or *FHL1* which suggests that there are additional genes involved in EDMD pathology (Gueneau et al., 2009; Meinke et al., 2011). Thus, EDMD likely has a broad spectrum of genetic causes, which will be revealed once whole genome sequencing becomes cheaper and more widely available. It will be interesting to learn if new targets also affect the nuclear lamina or act via different mechanisms.

Mutant lamin A variants affect nuclear morphology in myogenic cells

To investigate the pathogenic mechanism in detail, mutant lamin variants have to be studied in vitro and in vivo. Currently there are several mouse models available for *LMNA* associated muscular dystrophies including *lmna*-null mice, which are characterised by postnatal growth retardation, muscular dystrophy and progressive DCM also present features of other laminopathies (Nikolova et al., 2004; Sullivan et al., 1999). Other models available which resemble the human phenotype are knock-in mice which carry dominant *lmna* mutations p.N195K which causes cardiomyopathy (Mounkes et al., 2005) and p.H222P which results in skeletal muscle disease and cardiomyopathy (Arimura et al., 2005). Importantly, all the knock-in mouse models only show a phenotype when homozygous for the mutant alleles, in contrast with the heterozygous state in patients (www.umd.be/LMNA).

To explore pathogenic mechanisms induced by different *LMNA* mutations requires the analysis of many more mutations in parallel. However, to produce knock-in mouse models is a lengthy and expensive process, and because laminopathies are rare diseases, patient samples are generally difficult to obtain. The majority of pathogenic *LMNA* mutations are dominant, so in order to study their effects on cellular function overexpression studies have become widely accepted in wild-type cells with native lamin A/C (Favreau et al., 2004; Hakelien et al., 2008; Ostlund et al., 2001). I have chosen a retroviral expression system which, in comparison to transfection, yields moderate transgene expression with very high efficiencies even in primary cells.

Given the important function of satellite cells in muscle homeostasis and repair, they are a good candidate to explain the late onset and slow progression of the EDMD pathology (Morgan and Zammit, 2010). However, it is still unknown if dysfunctional satellite cells or myoblasts contribute to the pathology of EDMD (Gnocchi et al., 2008) although there is some evidence that mutant lamin protein interferes with myoblast function when expressed in mouse myoblasts (Favreau et al., 2004; Markiewicz et al., 2005), or in human myoblasts (Kandert et al., 2009). Mutant lamin A protein can functionally affect myoblasts at multiple stages during myogenic progression including, proliferation, cell cycle exit and differentiation.

I tested the effects of four EDMD mutations on nuclear morphology in myoblasts and found that two mutations (p.R25P and p.R249W) result in abnormal nuclear morphology and mislocalisation

of lamin B, which is similar to phenotypes induced by many other mutations exogenously expressed in various cell types (Ostlund et al., 2001; Raharjo et al., 2001), or found in human patient cells (Muchir et al., 2004). However, if and more importantly how these defects are associated with myoblast function is not well understood.

Interestingly, none of the four mutations affected proliferation or cell cycle in C2C12 cells. Additionally, no drastic defect in myogenic differentiation was observed, even when they were expressed in *lmna*-null primary myoblasts, to simulate a homozygous state. The only significant change noted was a slight increase in myogenic commitment of wild type satellite cells and C2C12 cells in presence of lamin A-N456I.

Importantly, all four mutations shared one common feature which was that they all induced nuclear alterations in fused myotubes from C2C12 myoblasts (p.R25P and p.R249W) or satellite cell derived myoblasts (p.N456I and p.R541P). Since some differences were observed in C2C12 cells they are likely to act via different mechanisms but which results in a similar phenotype in myotubes.

Lamin A interacts with SUN-domain proteins (Haque et al., 2006; Haque et al., 2010) and nesprins (Mislow et al., 2002; Zhang et al., 2005), main components of the LINC complex, which support the structural integrity of the nucleus (Mellad et al., 2011). Disruption of the LINC complex has been shown to induce defects in nuclear morphology (Khatau et al., 2009) and affect the localisation of skeletal muscle nuclei as well as strain transmission between the cell and nucleus (Zhang et al., 2010), while mutations in giant nesprins 1 and 2 result in a pathology resembling that of EDMD (Zhang et al., 2007). In addition, accumulation of Sun1 has recently been implicated in the pathology of *lmna*-null mice which also suffer from muscle dystrophy (Gnocchi et al., 2011; Sullivan et al., 1999). Furthermore, nuclei of cells with *LMNA* mutations have been shown to be less resistant to mechanical stress (J. Lammerding, personal communication) and ultrastructural analysis of myonuclei from EDMD patients reveals damage to the nuclear membrane and and leakage of chromatin into the cytoplasm (Fidzianska and Hausmanowa-Petrusewicz, 2003; Fidzianska et al., 1998; Park et al., 2009).

Taken together, this observations reinforce the hypothesis that mutations in *LMNA* or lamin interacting proteins result in a dysfunctional A-type lamin filament network, which might not be as flexible as a nuclear lamina composed of only wild-type forms and/or less able to integrate into the nuclear lamina, leading to increase susceptibility of nuclei to mechanical stress and the EDMD pathology. A contribution of dysfunctional satellite cells to the disease pathology (Gnocchi et al., 2008) seems unlikely for the four mutations tested in this study. However, they remain a potential contributing factor to EDMD pathology, at least for a subset of mutations (Favreau et al., 2004; Kandert et al., 2009; Markiewicz et al., 2005)

AON-mediated exon skipping of *LMNA* exon 5 as a potential therapy for particular laminopathies

With extensive research on the role of lamins and lamin interacting proteins in health and disease, therapies for laminopathies start to emerge. Treatments could either target the consequence of lamin A mutations indirectly, or defects in lamin A protein directly. Indirect treatment for example target the Erk1/2 pathway which has been shown to be active in *emd*-null and *lmna*$^{H222P/H222P}$ knock-in mice which both suffer from cardiac phenotypes resembling cardiomyopathy (Muchir et al., 2007a; Muchir et al., 2007b). Administration of Erk1/2 inhibitors, prior to the onset of heart disease has been shown to prevent left ventricular dilatation and deterioration of cardiac contractility (Muchir et al., 2009; Wu et al., 2011). While, modulating the Erk1/2 pathway has been shown to work in mice, human trials have not. Another example is an adipo-cytokine replacement therapy (such as leptin) which has been shown to improve, common metabolic phenotypes found in FPLD2 patients such as hyperglycemia, triglyceridaemia and hepatic steatosis (Park et al., 2007).

An example for a treatment which targets defective lamin A protein directly are farnesyltransferase inhibitors (FTIs) (Fong et al., 2006a; Toth et al., 2005; Yang et al., 2005; Yang et al., 2006). The expression of farnesylated lamin A (either caused by a cryptic splice site resulting in internal deletions in lamin A or mutations in the lamin A processing enzyme Zmpste24) is associated with nuclear blebs, defective DNA repair and premature senescence on a cellular level which translated into premature ageing phenotypes (Goldman et al., 2004; Liu et al., 2005; Moulson et al., 2007; Scaffidi and Misteli, 2005). Reducing the amount of farnesylated lamin A by applying FTIs has been shown to ameliorate nuclear phenotypes in mouse and human fibroblasts (Toth et al., 2005; Yang et al., 2005) as well as disease phenotypes including mean survival in animals (Fong et al., 2006a; Yang et al., 2006). Clinical trials for the use of FTIs in progeria are currently in progress under the supervision of Mark Kieran, at the Children's Hospital Boston, USA. Similarly, the restoration of full length lamin A expression (and restoration of normal lamina processing) by masking the cryptic splice site with antisense oligonucleotides (AONs), can revert abnormal nuclear phenotypes in HGPS cells, and has great potential for therapy (Scaffidi and Misteli, 2005).

Antisense oligonucleotides are also used to restore the reading frame by removing out of frame exons, or exons with premature termination codons (PTCs) (Aartsma-Rus and van Ommen, 2007; Hammond and Wood, 2011). An example where this is clinically relevant is in Duchenne muscular dystrophy, which is caused by loss of dystrophin expression due to nonsense mutations (Hoffman et al., 1987; Muntoni et al., 2003). By removing the mutated exon, expression of a shorter but partially functional dystrophin is restored (Dunckley et al., 1998) which has been shown to ameliorate the phenotype in the *mdx*-mouse (Alter et al., 2006; Mann et al., 2001). This led to the development of therapies for DMD which are now in clinical trial (Cirak et al., 2011; Goemans et al., 2011). The same rational can be applied to mutations in *LMNA*. If the deletion of a specific exon results in a protein product that is functionally superior to the mutated protein, it is a valid target for exon skipping therapy.

I have analysed the exon structure of *LMNA* and found that exons 3 and 5 both encode for 42 amino acids (6 complete heptad repeats) of the central rod domain of lamin A (appendix 1). The rod domains of cytoplasmic intermediate filament proteins also lack 6 heptad repeats (Weber et al., 1989) which led to the hypothesis that *LMNA* exons 3 and 5 are potentially redundant. In a series of proof-of-principle experiments I confirmed that deletion of exon 5, but not exon 3, results in a partially functional protein which can rescue nuclear abnormalities in *lmna*-null primary mouse embryonic fibroblasts, such as lamin B1 and emerin localisation as well as nuclear morphology.

The reason why exon 5 is apparently redundant, but not exon 3, is unexpected given the similar structural change their removal results in, and remains to be determined. One explanation might be that they differentially affect lamin binding proteins. Functional studies such as their effects on cell proliferation and differentiation are still outstanding. Since exon skipping therapy would also result in lamin C-Δ5, it needs to be included in these studies, preferably in combination with lamin A-Δ5.

The next step in the process is to design antisense oligonucleotides, test their skipping efficiency and try to rescue nuclear abnormalities in human cells from laminopathy patients. I have already obtained human dermal fibroblasts (kind gift from G. Bonne) which were isolated from an L-CMD patient with the missense mutation p.L302P (Quijano-Roy et al., 2008). Preliminary results show that lamin A/C and lamin B1 is mislocalised in more than 30% of all cells, which provides a good starting point to test the effectiveness of AONs. Unfortunately, there are currently no mouse models available with mutations in exon 5, to test the therapy *in vivo*. However, if experiments in human cells yield positive results it is definitely worth considering producing one.

To date 21 different mutations have been described in *LMNA* exon 5 which together, affect 7.9% of all reported patients (www.umd.be/LMNA). These mutations include missense mutations, nonsense mutations and one splice site mutation (see table 6.2). If lamin A-Δ5 is indeed functionally similar to the wild type protein, all of these mutations would be treatable.

However, current limitations of AON technology include inefficient skipping (Muntoni and Wood, 2011). This could be an issue since the majority of mutations in exon 5 are dominant mutations, which might need to be removed completely to treat the phenotype. In addition, incomplete skipping of exon 5 would result in the co-expression of six different A-type lamin variants: wild-type lamin A and C, mutated lamin A and C and skipped lamin A and C, which at the end might be more detrimental to the cell than higher levels of mutant and wild-type lamins A and C.

One of the mutations in exon 5 (p.R298C), results in AR-CMT2 which is characterised by myelination defects in peripheral neurons (De Sandre-Giovannoli et al., 2002). In this case partial skipping might be enough to ameliorate the phenotype, provided that lamin A-Δ5 performs like wild-type lamin A. However, tissue specific targeting of AONs is another limitation yet to overcome. Although progress has been made towards the identification of arginine-rich cell penetrating peptides which promote AON uptake in cardiomyocytes (Yin et al., 2009), technology to target the peripheral nervous system is not yet available (M.J. Wood, personal communication).

In future exon exchange technologies such as spliceosome-mediated RNA trans-splicing, may replace exon skipping (Puttaraju et al., 1999) but until such technologies become available and are efficient enough, AON mediated exon skipping remains the best possible alternative to target specific laminopathies.

Thesis conclusion

In conclusion, my work advances the current understanding of genotype-phenotype correlations in laminopathies as well as the involvement of satellite cells in the pathology of EDMD. Further, it provides proof-of-principle for exon skipping to target missense mutations in the *LMNA* gene, which one day may translate into therapy for laminopathies(Taimen et al., 2009; Taranum et al., 2012).

References

Aartsma-Rus, A., Singh, K.H., Fokkema, I.F., Ginjaar, I.B., van Ommen, G.J., den Dunnen, J.T., and van der Maarel, S.M. (2010). Therapeutic exon skipping for dysferlinopathies? European journal of human genetics : EJHG *18*, 889-894.

Aartsma-Rus, A., and van Ommen, G.J. (2007). Antisense-mediated exon skipping: a versatile tool with therapeutic and research applications. RNA *13*, 1609-1624.

Agarwal, A.K., Fryns, J.P., Auchus, R.J., and Garg, A. (2003). Zinc metalloproteinase, ZMPSTE24, is mutated in mandibuloacral dysplasia. Human molecular genetics *12*, 1995-2001.

Agarwal, A.K., Kazachkova, I., Ten, S., and Garg, A. (2008). Severe mandibuloacral dysplasia-associated lipodystrophy and progeria in a young girl with a novel homozygous Arg527Cys LMNA mutation. The Journal of clinical endocrinology and metabolism *93*, 4617-4623.

Alter, J., Lou, F., Rabinowitz, A., Yin, H., Rosenfeld, J., Wilton, S.D., Partridge, T.A., and Lu, Q.L. (2006). Systemic delivery of morpholino oligonucleotide restores dystrophin expression bodywide and improves dystrophic pathology. Nature medicine *12*, 175-177.

Alvarez-Erviti, L., Seow, Y., Yin, H., Betts, C., Lakhal, S., and Wood, M.J. (2011). Delivery of siRNA to the mouse brain by systemic injection of targeted exosomes. Nature biotechnology *29*, 341-345.

Andres, V., and Gonzalez, J.M. (2009). Role of A-type lamins in signaling, transcription, and chromatin organization. The Journal of cell biology *187*, 945-957.

Arbustini, E., Pilotto, A., Repetto, A., Grasso, M., Negri, A., Diegoli, M., Campana, C., Scelsi, L., Baldini, E., Gavazzi, A.*, et al.* (2002). Autosomal dominant dilated cardiomyopathy with atrioventricular block: a lamin A/C defect-related disease. Journal of the American College of Cardiology *39*, 981-990.

Arimura, T., Helbling-Leclerc, A., Massart, C., Varnous, S., Niel, F., Lacene, E., Fromes, Y., Toussaint, M., Mura, A.M., Keller, D.I.*, et al.* (2005). Mouse model carrying H222P-Lmna mutation develops muscular dystrophy and dilated cardiomyopathy similar to human striated muscle laminopathies. Human molecular genetics *14*, 155-169.

Asakura, A., Seale, P., Girgis-Gabardo, A., and Rudnicki, M.A. (2002). Myogenic specification of side population cells in skeletal muscle. The Journal of cell biology *159*, 123-134.

Astejada, M.N., Goto, K., Nagano, A., Ura, S., Noguchi, S., Nonaka, I., Nishino, I., and Hayashi, Y.K. (2007). Emerinopathy and laminopathy clinical, pathological and molecular features of muscular dystrophy with nuclear envelopathy in Japan. Acta myologica : myopathies and cardiomyopathies : official journal of the Mediterranean Society of Myology / edited by the Gaetano Conte Academy for the study of striated muscle diseases *26*, 159-164.

Bakay, M., Wang, Z., Melcon, G., Schiltz, L., Xuan, J., Zhao, P., Sartorelli, V., Seo, J., Pegoraro, E., Angelini, C.*, et al.* (2006). Nuclear envelope dystrophies show a transcriptional fingerprint suggesting disruption of Rb-MyoD pathways in muscle regeneration. Brain : a journal of neurology *129*, 996-1013.

Baker, N.A., Sept, D., Joseph, S., Holst, M.J., and McCammon, J.A. (2001). Electrostatics of nanosystems: application to microtubules and the ribosome. Proceedings of the National Academy of Sciences of the United States of America *98*, 10037-10041.

Bansal, D., Miyake, K., Vogel, S.S., Groh, S., Chen, C.C., Williamson, R., McNeil, P.L., and Campbell, K.P. (2003). Defective membrane repair in dysferlin-deficient muscular dystrophy. Nature *423*, 168-172.

Barrowman, J., Hamblet, C., Kane, M.S., and Michaelis, S. (2012). Requirements for efficient proteolytic cleavage of prelamin A by ZMPSTE24. PloS one *7*, e32120.

Beauchamp, J.R., Heslop, L., Yu, D.S., Tajbakhsh, S., Kelly, R.G., Wernig, A., Buckingham, M.E., Partridge, T.A., and Zammit, P.S. (2000). Expression of CD34 and Myf5 defines the majority of quiescent adult skeletal muscle satellite cells. The Journal of cell biology *151*, 1221-1234.

Ben-Harush, K., Wiesel, N., Frenkiel-Krispin, D., Moeller, D., Soreq, E., Aebi, U., Herrmann, H., Gruenbaum, Y., and Medalia, O. (2009). The supramolecular organization of the C. elegans nuclear lamin filament. Journal of molecular biology *386*, 1392-1402.

Benedetti, S., Bertini, E., Iannaccone, S., Angelini, C., Trisciani, M., Toniolo, D., Sferrazza, B., Carrera, P., Comi, G., Ferrari, M.*, et al.* (2005). Dominant LMNA mutations can cause combined muscular dystrophy and peripheral neuropathy. Journal of neurology, neurosurgery, and psychiatry *76*, 1019-1021.

Benedetti, S., Menditto, I., Degano, M., Rodolico, C., Merlini, L., D'Amico, A., Palmucci, L., Berardinelli, A., Pegoraro, E., Trevisan, C.P.*, et al.* (2007). Phenotypic clustering of lamin A/C mutations in neuromuscular patients. Neurology *69*, 1285-1292.

Bengtsson, L. (2007). What MAN1 does to the Smads. TGFbeta/BMP signaling and the nuclear envelope. The FEBS journal *274*, 1374-1382.

Bennett, C.F., and Swayze, E.E. (2010). RNA targeting therapeutics: molecular mechanisms of antisense oligonucleotides as a therapeutic platform. Annual review of pharmacology and toxicology *50*, 259-293.

Berger, R., Theodor, L., Shoham, J., Gokkel, E., Brok-Simoni, F., Avraham, K.B., Copeland, N.G., Jenkins, N.A., Rechavi, G., and Simon, A.J. (1996). The characterization and localization of the mouse thymopoietin/lamina-associated polypeptide 2 gene and its alternatively spliced products. Genome research *6*, 361-370.

Bergo, M.O., Gavino, B., Ross, J., Schmidt, W.K., Hong, C., Kendall, L.V., Mohr, A., Meta, M., Genant, H., Jiang, Y.*, et al.* (2002). Zmpste24 deficiency in mice causes spontaneous bone fractures, muscle weakness, and a prelamin A processing defect. Proceedings of the National Academy of Sciences of the United States of America *99*, 13049-13054.

Bernard, R., De Sandre-Giovannoli, A., Delague, V., and Levy, N. (2006). Molecular genetics of autosomal-recessive axonal Charcot-Marie-Tooth neuropathies. Neuromolecular medicine *8*, 87-106.

Bidault, G., Vatier, C., Capeau, J., Vigouroux, C., and Bereziat, V. (2011). LMNA-linked lipodystrophies: from altered fat distribution to cellular alterations. Biochemical Society transactions *39*, 1752-1757.

Bione, S., Maestrini, E., Rivella, S., Mancini, M., Regis, S., Romeo, G., and Toniolo, D. (1994). Identification of a novel X-linked gene responsible for Emery-Dreifuss muscular dystrophy. Nat Genet *8*, 323-327.

Blau, H.M., Chiu, C.P., and Webster, C. (1983). Cytoplasmic activation of human nuclear genes in stable heterocaryons. Cell *32*, 1171-1180.

Bollati, M., Barbiroli, A., Favalli, V., Arbustini, E., Charron, P., and Bolognesi, M. (2012). Structures of the lamin A/C R335W and E347K mutants: implications for dilated cardiolaminopathies. Biochemical and biophysical research communications *418*, 217-221.

Bonne, G., Di Barletta, M.R., Varnous, S., Becane, H.M., Hammouda, E.H., Merlini, L., Muntoni, F., Greenberg, C.R., Gary, F., Urtizberea, J.A.*, et al.* (1999). Mutations in the gene encoding lamin A/C cause autosomal dominant Emery-Dreifuss muscular dystrophy. Nat Genet *21*, 285-288.

Bonne, G., Leturcq, F., and Ben Yaou, R. (1993). Emery-Dreifuss Muscular Dystrophy. In GeneReviews, R.A. Pagon, T.D. Bird, C.R. Dolan, K. Stephens, and M.P. Adam, eds. (Seattle (WA)).

Bonne, G., Mercuri, E., Muchir, A., Urtizberea, A., Becane, H.M., Recan, D., Merlini, L., Wehnert, M., Boor, R., Reuner, U.*, et al.* (2000). Clinical and molecular genetic spectrum of autosomal dominant Emery-Dreifuss muscular dystrophy due to mutations of the lamin A/C gene. Annals of neurology *48*, 170-180.

Bork, P., Holm, L., and Sander, C. (1994). The immunoglobulin fold. Structural classification, sequence patterns and common core. Journal of molecular biology *242*, 309-320.

Broers, J.L., Kuijpers, H.J., Ostlund, C., Worman, H.J., Endert, J., and Ramaekers, F.C. (2005). Both lamin A and lamin C mutations cause lamina instability as well as loss of internal nuclear lamin organization. Exp Cell Res *304*, 582-592.

Broers, J.L., Machiels, B.M., van Eys, G.J., Kuijpers, H.J., Manders, E.M., van Driel, R., and Ramaekers, F.C. (1999). Dynamics of the nuclear lamina as monitored by GFP-tagged A-type lamins. Journal of cell science *112 (Pt 20)*, 3463-3475.

Broers, J.L., Ramaekers, F.C., Bonne, G., Yaou, R.B., and Hutchison, C.J. (2006). Nuclear lamins: laminopathies and their role in premature ageing. Physiological reviews *86*, 967-1008.

Brown, C.A., Lanning, R.W., McKinney, K.Q., Salvino, A.R., Cherniske, E., Crowe, C.A., Darras, B.T., Gominak, S., Greenberg, C.R., Grosmann, C.*, et al.* (2001). Novel and recurrent mutations in lamin A/C in patients with Emery-Dreifuss muscular dystrophy. American journal of medical genetics *102*, 359-367.

Brown, C.A., Scharner, J., Felice, K., Meriggioli, M.N., Tarnopolsky, M., Bower, M., Zammit, P.S., Mendell, J.R., and Ellis, J.A. (2011). Novel and recurrent EMD mutations in patients with Emery-Dreifuss muscular dystrophy, identify exon 2 as a mutation hot spot. Journal of human genetics *56*, 589-594.

Bryson-Richardson, R.J., and Currie, P.D. (2008). The genetics of vertebrate myogenesis. Nature reviews Genetics *9*, 632-646.

Busslinger, M., Moschonas, N., and Flavell, R.A. (1981). Beta + thalassemia: aberrant splicing results from a single point mutation in an intron. Cell *27*, 289-298.

Cao, H., and Hegele, R.A. (2003). LMNA is mutated in Hutchinson-Gilford progeria (MIM 176670) but not in Wiedemann-Rautenstrauch progeroid syndrome (MIM 264090). Journal of human genetics *48*, 271-274.

Capanni, C., Mattioli, E., Columbaro, M., Lucarelli, E., Parnaik, V.K., Novelli, G., Wehnert, M., Cenni, V., Maraldi, N.M., Squarzoni, S.*, et al.* (2005). Altered pre-lamin A processing is a common mechanism leading to lipodystrophy. Human molecular genetics *14*, 1489-1502.

Cavallo, L., Kleinjung, J., and Fraternali, F. (2003). POPS: A fast algorithm for solvent accessible surface areas at atomic and residue level. Nucleic acids research *31*, 3364-3366.

Charge, S.B., and Rudnicki, M.A. (2004). Cellular and molecular regulation of muscle regeneration. Physiological reviews *84*, 209-238.

Chaturvedi, L.S., Mukherjee, M., Srivastava, S., Mittal, R.D., and Mittal, B. (2001). Point mutation and polymorphism in Duchenne/Becker muscular dystrophy (D/BMD) patients. Experimental & molecular medicine *33*, 251-256.

Chen, C.Y., Chi, Y.H., Mutalif, R.A., Starost, M.F., Myers, T.G., Anderson, S.A., Stewart, C.L., and Jeang, K.T. (2012). Accumulation of the inner nuclear envelope protein sun1 is pathogenic in progeric and dystrophic laminopathies. Cell *149*, 565-577.

Chen, L., Lee, L., Kudlow, B.A., Dos Santos, H.G., Sletvold, O., Shafeghati, Y., Botha, E.G., Garg, A., Hanson, N.B., Martin, G.M.*, et al.* (2003). LMNA mutations in atypical Werner's syndrome. Lancet *362*, 440-445.

Cirak, S., Arechavala-Gomeza, V., Guglieri, M., Feng, L., Torelli, S., Anthony, K., Abbs, S., Garralda, M.E., Bourke, J., Wells, D.J.*, et al.* (2011). Exon skipping and dystrophin restoration in patients with Duchenne muscular dystrophy after systemic phosphorodiamidate morpholino oligomer treatment: an open-label, phase 2, dose-escalation study. Lancet *378*, 595-605.

Clements, L., Manilal, S., Love, D.R., and Morris, G.E. (2000). Direct interaction between emerin and lamin A. Biochemical and biophysical research communications *267*, 709-714.

Coffinier, C., Jung, H.J., Li, Z., Nobumori, C., Yun, U.J., Farber, E.A., Davies, B.S., Weinstein, M.M., Yang, S.H., Lammerding, J.*, et al.* (2010). Direct synthesis of lamin A, bypassing prelamin a processing, causes misshapen nuclei in fibroblasts but no detectable pathology in mice. The Journal of biological chemistry *285*, 20818-20826.

Coffinier, C., Jung, H.J., Nobumori, C., Chang, S., Tu, Y., Barnes, R.H., 2nd, Yoshinaga, Y., de Jong, P.J., Vergnes, L., Reue, K.*, et al.* (2011). Deficiencies in lamin B1 and lamin B2 cause neurodevelopmental defects and distinct nuclear shape abnormalities in neurons. Molecular biology of the cell *22*, 4683-4693.

Cohen, C., and Parry, D.A. (1990). Alpha-helical coiled coils and bundles: how to design an alpha-helical protein. Proteins *7*, 1-15.

Collins, C.A., Olsen, I., Zammit, P.S., Heslop, L., Petrie, A., Partridge, T.A., and Morgan, J.E. (2005). Stem cell function, self-renewal, and behavioral heterogeneity of cells from the adult muscle satellite cell niche. Cell *122*, 289-301.

Collins, C.A., and Zammit, P.S. (2009). Isolation and grafting of single muscle fibres. Methods Mol Biol *482*, 319-330.

Constantinescu, D., Gray, H.L., Sammak, P.J., Schatten, G.P., and Csoka, A.B. (2006). Lamin A/C expression is a marker of mouse and human embryonic stem cell differentiation. Stem Cells *24*, 177-185.

Conway, J.F., and Parry, D.A. (1990). Structural features in the heptad substructure and longer range repeats of two-stranded alpha-fibrous proteins. International journal of biological macromolecules *12*, 328-334.

Cooper, R.N., Tajbakhsh, S., Mouly, V., Cossu, G., Buckingham, M., and Butler-Browne, G.S. (1999). In vivo satellite cell activation via Myf5 and MyoD in regenerating mouse skeletal muscle. Journal of cell science *112 (Pt 17)*, 2895-2901.

Cooper, T.A., Wan, L., and Dreyfuss, G. (2009). RNA and disease. Cell *136*, 777-793.

Corey, D.R., and Abrams, J.M. (2001). Morpholino antisense oligonucleotides: tools for investigating vertebrate development. Genome biology *2*, REVIEWS1015.

Cornelison, D.D., and Wold, B.J. (1997). Single-cell analysis of regulatory gene expression in quiescent and activated mouse skeletal muscle satellite cells. Developmental biology *191*, 270-283.

Crisp, M., Liu, Q., Roux, K., Rattner, J.B., Shanahan, C., Burke, B., Stahl, P.D., and Hodzic, D. (2006). Coupling of the nucleus and cytoplasm: role of the LINC complex. The Journal of cell biology *172*, 41-53.

Csoka, A.B., Cao, H., Sammak, P.J., Constantinescu, D., Schatten, G.P., and Hegele, R.A. (2004). Novel lamin A/C gene (LMNA) mutations in atypical progeroid syndromes. Journal of medical genetics *41*, 304-308.

Dai, Q., Choy, E., Chiu, V., Romano, J., Slivka, S.R., Steitz, S.A., Michaelis, S., and Philips, M.R. (1998). Mammalian prenylcysteine carboxyl methyltransferase is in the endoplasmic reticulum. The Journal of biological chemistry *273*, 15030-15034.

Davies, B.S., Barnes, R.H., 2nd, Tu, Y., Ren, S., Andres, D.A., Spielmann, H.P., Lammerding, J., Wang, Y., Young, S.G., and Fong, L.G. (2010). An accumulation of non-farnesylated prelamin A causes cardiomyopathy but not progeria. Human molecular genetics *19*, 2682-2694.

Davies, B.S., Coffinier, C., Yang, S.H., Barnes, R.H., 2nd, Jung, H.J., Young, S.G., and Fong, L.G. (2011). Investigating the purpose of prelamin A processing. Nucleus *2*, 4-9.

Davies, B.S., Fong, L.G., Yang, S.H., Coffinier, C., and Young, S.G. (2009). The posttranslational processing of prelamin A and disease. Annual review of genomics and human genetics *10*, 153-174.

De Angelis, L., Berghella, L., Coletta, M., Lattanzi, L., Zanchi, M., Cusella-De Angelis, M.G., Ponzetto, C., and Cossu, G. (1999). Skeletal myogenic progenitors originating from embryonic dorsal aorta coexpress endothelial and myogenic markers and contribute to postnatal muscle growth and regeneration. The Journal of cell biology *147*, 869-878.

De Falco, G., Comes, F., and Simone, C. (2006). pRb: master of differentiation. Coupling irreversible cell cycle withdrawal with induction of muscle-specific transcription. Oncogene *25*, 5244-5249.

De Sandre-Giovannoli, A., Bernard, R., Cau, P., Navarro, C., Amiel, J., Boccaccio, I., Lyonnet, S., Stewart, C.L., Munnich, A., Le Merrer, M.*, et al.* (2003). Lamin a truncation in Hutchinson-Gilford progeria. Science *300*, 2055.

De Sandre-Giovannoli, A., Chaouch, M., Kozlov, S., Vallat, J.M., Tazir, M., Kassouri, N., Szepetowski, P., Hammadouche, T., Vandenberghe, A., Stewart, C.L.*, et al.* (2002). Homozygous defects in LMNA, encoding lamin A/C nuclear-envelope proteins, cause autosomal recessive axonal neuropathy in human (Charcot-Marie-Tooth disorder type 2) and mouse. American journal of human genetics *70*, 726-736.

Decaudain, A., Vantyghem, M.C., Guerci, B., Hecart, A.C., Auclair, M., Reznik, Y., Narbonne, H., Ducluzeau, P.H., Donadille, B., Lebbe, C.*, et al.* (2007). New metabolic phenotypes in laminopathies: LMNA mutations in patients with severe metabolic syndrome. The Journal of clinical endocrinology and metabolism *92*, 4835-4844.

Dechat, T., Adam, S.A., Taimen, P., Shimi, T., and Goldman, R.D. (2010). Nuclear lamins. Cold Spring Harbor perspectives in biology *2*, a000547.

Dechat, T., Gotzmann, J., Stockinger, A., Harris, C.A., Talle, M.A., Siekierka, J.J., and Foisner, R. (1998). Detergent-salt resistance of LAP2alpha in interphase nuclei and phosphorylation-dependent association with chromosomes early in nuclear assembly implies functions in nuclear structure dynamics. The EMBO journal *17*, 4887-4902.

Dechat, T., Korbei, B., Vaughan, O.A., Vlcek, S., Hutchison, C.J., and Foisner, R. (2000). Lamina-associated polypeptide 2alpha binds intranuclear A-type lamins. Journal of cell science *113 Pt 19*, 3473-3484.

Denecke, J., Brune, T., Feldhaus, T., Robenek, H., Kranz, C., Auchus, R.J., Agarwal, A.K., and Marquardt, T. (2006). A homozygous ZMPSTE24 null mutation in combination with a heterozygous mutation in the LMNA gene causes Hutchinson-Gilford progeria syndrome (HGPS): insights into the pathophysiology of HGPS. Human mutation *27*, 524-531.

Dhe-Paganon, S., Werner, E.D., Chi, Y.I., and Shoelson, S.E. (2002). Structure of the globular tail of nuclear lamin. The Journal of biological chemistry *277*, 17381-17384.

Doh, Y.J., Kim, H.K., Jung, E.D., Choi, S.H., Kim, J.G., Kim, B.W., and Lee, I.K. (2009). Novel LMNA gene mutation in a patient with Atypical Werner's Syndrome. The Korean journal of internal medicine *24*, 68-72.

Dolinsky, T.J., Czodrowski, P., Li, H., Nielsen, J.E., Jensen, J.H., Klebe, G., and Baker, N.A. (2007). PDB2PQR: expanding and upgrading automated preparation of biomolecular structures for molecular simulations. Nucleic acids research *35*, W522-525.

Dorner, D., Vlcek, S., Foeger, N., Gajewski, A., Makolm, C., Gotzmann, J., Hutchison, C.J., and Foisner, R. (2006). Lamina-associated polypeptide 2alpha regulates cell cycle progression and differentiation via the retinoblastoma-E2F pathway. The Journal of cell biology *173*, 83-93.

Dreuillet, C., Tillit, J., Kress, M., and Ernoult-Lange, M. (2002). In vivo and in vitro interaction between human transcription factor MOK2 and nuclear lamin A/C. Nucleic acids research *30*, 4634-4642.

Dunckley, M.G., Manoharan, M., Villiet, P., Eperon, I.C., and Dickson, G. (1998). Modification of splicing in the dystrophin gene in cultured Mdx muscle cells by antisense oligoribonucleotides. Human molecular genetics *7*, 1083-1090.

Egholm, M., Buchardt, O., Christensen, L., Behrens, C., Freier, S.M., Driver, D.A., Berg, R.H., Kim, S.K., Norden, B., and Nielsen, P.E. (1993). PNA hybridizes to complementary oligonucleotides obeying the Watson-Crick hydrogen-bonding rules. Nature *365*, 566-568.

Ellis, J.A., Craxton, M., Yates, J.R., and Kendrick-Jones, J. (1998). Aberrant intracellular targeting and cell cycle-dependent phosphorylation of emerin contribute to the Emery-Dreifuss muscular dystrophy phenotype. Journal of cell science *111 (Pt 6)*, 781-792.

Emerson, L.J., Holt, M.R., Wheeler, M.A., Wehnert, M., Parsons, M., and Ellis, J.A. (2009). Defects in cell spreading and ERK1/2 activation in fibroblasts with lamin A/C mutations. Biochimica et biophysica acta *1792*, 810-821.

Emery, A.E. (2000). Emery-Dreifuss muscular dystrophy - a 40 year retrospective. Neuromuscular disorders : NMD *10*, 228-232.

Emery, A.E. (2002). The muscular dystrophies. Lancet *359*, 687-695.

Emery, A.E., and Dreifuss, F.E. (1966). Unusual type of benign x-linked muscular dystrophy. Journal of neurology, neurosurgery, and psychiatry *29*, 338-342.

Erber, A., Riemer, D., Hofemeister, H., Bovenschulte, M., Stick, R., Panopoulou, G., Lehrach, H., and Weber, K. (1999). Characterization of the Hydra lamin and its gene: A molecular phylogeny of metazoan lamins. Journal of molecular evolution *49*, 260-271.

Eriksson, M., Brown, W.T., Gordon, L.B., Glynn, M.W., Singer, J., Scott, L., Erdos, M.R., Robbins, C.M., Moses, T.Y., Berglund, P.*, et al.* (2003). Recurrent de novo point mutations in lamin A cause Hutchinson-Gilford progeria syndrome. Nature *423*, 293-298.

Fairley, E.A., Kendrick-Jones, J., and Ellis, J.A. (1999). The Emery-Dreifuss muscular dystrophy phenotype arises from aberrant targeting and binding of emerin at the inner nuclear membrane. Journal of cell science *112 (Pt 15)*, 2571-2582.

Fan, X., Dion, P., Laganiere, J., Brais, B., and Rouleau, G.A. (2001). Oligomerization of polyalanine expanded PABPN1 facilitates nuclear protein aggregation that is associated with cell death. Human molecular genetics *10*, 2341-2351.

Farnsworth, C.C., Wolda, S.L., Gelb, M.H., and Glomset, J.A. (1989). Human lamin B contains a farnesylated cysteine residue. The Journal of biological chemistry *264*, 20422-20429.

Fatkin, D., MacRae, C., Sasaki, T., Wolff, M.R., Porcu, M., Frenneaux, M., Atherton, J., Vidaillet, H.J., Jr., Spudich, S., De Girolami, U.*, et al.* (1999). Missense mutations in the rod domain of the lamin A/C gene as causes of dilated cardiomyopathy and conduction-system disease. The New England journal of medicine *341*, 1715-1724.

Favreau, C., Delbarre, E., Courvalin, J.C., and Buendia, B. (2008). Differentiation of C2C12 myoblasts expressing lamin A mutated at a site responsible for Emery-Dreifuss muscular dystrophy is improved by inhibition of the MEK-ERK pathway and stimulation of the PI3-kinase pathway. Exp Cell Res *314*, 1392-1405.

Favreau, C., Higuet, D., Courvalin, J.C., and Buendia, B. (2004). Expression of a mutant lamin A that causes Emery-Dreifuss muscular dystrophy inhibits in vitro differentiation of C2C12 myoblasts. Molecular and cellular biology *24*, 1481-1492.

Fawcett, D.W. (1966). On the occurrence of a fibrous lamina on the inner aspect of the nuclear envelope in certain cells of vertebrates. The American journal of anatomy *119*, 129-145.

Fidzianska, A., and Hausmanowa-Petrusewicz, I. (2003). Architectural abnormalities in muscle nuclei. Ultrastructural differences between X-linked and autosomal dominant forms of EDMD. Journal of the neurological sciences *210*, 47-51.

Fidzianska, A., Toniolo, D., and Hausmanowa-Petrusewicz, I. (1998). Ultrastructural abnormality of sarcolemmal nuclei in Emery-Dreifuss muscular dystrophy (EDMD). Journal of the neurological sciences *159*, 88-93.

Foeger, N., Wiesel, N., Lotsch, D., Mucke, N., Kreplak, L., Aebi, U., Gruenbaum, Y., and Herrmann, H. (2006). Solubility properties and specific assembly pathways of the B-type lamin from Caenorhabditis elegans. Journal of structural biology *155*, 340-350.

Foisner, R., and Gerace, L. (1993). Integral membrane proteins of the nuclear envelope interact with lamins and chromosomes, and binding is modulated by mitotic phosphorylation. Cell *73*, 1267-1279.

Fokkema, I.F., den Dunnen, J.T., and Taschner, P.E. (2005). LOVD: easy creation of a locus-specific sequence variation database using an "LSDB-in-a-box" approach. Human mutation *26*, 63-68.

Fong, L.G., Frost, D., Meta, M., Qiao, X., Yang, S.H., Coffinier, C., and Young, S.G. (2006a). A protein farnesyltransferase inhibitor ameliorates disease in a mouse model of progeria. Science *311*, 1621-1623.

Fong, L.G., Ng, J.K., Lammerding, J., Vickers, T.A., Meta, M., Cote, N., Gavino, B., Qiao, X., Chang, S.Y., Young, S.R.*, et al.* (2006b). Prelamin A and lamin A appear to be dispensable in the nuclear lamina. The Journal of clinical investigation *116*, 743-752.

Fraternali, F., and Cavallo, L. (2002). Parameter optimized surfaces (POPS): analysis of key interactions and conformational changes in the ribosome. Nucleic acids research *30*, 2950-2960.

Frock, R.L., Kudlow, B.A., Evans, A.M., Jameson, S.A., Hauschka, S.D., and Kennedy, B.K. (2006). Lamin A/C and emerin are critical for skeletal muscle satellite cell differentiation. Genes & development *20*, 486-500.

Fuchs, E., and Weber, K. (1994). Intermediate filaments: structure, dynamics, function, and disease. Annual review of biochemistry *63*, 345-382.

Furukawa, K. (1999). LAP2 binding protein 1 (L2BP1/BAF) is a candidate mediator of LAP2-chromatin interaction. Journal of cell science *112 (Pt 15)*, 2485-2492.

Furukawa, K., and Hotta, Y. (1993). cDNA cloning of a germ cell specific lamin B3 from mouse spermatocytes and analysis of its function by ectopic expression in somatic cells. The EMBO journal *12*, 97-106.

Furukawa, K., Inagaki, H., and Hotta, Y. (1994). Identification and cloning of an mRNA coding for a germ cell-specific A-type lamin in mice. Exp Cell Res *212*, 426-430.

Garg, A., Speckman, R.A., and Bowcock, A.M. (2002). Multisystem dystrophy syndrome due to novel missense mutations in the amino-terminal head and alpha-helical rod domains of the lamin A/C gene. The American journal of medicine *112*, 549-555.

Geiger, S.K., Bar, H., Ehlermann, P., Walde, S., Rutschow, D., Zeller, R., Ivandic, B.T., Zentgraf, H., Katus, H.A., Herrmann, H.*, et al.* (2008). Incomplete nonsense-mediated decay of mutant lamin A/C mRNA provokes dilated cardiomyopathy and ventricular tachycardia. J Mol Med (Berl) *86*, 281-289.

Genschel, J., Bochow, B., Kuepferling, S., Ewert, R., Hetzer, R., Lochs, H., and Schmidt, H. (2001). A R644C mutation within lamin A extends the mutations causing dilated cardiomyopathy. Human mutation *17*, 154.

Gerace, L., and Blobel, G. (1980). The nuclear envelope lamina is reversibly depolymerized during mitosis. Cell *19*, 277-287.

Gerace, L., Blum, A., and Blobel, G. (1978). Immunocytochemical localization of the major polypeptides of the nuclear pore complex-lamina fraction. Interphase and mitotic distribution. The Journal of cell biology *79*, 546-566.

Gilchrist, S., Gilbert, N., Perry, P., Ostlund, C., Worman, H.J., and Bickmore, W.A. (2004). Altered protein dynamics of disease-associated lamin A mutants. BMC cell biology *5*, 46.

Gilford, H. (1897). On a Condition of Mixed Premature and Immature Development. Medico-chirurgical transactions *80*, 17-46 25.

Gnocchi, V.F., Ellis, J.A., and Zammit, P.S. (2008). Does satellite cell dysfunction contribute to disease progression in Emery-Dreifuss muscular dystrophy? Biochemical Society transactions *36*, 1344-1349.

Gnocchi, V.F., Scharner, J., Huang, Z., Brady, K., Lee, J.S., White, R.B., Morgan, J.E., Sun, Y.B., Ellis, J.A., and Zammit, P.S. (2011). Uncoordinated transcription and compromised muscle function in the lmna-null mouse model of Emery- Emery-Dreyfuss muscular dystrophy. PloS one *6*, e16651.

Gnocchi, V.F., White, R.B., Ono, Y., Ellis, J.A., and Zammit, P.S. (2009). Further characterisation of the molecular signature of quiescent and activated mouse muscle satellite cells. PloS one *4*, e5205.

Goemans, N.M., Tulinius, M., van den Akker, J.T., Burm, B.E., Ekhart, P.F., Heuvelmans, N., Holling, T., Janson, A.A., Platenburg, G.J., Sipkens, J.A.*, et al.* (2011). Systemic administration of PRO051 in Duchenne's muscular dystrophy. The New England journal of medicine *364*, 1513-1522.

Goldberg, M.W., Huttenlauch, I., Hutchison, C.J., and Stick, R. (2008). Filaments made from A- and B-type lamins differ in structure and organization. Journal of cell science *121*, 215-225.

Goldman, R.D., Shumaker, D.K., Erdos, M.R., Eriksson, M., Goldman, A.E., Gordon, L.B., Gruenbaum, Y., Khuon, S., Mendez, M., Varga, R.*, et al.* (2004). Accumulation of mutant lamin A causes progressive changes in nuclear architecture in Hutchinson-Gilford progeria syndrome. Proceedings of the National Academy of Sciences of the United States of America *101*, 8963-8968.

Gonzalez, J.M., Navarro-Puche, A., Casar, B., Crespo, P., and Andres, V. (2008). Fast regulation of AP-1 activity through interaction of lamin A/C, ERK1/2, and c-Fos at the nuclear envelope. The Journal of cell biology *183*, 653-666.

Gorza, L. (1990). Identification of a novel type 2 fiber population in mammalian skeletal muscle by combined use of histochemical myosin ATPase and anti-myosin monoclonal antibodies. J Histochem Cytochem *38*, 257-265.

Gotic, I., Leschnik, M., Kolm, U., Markovic, M., Haubner, B.J., Biadasiewicz, K., Metzler, B., Stewart, C.L., and Foisner, R. (2010a). Lamina-associated polypeptide 2alpha loss impairs heart function and stress response in mice. Circulation research *106*, 346-353.

Gotic, I., Schmidt, W.M., Biadasiewicz, K., Leschnik, M., Spilka, R., Braun, J., Stewart, C.L., and Foisner, R. (2010b). Loss of LAP2 alpha delays satellite cell differentiation and affects postnatal fiber-type determination. Stem Cells *28*, 480-488.

Granger, B., Gueneau, L., Drouin-Garraud, V., Pedergnana, V., Gagnon, F., Ben Yaou, R., Tezenas du Montcel, S., and Bonne, G. (2011). Modifier locus of the skeletal muscle involvement in Emery-Dreifuss muscular dystrophy. Human genetics *129*, 149-159.

Green, M.R. (1986). Pre-mRNA splicing. Annual review of genetics *20*, 671-708.

Grefte, S., Kuijpers-Jagtman, A.M., Torensma, R., and Von den Hoff, J.W. (2007). Skeletal muscle development and regeneration. Stem cells and development *16*, 857-868.

Gu, W., Schneider, J.W., Condorelli, G., Kaushal, S., Mahdavi, V., and Nadal-Ginard, B. (1993). Interaction of myogenic factors and the retinoblastoma protein mediates muscle cell commitment and differentiation. Cell *72*, 309-324.

Guelen, L., Pagie, L., Brasset, E., Meuleman, W., Faza, M.B., Talhout, W., Eussen, B.H., de Klein, A., Wessels, L., de Laat, W.*, et al.* (2008). Domain organization of human chromosomes revealed by mapping of nuclear lamina interactions. Nature *453*, 948-951.

Gueneau, L., Bertrand, A.T., Jais, J.P., Salih, M.A., Stojkovic, T., Wehnert, M., Hoeltzenbein, M., Spuler, S., Saitoh, S., Verschueren, A.*, et al.* (2009). Mutations of the FHL1 gene cause Emery-Dreifuss muscular dystrophy. American journal of human genetics *85*, 338-353.

Guo, K., Wang, J., Andres, V., Smith, R.C., and Walsh, K. (1995). MyoD-induced expression of p21 inhibits cyclin-dependent kinase activity upon myocyte terminal differentiation. Molecular and cellular biology *15*, 3823-3829.

Guttinger, S., Laurell, E., and Kutay, U. (2009). Orchestrating nuclear envelope disassembly and reassembly during mitosis. Nature reviews Molecular cell biology *10*, 178-191.

Hakelien, A.M., Delbarre, E., Gaustad, K.G., Buendia, B., and Collas, P. (2008). Expression of the myodystrophic R453W mutation of lamin A in C2C12 myoblasts causes promoter-specific and global epigenetic defects. Exp Cell Res *314*, 1869-1880.

Hammond, S.M., and Wood, M.J. (2011). Genetic therapies for RNA mis-splicing diseases. Trends in genetics : TIG *27*, 196-205.

Haque, F., Lloyd, D.J., Smallwood, D.T., Dent, C.L., Shanahan, C.M., Fry, A.M., Trembath, R.C., and Shackleton, S. (2006). SUN1 interacts with nuclear lamin A and cytoplasmic nesprins to provide a physical connection between the nuclear lamina and the cytoskeleton. Molecular and cellular biology *26*, 3738-3751.

Haque, F., Mazzeo, D., Patel, J.T., Smallwood, D.T., Ellis, J.A., Shanahan, C.M., and Shackleton, S. (2010). Mammalian SUN protein interaction networks at the inner nuclear membrane and their role in laminopathy disease processes. The Journal of biological chemistry *285*, 3487-3498.

Haraguchi, T., Holaska, J.M., Yamane, M., Koujin, T., Hashiguchi, N., Mori, C., Wilson, K.L., and Hiraoka, Y. (2004). Emerin binding to Btf, a death-promoting transcriptional repressor, is disrupted by a missense mutation that causes Emery-Dreifuss muscular dystrophy. European journal of biochemistry / FEBS *271*, 1035-1045.

Harborth, J., Elbashir, S.M., Bechert, K., Tuschl, T., and Weber, K. (2001). Identification of essential genes in cultured mammalian cells using small interfering RNAs. Journal of cell science *114*, 4557-4565.

Harbury, P.B., Zhang, T., Kim, P.S., and Alber, T. (1993). A switch between two-, three-, and four-stranded coiled coils in GCN4 leucine zipper mutants. Science *262*, 1401-1407.

Hellemans, J., Preobrazhenska, O., Willaert, A., Debeer, P., Verdonk, P.C., Costa, T., Janssens, K., Menten, B., Van Roy, N., Vermeulen, S.J.*, et al.* (2004). Loss-of-function mutations in LEMD3 result in osteopoikilosis, Buschke-Ollendorff syndrome and melorheostosis. Nat Genet *36*, 1213-1218.

Helmken, C., Hofmann, Y., Schoenen, F., Oprea, G., Raschke, H., Rudnik-Schoneborn, S., Zerres, K., and Wirth, B. (2003). Evidence for a modifying pathway in SMA discordant families: reduced SMN level decreases the amount of its interacting partners and Htra2-beta1. Human genetics *114*, 11-21.

Hennekam, R.C. (2006). Hutchinson-Gilford progeria syndrome: review of the phenotype. American journal of medical genetics Part A *140*, 2603-2624.

Hernandez, L., Roux, K.J., Wong, E.S., Mounkes, L.C., Mutalif, R., Navasankari, R., Rai, B., Cool, S., Jeong, J.W., Wang, H.*, et al.* (2010). Functional coupling between the extracellular matrix and nuclear lamina by Wnt signaling in progeria. Developmental cell *19*, 413-425.

Herrmann, H., and Aebi, U. (2004). Intermediate filaments: molecular structure, assembly mechanism, and integration into functionally distinct intracellular Scaffolds. Annual review of biochemistry *73*, 749-789.

Herrmann, H., Strelkov, S.V., Burkhard, P., and Aebi, U. (2009). Intermediate filaments: primary determinants of cell architecture and plasticity. The Journal of clinical investigation *119*, 1772-1783.

Hetzer, M.W. (2010). The nuclear envelope. Cold Spring Harbor perspectives in biology *2*, a000539.

Hoffman, E.P., Brown, R.H., Jr., and Kunkel, L.M. (1987). Dystrophin: the protein product of the Duchenne muscular dystrophy locus. Cell *51*, 919-928.

Hoger, T.H., Zatloukal, K., Waizenegger, I., and Krohne, G. (1990). Characterization of a second highly conserved B-type lamin present in cells previously thought to contain only a single B-type lamin. Chromosoma *99*, 379-390.

Holaska, J.M., Lee, K.K., Kowalski, A.K., and Wilson, K.L. (2003). Transcriptional repressor germ cell-less (GCL) and barrier to autointegration factor (BAF) compete for binding to emerin in vitro. The Journal of biological chemistry *278*, 6969-6975.

Hua, Y., Sahashi, K., Hung, G., Rigo, F., Passini, M.A., Bennett, C.F., and Krainer, A.R. (2010). Antisense correction of SMN2 splicing in the CNS rescues necrosis in a type III SMA mouse model. Genes & development *24*, 1634-1644.

Hua, Y., Vickers, T.A., Okunola, H.L., Bennett, C.F., and Krainer, A.R. (2008). Antisense masking of an hnRNP A1/A2 intronic splicing silencer corrects SMN2 splicing in transgenic mice. American journal of human genetics *82*, 834-848.

Huang, S., Risques, R.A., Martin, G.M., Rabinovitch, P.S., and Oshima, J. (2008). Accelerated telomere shortening and replicative senescence in human fibroblasts overexpressing mutant and wild-type lamin A. Exp Cell Res *314*, 82-91.

Hutchinson, J. (1886). Congenital Absence of Hair and Mammary Glands with Atrophic Condition of the Skin and its Appendages, in a Boy whose Mother had been almost wholly Bald from Alopecia Areata from the age of Six. Medico-chirurgical transactions *69*, 473-477.

Huxley, A.F., and Niedergerke, R. (1954). Structural changes in muscle during contraction; interference microscopy of living muscle fibres. Nature *173*, 971-973.

Huxley, H., and Hanson, J. (1954). Changes in the cross-striations of muscle during contraction and stretch and their structural interpretation. Nature *173*, 973-976.

Ibraghimov-Beskrovnaya, O., Ervasti, J.M., Leveille, C.J., Slaughter, C.A., Sernett, S.W., and Campbell, K.P. (1992). Primary structure of dystrophin-associated glycoproteins linking dystrophin to the extracellular matrix. Nature *355*, 696-702.

Irintchev, A., Zeschnigk, M., Starzinski-Powitz, A., and Wernig, A. (1994). Expression pattern of M-cadherin in normal, denervated, and regenerating mouse muscles. Developmental dynamics : an official publication of the American Association of Anatomists *199*, 326-337.

Ishikawa, H., Bischoff, R., and Holtzer, H. (1968). Mitosis and intermediate-sized filaments in developing skeletal muscle. The Journal of cell biology *38*, 538-555.

Ivorra, C., Kubicek, M., Gonzalez, J.M., Sanz-Gonzalez, S.M., Alvarez-Barrientos, A., O'Connor, J.E., Burke, B., and Andres, V. (2006). A mechanism of AP-1 suppression through interaction of c-Fos with lamin A/C. Genes & development *20*, 307-320.

Jakobs, P.M., Hanson, E.L., Crispell, K.A., Toy, W., Keegan, H., Schilling, K., Icenogle, T.B., Litt, M., and Hershberger, R.E. (2001). Novel lamin A/C mutations in two families with dilated cardiomyopathy and conduction system disease. Journal of cardiac failure *7*, 249-256.

Janmey, P.A., Shah, J.V., Janssen, K.P., and Schliwa, M. (1998). Viscoelasticity of intermediate filament networks. Sub-cellular biochemistry *31*, 381-397.

Janssen, I., Heymsfield, S.B., Wang, Z.M., and Ross, R. (2000). Skeletal muscle mass and distribution in 468 men and women aged 18-88 yr. J Appl Physiol *89*, 81-88.

Jepsen, J.S., Sorensen, M.D., and Wengel, J. (2004). Locked nucleic acid: a potent nucleic acid analog in therapeutics and biotechnology. Oligonucleotides *14*, 130-146.

Jimenez-Escrig, A., Gobernado, I., Garcia-Villanueva, M., and Sanchez-Herranz, A. (2012). Autosomal recessive Emery-Dreifuss muscular dystrophy caused by a novel mutation (R225Q) in the lamin A/C gene identified by exome sequencing. Muscle & nerve *45*, 605-610.

Jung, H.J., Nam, K.N., Son, M.S., Kang, H., Hong, J.W., Kim, J.W., and Lee, E.H. (2011). Indirubin-3'-oxime inhibits inflammatory activation of rat brain microglia. Neuroscience letters *487*, 139-143.

Kandert, S., Wehnert, M., Muller, C.R., Buendia, B., and Dabauvalle, M.C. (2009). Impaired nuclear functions lead to increased senescence and inefficient differentiation in human myoblasts with a dominant p.R545C mutation in the LMNA gene. European journal of cell biology *88*, 593-608.

Kapinos, L.E., Burkhard, P., Herrmann, H., Aebi, U., and Strelkov, S.V. (2011). Simultaneous formation of right- and left-handed anti-parallel coiled-coil interfaces by a coil2 fragment of human lamin A. Journal of molecular biology *408*, 135-146.

Kapinos, L.E., Schumacher, J., Mucke, N., Machaidze, G., Burkhard, P., Aebi, U., Strelkov, S.V., and Herrmann, H. (2010). Characterization of the head-to-tail overlap complexes formed by human lamin A, B1 and B2 "half-minilamin" dimers. Journal of molecular biology *396*, 719-731.

Karabinos, A., Schunemann, J., Meyer, M., Aebi, U., and Weber, K. (2003). The single nuclear lamin of Caenorhabditis elegans forms in vitro stable intermediate filaments and paracrystals with a reduced axial periodicity. Journal of molecular biology *325*, 241-247.

Karkkainen, S., Helio, T., Miettinen, R., Tuomainen, P., Peltola, P., Rummukainen, J., Ylitalo, K., Kaartinen, M., Kuusisto, J., Toivonen, L.*, et al.* (2004). A novel mutation, Ser143Pro, in the lamin A/C gene is common in finnish patients with familial dilated cardiomyopathy. European heart journal *25*, 885-893.

Katz, B. (1961). The terminations of the afferent nerve fibre in the muscle spindle of the frog. Philos Trans R Soc Lond (Biol) *243*, 221-240.

Khatau, S.B., Hale, C.M., Stewart-Hutchinson, P.J., Patel, M.S., Stewart, C.L., Searson, P.C., Hodzic, D., and Wirtz, D. (2009). A perinuclear actin cap regulates nuclear shape. Proceedings of the National Academy of Sciences of the United States of America *106*, 19017-19022.

Kim, Y., Sharov, A.A., McDole, K., Cheng, M., Hao, H., Fan, C.M., Gaiano, N., Ko, M.S., and Zheng, Y. (2011). Mouse B-type lamins are required for proper organogenesis but not by embryonic stem cells. Science *334*, 1706-1710.

Koenig, M., and Kunkel, L.M. (1990). Detailed analysis of the repeat domain of dystrophin reveals four potential hinge segments that may confer flexibility. The Journal of biological chemistry *265*, 4560-4566.

Kolb, T., Maass, K., Hergt, M., Aebi, U., and Herrmann, H. (2011). Lamin A and lamin C form homodimers and coexist in higher complex forms both in the nucleoplasmic fraction and in the lamina of cultured human cells. Nucleus *2*, 425-433.

Korfali, N., Srsen, V., Waterfall, M., Batrakou, D.G., Pekovic, V., Hutchison, C.J., and Schirmer, E.C. (2011). A flow cytometry-based screen of nuclear envelope transmembrane proteins identifies NET4/Tmem53 as involved in stress-dependent cell cycle withdrawal. PloS one *6*, e18762.

Kosho, T., Takahashi, J., Momose, T., Nakamura, A., Sakurai, A., Wada, T., Yoshida, K., Wakui, K., Suzuki, T., Kasuga, K.*, et al.* (2007). Mandibuloacral dysplasia and a novel LMNA mutation in a woman with severe progressive skeletal changes. American journal of medical genetics Part A *143A*, 2598-2603.

Krimm, I., Ostlund, C., Gilquin, B., Couprie, J., Hossenlopp, P., Mornon, J.P., Bonne, G., Courvalin, J.C., Worman, H.J., and Zinn-Justin, S. (2002). The Ig-like structure of the C-terminal domain of lamin A/C, mutated in muscular dystrophies, cardiomyopathy, and partial lipodystrophy. Structure *10*, 811-823.

LaBarge, M.A., and Blau, H.M. (2002). Biological progression from adult bone marrow to mononucleate muscle stem cell to multinucleate muscle fiber in response to injury. Cell *111*, 589-601.

Lacerra, G., Sierakowska, H., Carestia, C., Fucharoen, S., Summerton, J., Weller, D., and Kole, R. (2000). Restoration of hemoglobin A synthesis in erythroid cells from peripheral blood of thalassemic patients. Proceedings of the National Academy of Sciences of the United States of America *97*, 9591-9596.

Laemmli, U.K. (1970). Cleavage of structural proteins during the assembly of the head of bacteriophage T4. Nature *227*, 680-685.

Lammerding, J., Schulze, P.C., Takahashi, T., Kozlov, S., Sullivan, T., Kamm, R.D., Stewart, C.L., and Lee, R.T. (2004). Lamin A/C deficiency causes defective nuclear mechanics and mechanotransduction. The Journal of clinical investigation *113*, 370-378.

Lander, E.S., Linton, L.M., Birren, B., Nusbaum, C., Zody, M.C., Baldwin, J., Devon, K., Dewar, K., Doyle, M., FitzHugh, W.*, et al.* (2001). Initial sequencing and analysis of the human genome. Nature *409*, 860-921.

Lee, K.K., Haraguchi, T., Lee, R.S., Koujin, T., Hiraoka, Y., and Wilson, K.L. (2001). Distinct functional domains in emerin bind lamin A and DNA-bridging protein BAF. Journal of cell science *114*, 4567-4573.

Lepper, C., Partridge, T.A., and Fan, C.M. (2011). An absolute requirement for Pax7-positive satellite cells in acute injury-induced skeletal muscle regeneration. Development *138*, 3639-3646.

Lin, F., Morrison, J.M., Wu, W., and Worman, H.J. (2005). MAN1, an integral protein of the inner nuclear membrane, binds Smad2 and Smad3 and antagonizes transforming growth factor-beta signaling. Human molecular genetics *14*, 437-445.

Lin, F., and Worman, H.J. (1993). Structural organization of the human gene encoding nuclear lamin A and nuclear lamin C. The Journal of biological chemistry *268*, 16321-16326.

Liu, B., Wang, J., Chan, K.M., Tjia, W.M., Deng, W., Guan, X., Huang, J.D., Li, K.M., Chau, P.Y., Chen, D.J.*, et al.* (2005). Genomic instability in laminopathy-based premature aging. Nature medicine *11*, 780-785.

Liu, G.H., Barkho, B.Z., Ruiz, S., Diep, D., Qu, J., Yang, S.L., Panopoulos, A.D., Suzuki, K., Kurian, L., Walsh, C.*, et al.* (2011). Recapitulation of premature ageing with iPSCs from Hutchinson-Gilford progeria syndrome. Nature *472*, 221-225.

Liu, J., Rolef Ben-Shahar, T., Riemer, D., Treinin, M., Spann, P., Weber, K., Fire, A., and Gruenbaum, Y. (2000). Essential roles for Caenorhabditis elegans lamin gene in nuclear organization, cell cycle progression, and spatial organization of nuclear pore complexes. Molecular biology of the cell *11*, 3937-3947.

Lloyd, D.J., Trembath, R.C., and Shackleton, S. (2002). A novel interaction between lamin A and SREBP1: implications for partial lipodystrophy and other laminopathies. Human molecular genetics *11*, 769-777.

Lombardi, M.L., Jaalouk, D.E., Shanahan, C.M., Burke, B., Roux, K.J., and Lammerding, J. (2011). The interaction between nesprins and sun proteins at the nuclear envelope is critical for force transmission between the nucleus and cytoskeleton. The Journal of biological chemistry *286*, 26743-26753.

Lorson, C.L., Hahnen, E., Androphy, E.J., and Wirth, B. (1999). A single nucleotide in the SMN gene regulates splicing and is responsible for spinal muscular atrophy. Proceedings of the National Academy of Sciences of the United States of America *96*, 6307-6311.

Lussi, Y.C., Hugi, I., Laurell, E., Kutay, U., and Fahrenkrog, B. (2011). The nucleoporin Nup88 is interacting with nuclear lamin A. Molecular biology of the cell *22*, 1080-1090.

Machiels, B.M., Broers, J.L., Raymond, Y., de Ley, L., Kuijpers, H.J., Caberg, N.E., and Ramaekers, F.C. (1995). Abnormal A-type lamin organization in a human lung carcinoma cell line. European journal of cell biology *67*, 328-335.

Machiels, B.M., Zorenc, A.H., Endert, J.M., Kuijpers, H.J., van Eys, G.J., Ramaekers, F.C., and Broers, J.L. (1996). An alternative splicing product of the lamin A/C gene lacks exon 10. The Journal of biological chemistry *271*, 9249-9253.

Magracheva, E., Kozlov, S., Stewart, C.L., Wlodawer, A., and Zdanov, A. (2009). Structure of the lamin A/C R482W mutant responsible for dominant familial partial lipodystrophy (FPLD). Acta crystallographica Section F, Structural biology and crystallization communications *65*, 665-670.

Mamchaoui, K., Trollet, C., Bigot, A., Negroni, E., Chaouch, S., Wolff, A., Kandalla, P.K., Marie, S., Di Santo, J., St Guily, J.L.*, et al.* (2011). Immortalized pathological human myoblasts: towards a universal tool for the study of neuromuscular disorders. Skeletal muscle *1*, 34.

Mann, C.J., Honeyman, K., Cheng, A.J., Ly, T., Lloyd, F., Fletcher, S., Morgan, J.E., Partridge, T.A., and Wilton, S.D. (2001). Antisense-induced exon skipping and synthesis of dystrophin in the mdx mouse. Proceedings of the National Academy of Sciences of the United States of America *98*, 42-47.

Mansharamani, M., and Wilson, K.L. (2005). Direct binding of nuclear membrane protein MAN1 to emerin in vitro and two modes of binding to barrier-to-autointegration factor. The Journal of biological chemistry *280*, 13863-13870.

Maquat, L.E. (2005). Nonsense-mediated mRNA decay in mammals. Journal of cell science *118*, 1773-1776.

Margalit, A., Vlcek, S., Gruenbaum, Y., and Foisner, R. (2005). Breaking and making of the nuclear envelope. Journal of cellular biochemistry *95*, 454-465.

Mariappan, I., Gurung, R., Thanumalayan, S., and Parnaik, V.K. (2007). Identification of cyclin D3 as a new interaction partner of lamin A/C. Biochemical and biophysical research communications *355*, 981-985.

Markiewicz, E., Dechat, T., Foisner, R., Quinlan, R.A., and Hutchison, C.J. (2002). Lamin A/C binding protein LAP2alpha is required for nuclear anchorage of retinoblastoma protein. Molecular biology of the cell *13*, 4401-4413.

Markiewicz, E., Ledran, M., and Hutchison, C.J. (2005). Remodelling of the nuclear lamina and nucleoskeleton is required for skeletal muscle differentiation in vitro. Journal of cell science *118*, 409-420.

Martelli, A.M., Bortul, R., Tabellini, G., Faenza, I., Cappellini, A., Bareggi, R., Manzoli, L., and Cocco, L. (2002). Molecular characterization of protein kinase C-alpha binding to lamin A. Journal of cellular biochemistry *86*, 320-330.

Martins, S.B., Eide, T., Steen, R.L., Jahnsen, T., Skalhegg, B.S., and Collas, P. (2000). HA95 is a protein of the chromatin and nuclear matrix regulating nuclear envelope dynamics. Journal of cell science *113 Pt 21*, 3703-3713.

Mason, J.M., and Arndt, K.M. (2004). Coiled coil domains: stability, specificity, and biological implications. Chembiochem : a European journal of chemical biology *5*, 170-176.

Mattioli, E., Columbaro, M., Capanni, C., Maraldi, N.M., Cenni, V., Scotlandi, K., Marino, M.T., Merlini, L., Squarzoni, S., and Lattanzi, G. (2011). Prelamin A-mediated recruitment of SUN1 to the nuclear envelope directs nuclear positioning in human muscle. Cell death and differentiation *18*, 1305-1315.

Mauro, A. (1961). Satellite cell of skeletal muscle fibers. The Journal of biophysical and biochemical cytology *9*, 493-495.

McGrath, M.J., Cottle, D.L., Nguyen, M.A., Dyson, J.M., Coghill, I.D., Robinson, P.A., Holdsworth, M., Cowling, B.S., Hardeman, E.C., Mitchell, C.A.*, et al.* (2006). Four and a half LIM protein 1 binds myosin-binding protein C and regulates myosin filament formation and sarcomere assembly. The Journal of biological chemistry *281*, 7666-7683.

McNally, E.M., and Pytel, P. (2007). Muscle diseases: the muscular dystrophies. Annual review of pathology *2*, 87-109.

Meier, M., Padilla, G.P., Herrmann, H., Wedig, T., Hergt, M., Patel, T.R., Stetefeld, J., Aebi, U., and Burkhard, P. (2009). Vimentin coil 1A-A molecular switch involved in the initiation of filament elongation. Journal of molecular biology *390*, 245-261.

Meinke, P., Nguyen, T.D., and Wehnert, M.S. (2011). The LINC complex and human disease. Biochemical Society transactions *39*, 1693-1697.

Melcon, G., Kozlov, S., Cutler, D.A., Sullivan, T., Hernandez, L., Zhao, P., Mitchell, S., Nader, G., Bakay, M., Rottman, J.N.*, et al.* (2006). Loss of emerin at the nuclear envelope disrupts the Rb1/E2F and MyoD pathways during muscle regeneration. Human molecular genetics *15*, 637-651.

Mellad, J.A., Warren, D.T., and Shanahan, C.M. (2011). Nesprins LINC the nucleus and cytoskeleton. Current opinion in cell biology *23*, 47-54.

Mercuri, E., Brown, S.C., Nihoyannopoulos, P., Poulton, J., Kinali, M., Richard, P., Piercy, R.J., Messina, S., Sewry, C., Burke, M.M., *et al.* (2005). Extreme variability of skeletal and cardiac muscle involvement in patients with mutations in exon 11 of the lamin A/C gene. Muscle & nerve *31*, 602-609.

Merideth, M.A., Gordon, L.B., Clauss, S., Sachdev, V., Smith, A.C., Perry, M.B., Brewer, C.C., Zalewski, C., Kim, H.J., Solomon, B., *et al.* (2008). Phenotype and course of Hutchinson-Gilford progeria syndrome. The New England journal of medicine *358*, 592-604.

Mical, T.I., and Monteiro, M.J. (1998). The role of sequences unique to nuclear intermediate filaments in the targeting and assembly of human lamin B: evidence for lack of interaction of lamin B with its putative receptor. Journal of cell science *111 (Pt 23)*, 3471-3485.

Mislow, J.M., Holaska, J.M., Kim, M.S., Lee, K.K., Segura-Totten, M., Wilson, K.L., and McNally, E.M. (2002). Nesprin-1alpha self-associates and binds directly to emerin and lamin A in vitro. FEBS letters *525*, 135-140.

Mittelbronn, M., Hanisch, F., Gleichmann, M., Stotter, M., Korinthenberg, R., Wehnert, M., Bonne, G., Rudnik-Schoneborn, S., and Bornemann, A. (2006). Myofiber degeneration in autosomal dominant Emery-Dreifuss muscular dystrophy (AD-EDMD) (LGMD1B). Brain Pathol *16*, 266-272.

Moir, R.D., Donaldson, A.D., and Stewart, M. (1991). Expression in Escherichia coli of human lamins A and C: influence of head and tail domains on assembly properties and paracrystal formation. Journal of cell science *99 (Pt 2)*, 363-372.

Monteiro, M.J., Hicks, C., Gu, L., and Janicki, S. (1994). Determinants for intracellular sorting of cytoplasmic and nuclear intermediate filaments. The Journal of cell biology *127*, 1327-1343.

Morgan, J.E., and Zammit, P.S. (2010). Direct effects of the pathogenic mutation on satellite cell function in muscular dystrophy. Exp Cell Res *316*, 3100-3108.

Moss, F.P., and Leblond, C.P. (1971). Satellite cells as the source of nuclei in muscles of growing rats. The Anatomical record *170*, 421-435.

Motsch, I., Kaluarachchi, M., Emerson, L.J., Brown, C.A., Brown, S.C., Dabauvalle, M.C., and Ellis, J.A. (2005). Lamins A and C are differentially dysfunctional in autosomal dominant Emery-Dreifuss muscular dystrophy. European journal of cell biology *84*, 765-781.

Moulson, C.L., Fong, L.G., Gardner, J.M., Farber, E.A., Go, G., Passariello, A., Grange, D.K., Young, S.G., and Miner, J.H. (2007). Increased progerin expression associated with unusual LMNA mutations causes severe progeroid syndromes. Human mutation *28*, 882-889.

Mounkes, L.C., Kozlov, S., Hernandez, L., Sullivan, T., and Stewart, C.L. (2003). A progeroid syndrome in mice is caused by defects in A-type lamins. Nature *423*, 298-301.

Mounkes, L.C., Kozlov, S.V., Rottman, J.N., and Stewart, C.L. (2005). Expression of an LMNA-N195K variant of A-type lamins results in cardiac conduction defects and death in mice. Human molecular genetics *14*, 2167-2180.

Muchir, A., Bonne, G., van der Kooi, A.J., van Meegen, M., Baas, F., Bolhuis, P.A., de Visser, M., and Schwartz, K. (2000). Identification of mutations in the gene encoding lamins A/C in autosomal dominant limb girdle muscular dystrophy with atrioventricular conduction disturbances (LGMD1B). Human molecular genetics *9*, 1453-1459.

Muchir, A., Medioni, J., Laluc, M., Massart, C., Arimura, T., van der Kooi, A.J., Desguerre, I., Mayer, M., Ferrer, X., Briault, S., *et al.* (2004). Nuclear envelope alterations in fibroblasts

from patients with muscular dystrophy, cardiomyopathy, and partial lipodystrophy carrying lamin A/C gene mutations. Muscle & nerve *30*, 444-450.

Muchir, A., Pavlidis, P., Bonne, G., Hayashi, Y.K., and Worman, H.J. (2007a). Activation of MAPK in hearts of EMD null mice: similarities between mouse models of X-linked and autosomal dominant Emery Dreifuss muscular dystrophy. Human molecular genetics *16*, 1884-1895.

Muchir, A., Pavlidis, P., Decostre, V., Herron, A.J., Arimura, T., Bonne, G., and Worman, H.J. (2007b). Activation of MAPK pathways links LMNA mutations to cardiomyopathy in Emery-Dreifuss muscular dystrophy. The Journal of clinical investigation *117*, 1282-1293.

Muchir, A., Shan, J., Bonne, G., Lehnart, S.E., and Worman, H.J. (2009). Inhibition of extracellular signal-regulated kinase signaling to prevent cardiomyopathy caused by mutation in the gene encoding A-type lamins. Human molecular genetics *18*, 241-247.

Muchir, A., van Engelen, B.G., Lammens, M., Mislow, J.M., McNally, E., Schwartz, K., and Bonne, G. (2003). Nuclear envelope alterations in fibroblasts from LGMD1B patients carrying nonsense Y259X heterozygous or homozygous mutation in lamin A/C gene. Exp Cell Res *291*, 352-362.

Muntoni, F., Bonne, G., Goldfarb, L.G., Mercuri, E., Piercy, R.J., Burke, M., Yaou, R.B., Richard, P., Recan, D., Shatunov, A.*, et al.* (2006). Disease severity in dominant Emery Dreifuss is increased by mutations in both emerin and desmin proteins. Brain : a journal of neurology *129*, 1260-1268.

Muntoni, F., Brown, S., Sewry, C., and Patel, K. (2002). Muscle development genes: their relevance in neuromuscular disorders. Neuromuscular disorders : NMD *12*, 438-446.

Muntoni, F., Torelli, S., and Ferlini, A. (2003). Dystrophin and mutations: one gene, several proteins, multiple phenotypes. Lancet neurology *2*, 731-740.

Muntoni, F., and Wood, M.J. (2011). Targeting RNA to treat neuromuscular disease. Nature reviews Drug discovery *10*, 621-637.

Naetar, N., Korbei, B., Kozlov, S., Kerenyi, M.A., Dorner, D., Kral, R., Gotic, I., Fuchs, P., Cohen, T.V., Bittner, R.*, et al.* (2008). Loss of nucleoplasmic LAP2alpha-lamin A complexes causes erythroid and epidermal progenitor hyperproliferation. Nature cell biology *10*, 1341-1348.

Nagano, A., Koga, R., Ogawa, M., Kurano, Y., Kawada, J., Okada, R., Hayashi, Y.K., Tsukahara, T., and Arahata, K. (1996). Emerin deficiency at the nuclear membrane in patients with Emery-Dreifuss muscular dystrophy. Nat Genet *12*, 254-259.

Navarro, C.L., De Sandre-Giovannoli, A., Bernard, R., Boccaccio, I., Boyer, A., Genevieve, D., Hadj-Rabia, S., Gaudy-Marqueste, C., Smitt, H.S., Vabres, P.*, et al.* (2004). Lamin A and ZMPSTE24 (FACE-1) defects cause nuclear disorganization and identify restrictive dermopathy as a lethal neonatal laminopathy. Human molecular genetics *13*, 2493-2503.

Nielsen, P.E., Egholm, M., Berg, R.H., and Buchardt, O. (1991). Sequence-selective recognition of DNA by strand displacement with a thymine-substituted polyamide. Science *254*, 1497-1500.

Nikolova, V., Leimena, C., McMahon, A.C., Tan, J.C., Chandar, S., Jogia, D., Kesteven, S.H., Michalicek, J., Otway, R., Verheyen, F.*, et al.* (2004). Defects in nuclear structure and function promote dilated cardiomyopathy in lamin A/C-deficient mice. The Journal of clinical investigation *113*, 357-369.

Nitta, R.T., Jameson, S.A., Kudlow, B.A., Conlan, L.A., and Kennedy, B.K. (2006). Stabilization of the retinoblastoma protein by A-type nuclear lamins is required for INK4A-mediated cell cycle arrest. Molecular and cellular biology *26*, 5360-5372.

North, A.C., Steinert, P.M., and Parry, D.A. (1994). Coiled-coil stutter and link segments in keratin and other intermediate filament molecules: a computer modeling study. Proteins *20*, 174-184.

Novelli, G., Muchir, A., Sangiuolo, F., Helbling-Leclerc, A., D'Apice, M.R., Massart, C., Capon, F., Sbraccia, P., Federici, M., Lauro, R.*, et al.* (2002). Mandibuloacral dysplasia is caused by a mutation in LMNA-encoding lamin A/C. American journal of human genetics *71*, 426-431.

Olins, A.L., Rhodes, G., Welch, D.B., Zwerger, M., and Olins, D.E. (2010). Lamin B receptor: multi-tasking at the nuclear envelope. Nucleus *1*, 53-70.

Ono, Y., Calhabeu, F., Morgan, J.E., Katagiri, T., Amthor, H., and Zammit, P.S. (2011). BMP signalling permits population expansion by preventing premature myogenic differentiation in muscle satellite cells. Cell death and differentiation *18*, 222-234.

Ostlund, C., Bonne, G., Schwartz, K., and Worman, H.J. (2001). Properties of lamin A mutants found in Emery-Dreifuss muscular dystrophy, cardiomyopathy and Dunnigan-type partial lipodystrophy. Journal of cell science *114*, 4435-4445.

Ozaki, T., Saijo, M., Murakami, K., Enomoto, H., Taya, Y., and Sakiyama, S. (1994). Complex formation between lamin A and the retinoblastoma gene product: identification of the domain on lamin A required for its interaction. Oncogene *9*, 2649-2653.

Ozawa, E., Mizuno, Y., Hagiwara, Y., Sasaoka, T., and Yoshida, M. (2005). Molecular and cell biology of the sarcoglycan complex. Muscle & nerve *32*, 563-576.

Ozawa, R., Hayashi, Y.K., Ogawa, M., Kurokawa, R., Matsumoto, H., Noguchi, S., Nonaka, I., and Nishino, I. (2006). Emerin-lacking mice show minimal motor and cardiac dysfunctions with nuclear-associated vacuoles. The American journal of pathology *168*, 907-917.

Padiath, Q.S., Saigoh, K., Schiffmann, R., Asahara, H., Yamada, T., Koeppen, A., Hogan, K., Ptacek, L.J., and Fu, Y.H. (2006). Lamin B1 duplications cause autosomal dominant leukodystrophy. Nat Genet *38*, 1114-1123.

Padmakumar, V.C., Libotte, T., Lu, W., Zaim, H., Abraham, S., Noegel, A.A., Gotzmann, J., Foisner, R., and Karakesisoglou, I. (2005). The inner nuclear membrane protein Sun1 mediates the anchorage of Nesprin-2 to the nuclear envelope. Journal of cell science *118*, 3419-3430.

Pappas, G.D. (1956). The fine structure of the nuclear envelope of Amoeba proteus. The Journal of biophysical and biochemical cytology *2*, 431-434.

Paradisi, M., McClintock, D., Boguslavsky, R.L., Pedicelli, C., Worman, H.J., and Djabali, K. (2005). Dermal fibroblasts in Hutchinson-Gilford progeria syndrome with the lamin A G608G mutation have dysmorphic nuclei and are hypersensitive to heat stress. BMC cell biology *6*, 27.

Park, J.Y., Javor, E.D., Cochran, E.K., DePaoli, A.M., and Gorden, P. (2007). Long-term efficacy of leptin replacement in patients with Dunnigan-type familial partial lipodystrophy. Metabolism: clinical and experimental *56*, 508-516.

Park, Y.E., Hayashi, Y.K., Goto, K., Komaki, H., Hayashi, Y., Inuzuka, T., Noguchi, S., Nonaka, I., and Nishino, I. (2009). Nuclear changes in skeletal muscle extend to satellite cells in autosomal dominant Emery-Dreifuss muscular dystrophy/limb-girdle muscular dystrophy 1B. Neuromuscular disorders : NMD *19*, 29-36.

Parry, D.A., Fraser, R.D., and Squire, J.M. (2008). Fifty years of coiled-coils and alpha-helical bundles: a close relationship between sequence and structure. Journal of structural biology *163*, 258-269.

Pederson, T. (2011). The nucleus introduced. Cold Spring Harbor perspectives in biology *3*.

Pekovic, V., Harborth, J., Broers, J.L., Ramaekers, F.C., van Engelen, B., Lammens, M., von Zglinicki, T., Foisner, R., Hutchison, C., and Markiewicz, E. (2007). Nucleoplasmic LAP2alpha-lamin A complexes are required to maintain a proliferative state in human fibroblasts. The Journal of cell biology *176*, 163-172.

Pendas, A.M., Zhou, Z., Cadinanos, J., Freije, J.M., Wang, J., Hultenby, K., Astudillo, A., Wernerson, A., Rodriguez, F., Tryggvason, K.*, et al.* (2002). Defective prelamin A processing and muscular and adipocyte alterations in Zmpste24 metalloproteinase-deficient mice. Nat Genet *31*, 94-99.

Perriard, J.C., Hirschy, A., and Ehler, E. (2003). Dilated cardiomyopathy: a disease of the intercalated disc? Trends in cardiovascular medicine *13*, 30-38.

Perrot, A., Hussein, S., Ruppert, V., Schmidt, H.H., Wehnert, M.S., Duong, N.T., Posch, M.G., Panek, A., Dietz, R., Kindermann, I.*, et al.* (2009). Identification of mutational hot spots in LMNA encoding lamin A/C in patients with familial dilated cardiomyopathy. Basic research in cardiology *104*, 90-99.

Peter, A., and Stick, R. (2012). Evolution of the lamin protein family: What introns can tell. Nucleus *3*.

Pethig, K., Genschel, J., Peters, T., Wilhelmi, M., Flemming, P., Lochs, H., Haverich, A., and Schmidt, H.H. (2005). LMNA mutations in cardiac transplant recipients. Cardiology *103*, 57-62.

Plasilova, M., Chattopadhyay, C., Pal, P., Schaub, N.A., Buechner, S.A., Mueller, H., Miny, P., Ghosh, A., and Heinimann, K. (2004). Homozygous missense mutation in the lamin A/C gene causes autosomal recessive Hutchinson-Gilford progeria syndrome. Journal of medical genetics *41*, 609-614.

Pros, E., Fernandez-Rodriguez, J., Canet, B., Benito, L., Sanchez, A., Benavides, A., Ramos, F.J., Lopez-Ariztegui, M.A., Capella, G., Blanco, I.*, et al.* (2009). Antisense therapeutics for neurofibromatosis type 1 caused by deep intronic mutations. Human mutation *30*, 454-462.

Puckelwartz, M.J., Kessler, E., Zhang, Y., Hodzic, D., Randles, K.N., Morris, G., Earley, J.U., Hadhazy, M., Holaska, J.M., Mewborn, S.K.*, et al.* (2009). Disruption of nesprin-1 produces an Emery Dreifuss muscular dystrophy-like phenotype in mice. Human molecular genetics *18*, 607-620.

Puttaraju, M., Jamison, S.F., Mansfield, S.G., Garcia-Blanco, M.A., and Mitchell, L.G. (1999). Spliceosome-mediated RNA trans-splicing as a tool for gene therapy. Nature biotechnology *17*, 246-252.

Quijano-Roy, S., Mbieleu, B., Bonnemann, C.G., Jeannet, P.Y., Colomer, J., Clarke, N.F., Cuisset, J.M., Roper, H., De Meirleir, L., D'Amico, A.*, et al.* (2008). De novo LMNA mutations cause a new form of congenital muscular dystrophy. Annals of neurology *64*, 177-186.

Raffaele Di Barletta, M., Ricci, E., Galluzzi, G., Tonali, P., Mora, M., Morandi, L., Romorini, A., Voit, T., Orstavik, K.H., Merlini, L.*, et al.* (2000). Different mutations in the LMNA gene cause autosomal dominant and autosomal recessive Emery-Dreifuss muscular dystrophy. American journal of human genetics *66*, 1407-1412.

Raharjo, W.H., Enarson, P., Sullivan, T., Stewart, C.L., and Burke, B. (2001). Nuclear envelope defects associated with LMNA mutations cause dilated cardiomyopathy and Emery-Dreifuss muscular dystrophy. Journal of cell science *114*, 4447-4457.

Rajendran, V., Purohit, R., and Sethumadhavan, R. (2011). In silico investigation of molecular mechanism of laminopathy caused by a point mutation (R482W) in lamin A/C protein. Amino acids.

Rankin, J., Auer-Grumbach, M., Bagg, W., Colclough, K., Nguyen, T.D., Fenton-May, J., Hattersley, A., Hudson, J., Jardine, P., Josifova, D.*, et al.* (2008). Extreme phenotypic diversity and nonpenetrance in families with the LMNA gene mutation R644C. American journal of medical genetics Part A *146A*, 1530-1542.

Razafsky, D., and Hodzic, D. (2009). Bringing KASH under the SUN: the many faces of nucleo-cytoskeletal connections. The Journal of cell biology *186*, 461-472.

Rebbapragada, I., and Lykke-Andersen, J. (2009). Execution of nonsense-mediated mRNA decay: what defines a substrate? Current opinion in cell biology *21*, 394-402.

Relaix, F., Rocancourt, D., Mansouri, A., and Buckingham, M. (2004). Divergent functions of murine Pax3 and Pax7 in limb muscle development. Genes & development *18*, 1088-1105.

Renou, L., Stora, S., Yaou, R.B., Volk, M., Sinkovec, M., Demay, L., Richard, P., Peterlin, B., and Bonne, G. (2008). Heart-hand syndrome of Slovenian type: a new kind of laminopathy. Journal of medical genetics *45*, 666-671.

Rincon, A., Aguado, C., Desviat, L.R., Sanchez-Alcudia, R., Ugarte, M., and Perez, B. (2007). Propionic and methylmalonic acidemia: antisense therapeutics for intronic variations causing aberrantly spliced messenger RNA. American journal of human genetics *81*, 1262-1270.

Rosenblatt, J.D., Lunt, A.I., Parry, D.J., and Partridge, T.A. (1995). Culturing satellite cells from living single muscle fiber explants. In vitro cellular & developmental biology Animal *31*, 773-779.

Roux, K.J., Crisp, M.L., Liu, Q., Kim, D., Kozlov, S., Stewart, C.L., and Burke, B. (2009). Nesprin 4 is an outer nuclear membrane protein that can induce kinesin-mediated cell polarization. Proceedings of the National Academy of Sciences of the United States of America *106*, 2194-2199.

Rudnik-Schoneborn, S., Botzenhart, E., Eggermann, T., Senderek, J., Schoser, B.G., Schroder, R., Wehnert, M., Wirth, B., and Zerres, K. (2007). Mutations of the LMNA gene can mimic autosomal dominant proximal spinal muscular atrophy. Neurogenetics *8*, 137-142.

Rybakova, I.N., Patel, J.R., and Ervasti, J.M. (2000). The dystrophin complex forms a mechanically strong link between the sarcolemma and costameric actin. The Journal of cell biology *150*, 1209-1214.

Sacco, A., Mourkioti, F., Tran, R., Choi, J., Llewellyn, M., Kraft, P., Shkreli, M., Delp, S., Pomerantz, J.H., Artandi, S.E.*, et al.* (2010). Short telomeres and stem cell exhaustion model Duchenne muscular dystrophy in mdx/mTR mice. Cell *143*, 1059-1071.

Sakaki, M., Koike, H., Takahashi, N., Sasagawa, N., Tomioka, S., Arahata, K., and Ishiura, S. (2001). Interaction between emerin and nuclear lamins. Journal of biochemistry *129*, 321-327.

Sasseville, A.M., and Langelier, Y. (1998). In vitro interaction of the carboxy-terminal domain of lamin A with actin. FEBS letters *425*, 485-489.

Savage, D.B., Soos, M.A., Powlson, A., O'Rahilly, S., McFarlane, I., Halsall, D.J., Barroso, I., Thomas, E.L., Bell, J.D., Scobie, I.*, et al.* (2004). Familial partial lipodystrophy associated with compound heterozygosity for novel mutations in the LMNA gene. Diabetologia *47*, 753-756.

Scaffidi, P., and Misteli, T. (2005). Reversal of the cellular phenotype in the premature aging disease Hutchinson-Gilford progeria syndrome. Nature medicine *11*, 440-445.

Scharner, J., Brown, C.A., Bower, M., Iannaccone, S.T., Khatri, I.A., Escolar, D., Gordon, E., Felice, K., Crowe, C.A., Grosmann, C.*, et al.* (2011). Novel LMNA mutations in patients with Emery-Dreifuss muscular dystrophy and functional characterization of four LMNA mutations. Human mutation *32*, 152-167.

Scharner, J., Gnocchi, V.F., Ellis, J.A., and Zammit, P.S. (2010). Genotype-phenotype correlations in laminopathies: how does fate translate? Biochemical Society transactions *38*, 257-262.

Scharner, J., and Zammit, P.S. (2011). The muscle satellite cell at 50: the formative years. Skeletal muscle *1*, 28.

Schiaffino, S., and Reggiani, C. (2011). Fiber types in mammalian skeletal muscles. Physiological reviews *91*, 1447-1531.

Schirmer, E.C., Florens, L., Guan, T., Yates, J.R., 3rd, and Gerace, L. (2003). Nuclear membrane proteins with potential disease links found by subtractive proteomics. Science *301*, 1380-1382.

Schirmer, E.C., Guan, T., and Gerace, L. (2001). Involvement of the lamin rod domain in heterotypic lamin interactions important for nuclear organization. The Journal of cell biology *153*, 479-489.

Schmidt, W.K., Tam, A., Fujimura-Kamada, K., and Michaelis, S. (1998). Endoplasmic reticulum membrane localization of Rce1p and Ste24p, yeast proteases involved in carboxyl-terminal CAAX protein processing and amino-terminal a-factor cleavage. Proceedings of the National Academy of Sciences of the United States of America *95*, 11175-11180.

Schultz, E., Gibson, M.C., and Champion, T. (1978). Satellite cells are mitotically quiescent in mature mouse muscle: an EM and radioautographic study. The Journal of experimental zoology *206*, 451-456.

Seale, P., Sabourin, L.A., Girgis-Gabardo, A., Mansouri, A., Gruss, P., and Rudnicki, M.A. (2000). Pax7 is required for the specification of myogenic satellite cells. Cell *102*, 777-786.

Sewry, C.A., Brown, S.C., Mercuri, E., Bonne, G., Feng, L., Camici, G., Morris, G.E., and Muntoni, F. (2001). Skeletal muscle pathology in autosomal dominant Emery-Dreifuss muscular dystrophy with lamin A/C mutations. Neuropathology and applied neurobiology *27*, 281-290.

Shackleton, S., Lloyd, D.J., Jackson, S.N., Evans, R., Niermeijer, M.F., Singh, B.M., Schmidt, H., Brabant, G., Kumar, S., Durrington, P.N.*, et al.* (2000). LMNA, encoding lamin A/C, is mutated in partial lipodystrophy. Nat Genet *24*, 153-156.

Shackleton, S., Smallwood, D.T., Clayton, P., Wilson, L.C., Agarwal, A.K., Garg, A., and Trembath, R.C. (2005). Compound heterozygous ZMPSTE24 mutations reduce prelamin A processing and result in a severe progeroid phenotype. Journal of medical genetics *42*, e36.

Shimi, T., Pfleghaar, K., Kojima, S., Pack, C.G., Solovei, I., Goldman, A.E., Adam, S.A., Shumaker, D.K., Kinjo, M., Cremer, T.*, et al.* (2008). The A- and B-type nuclear lamin networks: microdomains involved in chromatin organization and transcription. Genes & development *22*, 3409-3421.

Shumaker, D.K., Lee, K.K., Tanhehco, Y.C., Craigie, R., and Wilson, K.L. (2001). LAP2 binds to BAF.DNA complexes: requirement for the LEM domain and modulation by variable regions. The EMBO journal *20*, 1754-1764.

Shumaker, D.K., Lopez-Soler, R.I., Adam, S.A., Herrmann, H., Moir, R.D., Spann, T.P., and Goldman, R.D. (2005). Functions and dysfunctions of the nuclear lamin Ig-fold domain in nuclear assembly, growth, and Emery-Dreifuss muscular dystrophy. Proceedings of the National Academy of Sciences of the United States of America *102*, 15494-15499.

Shumaker, D.K., Solimando, L., Sengupta, K., Shimi, T., Adam, S.A., Grunwald, A., Strelkov, S.V., Aebi, U., Cardoso, M.C., and Goldman, R.D. (2008). The highly conserved nuclear lamin Ig-fold binds to PCNA: its role in DNA replication. The Journal of cell biology *181*, 269-280.

Simha, V., Agarwal, A.K., Oral, E.A., Fryns, J.P., and Garg, A. (2003). Genetic and phenotypic heterogeneity in patients with mandibuloacral dysplasia-associated lipodystrophy. The Journal of clinical endocrinology and metabolism *88*, 2821-2824.

Simon, D.N., Zastrow, M.S., and Wilson, K.L. (2010). Direct actin binding to A- and B-type lamin tails and actin filament bundling by the lamin A tail. Nucleus *1*, 264-272.

Smith, T.A., Strelkov, S.V., Burkhard, P., Aebi, U., and Parry, D.A. (2002). Sequence comparisons of intermediate filament chains: evidence of a unique functional/structural role for coiled-coil segment 1A and linker L1. Journal of structural biology *137*, 128-145.

Sparrow, J.C., and Schock, F. (2009). The initial steps of myofibril assembly: integrins pave the way. Nature reviews Molecular cell biology *10*, 293-298.

Steen, R.L., and Collas, P. (2001). Mistargeting of B-type lamins at the end of mitosis: implications on cell survival and regulation of lamins A/C expression. The Journal of cell biology *153*, 621-626.

Stenson, P.D., Mort, M., Ball, E.V., Howells, K., Phillips, A.D., Thomas, N.S., and Cooper, D.N. (2009). The Human Gene Mutation Database: 2008 update. Genome medicine *1*, 13.

Stewart, C., and Burke, B. (1987). Teratocarcinoma stem cells and early mouse embryos contain only a single major lamin polypeptide closely resembling lamin B. Cell *51*, 383-392.

Stierle, V., Couprie, J., Ostlund, C., Krimm, I., Zinn-Justin, S., Hossenlopp, P., Worman, H.J., Courvalin, J.C., and Duband-Goulet, I. (2003). The carboxyl-terminal region common to lamins A and C contains a DNA binding domain. Biochemistry *42*, 4819-4828.

Straub, V., Rafael, J.A., Chamberlain, J.S., and Campbell, K.P. (1997). Animal models for muscular dystrophy show different patterns of sarcolemmal disruption. The Journal of cell biology *139*, 375-385.

Strelkov, S.V., Schumacher, J., Burkhard, P., Aebi, U., and Herrmann, H. (2004). Crystal structure of the human lamin A coil 2B dimer: implications for the head-to-tail association of nuclear lamins. Journal of molecular biology *343*, 1067-1080.

Stuurman, N., Heins, S., and Aebi, U. (1998). Nuclear lamins: their structure, assembly, and interactions. Journal of structural biology *122*, 42-66.

Sullivan, T., Escalante-Alcalde, D., Bhatt, H., Anver, M., Bhat, N., Nagashima, K., Stewart, C.L., and Burke, B. (1999). Loss of A-type lamin expression compromises nuclear envelope integrity leading to muscular dystrophy. The Journal of cell biology *147*, 913-920.

Sylvius, N., Bonne, G., Straatman, K., Reddy, T., Gant, T.W., and Shackleton, S. (2011). MicroRNA expression profiling in patients with lamin A/C-associated muscular dystrophy. FASEB journal : official publication of the Federation of American Societies for Experimental Biology *25*, 3966-3978.

Szeverenyi, I., Cassidy, A.J., Chung, C.W., Lee, B.T., Common, J.E., Ogg, S.C., Chen, H., Sim, S.Y., Goh, W.L., Ng, K.W.*, et al.* (2008). The Human Intermediate Filament Database: comprehensive information on a gene family involved in many human diseases. Human mutation *29*, 351-360.

Taimen, P., Pfleghaar, K., Shimi, T., Moller, D., Ben-Harush, K., Erdos, M.R., Adam, S.A., Herrmann, H., Medalia, O., Collins, F.S.*, et al.* (2009). A progeria mutation reveals functions for lamin A in nuclear assembly, architecture, and chromosome organization. Proceedings of the National Academy of Sciences of the United States of America *106*, 20788-20793.

Tamaki, T., Akatsuka, A., Ando, K., Nakamura, Y., Matsuzawa, H., Hotta, T., Roy, R.R., and Edgerton, V.R. (2002). Identification of myogenic-endothelial progenitor cells in the interstitial spaces of skeletal muscle. The Journal of cell biology *157*, 571-577.

Taranum, S., Vaylann, E., Meinke, P., Abraham, S., Yang, L., Neumann, S., Karakesisoglou, I., Wehnert, M., and Noegel, A.A. (2012). LINC complex alterations in DMD and EDMD/CMT fibroblasts. European journal of cell biology *article in press (doi 10.1016/j.ejcb.2012.03.003)*.

Tatsumi, R., and Allen, R.E. (2004). Active hepatocyte growth factor is present in skeletal muscle extracellular matrix. Muscle & nerve *30*, 654-658.

Tatsumi, R., Anderson, J.E., Nevoret, C.J., Halevy, O., and Allen, R.E. (1998). HGF/SF is present in normal adult skeletal muscle and is capable of activating satellite cells. Developmental biology *194*, 114-128.

Taylor, M.R., Fain, P.R., Sinagra, G., Robinson, M.L., Robertson, A.D., Carniel, E., Di Lenarda, A., Bohlmeyer, T.J., Ferguson, D.A., Brodsky, G.L.*, et al.* (2003). Natural history of dilated cardiomyopathy due to lamin A/C gene mutations. Journal of the American College of Cardiology *41*, 771-780.

Tazir, M., Azzedine, H., Assami, S., Sindou, P., Nouioua, S., Zemmouri, R., Hamadouche, T., Chaouch, M., Feingold, J., Vallat, J.M.*, et al.* (2004). Phenotypic variability in autosomal recessive axonal Charcot-Marie-Tooth disease due to the R298C mutation in lamin A/C. Brain : a journal of neurology *127*, 154-163.

Teplova, M., Minasov, G., Tereshko, V., Inamati, G.B., Cook, P.D., Manoharan, M., and Egli, M. (1999). Crystal structure and improved antisense properties of 2'-O-(2-methoxyethyl)-RNA. Nature structural biology *6*, 535-539.

Toth, J.I., Yang, S.H., Qiao, X., Beigneux, A.P., Gelb, M.H., Moulson, C.L., Miner, J.H., Young, S.G., and Fong, L.G. (2005). Blocking protein farnesyltransferase improves nuclear shape in fibroblasts from humans with progeroid syndromes. Proceedings of the National Academy of Sciences of the United States of America *102*, 12873-12878.

Tsai, M.Y., Wang, S., Heidinger, J.M., Shumaker, D.K., Adam, S.A., Goldman, R.D., and Zheng, Y. (2006). A mitotic lamin B matrix induced by RanGTP required for spindle assembly. Science *311*, 1887-1893.

Tzur, Y.B., Wilson, K.L., and Gruenbaum, Y. (2006). SUN-domain proteins: 'Velcro' that links the nucleoskeleton to the cytoskeleton. Nature reviews Molecular cell biology *7*, 782-788.

Ulbert, S., Platani, M., Boue, S., and Mattaj, I.W. (2006). Direct membrane protein-DNA interactions required early in nuclear envelope assembly. The Journal of cell biology *173*, 469-476.

Van Berlo, J.H., Voncken, J.W., Kubben, N., Broers, J.L., Duisters, R., van Leeuwen, R.E., Crijns, H.J., Ramaekers, F.C., Hutchison, C.J., and Pinto, Y.M. (2005). A-type lamins are essential

for TGF-beta1 induced PP2A to dephosphorylate transcription factors. Human molecular genetics *14*, 2839-2849.

van der Kooi, A.J., Bonne, G., Eymard, B., Duboc, D., Talim, B., Van der Valk, M., Reiss, P., Richard, P., Demay, L., Merlini, L.*, et al.* (2002). Lamin A/C mutations with lipodystrophy, cardiac abnormalities, and muscular dystrophy. Neurology *59*, 620-623.

van der Kooi, A.J., van Meegen, M., Ledderhof, T.M., McNally, E.M., de Visser, M., and Bolhuis, P.A. (1997). Genetic localization of a newly recognized autosomal dominant limb-girdle muscular dystrophy with cardiac involvement (LGMD1B) to chromosome 1q11-21. American journal of human genetics *60*, 891-895.

van Engelen, B.G., Muchir, A., Hutchison, C.J., van der Kooi, A.J., Bonne, G., and Lammens, M. (2005). The lethal phenotype of a homozygous nonsense mutation in the lamin A/C gene. Neurology *64*, 374-376.

van Tintelen, J.P., Tio, R.A., Kerstjens-Frederikse, W.S., van Berlo, J.H., Boven, L.G., Suurmeijer, A.J., White, S.J., den Dunnen, J.T., te Meerman, G.J., Vos, Y.J.*, et al.* (2007). Severe myocardial fibrosis caused by a deletion of the 5' end of the lamin A/C gene. Journal of the American College of Cardiology *49*, 2430-2439.

Vaughan, A., Alvarez-Reyes, M., Bridger, J.M., Broers, J.L., Ramaekers, F.C., Wehnert, M., Morris, G.E., Whitfield, W.G.F., and Hutchison, C.J. (2001). Both emerin and lamin C depend on lamin A for localization at the nuclear envelope. Journal of cell science *114*, 2577-2590.

Venables, R.S., McLean, S., Luny, D., Moteleb, E., Morley, S., Quinlan, R.A., Lane, E.B., and Hutchison, C.J. (2001). Expression of individual lamins in basal cell carcinomas of the skin. British journal of cancer *84*, 512-519.

Vergnes, L., Peterfy, M., Bergo, M.O., Young, S.G., and Reue, K. (2004). Lamin B1 is required for mouse development and nuclear integrity. Proceedings of the National Academy of Sciences of the United States of America *101*, 10428-10433.

Verstraeten, V.L., Broers, J.L., van Steensel, M.A., Zinn-Justin, S., Ramaekers, F.C., Steijlen, P.M., Kamps, M., Kuijpers, H.J., Merckx, D., Smeets, H.J.*, et al.* (2006). Compound heterozygosity for mutations in LMNA causes a progeria syndrome without prelamin A accumulation. Human molecular genetics *15*, 2509-2522.

Vigouroux, C., Auclair, M., Dubosclard, E., Pouchelet, M., Capeau, J., Courvalin, J.C., and Buendia, B. (2001). Nuclear envelope disorganization in fibroblasts from lipodystrophic patients with heterozygous R482Q/W mutations in the lamin A/C gene. Journal of cell science *114*, 4459-4468.

Vorburger, K., Kitten, G.T., and Nigg, E.A. (1989). Modification of nuclear lamin proteins by a mevalonic acid derivative occurs in reticulocyte lysates and requires the cysteine residue of the C-terminal CXXM motif. The EMBO journal *8*, 4007-4013.

Vytopil, M., Benedetti, S., Ricci, E., Galluzzi, G., Dello Russo, A., Merlini, L., Boriani, G., Gallina, M., Morandi, L., Politano, L.*, et al.* (2003). Mutation analysis of the lamin A/C gene (LMNA) among patients with different cardiomuscular phenotypes. Journal of medical genetics *40*, e132.

Vytopil, M., Ricci, E., Dello Russo, A., Hanisch, F., Neudecker, S., Zierz, S., Ricotti, R., Demay, L., Richard, P., Wehnert, M.*, et al.* (2002). Frequent low penetrance mutations in the Lamin A/C gene, causing Emery Dreifuss muscular dystrophy. Neuromuscular disorders : NMD *12*, 958-963.

Watson, J.V., Chambers, S.H., and Smith, P.J. (1987). A pragmatic approach to the analysis of DNA histograms with a definable G1 peak. Cytometry *8*, 1-8.

Webb, R.C. (2003). Smooth muscle contraction and relaxation. Advances in physiology education *27*, 201-206.

Weber, K., Plessmann, U., Dodemont, H., and Kossmagk-Stephan, K. (1988). Amino acid sequences and homopolymer-forming ability of the intermediate filament proteins from an invertebrate epithelium. The EMBO journal *7*, 2995-3001.

Weber, K., Plessmann, U., and Ulrich, W. (1989). Cytoplasmic intermediate filament proteins of invertebrates are closer to nuclear lamins than are vertebrate intermediate filament proteins; sequence characterization of two muscle proteins of a nematode. The EMBO journal *8*, 3221-3227.

Webster, C., and Blau, H.M. (1990). Accelerated age-related decline in replicative life-span of Duchenne muscular dystrophy myoblasts: implications for cell and gene therapy. Somatic cell and molecular genetics *16*, 557-565.

Wente, S.R., and Rout, M.P. (2010). The nuclear pore complex and nuclear transport. Cold Spring Harbor perspectives in biology *2*, a000562.

Wiesel, N., Mattout, A., Melcer, S., Melamed-Book, N., Herrmann, H., Medalia, O., Aebi, U., and Gruenbaum, Y. (2008). Laminopathic mutations interfere with the assembly, localization, and dynamics of nuclear lamins. Proceedings of the National Academy of Sciences of the United States of America *105*, 180-185.

Wilhelmsen, K., Litjens, S.H., Kuikman, I., Tshimbalanga, N., Janssen, H., van den Bout, I., Raymond, K., and Sonnenberg, A. (2005). Nesprin-3, a novel outer nuclear membrane protein, associates with the cytoskeletal linker protein plectin. The Journal of cell biology *171*, 799-810.

Willis, N.D., Cox, T.R., Rahman-Casans, S.F., Smits, K., Przyborski, S.A., van den Brandt, P., van Engeland, M., Weijenberg, M., Wilson, R.G., de Bruine, A.*, et al.* (2008). Lamin A/C is a risk biomarker in colorectal cancer. PloS one *3*, e2988.

Wilson, K.L., and Foisner, R. (2010). Lamin-binding Proteins. Cold Spring Harbor perspectives in biology *2*, a000554.

Wolf, C.M., Wang, L., Alcalai, R., Pizard, A., Burgon, P.G., Ahmad, F., Sherwood, M., Branco, D.M., Wakimoto, H., Fishman, G.I.*, et al.* (2008). Lamin A/C haploinsufficiency causes dilated cardiomyopathy and apoptosis-triggered cardiac conduction system disease. Journal of molecular and cellular cardiology *44*, 293-303.

Worman, H.J. (2012). Nuclear lamins and laminopathies. The Journal of pathology *226*, 316-325.

Worman, H.J., and Bonne, G. (2007). "Laminopathies": a wide spectrum of human diseases. Exp Cell Res *313*, 2121-2133.

Worman, H.J., Evans, C.D., and Blobel, G. (1990). The lamin B receptor of the nuclear envelope inner membrane: a polytopic protein with eight potential transmembrane domains. The Journal of cell biology *111*, 1535-1542.

Worman, H.J., Fong, L.G., Muchir, A., and Young, S.G. (2009). Laminopathies and the long strange trip from basic cell biology to therapy. The Journal of clinical investigation *119*, 1825-1836.

Wu, B., Moulton, H.M., Iversen, P.L., Jiang, J., Li, J., Spurney, C.F., Sali, A., Guerron, A.D., Nagaraju, K., Doran, T.*, et al.* (2008). Effective rescue of dystrophin improves cardiac function in dystrophin-deficient mice by a modified morpholino oligomer. Proceedings of the National Academy of Sciences of the United States of America *105*, 14814-14819.

Wu, W., Muchir, A., Shan, J., Bonne, G., and Worman, H.J. (2011). Mitogen-activated protein kinase inhibitors improve heart function and prevent fibrosis in cardiomyopathy caused by mutation in lamin A/C gene. Circulation *123*, 53-61.

Wydner, K.L., McNeil, J.A., Lin, F., Worman, H.J., and Lawrence, J.B. (1996). Chromosomal assignment of human nuclear envelope protein genes LMNA, LMNB1, and LBR by fluorescence in situ hybridization. Genomics *32*, 474-478.

Xu, J. (2005). Preparation, culture, and immortalization of mouse embryonic fibroblasts. Current protocols in molecular biology / edited by Frederick M Ausubel [et al] *Chapter 28*, Unit 28 21.

Yaffe, D., and Saxel, O. (1977). Serial passaging and differentiation of myogenic cells isolated from dystrophic mouse muscle. Nature *270*, 725-727.

Yang, S.H., Bergo, M.O., Toth, J.I., Qiao, X., Hu, Y., Sandoval, S., Meta, M., Bendale, P., Gelb, M.H., Young, S.G.*, et al.* (2005). Blocking protein farnesyltransferase improves nuclear blebbing in mouse fibroblasts with a targeted Hutchinson-Gilford progeria syndrome mutation. Proceedings of the National Academy of Sciences of the United States of America *102*, 10291-10296.

Yang, S.H., Chang, S.Y., Yin, L., Tu, Y., Hu, Y., Yoshinaga, Y., de Jong, P.J., Fong, L.G., and Young, S.G. (2011). An absence of both lamin B1 and lamin B2 in keratinocytes has no effect on cell proliferation or the development of skin and hair. Human molecular genetics *20*, 3537-3544.

Yang, S.H., Meta, M., Qiao, X., Frost, D., Bauch, J., Coffinier, C., Majumdar, S., Bergo, M.O., Young, S.G., and Fong, L.G. (2006). A farnesyltransferase inhibitor improves disease phenotypes in mice with a Hutchinson-Gilford progeria syndrome mutation. The Journal of clinical investigation *116*, 2115-2121.

Yates, J.R., and Wehnert, M. (1999). The Emery-Dreifuss Muscular Dystrophy Mutation Database. Neuromuscular disorders : NMD *9*, 199.

Ye, Q., Callebaut, I., Pezhman, A., Courvalin, J.C., and Worman, H.J. (1997). Domain-specific interactions of human HP1-type chromodomain proteins and inner nuclear membrane protein LBR. The Journal of biological chemistry *272*, 14983-14989.

Ye, Q., and Worman, H.J. (1994). Primary structure analysis and lamin B and DNA binding of human LBR, an integral protein of the nuclear envelope inner membrane. The Journal of biological chemistry *269*, 11306-11311.

Ye, Q., and Worman, H.J. (1996). Interaction between an integral protein of the nuclear envelope inner membrane and human chromodomain proteins homologous to Drosophila HP1. The Journal of biological chemistry *271*, 14653-14656.

Yin, H., Moulton, H.M., Betts, C., Seow, Y., Boutilier, J., Iverson, P.L., and Wood, M.J. (2009). A fusion peptide directs enhanced systemic dystrophin exon skipping and functional restoration in dystrophin-deficient mdx mice. Human molecular genetics *18*, 4405-4414.

Yin, H., Moulton, H.M., Seow, Y., Boyd, C., Boutilier, J., Iverson, P., and Wood, M.J. (2008). Cell-penetrating peptide-conjugated antisense oligonucleotides restore systemic muscle and cardiac dystrophin expression and function. Human molecular genetics *17*, 3909-3918.

Youn, G.J., Uzunyan, M., Vachon, L., Johnson, J., Winder, T.L., and Yano, S. (2010). Autosomal recessive LMNA mutation causing restrictive dermopathy. Clinical genetics *78*, 199-200.

Zammit, P.S. (2008). All muscle satellite cells are equal, but are some more equal than others? Journal of cell science *121*, 2975-2982.

Zammit, P.S., Golding, J.P., Nagata, Y., Hudon, V., Partridge, T.A., and Beauchamp, J.R. (2004). Muscle satellite cells adopt divergent fates: a mechanism for self-renewal? The Journal of cell biology *166*, 347-357.

Zammit, P.S., Partridge, T.A., and Yablonka-Reuveni, Z. (2006a). The skeletal muscle satellite cell: the stem cell that came in from the cold. J Histochem Cytochem *54*, 1177-1191.

Zammit, P.S., Relaix, F., Nagata, Y., Ruiz, A.P., Collins, C.A., Partridge, T.A., and Beauchamp, J.R. (2006b). Pax7 and myogenic progression in skeletal muscle satellite cells. Journal of cell science *119*, 1824-1832.

Zastrow, M.S., Vlcek, S., and Wilson, K.L. (2004). Proteins that bind A-type lamins: integrating isolated clues. Journal of cell science *117*, 979-987.

Zhang, F.L., and Casey, P.J. (1996). Protein prenylation: molecular mechanisms and functional consequences. Annual review of biochemistry *65*, 241-269.

Zhang, J., Felder, A., Liu, Y., Guo, L.T., Lange, S., Dalton, N.D., Gu, Y., Peterson, K.L., Mizisin, A.P., Shelton, G.D.*, et al.* (2010). Nesprin 1 is critical for nuclear positioning and anchorage. Human molecular genetics *19*, 329-341.

Zhang, J., Lian, Q., Zhu, G., Zhou, F., Sui, L., Tan, C., Mutalif, R.A., Navasankari, R., Zhang, Y., Tse, H.F.*, et al.* (2011). A human iPSC model of Hutchinson Gilford Progeria reveals vascular smooth muscle and mesenchymal stem cell defects. Cell stem cell *8*, 31-45.

Zhang, Q., Bethmann, C., Worth, N.F., Davies, J.D., Wasner, C., Feuer, A., Ragnauth, C.D., Yi, Q., Mellad, J.A., Warren, D.T.*, et al.* (2007). Nesprin-1 and -2 are involved in the pathogenesis of Emery Dreifuss muscular dystrophy and are critical for nuclear envelope integrity. Human molecular genetics *16*, 2816-2833.

Zhang, Q., Ragnauth, C.D., Skepper, J.N., Worth, N.F., Warren, D.T., Roberts, R.G., Weissberg, P.L., Ellis, J.A., and Shanahan, C.M. (2005). Nesprin-2 is a multi-isomeric protein that binds lamin and emerin at the nuclear envelope and forms a subcellular network in skeletal muscle. Journal of cell science *118*, 673-687.

Zhen, Y.Y., Libotte, T., Munck, M., Noegel, A.A., and Korenbaum, E. (2002). NUANCE, a giant protein connecting the nucleus and actin cytoskeleton. Journal of cell science *115*, 3207-3222.

Appendix 1: Sequence alignment of intermediate filament central rod domains

The central rod domain of eight different human intermediate filament proteins is shown. The sequences were obtained from the UniProt protein sequence database (www.uniprot.org) and aligned using the free online tool Clustal2W (available at: www.ebi.ac.uk/Tools/msa/clustalw2). Coils 1a, 1b, 2a and 2b as well as linker regions L1, L12 and L2 are indicated above the sequence. The heptad repeat position for each residue (a-g) is indicated as well. The sequence encoded by *LMNA* exons 3 or 5 is highlighted in red; NF-L, Neurofilament light; (.) semi-conserved; (:) conserved; (*) identical.

Appendix 2: Alignment of the lamin A protein sequence from three different species

```
                                  Head <---|_________________Coil 1a_______________|     L1     |_______________________________________________
Homo sapiens       METPSQRRATRSGAQASSTPLSPTRITRLQEKEDLQELNDRLAVYIDRVRSLETENAGLRLRITESEEVVSREVSGIKAAYEAELGDARKTLDSVAKERARLQLELSKVREEFKELKARN 120
Mus musculus       METPSQRRATRSGAQASSTPLSPTRITRLQEKEDLQELNDRLAVYIDRVRSLETENAGLRLRITESEEVVSREVSGIKAAYEAELGDARKTLDSVAKERARLQLELSKVREEFKELKARN 120
Xenopus laevis     METPGQKRATRS----THTPLSPTRITRLQEKEDLQGLNDRLAVYIDKVRSLELENARLRLRITESEDVISREVTGIKSAYETELADARKTLDSVAKERARLQLELSKIREEHKELKARN 116
                   ****.*:*****    : ****************** **********:***** *** *********:*:****:***:***:**.*********************:***.*******

                   ____________________________________Coil 1b_________________________________________________________|        L12        |
Homo sapiens       TKKEGDLIAAQARLKDLEALLNSKEAALSTALSEKRTLEGELHDLRGQVAKLEAALGEAKKQLQDEMLRRVDAENRLQTMKEELDFQKNIYSEELRETKRRHETRLVEIDNGKQREFESR 240
Mus musculus       TKKEGDLLAAQARLKDLEALLNSKEAALSTALSEKRTLEGELHDLRGQVAKLEAALGEAKKQLQDEMLRRVDAENRLQTLKEELDFQKNIYSEELRETKRRHETRLVEIDNGKQREFESR 240
Xenopus laevis     AKKESDLLTAQARLKDLEALLNSKDAALTTALGEKRNLENEIRELKAHIAKLEASLADTKKQLQDEMLRRVDTENRNQTLKEELEFQKSIYNEEMRETKRRHETRLVEVDNGRQREFESK 236
                   :***.**::**************:***:***.***.**.*:::*:.::*****:*.::*************:***  **:****:***.**.**:*************:***:******:

                   ____Coil 2a_____|   L2   |______________________________________Coil 2B______________________________________________________
Homo sapiens       LADALQELRAQHEDQVEQYKKELEKTYSAKLDNARQSAERNSNLVGAAHEELQQSRIRIDSLSAQLSQLQKQLAAKEAKLRDLEDSLARERDTSRRLLAEKEREMAEMRARMQQQLDEYQ 360
Mus musculus       LADALQELRAQHEDQVEQYKKELEKTYSAKLDNARQSAERNSNLVGAAHEELQQSRIRIDSLSAQLSQLQKQLAAKEAKLRDLEDSLARERDTSRRLLAEKEREMAEMRARMQQQLDEYQ 360
Xenopus laevis     LADALHELRAQHEGQIGLYKEELGKTYNAKLENAKQSAERNSSLVGEAQEEIQQSRIRIDSLSAQLSQLQKQLAAREAKLRDLEDAYARERDSSRRLLADKDREMAEMRARMQQQLDEYQ 356
                   *****:*******.*:  **:** ***.***:**:*******.*** *:**:**********************:*********:  *****:******:*:*****************

                   _____________________|---> Tail                                      |--->                        Ig-fold domain
Homo sapiens       ELLDIKLALDMEIHAYRKLLEGEEERLRLSPSPTSQ-RSRGRASSHSSQTQGGGSVTKKRKLESTESRSS-FSQHARTSGRVAVEEVDEEGKFVRLRNKSNEDQSMGNWQIKRQNGDDPL 478
Mus musculus       ELLDIKLALDMEIHAYRKLLEGEEERLRLSPSPTSQ-RSRGRASSHSSQSQGGGSVTKKRKLESSESRSS-FSQHARTSGRVAVEEVDEEGKFVRLRNKSNEDQSMGNWQIRRQNGDDPL 478
Xenopus laevis     ELLDIKLALDMEINAYRKLLEGEEERLRLSPSPNTQKRSARTIASHSG-AHISSSASKRRRLEEGESRSSSFTQHARTTGKVSVEEVDPEGKYVRLRNKSNEDQSLGNWQIKRQIGDETP 475
                   *************:*******************.:* **    :***. :: ..*.:*:*:**. ***** *:*****:*:*:***** ***:***********:*****:** **:.

                                                                                         <---|
Homo sapiens       LTYRFPPKFTLKAGQVVTIWAAGAGATHSPPTDLVWKAQNTWGCGNSLRTALINSTGEEVAMRKLVRSVTVVED--DEDEDGDDLLHHHHGSHCSS---SGDPAEYNLRSRTVLCGTCGQ 593
Mus musculus       MTYRFPPKFTLKAGQVVTIWASGAGATHSPPTDLVWKAQNTWGCGSSLRTALINSTGEEVAMRKLVRSLTMVEDNEDDDEDGEELLHHHRGSHCSG---SGDPAEYNLRSRTVLCGTCGQ 595
Xenopus laevis     IVYKFPPRLTLKAGQTVTIWASGAGATNSPPSDLVWKAQSSWGTGDSIRTALLTSSNEEVAMRKLVRTVVINDE-DDEDNDDMEHHHHHHHHHHDGQNSSGDPGEYNLRSRTIVCTSCGR 594
                   :.*:***::******.*****:*****:***:*******.:** *.*:****:.*:.**********::.: ::  *:*:*. :  ***:  * ..   ****.********::* :**:

Homo sapiens       PADKASASGSGA-QVGGPISSGSSASSVTVTRSYRSVGGSGGGS-FGDNLVTRSYLLGNSSPRTQSPQNCSIM 664
Mus musculus       PADKA-AGGAGA-QVGGSISSGSSASSVTVTRSFRSVGGSGGGS-FGDNLVTRSYLLGNSSPRSQSSQNCSIM 665
Xenopus laevis     PAEKSVLASQGSGLVTG--SSGSSSSSVTLTRTYRSTGGTSGGSGLGESPVTRNFIVGNGQRAQVAPQNCSIM 665
                   **:*:  .. *:  * *  *****:****:**::**.**:.*** :*:. ***.:::**..    :.******
```

(In the Homo sapiens sequence of the last block, RSYLLG is printed in bold.)

The lamin A protein sequence from three different species is shown. The sequences were obtained from the UniProt protein sequence database (www.uniprot.org) and aligned using the free online tool Clustal2W (available at: www.ebi.ac.uk/Tools/msa/clustalw2). The location of coils 1a, 1b, 2a and 2b as well as linker regions L1, L12 and L2 and the Ig-fold are indicated above the sequence; (.) semi-conserved; (:) conserved; (*) identical.

Appendix 3: Classification and structures of the 20 standard amino acids

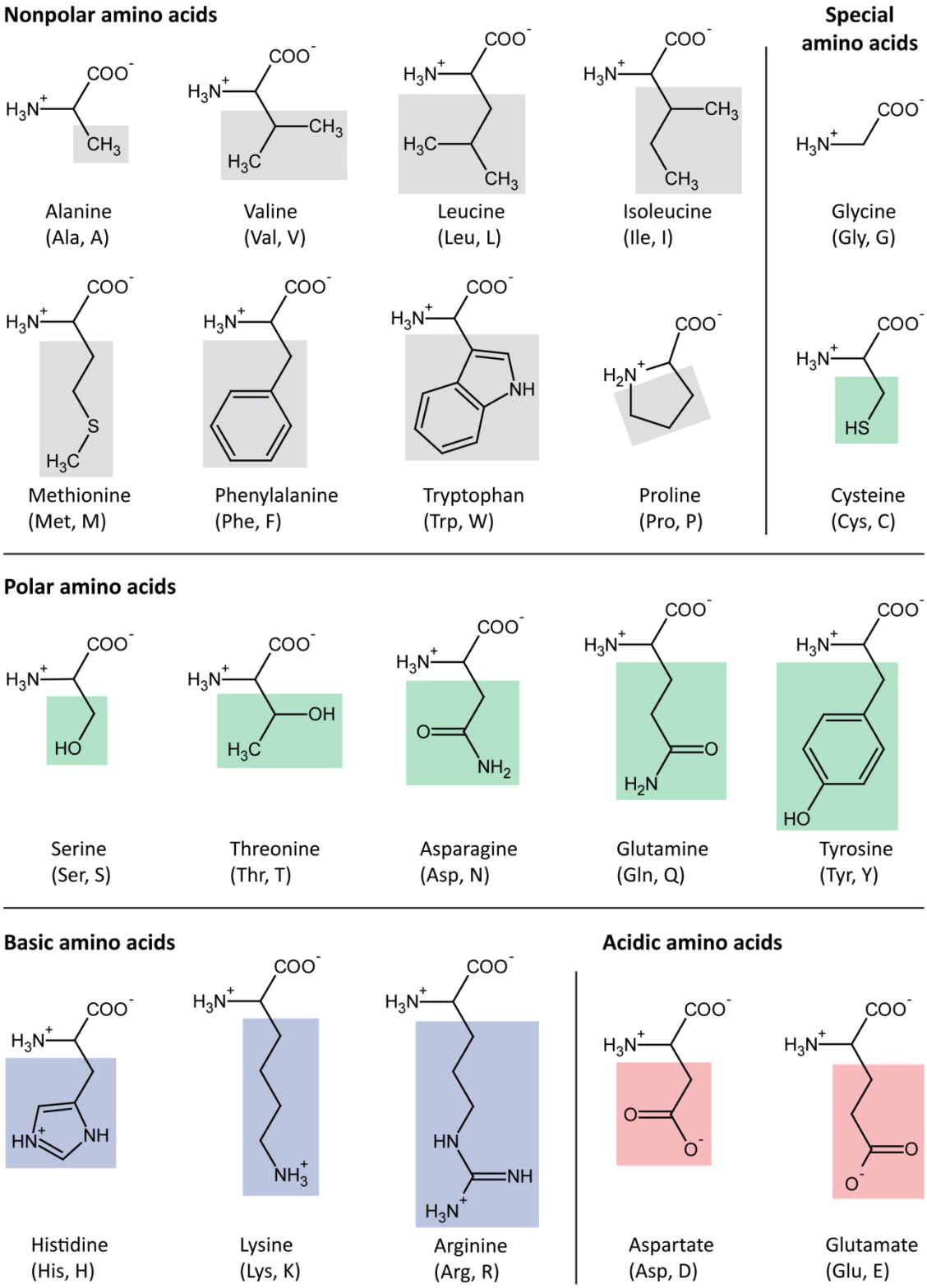

The ionisation state of the amino acids and their R-groups shown in this illustration represents the dominant form at pH7. The R-groups are highlighted by coloured boxes indicating nonpolar (grey), polar (green), positively charged (blue) and negatively charged (red) side chains. The structures were drawn using ACD Chemsketch.